

Drivers of plant nutrient acquisition and allocation strategies and their influence
on plant responses to environmental change

by

Evan A. Perkowski, B.S.

A Dissertation

In

Biological Sciences

Submitted to the Graduate Faculty
of Texas Tech University in
Partial Fulfillment of
the Requirements for
the Degree of

Doctor of Philosophy

Approved

Nicholas G. Smith, Ph.D.
Chair of Committee

Aimée T. Classen, Ph.D.

Natasja van Gestel, Ph.D.

Lindsey C. Slaughter, Ph.D.

Dylan W. Schwilk, Ph.D.

Mark Sheridan, Ph.D.
Dean of the Graduate School

May 2023

Copyright 2023, Evan A. Perkowski

Acknowledgements

This dissertation was made possible by the mentorship, collaboration, and friendship of many people. I am so thankful to be surrounded by such supportive and helpful mentors, peers, and friends that have made navigating through graduate school and finishing this dissertation an enjoyable experience. Specifically, I am thankful for the incredible mentorship of my advisor and committee chair, Dr. Nick Smith, who provided invaluable insight and tools that have helped shape me into the plant ecophysiological I claim to be today. I am also indebted to my committee members, Drs. Aimée Classen, Natasja van Gestel, Dylan Schwilk, and Lindsey Slaughter, for useful feedback, invaluable support, and encouragement as I planned and implemented experiments.

I am also thankful for past and present members of the EcoHealth lab for encouragement, support, and extracurricular activities that made time inside and outside the lab enjoyable and memorable. Particular thanks go to Dr. Lizz Waring, Dr. Xiulin Gao, Helen Scott, and Risa McNellis, Billi Jean Petermann, and the late Dr. Kris Petterson, all of whom were invaluable to helping me navigate my first year. I am especially thankful for the mentorship and friendship of Dr. Lizz Waring, as our weekly coffee chats were instrumental for helping me feel welcome in Lubbock and acclimate to life as a graduate student. I am also grateful for the friendship of Billi Jean Petermann and the late Dr. Kris Petterson for their encouragement and willingness to discuss microbial symbioses over coffee on random Saturday mornings.

Additional thanks go out to Isa Beltran, Snehanjana Chatterjee, Jeff Chi-

eppa, Peter Eludini, Zinny Ezekannagha, Hannah German, Eve Gray, Monika Kelley, Azaj Mahmud, Jorge Ochoa, Brad Posch, Avery Schoenherr, Christine Vanginault, and Jose Villeda for help with experiments or for lending an ear over puzzling results. I am also thankful for collaborators Dr. Christy Goodale and Dave Frey, who provided invaluable insight for the second experimental chapter.

I would like to thank my undergraduate advisor, Dr. Janice Krumm, for continued mentorship and friendship and for insightful advice about navigating graduate school, but most of all for helping me realize my career aspirations and pushing me to pursue this endeavor. Additional thanks go out to my family, particularly my parents, partner, and dog for continued support and distractions outside the lab. The experiments included here would not have been possible without their emotional and monetary support.

This work was made possible from funding by the NSF, USDA, Braun and Gresham, PLLC., and was a contribution to the LEMONTREE (Land Ecosystem Models based On New Theory, obseRvations and ExperimEnts) project. The LEMONTREE project is funded through the generosity of Eric and Wendy Schmidt by recommendation of the Schmidt Futures programme and the Imperial College initiative on Grand Challenges in Ecosystems and the Environment. This work was also funded by graduate student research awards from Texas Tech University and the Botanical Society of America.

I have inevitably missed mentioning folks that were instrumental to the completion of these experiments and contributed to my development as a plant ecophysiological. Please know that I am grateful and appreciative of our interactions.

Table of Contents

Acknowledgements	ii
Abstract	ix
List of Tables	xi
List of Figures	xv
1. Introduction	1
2. Structural carbon costs to acquire nitrogen are determined by nitrogen and light availability in two species with different nitrogen acquisition strategies	7
2.1 Introduction	7
2.2 Methods	11
2.2.1 <i>Experiment setup</i>	11
2.2.2 <i>Plant measurements and calculations</i>	12
2.2.3 <i>Statistical analyses</i>	13
2.3 Results	15
2.3.1 <i>Carbon costs to acquire nitrogen</i>	15
2.3.2 <i>Whole plant nitrogen biomass</i>	18
2.3.3 <i>Root carbon biomass</i>	20
2.3.4 <i>Root nodule biomass</i>	22
2.4 Discussion	26
2.4.1 <i>Carbon costs to acquire nitrogen increase with light availability and decrease with fertilization</i>	26
2.4.2 <i>Modeling implications</i>	28
2.4.3 <i>Study limitations</i>	30
2.4.4 <i>Conclusions</i>	33
3. Soil nitrogen availability modifies leaf nitrogen economies in mature temperate deciduous forests: a direct test of photosynthetic least-cost theory	34
3.1 Introduction	34

3.2 Methods	38
3.2.1 <i>Study site description</i>	38
3.2.2 <i>Experimental design</i>	39
3.2.3 <i>Leaf gas exchange and trait measurements</i>	39
3.2.4 A_{net}/C_i curve-fitting and parameter estimation	42
3.2.5 Proportion of leaf nitrogen allocated to photosynthesis and structure	44
3.2.6 Tradeoffs between nitrogen and water use	46
3.2.7 Soil nitrogen availability and pH	46
3.2.8 Statistical analyses	48
3.3 Results	50
3.3.1 Leaf nitrogen content	50
3.3.2 Net photosynthesis and leaf biochemistry	53
3.3.3 Leaf nitrogen allocation	56
3.3.4 Tradeoffs between nitrogen and water use	59
3.4 Discussion	62
3.4.1 Soil nitrogen availability modifies tradeoffs between nitrogen and water use	63
3.4.2 Soil pH did not modify tradeoffs between nitrogen and water usage	65
3.4.3 Species identity explains a large amount of variation in leaf and whole plant traits	66
3.4.4 Implications for photosynthetic least-cost theory model development	67
3.4.5 Conclusions	69
4. The relative cost of resource use for photosynthesis drives variance in leaf nitrogen content across a climate and soil resource availability gradient	70
4.1 Introduction	70
4.2 Methods	76
4.2.1 Site descriptions and sampling methodology	76

4.2.2 <i>Leaf trait measurements</i>	77
4.2.3 <i>Site climate data</i>	82
4.2.4 <i>Site edaphic characteristics</i>	82
4.2.5 <i>Plant functional group assignments</i>	84
4.2.6 <i>Data analysis</i>	85
4.3 Results	88
4.3.1 <i>Cost to acquire nitrogen relative to water</i>	88
4.3.2 <i>Leaf $C_i:C_a$</i>	92
4.3.3 <i>Leaf nitrogen content</i>	95
4.3.4 <i>Structural equation model</i>	99
4.4 Discussion	102
4.4.1 <i>Negative effects of leaf $C_i:C_a$ on N_{area} are driven by reductions in M_{area}, not N_{mass}</i>	102
4.4.2 <i>Soil nitrogen availability increases N_{area} through changes in β</i>	104
4.4.3 <i>Soil moisture increases N_{area} by facilitating increases in soil nitrogen availability</i>	105
4.4.4 <i>Indirect effects of climate on N_{area} are mediated through changes in leaf $C_i:C_a$ and β</i>	106
4.4.5 <i>Species identity traits modify effects of the environment on β, leaf $C_i:C_a$, and N_{area}</i>	107
4.4.6 <i>Next steps for optimality model development</i>	108
4.4.7 <i>Conclusions</i>	109
5. Optimal resource investment to photosynthetic capacity maximizes nutrient allocation to whole plant growth under elevated CO ₂	111
5.1 Introduction	111
5.2 Methods	116
5.2.1 <i>Seed treatments and experimental design</i>	116
5.2.2 <i>Growth chamber conditions</i>	117
5.2.3 <i>Leaf gas exchange measurements</i>	119

5.2.4 <i>Leaf trait measurements</i>	120
5.2.5 <i>A/C_i curve fitting and parameter estimation</i>	122
5.2.6 <i>Stomatal limitation</i>	122
5.2.7 <i>Proportion of leaf nitrogen allocated to photosynthesis and structure</i>	123
5.2.8 <i>Whole plant traits</i>	125
5.2.9 <i>Statistical analyses</i>	127
5.3 Results	129
5.3.1 <i>Leaf nitrogen and chlorophyll content</i>	129
5.3.2 <i>Leaf biochemistry and stomatal conductance</i>	133
5.3.3 <i>Leaf nitrogen allocation</i>	137
5.3.4 <i>Whole plant traits</i>	141
5.3.5 <i>Nitrogen fixation</i>	145
5.4 Discussion	149
5.4.1 <i>Soil nitrogen fertilization has divergent effects on leaf and whole plant acclimation responses to CO₂</i>	150
5.4.2 <i>Implications for future model development</i>	153
5.4.3 <i>Study limitations and future directions</i>	155
5.4.4 <i>Conclusions</i>	156
6. Conclusions	158
References	168
Appendix A: Supplemental material for "Structural carbon costs to acquire nitrogen are determined by nitrogen and light availability in two species with different nitrogen acquisition strategies"	205
Appendix B: Supplemental material for "Soil nitrogen availability modifies leaf nitrogen economies in mature temperate deciduous forests: a direct test of photosynthetic least-cost theory"	209

Appendix C: Supplemental material for "The relative cost of resource use for photosynthesis drives variance in leaf nitrogen content across a climate and soil resource availability gradient"	214
Appendix D: Supplemental material for "Optimal resource investment to photosynthetic capacity maximizes nutrient allocation to whole plant growth under elevated CO₂" . . .	220

Abstract

Photosynthesis is the largest carbon flux between the atmosphere and terrestrial biosphere and is constrained by ecosystem nutrient cycle dynamics, which causes terrestrial biosphere models to be sensitive to the formulation of photosynthetic processes. Terrestrial biosphere models exhibit high divergence in simulated carbon and nitrogen fluxes under future environmental conditions, which may be due to uncertainty in the acclimation response of photosynthetic processes to environmental change. Photosynthetic least-cost theory provides a promising framework for understanding effects of climatic and edaphic factors on photosynthetic acclimation responses to changing environments. Yet, empirical tests of the theory are rare, limiting our ability to assess whether the theory is suitable for implementation in next-generation terrestrial biosphere models.

Here, I present four experiments designed to test assumptions of photosynthetic least-cost theory. Experiment chapters are flanked by a general introduction chapter and conclusions chapter. The first experimental chapter quantifies structural carbon costs to acquire nitrogen in *Glycine max* and *Gossypium hirsutum* grown under four nitrogen fertilization levels and four light availability levels in a full factorial greenhouse experiment. I find that carbon costs to acquire nitrogen in both species increase with increasing light availability and decrease with increasing fertilization, though responses to fertilization in *G. max* were markedly less than *G. hirsutum*. The second experimental chapter quantifies leaf nitrogen and photosynthetic traits in upper canopy leaves of deciduous trees growing in a 9-year nitrogen-by-sulfur field manipulation experiment. I find evidence for nitrogen-

water use tradeoffs with increasing soil nitrogen availability, evidenced through a negative relationship between leaf nitrogen content and ratio of leaf intercellular CO₂ concentration to atmospheric CO₂ concentration (leaf $C_i:C_a$) and stronger increase in leaf nitrogen content with increasing soil nitrogen availability than leaf $C_i:C_a$. The third experiment investigates variance in leaf nitrogen content across a climate and soil resource availability gradient in Texan grasslands, showing that effects of soil resource availability and climate on leaf nitrogen content are driven by changes in leaf $C_i:C_a$. Finally, the fourth experiment quantifies leaf and whole plant acclimation responses in *G. max* grown under two atmospheric CO₂ levels, with and without inoculation with *Bradyrhizobium japonicum*, and across nine nitrogen fertilization treatments in a full factorial growth chamber experiment. I find that leaf acclimation responses to CO₂ were independent of soil nitrogen fertilization and inoculation treatment, though increased whole plant growth under elevated CO₂ was enhanced with increasing soil nitrogen fertilization and in inoculated pots under low nitrogen fertilization.

Experiments included in this dissertation provide consistent support for patterns expected from photosynthetic least-cost theory. The use of multiple experimental approaches allowed me to examine mechanisms driving patterns expected from the theory and investigate whether these patterns occur in the field across environmental gradients. Findings from these chapters challenge common paradigms in plant ecophysiology, providing empirical evidence suggesting that including photosynthetic least-cost frameworks in terrestrial biosphere models may improve the longstanding observed divergence in simulated outcomes across terrestrial biosphere model products.

List of Tables

2.1	Analysis of variance results exploring species-specific effects of light availability, nitrogen fertilization, and their interactions on carbon costs to acquire nitrogen, whole-plant nitrogen biomass, and root carbon biomass	16
2.2	Analysis of variance results exploring effects of light availability, nitrogen fertilization, and their interactions on <i>G. max</i> root nodule biomass and the ratio of root nodule biomass to root biomass	23
2.3	Slopes of the regression line describing the relationship between each dependent variable and nitrogen fertilization at each light level	24
3.1	Effects of soil nitrogen availability, soil pH, and species on leaf nitrogen content per unit leaf area, leaf nitrogen content per unit leaf mass, and leaf mass per unit leaf area	51
3.2	Effects of soil nitrogen availability, soil pH, species, and N_{area} on net photosynthesis, the maximum rate of Rubisco carboxylation, the maximum rate of RuBP regeneration, and the ratio of the maximum rate of RuBP regeneration to the maximum rate of Rubisco carboxylation	54
3.3	Effects of soil nitrogen availability, soil pH, and species on the proportion of leaf nitrogen content allocated to photosynthesis, Rubisco, bioenergetics, and structure	57

3.4 Effects of soil nitrogen availability, soil pH, species, and N_{area} on χ , photosynthetic nitrogen use efficiency, leaf nitrogen content per unit χ , and maximum Rubisco carboxylation rate per unit χ	60
4.1 Site locality information, sampling year, 2006-2020 mean annual precipitation, mean annual temperature, and water holding capacity	80
4.2 Effects of soil moisture, soil nitrogen availability, and plant functional group on β	89
4.3 Effects of soil moisture, soil nitrogen availability, and plant functional group on leaf $C_i:C_a$	93
4.4 Effects of soil moisture, soil nitrogen availability, plant functional group, and leaf $C_i:C_a$ on leaf nitrogen content per unit leaf area, leaf nitrogen content per unit leaf biomass, and leaf biomass per unit leaf area	97
4.5 Structural equation model results investigating direct effects of climatic and soil resource availability on leaf nitrogen content	100
5.1 Effects of soil nitrogen fertilization, inoculation, and CO ₂ treatments on leaf nitrogen content per unit leaf area, leaf nitrogen content per unit leaf mass, leaf mass per unit leaf area, and chlorophyll content per unit leaf area	131

5.2	Effects of soil nitrogen fertilization, inoculation, and CO ₂ on the maximum rate of Rubisco carboxylation, the maximum rate of RuBP regeneration, dark respiration, the ratio of the maximum rate of RuBP regeneration to the maximum rate of Rubisco carboxylation, stomatal conductance, and stomatal limitation	135
5.3	Effects of soil nitrogen fertilization, inoculation, and CO ₂ on the fraction of leaf nitrogen allocated to Rubisco, bioenergetics, light harvesting proteins, photosynthesis, and structure	139
5.4	Effects of CO ₂ , fertilization, and inoculation on total leaf area, whole plant biomass, carbon costs to acquire nitrogen, belowground carbon biomass, and whole plant nitrogen biomass	143
5.5	Effects of CO ₂ , fertilization, and inoculation on root nodule biomass, plant investments in symbiotic nitrogen fixation, and percent nitrogen fixed from the atmosphere	147
A1	Summary table containing volumes of compounds used to create modified Hoagland's solutions for each soil nitrogen fertilization treatment	205
A2	Analysis of variance results exploring species-specific effects of light availability, nitrogen fertilization, and their interactions on the ratio of whole plant biomass to pot volume	206
A3	Slopes of the regression line describing the relationship between each dependent variable and nitrogen fertilization at each light level	207

B1	Sample sizes of each species, abbreviated by their USDA NRCS PLANTS database code, within each plot at each site	209
B2	Analysis of variance results exploring the linear effect of leaf temperature on net photosynthesis rate and stomatal conductance measured at 400 $\mu\text{mol mol}^{-1}$ CO ₂	210
B3	Second order log-polynomial regression coefficients that described the effect of leaf temperature on net photosynthesis and stomatal conductance measured at 400 $\mu\text{mol mol}^{-1}$ CO ₂	211
B4	Mean, standard error, and 95% confidence interval ranges of soil nitrogen availability estimates across all measured plots	212
C1	List of sampled species and their plant functional group assignment	216
C2	List of sampled species and their plant functional group assignment (cont.)	217
C3	Model selection results for soil moisture and vapor pressure deficit	218
D1	Summary table containing volumes of compounds used to create modified Hoagland's solutions for each soil nitrogen fertilization treatment	220
D2	Summary of the daily growth chamber growing condition program	221
D3	Effects of CO ₂ , fertilization, and inoculation on whole plant biomass: pot volume	222

List of Figures

2.1 Relationships between soil nitrogen fertilization and light availability on carbon costs to acquire nitrogen in <i>G. hirsutum</i> and <i>G. max</i>	17
2.2 Relationships between soil nitrogen fertilization and light availability on whole-plant nitrogen biomass in <i>G. hirsutum</i> and <i>G. max</i>	19
2.3 Relationships between soil nitrogen fertilization and light availability on root carbon biomass in <i>G. hirsutum</i> and <i>G. max</i>	21
2.4 Effects of shade cover and nitrogen fertilization on root nodule biomass and the ratio of root nodule biomass to root biomass in <i>G. max</i>	25
3.1 Effects of soil nitrogen availability and species on leaf nitrogen content per unit leaf area, leaf nitrogen content per unit leaf biomass, and leaf mass per leaf area	52
3.2 Effects of soil nitrogen availability, species, and leaf nitrogen content on net photosynthesis, maximum Rubisco carboxylation rate, and maximum RuBP regeneration rate	55
3.3 Effects of soil nitrogen availability, species, and leaf nitrogen content on the fraction of leaf nitrogen allocated to photosynthesis and structure	58
3.4 Effects of soil N availability, species, and leaf N content on tradeoffs between nitrogen and water use	61

4.1	Site locations along 2006-2020 mean annual precipitation and mean annual temperature gradients in Texas, USA.	81
4.2	Effects of soil nitrogen availability and soil moisture on the cost of acquiring and using nitrogen	91
4.3	Effects of 4-day mean vapor pressure deficit, 2-day soil moisture (per water holding capacity), and soil nitrogen availability on leaf $C_i:C_a$	94
4.4	Effects of leaf $C_i:C_a$, soil nitrogen availability, and soil moisture on leaf nitrogen content per unit leaf area, leaf nitrogen content per unit leaf biomass, and leaf mass per area.	98
4.5	Structural equation model results exploring drivers of N_{area}	101
5.1	Effects of CO_2 , fertilization, and inoculation on leaf nitrogen per unit leaf area, leaf nitrogen content, leaf mass per unit leaf area, and chlorophyll content per unit leaf area	132
5.2	Effects of CO_2 , fertilization, and inoculation on maximum rate of Rubisco carboxylation, the maximum rate of RuBP regeneration, and the ratio of the maximum rate of RuBP regeneration to the maximum rate of Rubisco carboxylation leaf mass per unit leaf area, dark respiration, stomatal conductance, and stomatal limitation .	136
5.3	Effects of CO_2 , fertilization, and inoculation on the relative fraction of leaf nitrogen allocated to photosynthesis and the fraction of leaf nitrogen allocated to structure	140

5.4	Effects of CO ₂ , fertilization, and inoculation on total leaf area, total biomass, and structural carbon costs to acquire nitrogen	144
5.5	Effects of CO ₂ , fertilization, and inoculation on nodule biomass, nodule biomass: root biomass, and percent nitrogen fixed from the atmosphere	148
A1	Effects of shade cover and nitrogen fertilization on the ratio of plant biomass to rooting volume in <i>G. hirsutum</i> and <i>G. max</i>	208
B1	Effects of leaf temperature on net photosynthesis rate and stomatal conductance values when measured at 400 $\mu\text{mol mol}^{-1}$ CO ₂ . . .	213
C1	Model selection results exploring relevant timescales for soil moisture and vapor pressure deficit	219
D1	Relationships between area-based leaf nitrogen content, mass-based leaf nitrogen content, and leaf mass per unit leaf area measured on the focal leaf used to generate A_{net}/C_i curves and leaf nitrogen content measured on the leaf used for chlorophyll extractions . . .	223
D2	Effects of CO ₂ , fertilization, and inoculation on the ratio of whole plant biomass to pot volume	224

1 Chapter 1

2 Introduction

3 Photosynthesis represents the largest carbon flux between the atmosphere
4 and biosphere, and is regulated by complex ecosystem carbon and nutrient cy-
5 cles (Hungate et al. 2003; IPCC 2021). As a result, the inclusion of robust,
6 empirically tested representations of photosynthetic processes is critical in order
7 for terrestrial biosphere models to accurately and reliably simulate carbon and
8 nutrient fluxes between the atmosphere and terrestrial biosphere (Oreskes et al.
9 1994; Smith and Dukes 2013; Prentice et al. 2015; Wieder et al. 2015). De-
10 spite evidence that the inclusion of coupled carbon and nutrient cycles can reduce
11 model uncertainty, widespread divergence in predicted carbon and nutrient fluxes
12 is still apparent across model products (Friedlingstein et al. 2014; Arora et al.
13 2020; Davies-Barnard et al. 2020). Divergence in predicted carbon and nutrient
14 fluxes across terrestrial biosphere models may be due to an incomplete under-
15 standing of how plants acclimate to changing environments (Smith and Dukes
16 2013; Davies-Barnard et al. 2020), as terrestrial biosphere models are sensitive to
17 the formulation of photosynthetic processes (Bonan et al. 2011; Ziehn et al. 2011;
18 Booth et al. 2012; Smith et al. 2016; Smith et al. 2017; Rogers et al. 2017).

Many terrestrial biosphere models predict leaf-level photosynthesis through linear relationships between area-based leaf nitrogen content and the maximum rate of Ribulose-1,5-bisphosphate carboxylase/oxygenase (“Rubisco”), following the idea that large fractions of leaf nitrogen content are allocated to the construction and maintenance of Rubisco and other photosynthetic enzymes (Evans

24 1989). The inclusion of coupled carbon and nutrient cycles in terrestrial bio-
25 sphere models (Shi et al. 2016; Braghieri et al. 2022) allows for the prediction
26 of leaf nitrogen content through soil nitrogen availability, which causes models to
27 indirectly predict photosynthetic processes through shifts in soil nitrogen avail-
28 ability (Smith et al. 2014; Lawrence et al. 2019). While these patterns are
29 commonly observed in ecosystems globally (Brix 1971; Evans 1989; Firn et al.
30 2019; Liang et al. 2020), this formulation does not allow for the prediction of
31 leaf and whole plant acclimation responses to changing environments (Smith and
32 Dukes 2013; Rogers et al. 2017; Harrison et al. 2021), and suggests that constant
33 leaf nitrogen-photosynthesis relationships are ubiquitous across ecosystems.

34 Photosynthetic least-cost theory (Prentice et al. 2014; Wang et al. 2017;
35 Smith et al. 2019; Paillassa et al. 2020; Scott and Smith 2022; Harrison et al.
36 2021) provides a framework for predicting leaf and whole plant acclimation re-
37 sponds to environmental change. The theory, which unifies optimal coordination
38 (Chen et al. 1993; Maire et al. 2012) and least-cost (Wright et al. 2003) theo-
39 ries, posits that plants optimize leaf net photosynthesis rates by minimizing the
40 summed cost of nutrient and water use. Minimized costs of nutrient and water use
41 at the leaf level optimizes leaf photosynthesis by allowing net photosynthesis to be
42 equally co-limited by the maximum rate of Rubisco carboxylation and the max-
43 imum rate of Ribulose-1,5-bisphosphate (RuBP) regeneration (Chen et al. 1993;
44 Maire et al. 2012). The theory indicates that costs of nutrient and water use
45 are substitutable such that, in a given environment, optimal photosynthesis rates
46 can be achieved by sacrificing inefficient use of a relatively more abundant (and
47 less costly to acquire) resource for more efficient use of a relatively less abundant

48 (and more costly to acquire) resource. This may result in changes in the ratio of
49 the cost to acquire and use nutrients relative to the cost to acquire and use water
50 (i.e., β) across environmental gradients. For example, plants may respond to an
51 increase in soil nitrogen availability by increasing leaf nitrogen allocation and de-
52 creasing stomatal conductance, allowing a given net photosynthesis rate achieved
53 through reduced nitrogen use efficiency and increased water use efficiency. The
54 theory predicts that β is positively correlated with the ratio of intercellular CO₂
55 to atmospheric CO₂ (leaf C_i:C_a), which is determined by factors that influence
56 leaf nutrient demand to build and maintain photosynthetic enzymes, such as at-
57 mospheric CO₂, temperature, vapor pressure deficit, or light availability (Prentice
58 et al. 2014; Wang et al. 2017; Smith et al. 2019; Stocker et al. 2020). Thus,
59 photosynthetic least-cost theory provides a promising framework for understand-
60 ing integrated plant acclimation responses to changes in climatic and edaphic
61 gradients.

62 Optimality models that use patterns expected from photosynthetic least-
63 cost theory have been developed for both C₃ (Wang et al. 2017; Smith et al. 2019;
64 Stocker et al. 2020) and more recently for C₄ species (Scott and Smith 2022).
65 Such models show broad agreement with patterns observed across environmental
66 gradients (Smith et al. 2019; Stocker et al. 2020; Paillassa et al. 2020; Querejeta
67 et al. 2022; Westerband et al. 2023), and are capable of reconciling dynamic
68 leaf nitrogen-photosynthesis relationships and acclimation responses to elevated
69 CO₂, temperature, light availability, and vapor pressure deficit (Dong et al. 2017;
70 Dong et al. 2020; Smith and Keenan 2020; Luo et al. 2021; Peng et al. 2021;
71 Dong et al. 2022; Dong et al. 2022; Querejeta et al. 2022; Westerband et al.

72 2023). Current versions of optimality models that invoke patterns expected from
73 photosynthetic least-cost theory hold β constant across growing environments.
74 As growing evidence suggests that costs of nutrient use are plastic across resource
75 availability and climatic gradients in species with different nutrient acquisition
76 strategies (Fisher et al. 2010; Brzostek et al. 2014; Terrer et al. 2018; Allen et al.
77 2020), one might expect that β should dynamically change across environments
78 and in species with different nutrient acquisition strategies.

79 Patterns expected from photosynthetic least-cost theory have recently been
80 shown to occur across broad environmental gradients. Despite this, a limited num-
81 ber of studies have investigated how β varies across edaphic and climatic gradients
82 and how variance in β might scale to influence leaf nutrient-water use tradeoffs
83 (Lavergne et al. 2020; Paillassa et al. 2020). Furthermore, no previous study has
84 investigated whether β varies in species with different nutrient acquisition strate-
85 gies, or if changes in β due to changes in edaphic characteristics scale to influence
86 leaf or whole plant acclimation responses to changing environments. The lack of
87 such studies provided motivation for the experimental chapters included in this
88 dissertation.

89 In this dissertation, I use a combination of greenhouse, field manipulation,
90 environmental gradient, and growth chamber experiments to quantify leaf and
91 whole plant acclimation responses across various climatic and edaphic conditions
92 and species representing different nutrient acquisition strategies. Together, these
93 experiments evaluate patterns expected from photosynthetic least-cost theory and
94 test mechanisms predicted to drive responses expected from theory. The empirical
95 data collected in these experiments provide important information needed to re-

96 fine existing optimality models that include photosynthetic least-cost frameworks,
97 and could help determine whether such models are suitable for implementing in
98 next-generation terrestrial biosphere models. While theory suggests that plants
99 acclimate across environments by minimizing the summed cost of nutrients relative
100 to water, I chose to isolate effects of soil nitrogen availability on costs of nitrogen
101 acquisition relative to water for the sake of brevity. I acknowledge that patterns
102 expected from theory may be modified by other nutrients (e.g., phosphorus) or
103 other edaphic characteristics (Smith et al. 2019; Paillassa et al. 2020; Westerband
104 et al. 2023), and, though not included here, should also be investigated.

105 In the first experimental chapter, I re-analyze data from a greenhouse ex-
106 periment that grew *Glycine max* and *Gossypium hirsutum* seedlings under full-
107 factorial combinations of four light treatments and four fertilization treatments
108 to examine effects of nitrogen and light availability on structural carbon costs to
109 acquire nitrogen. In the second experimental chapter, I measure leaf physiological
110 traits in the upper canopy of mature trees growing in a 9-year nitrogen-by-pH
111 field manipulation experiment to assess whether changes in soil nitrogen availabil-
112 ity or soil pH modify nitrogen-water use tradeoffs expected from photosynthetic
113 least-cost theory. In the third experimental chapter, I investigate primary drivers
114 of leaf nitrogen content across a broad precipitation and soil nitrogen availability
115 gradient in Texan grasslands. In the fourth experimental chapter, I use growth
116 chambers to quantify leaf and whole plant acclimation responses to CO₂ in *Glycine*
117 *max* grown across a soil nitrogen fertilization gradient. I also manipulate nutrient
118 acquisition strategy by controlling whether *Glycine max* seedlings were able to
119 form associations with symbiotic nitrogen-fixing bacteria.

120 Across experiments, I find consistent support for patterns expected from
121 photosynthetic least-cost theory, showing that shifts in edaphic characteristics
122 predictably alter β , and that β facilitates changes in leaf nitrogen-water use
123 tradeoffs and leaf nitrogen-photosynthesis relationships. I also show that costs
124 of nitrogen acquisition vary in species with different nitrogen acquisition strate-
125 gies. Finally, I show strong evidence suggesting that leaf acclimation responses to
126 elevated CO₂ are decoupled from soil nitrogen availability and inoculation with
127 symbiotic nitrogen-fixing bacteria. It is my hope that these experiments will en-
128 courage future iterations of optimality models that adopt photosynthetic least-cost
129 frameworks to consider frameworks for implementing dynamic β values across soil
130 resource availability gradients and in species with different nutrient acquisition
131 strategies.

132 The four experimental chapters included in this dissertation are presented
133 either as previously published journal articles or as manuscript drafts currently
134 in preparation for journal submission. Specifically, the first experimental chapter
135 was published in *Journal of Experimental Botany* in 2021 and the second chapter
136 is currently in review, while the third and fourth chapters are each in preparation
137 for journal submission. The dissertation concludes with a sixth chapter that sum-
138 marizes experiment findings, briefly synthesizes common themes observed across
139 experiments, and provides some suggestions for future experimentation.

140

Chapter 2

141

Structural carbon costs to acquire nitrogen are determined by
142 nitrogen and light availability in two species with different nitrogen
143 acquisition strategies

144 Perkowski EA, EF Waring, NG Smith, "Root mass carbon costs to acquire nitro-
145 gen are determined by nitrogen and light availability in two species with different
146 nitrogen acquisition strategies", *Journal of Experimental Botany*, 2021, Volume
147 72, Issue 15, Pages 5766-5776, by permission of Oxford University Press

148 2.1 Introduction

149 Carbon and nitrogen cycles are tightly coupled in terrestrial ecosystems. This
150 tight coupling influences photosynthesis (Walker et al. 2014; Rogers et al. 2017),
151 net primary productivity (LeBauer and Treseder 2008; Thomas et al. 2013), de-
152 composition (Cornwell et al. 2008; Bonan et al. 2013; Sulman et al. 2019), and
153 plant resource competition (Gill and Finzi 2016; Xu-Ri and Prentice 2017). Ter-
154 restrial biosphere models are beginning to include connected carbon and nitrogen
155 cycles to improve the realism of their simulations (Fisher et al. 2010; Brzostek
156 et al. 2014; Wieder et al. 2015; Shi et al. 2016; Zhu et al. 2019). Simula-
157 tions from these models indicate that coupling carbon and nitrogen cycles can
158 drastically influence future biosphere-atmosphere feedbacks under global change,
159 such as elevated carbon dioxide or nitrogen deposition (Thornton et al. 2007;
160 Goll et al. 2012; Wieder et al. 2015; Wieder et al. 2019). Nonetheless, there
161 are still limitations in our quantitative understanding of connected carbon and
162 nitrogen dynamics (Thomas et al. 2015; Meyerholt et al. 2016; Rogers et al.
163 2017; Exbrayat et al. 2018; Shi et al. 2019), forcing models to make potentially
164 unreliable assumptions.

165 Plant nitrogen acquisition is a process in terrestrial ecosystems by which
166 carbon and nitrogen are tightly coupled (Vitousek and Howarth 1991; Delaire et al.
167 2005; Brzostek et al. 2014). Plants must allocate carbon belowground to produce
168 and maintain root systems or exchange with symbiotic soil microbes in order to
169 acquire nitrogen (Högberg et al. 2008; Högberg et al. 2010). Thus, plants have an
170 inherent carbon cost associated with acquiring nitrogen, which can include both
171 direct energetic costs associated with nitrogen acquisition and indirect structural
172 costs associated with allocation (Gutschick 1981; Rastetter et al. 2001; Vitousek
173 et al. 2002; Menge et al. 2008). Model simulations (Fisher et al. 2010; Brzostek
174 et al. 2014; Shi et al. 2016; Allen et al. 2020) and meta-analyses (Terrer et al.
175 2018) suggest that these carbon costs vary between species, particularly those with
176 different nitrogen acquisition strategies. For example, simulations using iterations
177 of the Fixation and Uptake of Nitrogen (FUN) model indicate that species that
178 acquire nitrogen from non-symbiotic active uptake pathways (e.g. mass flow)
179 generally have larger carbon costs to acquire nitrogen than species that acquire
180 nitrogen through symbiotic associations with nitrogen-fixing bacteria (Brzostek
181 et al. 2014; Allen et al. 2020).

182 Carbon costs to acquire nitrogen likely vary in response to changes in soil
183 nitrogen availability. For example, if the primary mode of nitrogen acquisition
184 is through non-symbiotic active uptake, then nitrogen availability could decrease
185 carbon costs to acquire nitrogen as a result of increased per-root nitrogen up-
186 take (Franklin et al. 2009; Wang et al. 2018). However, if the primary mode of
187 nitrogen acquisition is through symbiotic active uptake, then nitrogen availabil-
188 ity may incur additional carbon costs to acquire nitrogen if it causes microbial

189 symbionts to shift toward parasitism along the parasitism–mutualism continuum
190 (Johnson et al. 1997; Hoek et al. 2016; Friel and Friesen 2019) or if it reduces
191 the nitrogen acquisition capacity of a microbial symbiont (van Diepen et al. 2007;
192 Soudzilovskaia et al. 2015; Muñoz et al. 2016). Species may respond to shifts in
193 soil nitrogen availability by switching their primary mode of nitrogen acquisition
194 to a strategy with lower carbon costs to acquire nitrogen in order to maximize
195 the magnitude of nitrogen acquired from a belowground carbon investment and
196 outcompete other individuals for soil resources (Rastetter et al. 2001; Menge et al.
197 2008).

198 Environmental conditions that affect plant nitrogen demand (e.g., CO₂,
199 light availability) could also affect plant carbon costs to acquire nitrogen. For
200 example, an increase in plant nitrogen demand could increase carbon costs to
201 acquire nitrogen if this increases the carbon that must be allocated belowground
202 to acquire a proportional amount of nitrogen (Kulmatiski et al. 2017; Noyce
203 et al. 2019). This could be driven by a temporary state of diminishing return
204 associated with investing carbon toward building and maintaining structures that
205 are necessary to support enhanced nitrogen uptake, such as fine roots (Matamala
206 and Schlesinger 2000; Norby et al. 2004; Arndal et al. 2018), mycorrhizal hyphae
207 (Saleh et al. 2020), or root nodules (Parvin et al. 2020). Alternatively, if the
208 environmental factor that increases plant nitrogen demand causes nitrogen to
209 become more limiting in the system (e.g. atmospheric CO₂) (Luo et al. 2004;
210 LeBauer and Treseder 2008; Vitousek et al. 2010; Liang et al. 2016), species
211 might switch their primary mode of nitrogen acquisition to a strategy with lower
212 relative carbon costs to acquire nitrogen in order to gain a competitive advantage

213 over species with either different or more limited modes of nitrogen acquisition
214 (Ainsworth and Long 2005; Taylor and Menge 2018).

215 Using a plant economics approach, I examined the influence of plant ni-
216 trogen demand and soil nitrogen availability on plant carbon costs to acquire
217 nitrogen. This was done by growing a species capable of forming associations
218 with nitrogen-fixing bacteria (*Glycine max* L. (Merr)) and a species not capable
219 of forming these associations (*Gossypium hirsutum* L.) under four levels of light
220 availability (plant nitrogen demand proxy) and four levels of soil nitrogen fertil-
221 ization (soil nitrogen availability proxy) in a full-factorial, controlled greenhouse
222 experiment. These species are commonly used in regional west Texan cropping
223 systems and have fast growth rates, but differ in growth form (*Gossypium hir-*
224 *sutum* is a perennial woody species, *G. max* is an annual herbaceous species).
225 Species were selected as a hypothesis generation exercise to determine whether ef-
226 fects of fertilization and light availability on carbon costs to acquire nitrogen were
227 directionally similar across species, though this selection does limit my ability to
228 deduce mechanisms that drive species differences across treatment combinations.
229 I used this experimental design to test the following hypotheses:

- 230 1. An increase in plant nitrogen demand due to increasing light availability will
231 increase carbon costs to acquire nitrogen through a proportionally larger
232 increase in belowground carbon than whole-plant nitrogen acquisition. This
233 will be the result of an increased investment of carbon toward belowground
234 structures that support enhanced nitrogen uptake, but at a lower nitrogen
235 return.
- 236 2. An increase in soil nitrogen availability will decrease carbon costs to acquire

237 nitrogen as a result of increased per root nitrogen uptake in *G. hirsutum*.
238 However, soil nitrogen availability will not affect carbon costs to acquire
239 nitrogen in *G. max* because of the already high return of nitrogen supplied
240 through nitrogen fixation.

241 2.2 Methods

242 2.2.1 *Experiment setup*

243 *Gossypium hirsutum* and *G. max*. were planted in individual 3 liter pots (NS-300;
244 Nursery Supplies, Orange, CA, USA) containing a 3:1 mix of unfertilized potting
245 mix (Sungro Sunshine Mix #2, Agawam, MA, USA) to native soil extracted from
246 an agricultural field most recently planted with *G. max* at the USDA-ARS Lab-
247 oratory in Lubbock, TX, USA (33.59°N, -101.90°W). The field soil was classified
248 as Amarillo fine sandy loam (75% sand, 10% silt, 15% clay). Upon planting,
249 all *G. max* pots were inoculated with *Bradyrhizobium japonicum* (Verdesian N-
250 Dure™ Soybean, Cary, NC, USA) to stimulate root nodulation. Individuals of
251 both species were grown under similar, unshaded, ambient greenhouse conditions
252 for 2 weeks to germinate and begin vegetative growth.

253 Three blocks were set up in the greenhouse, each containing four light
254 treatments created using shade cloth that reduced incoming radiation by either 0
255 (full sun), 30, 50, or 80%. Two weeks post-germination, individuals were randomly
256 placed in the four light treatments in each block. Individuals received one of four
257 nitrogen fertilization doses as 100mL of a modified Hoagland solution (Hoagland
258 and Arnon 1950) equivalent to either 0, 70, 210, or 630 ppm N twice per week
259 within each light treatment. Nitrogen fertilization doses were received as topical

260 agents to the soil surface. Each Hoagland solution was modified to keep concen-
261 trations of other macro- and micronutrients equivalent (Table A1). Plants were
262 routinely well watered to eliminate water stress.

263 2.2.2 *Plant measurements and calculations*

264 Each individual was harvested after 5 weeks of treatment, and biomass was sepa-
265 rated by organ type (leaves, stems, and roots). Nodules on *G. max* roots were also
266 harvested. Except for the 0% shade cover and 630 ppm N treatment combination,
267 all treatment combinations in both species had lower average dry biomass:pot vol-
268 ume ratios than the 1:1 ratio recommended by Poorter et al. (2012) to minimize
269 the likelihood of pot volume-induced growth limitation (Table A2, A3; Fig. A1).

270 All harvested material was dried, weighed, and ground by organ type.
271 Carbon and nitrogen content (g g^{-1}) was determined by subsampling from ground
272 and homogenized biomass of each organ type using an elemental analyzer (Costech
273 4010; Costech, Inc., Valencia, CA, USA). I scaled these values to total leaf, stem,
274 and root carbon and nitrogen biomass (g) by multiplying dry biomass of each
275 organ type by carbon or nitrogen content of each corresponding organ type. Whole
276 plant nitrogen biomass (g) was calculated as the sum of total leaf (g), stem (g),
277 and root (g) nitrogen biomass. Root nodule carbon biomass was not included in
278 the calculation of root carbon biomass; however, relative plant investment toward
279 root or root nodule standing stock was estimated as the ratio of root biomass to
280 root nodule biomass (g g^{-1}), following similar metrics to those adopted by Dovrat
281 et al. (2018) and Dovrat et al. (2020).

282 Carbon costs to acquire nitrogen (N_{cost} ; gC gN^{-1}) were estimated as the

283 ratio of total root carbon biomass (C_{bg} ; gC) to whole-plant nitrogen biomass
284 (N_{wp} ; gN). This calculation quantifies the relationship between carbon spent on
285 nitrogen acquisition and whole plant nitrogen acquisition by using root carbon
286 biomass as a proxy for estimating the magnitude of carbon allocated toward ni-
287 trogen acquisition. This calculation therefore assumes that the magnitude of root
288 carbon standing stock is proportional to carbon transferred to root nodules or my-
289 corrhizae, or lost through root exudation or turnover. The assumption has been
290 supported in species that associate with ectomycorrhizal fungi (Hobbie 2006; Hob-
291 bie and Hobbie 2008), but is less clear in species that acquire nitrogen through
292 non-symbiotic active uptake or symbiotic nitrogen fixation. It is also unclear
293 whether relationships between root carbon standing stock and carbon transfer to
294 root nodules are similar in magnitude to carbon lost through exudation or when
295 allocated toward other active uptake pathways. Thus, because of the way mea-
296 surements were calculated, proximal values of carbon costs to acquire nitrogen are
297 underestimates.

298 2.2.3 *Statistical analyses*

299 I explored the effects of light and nitrogen availability on carbon costs to acquire
300 nitrogen using separate linear mixed-effects models for each species. Models in-
301 cluded shade cover, nitrogen fertilization, and interactions between shade cover
302 and nitrogen fertilization as continuous fixed effects, and also included block as a
303 random intercept term. Three separate models for each species were built with
304 this independent variable structure for three different dependent variables: (i)
305 carbon costs to acquire nitrogen (gC gN⁻¹); (ii) whole plant nitrogen biomass

306 (denominator of carbon cost to acquire nitrogen; gN); and (iii) belowground car-
307 bon biomass (numerator of carbon cost to acquire nitrogen; gC). I constructed two
308 additional models for *G. max* with the same model structure described above to
309 investigate the effects of light availability and nitrogen fertilization on root nodule
310 biomass (g) and the ratio of root nodule biomass to root biomass (unitless).

311 I used Shapiro–Wilk tests of normality to determine whether species spe-
312 cific linear mixed-effects model residuals followed a normal distribution. Zero
313 models satisfied residual normality assumptions when models were fit using un-
314 transformed data (Shapiro–Wilk: $p<0.05$ in all cases). I attempted to satisfy
315 residual normality assumptions by first fitting models using dependent variables
316 that were natural-log transformed. If residual normality assumptions were still
317 not met (Shapiro–Wilk: $p<0.05$), then models were fit using dependent variables
318 that were square root transformed. All residual normality assumptions were satis-
319 fied when models were fit with either a natural-log or square root transformation
320 (Shapiro–Wilk: $p>0.05$ in all cases). Specifically, I natural-log transformed *G.*
321 *hirsutum* carbon costs to acquire nitrogen and *G. hirsutum* whole-plant nitrogen
322 biomass. I also square root transformed *G. max* carbon costs to acquire nitrogen,
323 *G. max* whole-plant nitrogen biomass, root carbon biomass in both species, *G.*
324 *max* root nodule biomass, and the *G. max* ratio of root nodule biomass to root
325 biomass. I used the ‘lmer’ function in the ‘lme4’ R package (Bates et al. 2015) to
326 fit each model and the ‘Anova’ function in the ‘car’ R package (Fox and Weisberg
327 2019) to calculate Wald’s χ^2 to determine the significance ($\alpha=0.05$) of each fixed
328 effect coefficient. Finally, I used the ‘emmeans’ R package (Lenth 2019) to conduct
329 post-hoc comparisons of our treatment combinations using Tukey’s tests. Degrees

330 of freedom for all Tukey's tests were approximated using the Kenward–Roger ap-
331 proach (Kenward and Roger 1997). All analyses and plots were conducted in R
332 version 4.0.1 (R Core Team 2021).

333 2.3 Results

334 2.3.1 *Carbon costs to acquire nitrogen*

335 Carbon costs to acquire nitrogen in *G. hirsutum* increased with increasing light
336 availability ($p<0.001$; Table 2.1; Fig. 2.1) and decreased with increasing nitrogen
337 fertilization ($p<0.001$; Table 2.1; Fig. 2.1). There was no interaction between
338 light availability and nitrogen fertilization ($p=0.486$, Table 2.1; Fig. 2.1).

339 Carbon costs to acquire nitrogen in *G. max* also increased with increasing
340 light availability ($p<0.001$, Table 2.1; Fig. 2.1) and decreased with increasing
341 nitrogen fertilization ($p<0.001$; Table 2.1; Fig. 2.1). There was no interaction
342 between light availability and nitrogen fertilization ($p=0.261$, Table 2.1; Fig. 2.1).

Table 2.1. Analysis of variance results exploring species-specific effects of light availability, nitrogen fertilization, and their interactions on carbon costs to acquire nitrogen (N_{cost} ; gC gN $^{-1}$), whole plant nitrogen biomass (N_{wp} ; gN), and root carbon biomass (C_{bg} ; gC)

	N_{cost}			N_{wp}			C_{bg}			
	df	Coefficient	χ^2	p	Coefficient	χ^2	p	Coefficient	χ^2	p
<i>G. hirsutum</i>										
Intercept		1.594	-	-	-3.232	-	-	0.432	-	-
Light (L)	1	$-1.09 * 10^{-2}$	56.494	<0.001	$-6.41 * 10^{-3}$	91.275	<0.001	$-2.62 * 10^{-3}$	169.608	<0.001
Nitrogen (N)	1	$-1.34 * 10^{-3}$	54.925	<0.001	$1.83 * 10^{-3}$	118.784	<0.001	$1.15 * 10^{-4}$	2.901	<i>0.089</i>
L*N	1	$3.88 * 10^{-6}$	0.485	0.486	$-1.34 * 10^{-5}$	10.721	0.001	$-1.67 * 10^{-6}$	3.140	<i>0.076</i>
<i>G. max</i>										
Intercept		1.877	-	-	0.239	-	-	0.438	-	-
Light (L)	1	$-7.67 * 10^{-3}$	174.156	<0.001	$-6.72 * 10^{-4}$	39.799	<0.001	$-2.55 * 10^{-3}$	194.548	<0.001
Nitrogen (N)	1	$-2.35 * 10^{-4}$	21.948	<0.001	$1.55 * 10^{-4}$	70.771	<0.001	$2.52 * 10^{-4}$	19.458	<0.001
L*N	1	$-2.89 * 10^{-6}$	1.262	0.261	$-6.32 * 10^{-7}$	1.435	0.231	$-3.16 * 10^{-6}$	10.803	0.001

16

343 *Significance determined using Wald's χ^2 tests ($p=0.05$). P -values less than 0.05 are in bold and p -values between
 344 0.05 and 0.1 are italicized. Negative coefficients for light treatments indicate a positive effect of increasing light
 345 availability on all response variables, as light availability is treated as percent shade cover in all linear mixed-effects
 346 models.

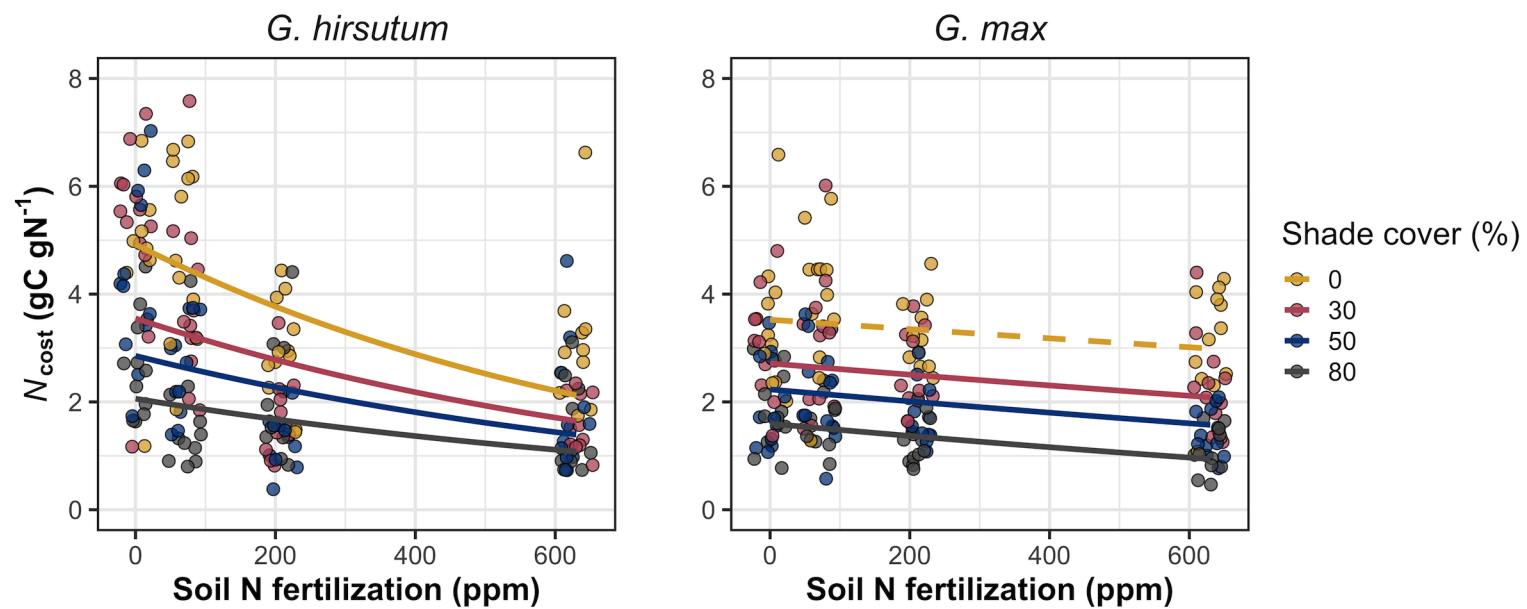


Figure 2.1. Relationships between soil nutrient fertilization and light availability on carbon costs to acquire nitrogen in *G. hirsutum* and *G. max*. Nitrogen fertilization treatments are represented on the x-axis. Shade cover treatments are represented through colored points and trendlines. Trendlines were created by back-transforming marginal mean slopes and intercepts from species-specific linear mixed-effects models. These values were calculated using the ‘emtrends’ and ‘emmeans’ functions in the ‘emmeans’ R package (Lenth 2019). Yellow points and trendlines represent the 0% shade cover treatment, red points and trendlines represent the 30% shade cover treatment, blue points and trendlines represent the 50% shade cover treatment, and gray points and trendlines represent the 80% shade cover treatment. Solid trendlines indicate slopes that are significantly different from zero (Tukey: $p < 0.05$), while dashed trendlines indicate slopes that are not statistically different from zero.

347 2.3.2 *Whole plant nitrogen biomass*

348 Whole plant nitrogen biomass in *G. hirsutum* was driven by an interaction between
349 light availability and nitrogen fertilization ($p=0.001$; Table 2.1; Fig. 2.2). This
350 interaction indicated a greater stimulation of whole-plant nitrogen biomass by
351 nitrogen fertilization as light levels increased (Table 2.1; Fig. 2.2).

352 Whole plant nitrogen biomass in *G. max* increased with increasing light
353 availability ($p<0.001$) and nitrogen fertilization ($p<0.001$), with no interaction
354 between light availability and nitrogen fertilization ($p=0.231$; Table 2.1; Fig. 2.2).

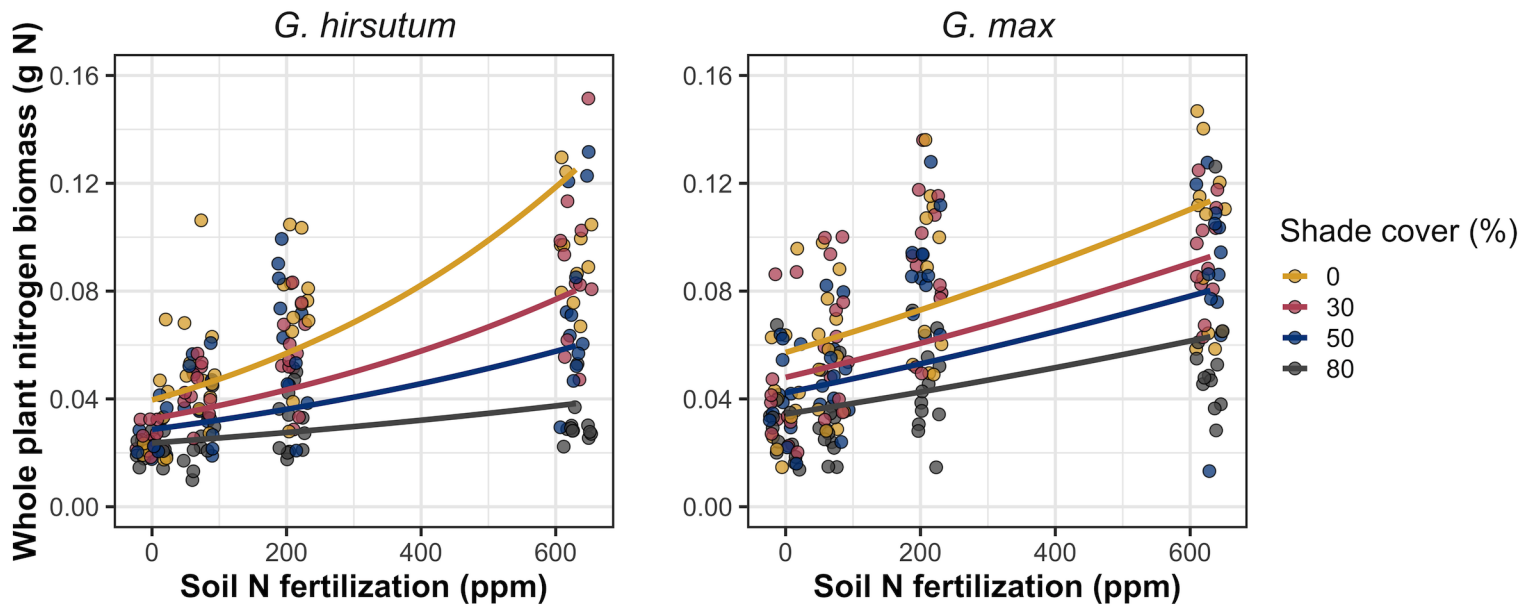


Figure 2.2. Relationships between soil nutrient fertilization and light availability on whole-plant nitrogen biomass in *G. hirsutum* and *G. max*. Whole-plant nitrogen biomass is the denominator of the carbon cost to acquire nitrogen calculation. Nitrogen fertilization treatments are represented on the x-axis. Shade cover treatments are represented through colored points and trendlines. Trendlines were created by back-transforming marginal mean slopes and intercepts from species-specific linear mixed-effects models. These values were calculated using the ‘emtrends’ and ‘emmeans’ functions in the ‘emmeans’ R package (Lenth 2019). Points are jittered for visibility. Colored points and trendlines are as explained in Fig. 2.1. Solid trendlines indicate slopes that are significantly different from zero (Tukey: $p < 0.05$), while dashed trendlines indicate slopes that are not statistically different from zero.

355 2.3.3 *Root carbon biomass*

356 Root carbon biomass in *G. hirsutum* significantly increased with increasing light
357 availability ($p<0.001$; Table 2.1; Fig. 2.3) and marginally increased with nitrogen
358 fertilization ($p=0.089$; Table 2.1; Fig. 2.3). There was also a marginal interaction
359 between light availability and nitrogen fertilization ($p=0.076$; Table 2.1), driven by
360 an increase in the positive response of root carbon biomass to increasing nitrogen
361 fertilization as light availability increased (Table 2.3). This pattern resulted in
362 significantly positive trends between root carbon biomass and nitrogen fertilization
363 in the two highest light treatments (Tukey: $p<0.05$ in both cases; Table 2.3;
364 Fig. 2.3) and no effect of nitrogen fertilization in the two lowest light treatments
365 (Tukey: $p>0.05$ in both cases; Table 2.3; Fig. 2.3).

366 There was an interaction between light availability and nitrogen fertiliza-
367 tion on root carbon biomass in *G. max* ($p=0.001$; Table 2.1; Fig. 2.3). Post-hoc
368 analyses indicated that the positive effects of nitrogen fertilization on *G. max*
369 root carbon biomass increased with increasing light availability (Table 2.3; Fig.
370 2.3). There were also positive individual effects of increasing nitrogen fertilization
371 ($p<0.001$; Table 2.3) and light availability ($p<0.001$; Table 2.3) on *G. max* root
372 carbon biomass (Table 2.1; Fig. 2.3).

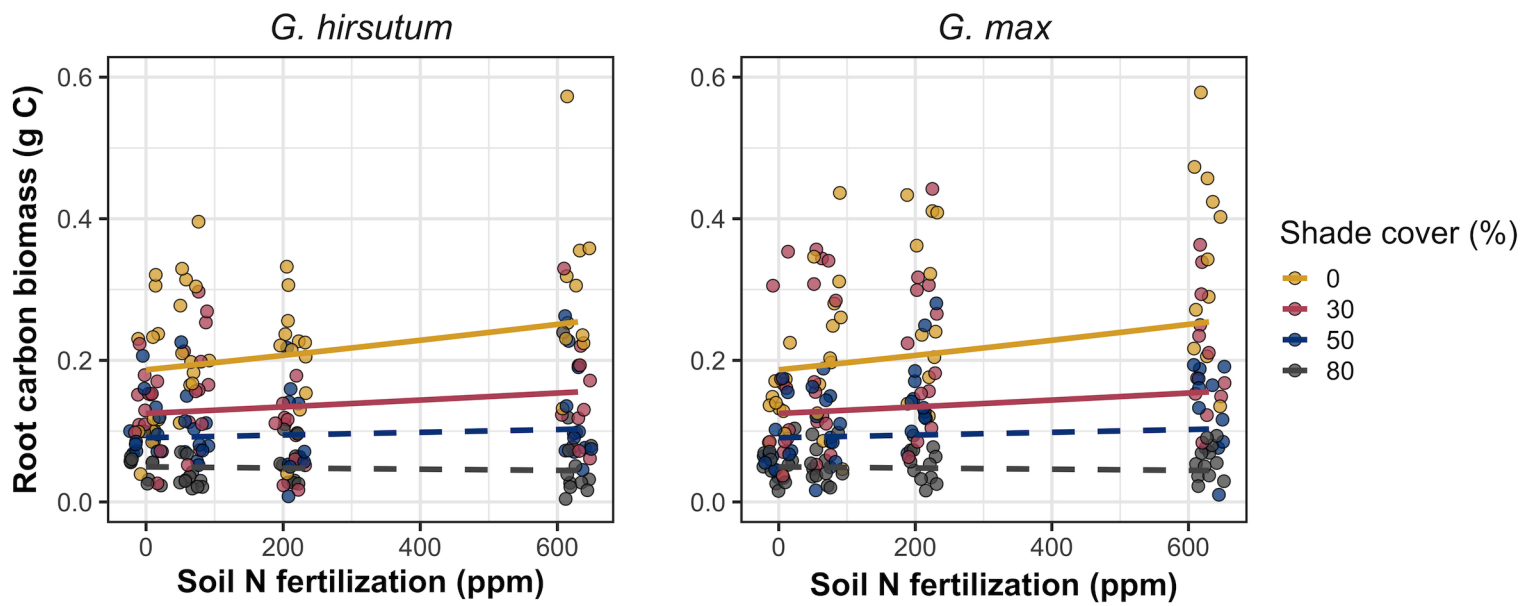


Figure 2.3. Relationships between soil nutrient fertilization and light availability on root carbon biomass in *G. hirsutum* and *G. max*. Root carbon biomass is the numerator of the carbon cost to acquire nitrogen calculation. Nitrogen fertilization treatments are represented on the x-axis. Colored points and trendlines are as explained in Fig. 2.1. Trendlines were created by back-transforming marginal mean slopes and intercepts from species-specific linear mixed-effects models. These values were calculated using the ‘emtrends’ and ‘emmeans’ functions in the ‘emmeans’ R package (Lenth 2019). Points are jittered for visibility. Colored points and trendlines are as explained in Fig. 2.1.

373 2.3.4 *Root nodule biomass*

374 Root nodule biomass in *G. max* increased with increasing light availability ($p <$
375 0.001; Table 2.2; Fig. 2.4a) and decreased with increasing nitrogen fertilization
376 ($p < 0.001$; Table 2.2; Fig. 2.4a). There was no interaction between nitrogen
377 fertilization and light availability ($p = 0.133$; Table 2.2; Fig. 2.4a). The ratio of
378 root nodule biomass to root biomass did not change in response to light availability
379 ($p = 0.481$; Table 2.2; Fig. 2.4b) but decreased with increasing nitrogen fertilization
380 ($p < 0.001$; Table 2.2; Fig. 2.4b). There was no interaction between nitrogen
381 fertilization and light availability on the ratio of root nodule biomass to root
382 biomass ($p = 0.621$; Table 2.2; Fig. 2.4b).

Table 2.2. Analysis of variance results exploring effects of light availability, nitrogen fertilization, and their interactions on *G. max* root nodule biomass (g) and the ratio of root nodule biomass to root biomass (g g⁻¹)*

	Nodule biomass			Nodule biomass: root biomass			<i>p</i>
	df	Coefficient	χ^2	<i>p</i>	Coefficient	χ^2	
(Intercept)		$3.02 * 10^{-1}$	-	-	$4.48 * 10^{-1}$	-	-
Light (L)	1	$-1.81 * 10^{-3}$	72.964	<0.001	$-8.76 * 10^{-5}$	0.496	0.481
Nitrogen (N)	1	$-2.83 * 10^{-4}$	115.377	<0.001	$-5.09 * 10^{-4}$	156.476	<0.001
L*N	1	$1.14 * 10^{-6}$	2.226	0.133	$-7.30 * 10^{-7}$	0.244	0.621

383 *Significance determined using Wald's χ^2 tests ($\alpha=0.05$). *P*-values less than 0.05 are in bold. Negative coefficients for
 384 light treatments indicate a positive effect of increasing light availability on all response variables, as light availability
 385 is treated as percent shade cover in all linear mixed-effects models. Root nodule biomass and nodule biomass: root
 386 biomass models were only constructed for *G. max* because *G. hirsutum* was not inoculated with *B. japonicum* and
 387 is not capable of forming root nodules.

Table 2.3. Slopes of the regression line describing the relationship between each dependent variable and nitrogen fertilization at each light level*

Shade cover	Carbon cost to acquire nitrogen	Whole plant nitrogen biomass	Belowground carbon biomass	Root nodule biomass	Nodule biomass: root biomass
<i>G. hirsutum</i>					
0%	$-1.34 * 10^{-3a}$	$1.83 * 10^{-3a}$	$1.15 * 10^{-4b}$	-	-
30%	$-1.22 * 10^{-3a}$	$1.43 * 10^{-3a}$	$1.17 * 10^{-4b}$	-	-
50%	$-1.14 * 10^{-3a}$	$1.17 * 10^{-3a}$	$3.12 * 10^{-5b}$	-	-
80%	$-1.02 * 10^{-3a}$	$7.66 * 10^{-4a}$	$-1.89 * 10^{-6b}$	-	-
<i>G. max</i>					
0%	$-2.35 * 10^{-4b}$	$1.55 * 10^{-5b}$	$2.51 * 10^{-4b}$	$-2.83 * 10^{-4b}$	$-5.09 * 10^{-4b}$
30%	$-3.22 * 10^{-4b}$	$1.35 * 10^{-5b}$	$1.57 * 10^{-4b}$	$-2.49 * 10^{-4b}$	$-5.31 * 10^{-4b}$
50%	$-3.80 * 10^{-4b}$	$1.23 * 10^{-5b}$	$9.37 * 10^{-5b}$	$-2.26 * 10^{-4b}$	$-5.45 * 10^{-4b}$
80%	$-4.66 * 10^{-4b}$	$1.04 * 10^{-5b}$	$-9.95 * 10^{-7b}$	$-1.92 * 10^{-4b}$	$-5.67 * 10^{-4b}$

* Slopes represent estimated marginal mean slopes from linear mixed-effects models described in the Methods. Slopes were calculated using the ‘emmeans’ R package (Lenth 2019). Superscripts indicate slopes fit to natural-log (^a) or square root (^b) transformed data. Slopes statistically different from zero (Tukey: $p < 0.05$) are indicated in bold. Marginally significant slopes (Tukey: $0.05 < p < 0.1$) are italicized.

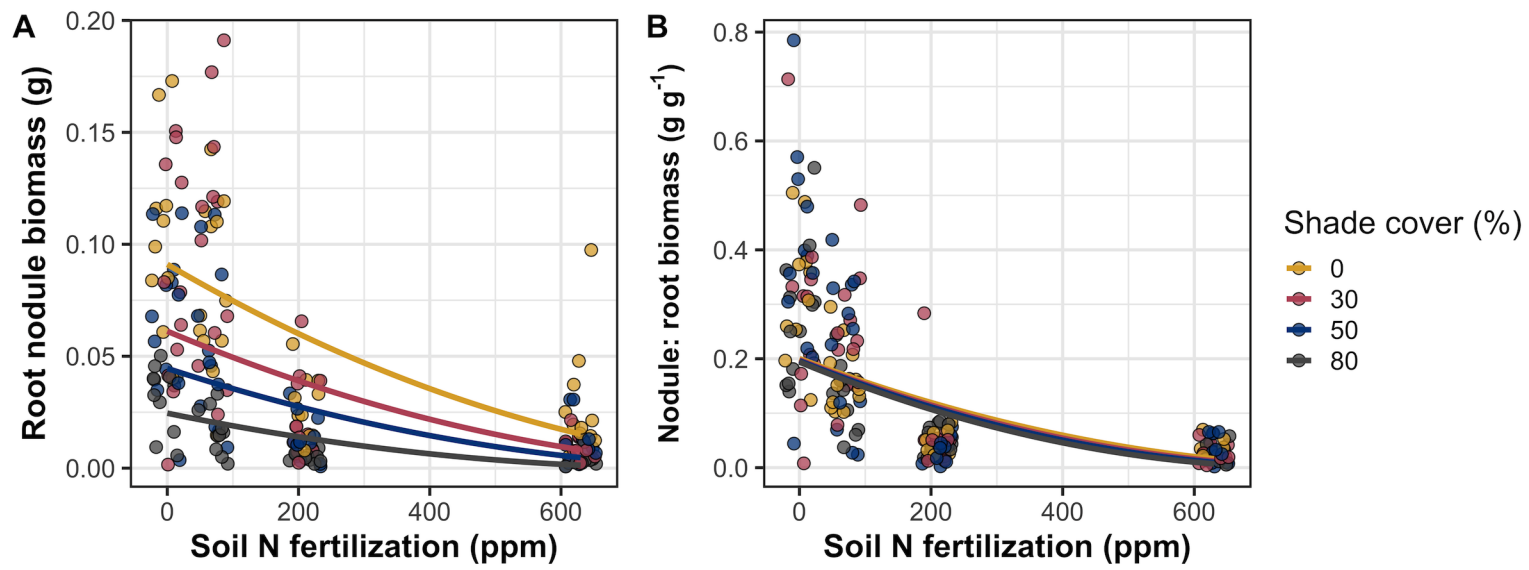


Figure 2.4. Effects of shade cover and nitrogen fertilization on root nodule biomass (a) and the ratio of root nodule biomass to root biomass (b) in *G. max*. Nitrogen fertilization treatments are represented on the x-axis. Shade cover treatments are represented through colored points and trendlines. Trendlines were created by back-transforming marginal mean slopes and intercepts from species-specific linear mixed-effects models. These values were calculated using the ‘emtrends’ and ‘emmeans’ functions in the ‘emmeans’ R package (Lenth 2019). Points are jittered for visibility. Yellow points and trendlines represent the 0% shade cover treatment, blue points and trendlines represent the 30% shade cover treatment, green points and trendlines represent the 50% shade cover treatment, and purple points and trendlines represent the 80% shade cover treatment. Solid trendlines indicate slopes that are significantly different from zero (Tukey: $p < 0.05$), while dashed trendlines indicate slopes that are not statistically different from zero.

392 2.4 Discussion

393 In this chapter, I determined the effects of light availability and soil nitrogen
394 fertilization on root mass carbon costs to acquire nitrogen in *G. hirsutum* and *G.*
395 *max*. In support of my hypotheses, I found that carbon costs to acquire nitrogen
396 generally increased with increasing light availability and decreased with increasing
397 soil nitrogen fertilization in both species. These findings suggest that carbon costs
398 to acquire nitrogen are determined by factors that influence plant nitrogen demand
399 and soil nitrogen availability. In contrast to my second hypothesis, root nodulation
400 data suggested that *G. max* and *G. hirsutum* achieved similar directional carbon
401 cost responses to nitrogen fertilization despite a likely shift in *G. max* allocation
402 from nodulation to root biomass along the nitrogen fertilization gradient.

403 2.4.1 *Carbon costs to acquire nitrogen increase with light availability and*
404 *decrease with fertilization*

405 Both *G. max* and *G. hirsutum* experienced an increase in carbon costs to ac-
406 quire nitrogen due to increasing light availability. These patterns were driven by
407 a larger increase in root carbon biomass than whole-plant nitrogen biomass. In-
408 creases in root carbon biomass due to factors that increase plant nitrogen demand
409 are a commonly observed pattern, as carbon allocated belowground provides sub-
410 strate needed to produce and maintain structures that satisfy aboveground plant
411 nitrogen demand (Nadelhoffer and Raich 1992; Giardina et al. 2005; Raich et al.
412 2014). Findings suggest that plants allocate relatively more carbon for acquiring
413 nitrogen when demand increases over short temporal scales, which may cause a
414 temporary state of diminishing return due to asynchrony between belowground

415 carbon and whole-plant nitrogen responses to plant nitrogen demand (Kulmatiski
416 et al. 2017; Noyce et al. 2019). These responses might be attributed to a temporal
417 lag associated with producing structures that enhance nitrogen acquisition. For
418 example, fine roots (Matamala and Schlesinger 2000; Norby et al. 2004; Arndal
419 et al. 2018) and root nodules (Parvin et al. 2020) take time to build and first
420 require the construction of coarse roots. Thus, full nitrogen returns from these
421 investments may not occur immediately (Kayler et al. 2010; Kayler et al. 2017),
422 and may vary by species acquisition strategy. I speculate that increases in ni-
423 trogen acquisition from a given carbon investment may occur beyond the 5-week
424 scope of this experiment. A similar study conducted over a longer temporal scale
425 would address this.

426 Increasing soil nitrogen fertilization generally decreased carbon costs to
427 acquire nitrogen in both species. These patterns were driven by a larger increase
428 in whole-plant nitrogen biomass than root carbon biomass. In *G. hirsutum*, re-
429 ductions in carbon costs to acquire nitrogen may have been due to an increase in
430 per-root nitrogen uptake, allowing individuals to maximize the amount of nitro-
431 gen acquired from a belowground carbon investment. Interestingly, increased soil
432 nitrogen fertilization increased whole-plant nitrogen biomass in *G. max* despite
433 reductions in root nodule biomass that likely reduced the nitrogen-fixing capac-
434 ity of *G. max* (Andersen et al. 2005; Muñoz et al. 2016). While reductions in
435 root nodulation due to increased soil nitrogen availability are commonly observed
436 (Gibson and Harper 1985; Fujikake et al. 2003), root nodulation responses were
437 observed in tandem with increased root carbon biomass, implying that *G. max*
438 shifted relative carbon allocation from nitrogen fixation to soil nitrogen acquisition

439 (Markham and Zekveld 2007; Dovrat et al. 2020). This was likely because there
440 was a reduction in the carbon cost advantage of acquiring fixed nitrogen relative
441 to soil nitrogen, and suggests that species capable of associating with symbiotic
442 nitrogen-fixing bacteria shift their relative nitrogen acquisition pathway to opti-
443 mize nitrogen uptake (Rastetter et al. 2001). Future studies should investigate
444 these patterns with a larger quantity of phylogenetically related species, or differ-
445 ent varieties of a single species that differ in their ability to form associations with
446 symbiotic nitrogen-fixing bacteria to more directly test the impact of nitrogen
447 fixation on the patterns observed in this study.

448 2.4.2 *Modeling implications*

449 Carbon costs to acquire nitrogen are subsumed in the general discussion of eco-
450 nomic analogies to plant resource uptake (Bloom et al. 1985; Rastetter et al.
451 2001; Vitousek et al. 2002; Phillips et al. 2013; Terrer et al. 2018; Henneron et al.
452 2020). Despite this, terrestrial biosphere models rarely include costs of nitrogen
453 acquisition to predict plant nitrogen uptake. There is currently one plant resource
454 uptake model, the Fixation and Uptake of Nitrogen model (FUN), that quantita-
455 tively predicts carbon costs to acquire nitrogen within a framework for predicting
456 plant nitrogen uptake for different nitrogen acquisition strategies (Fisher et al.
457 2010; Brzostek et al. 2014). Iterations of FUN are currently coupled to two ter-
458 restrial biosphere models: the Community Land Model 5.0 and the Joint UK Land
459 Environment Simulator (Clark et al. 2011; Shi et al. 2016; Lawrence et al. 2019).
460 Recent work suggests that coupling FUN to CLM 5.0 caused a large overpredic-
461 tion of plant nitrogen uptake associated with nitrogen fixation (Davies-Barnard

462 et al. 2020) compared to other terrestrial biosphere model products. Thus, em-
463 pirical data from manipulative experiments that explicitly quantify carbon costs
464 to acquire nitrogen in species capable of associating with nitrogen-fixing bacteria
465 across different environmental contexts is an important step toward identifying
466 potential biases in models such as FUN.

467 These findings support the FUN formulation of carbon costs to acquire
468 nitrogen in response to soil nitrogen availability. FUN calculates carbon costs
469 to acquire nitrogen based on the sum of carbon costs to acquire nitrogen via ni-
470 trogen fixation, mycorrhizal active uptake, non-mycorrhizal active uptake, and
471 retranslocation (Fisher et al. 2010; Brzostek et al. 2014). Carbon costs to acquire
472 nitrogen via mycorrhizal or non-mycorrhizal active uptake pathways are derived
473 as a function of nitrogen availability, root biomass, and two parameterized values
474 based on nitrogen acquisition strategy (Brzostek et al. 2014). Due to this, FUN
475 simulates a net decrease in carbon costs to acquire nitrogen with increasing ni-
476 trogen availability for mycorrhizal and non-mycorrhizal active uptake pathways,
477 assuming constant root biomass. This was a pattern I observed in *G. hirsutum* re-
478 gardless of light availability. In contrast, FUN would not simulate a net change in
479 carbon costs to acquire nitrogen via nitrogen fixation due to nitrogen availability.
480 This is because carbon costs to acquire nitrogen via nitrogen fixation are derived
481 from a well established function of soil temperature, which is independent of soil
482 nitrogen availability (Houlton et al. 2008; Fisher et al. 2010). I observed a net
483 reduction in carbon costs to acquire nitrogen in *G. max*, except when individu-
484 als were grown under 0% shade cover. While a net reduction of carbon costs in
485 response to nitrogen fertilization runs counter to nitrogen fixation carbon costs

486 simulated by FUN, these patterns were likely because *G. max* individuals switched
487 their primary mode of nitrogen acquisition from symbiotic nitrogen fixation to a
488 non-symbiotic active uptake pathway.

489 2.4.3 *Study limitations*

490 The metric used in this study to determine carbon costs to acquire nitrogen has
491 several limitations. Most notably, this metric uses root carbon biomass as a proxy
492 for estimating the amount of carbon spent on nitrogen acquisition. Although it is
493 true that most carbon allocated belowground has at least an indirect structural
494 role in acquiring soil resources, it remains unclear whether this assumption holds
495 true for species that acquire nitrogen via symbiotic nitrogen fixation. I also cannot
496 quantify carbon lost through root exudates or root turnover, which may increase
497 due to factors that increase plant nitrogen demand (Tingey et al. 2000; Phillips
498 et al. 2011), and can increase the magnitude of available nitrogen from soil organic
499 matter through priming effects on soil microbial communities (Uselman et al.
500 2000; Bengtson et al. 2012). It is also not clear whether these assumptions
501 hold under all environmental conditions, such as those that shift belowground
502 carbon allocation toward a different mode of nitrogen acquisition (Taylor and
503 Menge 2018; Friel and Friesen 2019) or between species with different acquisition
504 strategies. In this study, increasing soil nitrogen fertilization increased carbon
505 investment to roots relative to carbon transferred to root nodules. By assuming
506 that carbon allocated to root carbon was proportional to carbon allocated to
507 root nodules across all treatment combinations, these observed responses to soil
508 nitrogen fertilization were likely to be overestimated in *G. max*. I encourage future

509 research to quantify these carbon fates independently.

510 Carbon costs to acquire nitrogen decreased with increasing fertilization
511 more strongly in *G. hirsutum* than *G. max*, a pattern that may have been driven
512 by decreased investment to symbiotic nitrogen-fixing bacteria with increasing fer-
513 tilization in *G. max*. However, species differed by more than just acquisition
514 strategy, as *G. hirsutum* is a woody perennial species and *G. max* is a herba-
515 ceous annual species. Therefore, assigning causality to the stronger reduction
516 in costs of nitrogen acquisition in *G. hirsutum* is a challenge, and only provides
517 anecdotal evidence that such patterns are generalizable across species. As previ-
518 ously mentioned, future experiments should attempt to measure such responses
519 across a wider range of phylogenetically similar species or in a single species while
520 explicitly controlling the source of nitrogen uptake.

521 Researchers conducting pot experiments must carefully choose pot volume
522 to minimize the likelihood of growth limitations induced by pot volume (Poorter
523 et al. 2012). Poorter et al. (2012) indicate that researchers are likely to avoid
524 growth limitations associated with pot volume if measurements are collected when
525 the plant biomass:pot volume ratio is less than 1 g L^{-1} . In this experiment, all
526 treatment combinations in both species had biomass:pot volume ratios less than
527 1 g L^{-1} except for *G. max* and *G. hirsutum* that were grown under 0% shade
528 cover and had received 630 ppm N. Specifically, *G. max* and *G. hirsutum* had
529 average respective biomass:pot volume ratios of $1.24 \pm 0.07 \text{ g L}^{-1}$ and 1.34 ± 0.13
530 g L^{-1} , when grown under 0% shade cover and received 630 ppm N (Table A2,
531 A3; Fig. A1). If growth in this treatment combination was limited by pot vol-
532 ume, then individuals may have had larger carbon costs to acquire nitrogen than

533 would be expected if they were grown in larger pots. This pot volume induced
534 growth limitation could cause a reduction in per-root nitrogen uptake associated
535 with more densely packed roots, which could reduce the positive effect of nitro-
536 gen fertilization on whole-plant nitrogen biomass relative to root carbon biomass
537 (Poorter et al. 2012).

538 Pot size may have limited plant growth, which provides a possible expla-
539 nation for the marginally insignificant effect of increasing nitrogen fertilization on
540 *G. max* carbon costs to acquire nitrogen when grown under 0% shade cover. This
541 is because the regression line describing the relationship between carbon costs to
542 acquire nitrogen and nitrogen fertilization in *G. max* grown under 0% shade cover
543 would have flattened if growth limitation had caused larger than expected carbon
544 costs to acquire nitrogen in the 0% shade cover, 630 ppm N treatment combi-
545 nation. This may have been exacerbated by the fact that *G. max* likely shifted
546 relative carbon allocation from nitrogen fixation to soil nitrogen acquisition, which
547 could have increased the negative effect of more densely packed roots on nitrogen
548 uptake. These patterns could have also occurred in *G. hirsutum* grown under 0%
549 shade cover; however, there was no change in the effect of nitrogen fertilization on
550 *G. hirsutum* carbon costs to acquire nitrogen grown under 0% shade cover relative
551 to other shade cover treatments. Regardless, the possibility of growth limitation
552 due to pot volume suggests that effects of increasing nitrogen fertilization on car-
553 bon costs to acquire nitrogen in both species grown under 0% shade cover could
554 have been underestimated. Follow-up studies using a similar experimental design
555 with a larger pot volume would be necessary in order to determine whether these
556 patterns were impacted by pot volume-induced growth limitation.

557 2.4.4 *Conclusions*

558 In conclusion, this chapter provides empirical evidence that carbon costs to ac-
559 quire nitrogen are influenced by light availability and soil nitrogen fertilization
560 in a species capable of acquiring nitrogen via symbiotic nitrogen fixation and a
561 species not capable of forming such associations. We show that carbon costs to
562 acquire nitrogen generally increase with increasing light availability and decrease
563 with increasing nitrogen fertilization. This chapter provides important empirical
564 data needed to evaluate the formulation of carbon costs to acquire nitrogen in
565 terrestrial biosphere models, particularly carbon costs to acquire nitrogen that
566 are associated with symbiotic nitrogen fixation. Findings broadly support the
567 general formulation of these carbon costs in the FUN biogeochemical model in
568 response to shifts in nitrogen availability. However, there is a need for future
569 studies to explicitly quantify carbon costs to acquire nitrogen under different en-
570 vironmental contexts, over longer temporal scales, and using larger selections of
571 phylogenetically related species. In addition, I suggest that future studies mini-
572 mize the limitations associated with the metric used here by explicitly measuring
573 belowground carbon fates independently.

574

Chapter 3

575 Soil nitrogen availability modifies leaf nitrogen economies in mature
576 temperate deciduous forests: a direct test of photosynthetic least-cost
577 theory

578 3.1 Introduction

579 Photosynthesis represents the largest carbon flux between the atmosphere and
580 land surface (IPCC 2021), and plays a central role in biogeochemical cycling at
581 multiple spatial and temporal scales (Vitousek and Howarth 1991; LeBauer and
582 Treseder 2008; Kaiser et al. 2015; Wieder et al. 2015). Therefore, carbon and
583 energy fluxes simulated by terrestrial biosphere models are sensitive to the formu-
584 lation of photosynthetic processes (Ziehn et al. 2011; Bonan et al. 2011; Booth
585 et al. 2012; Smith et al. 2016; Smith et al. 2017) and must be represented using
586 robust, empirically tested processes (Prentice et al. 2015; Wieder et al. 2019).
587 Current formulations of photosynthesis vary across terrestrial biosphere models
588 (Smith and Dukes 2013; Rogers et al. 2017), which causes variation in modeled
589 ecosystem processes (Knorr 2000; Knorr and Heimann 2001; Bonan et al. 2011;
590 Friedlingstein et al. 2014) and casts uncertainty on the ability of these models to
591 accurately predict terrestrial ecosystem responses and feedbacks to global change
592 (Zaehle et al. 2005; Schaefer et al. 2012; Davies-Barnard et al. 2020).

593 Terrestrial biosphere models commonly represent C₃ photosynthesis thr-
594 ough variants of the Farquhar et al. (1980) biochemical model (Smith and Dukes
595 2013; Rogers 2014; Rogers et al. 2017). This well-tested photosynthesis model
596 estimates leaf-level carbon assimilation, or photosynthetic capacity, as a function
597 of the maximum rate of Ribulose-1,5-bisphosphate carboxylase-oxygenase (Ru-

598 bisco) carboxylation (V_{cmax}) and the maximum rate of Ribulose-1,5-bisphosphate
599 (RuBP) regeneration (J_{max}) (Farquhar et al. 1980). Many terrestrial biosphere
600 models predict these model inputs through plant functional group specific linear
601 relationships between leaf nutrient content and V_{cmax} (Smith and Dukes 2013;
602 Rogers 2014; Rogers et al. 2017) under the tenet that a large fraction of leaf nu-
603 trients, and nitrogen in particular, are partitioned toward building and maintain-
604 ing enzymes that support photosynthetic capacity, such as Rubisco (Brix 1971;
605 Gulmon and Chu 1981; Evans 1989; Kattge et al. 2009; Walker et al. 2014).
606 Terrestrial biosphere models predict leaf nutrient content from soil nutrient avail-
607 ability based on the assumption that increasing soil nutrients generally increases
608 leaf nutrients (Firn et al. 2019; Li et al. 2020; Liang et al. 2020) which, in the
609 case of nitrogen, often corresponds with an increase in photosynthetic processes
610 (Li et al. 2020; Liang et al. 2020).

611 Recent work calls the generality of relationships between soil nutrient avail-
612 ability, leaf nutrient content, and photosynthetic capacity into question, suggest-
613 ing instead that leaf nutrients and photosynthetic capacity are better predicted as
614 an integrated product of aboveground climate, leaf traits, and soil nutrient avail-
615 ability, rather than soil nutrient availability alone (Dong et al. 2017; Dong et al.
616 2020; Dong et al. 2022; Firn et al. 2019; Smith et al. 2019; Peng et al. 2021).
617 It has been reasoned that this result is because plants allocate added nutrients to
618 growth and storage rather than alterations in leaf chemistry (Smith et al. 2019),
619 perhaps as a result of nutrient limitation of primary productivity (LeBauer and
620 Treseder 2008; Fay et al. 2015). Additionally, recent work suggests that relation-
621 ships between leaf nutrient content and photosynthesis vary across environments,

622 and that the proportion of leaf nutrient content allocated to photosynthetic tis-
623 sue varies over space and time with plant acclimation and adaptation responses
624 to light availability, vapor pressure deficit, soil pH, soil nutrient availability, and
625 environmental factors that influence leaf mass per area (Pons and Pearcy 1994;
626 Niinemets and Tenhunen 1997; Evans and Poorter 2001; Hikosaka and Shigeno
627 2009; Ghimire et al. 2017; Onoda et al. 2017; Luo et al. 2021). The use of linear
628 relationships between leaf nutrient content and V_{cmax} to predict photosynthetic
629 capacity, as commonly used in terrestrial biosphere models (Rogers 2014), is not
630 capable of detecting such responses.

631 Photosynthetic least-cost theory provides an alternative framework for un-
632 derstanding relationships between soil nutrient availability, leaf nutrient content,
633 and photosynthetic capacity (Harrison et al. 2021). Using a two-input microeco-
634 nomics approach (Wright et al. 2003), the theory posits that plants acclimate to a
635 given environment by optimizing leaf photosynthesis rates at the lowest summed
636 cost of using nutrients and water (Prentice et al. 2014; Wang et al. 2017; Smith
637 et al. 2019; Paillassa et al. 2020). Across resource availability gradients, the
638 theory predicts that optimal photosynthetic rates can be achieved by trading less
639 efficient use of a more abundant (or less costly) resource to acquire for more ef-
640 ficient use of a less abundant (or more costly) resource to acquire. For example,
641 an increase in soil nutrient availability should reduce the cost of acquiring and
642 using nutrients (Bae et al. 2015; Eastman et al. 2021; Perkowski et al. 2021),
643 which could increase leaf nutrient investments in photosynthetic proteins to allow
644 similar photosynthetic rates to be achieved with greater nutrient use (reduced
645 nutrient use efficiency) and reduced water use (greater water use efficiency). The

646 theory suggests similar tradeoffs in response to increasing soil pH (Paillassa et al.
647 2020), specifically, that increasing soil pH should reduce the cost of acquiring soil
648 nutrients due to an increase in plant-available nutrient concentration (Paillassa
649 et al. 2020; Dong et al. 2022). The theory is also capable of reconciling dynamic
650 leaf nutrient-photosynthesis relationships at global scales (Luo et al. 2021).

651 Patterns expected from photosynthetic least-cost theory have recently re-
652 ceived empirical support both in global environmental gradient (Smith et al.
653 2019; Paillassa et al. 2020; Luo et al. 2021; Querejeta et al. 2022; Westerband
654 et al. 2023) and local manipulative invasion (Bialic-Murphy et al. 2021) stud-
655 ies. However, nutrient addition experiments that directly examine nutrient-water
656 use tradeoffs expected from the theory are rare (but see Guerrieri et al. 2011),
657 and only global gradient studies testing the theory have considered soil pH in
658 their analyses. Therefore, empirical data collected from nutrient addition and soil
659 pH manipulation experiments are critical to test mechanisms driving responses
660 predicted by the theory.

661 In this study, I measured leaf responses to soil nitrogen availability in five
662 deciduous tree species growing in the upper canopy of mature closed canopy tem-
663 perate forests in the northeastern United States. Soil nitrogen availability and
664 pH were manipulated through a nitrogen-by-pH field manipulation experiment
665 with treatments applied since 2011, eight years prior to measurement. Two dif-
666 ferent soil nitrogen treatments were applied to increase nitrogen availability with
667 opposing effects on soil pH. An additional nitrogen-free acidifying treatment was
668 applied to decrease soil pH. I hypothesized that increased soil nitrogen availabil-
669 ity would enable plants to create more photosynthetic enzymes per leaf, allowing

670 similar photosynthetic rates achieved with reduced leaf C_i:C_a and increased leaf
671 nitrogen content allocated to photosynthetic leaf tissue. I expected that this re-
672 sponse would be driven by a reduction in the cost of acquiring nitrogen, which
673 would cause trees to sacrifice efficient nitrogen use to enable more efficient use of
674 other limiting resources (i.e., water). Finally, I hypothesized similar leaf responses
675 to increasing soil pH.

676 3.2 Methods

677 3.2.1 *Study site description*

678 I conducted this study in summer 2019 at three stands located within a 20-km ra-
679 dius of Ithaca, NY, USA (42.444 °N, 76.502 °W). All stands contain mature,
680 closed-canopy forests dominated by deciduous tree species. Stands contained
681 abundant sugar maple (*Acer saccharum* Marshall), American beech (*Fagus gran-*
682 *difolia* Ehrh.), and white ash (*Fraxinus americana* L.), accounting for 43%, 15%,
683 and 17% of the total aboveground biomass across the three stands, respectively,
684 with less frequent red maple (*Acer rubrum* L.; 9% of total aboveground biomass)
685 and red oak occurrences (*Quercus rubra* L.; 10% of total aboveground biomass).
686 Soils at each site were broadly classified as a channery silt loam Inceptisols using
687 the USDA NRCS Web Soil Survey data product (Soil Survey Staff 2022). Between
688 2006 and 2020, study sites averaged 972 mm of precipitation per year and had an
689 average temperature of 7.9 °C per a weather station located near the Cornell Uni-
690 versity campus (42.449 °N, 76.449 °W) part of the NOAA NCEI Global Historical
691 Climatology Network (Menne et al. 2012).

692 3.2.2 *Experimental design*

693 Four 40 m x 40 m plots were set up at each site in 2009, each with an additional
694 10 m buffer along plot perimeters (60 m x 60 m total). The plots were set up as a
695 nitrogen-by-pH field manipulation experiment, with one each of four treatments at
696 each site. Two nitrogen treatments were applied, both at 50 kg N ha⁻¹ yr⁻¹, as ei-
697 ther sodium nitrate (NaNO₃) to raise soil pH, or ammonium sulfate ((NH₄)₂SO₄)
698 to acidify; an elemental sulfur treatment was selected to acidify without nitro-
699 gen, applied at the same rate of S addition from the ammonium sulfate plot (57
700 kg S ha⁻¹ yr⁻¹); and control plots received no additions. All amendments were
701 added in pelletized form using hand-held fertilizer spreaders to both the main
702 plots and buffers. Amendments were divided into three equal doses distributed
703 across the growing season from 2011-2017 and added as a single dose from 2018
704 onward. During 2019, plots were fertilized during the week of May 20.

705 3.2.3 *Leaf gas exchange and trait measurements*

706 I sampled one leaf each from 6 to 10 individuals per plot between June 25 and
707 July 12, 2019 for gas exchange measurements (Table B1), between one and two
708 months after fertilization. Leaves were collected from deciduous broadleaf trees
709 represented across all sites and plots and were replicated in efforts to mimic the
710 species abundance of each plot at each site. I attempted to collect leaves from
711 the upper canopy to reduce differential shading effects on leaf physiology. Leaves
712 were accessed by pulling down small branches using an arborist's slingshot and
713 weighted beanbag attached to a throw line. Branches were immediately recut
714 under deionized water and remained submerged to reduce stomatal closure and

715 avoid xylem embolism, as done in Smith and Dukes (2018), until gas exchange
716 data were collected.

717 Randomly selected leaves with little to no visible external damage were
718 attached to a Li-COR LI-6800 (Li-COR Bioscience, Lincoln, Nebraska, USA)
719 portable photosynthesis machine to measure net photosynthesis (A_{net} ; $\mu\text{mol m}^{-2}$
720 s^{-1}), stomatal conductance (g_{sw} ; $\text{mol m}^{-2} \text{s}^{-1}$), and intercellular CO_2 concentra-
721 tion (C_i ; $\mu\text{mol mol}^{-1}$) at different reference CO_2 concentrations (C_a ; $\mu\text{mol mol}^{-1}$)
722 concentrations (i.e., an A_{net}/C_i curve) under saturating light conditions (2,000
723 $\mu\text{mol m}^{-2} \text{s}^{-1}$). Reference CO_2 concentrations followed the sequence: 400, 300,
724 200, 100, 50, 400, 400, 600, 800, 1000, 1200, 1500, and 2000 $\mu\text{mol mol}^{-1} \text{CO}_2$.
725 Leaf temperatures were not controlled in the cuvette and ranged from 21.8 °C
726 to 31.7 °C (mean±SD: 27.2±2.2 °C). A linear and second order log-polynomial
727 regression suggested no effect of temperature on stomatal conductance measured
728 at 400 $\mu\text{mol mol}^{-1} \text{CO}_2$ or net photosynthesis measured at 400 $\mu\text{mol mol}^{-1} \text{CO}_2$
729 (Table B2, B3; Fig. B1). All A_{net}/C_i curves were generated within one hour of
730 branch severance.

731 Leaf morphological and chemical traits were collected on the same leaf used
732 to generate each A_{net}/C_i curve. Images of each leaf were taken using a flat-bed
733 scanner to determine fresh leaf area using the ‘LeafArea’ R package (Katabuchi
734 2015), which automates leaf area calculations using ImageJ software (Schneider
735 et al. 2012). Each leaf was dried at 65°C for at least 48 hours, weighed, and
736 ground using a Retsch MM200 ball mill grinder (Verder Scientific, Inc., Newtown,
737 PA, USA) until homogenized. Leaf mass per unit leaf area (M_{area} , g m^{-2}) was
738 calculated as the ratio of dry leaf biomass to fresh leaf area. Using a subsample

739 of ground and homogenized leaf biomass, leaf nitrogen content (N_{mass} ; gN g⁻¹)
740 and leaf $\delta^{13}\text{C}$ (‰, relative to Vienna Pee Dee Belemnite international reference
741 standard) were measured at the Cornell Stable Isotope Lab with an elemental
742 analyzer (NC 2500, CE Instruments, Wigan, UK) interfaced to an isotope ratio
743 mass spectrometer (Delta V Isotope Ratio Mass Spectrometer, ThermoFisher Sci-
744 entific, Waltham, MA, USA). Leaf nitrogen content per unit leaf area (N_{area} ; gN
745 m⁻²) was calculated by multiplying N_{mass} by M_{area} .

746 I used leaf $\delta^{13}\text{C}$ values to estimate χ (unitless), which is an isotope-derived
747 estimate of the leaf $C_i:C_a$ ratio. While intercellular and atmospheric CO₂ concen-
748 trations were directly measured during each A_{net}/C_i curve, deriving χ from $\delta^{13}\text{C}$
749 provides a more integrative estimate of the leaf $C_i:C_a$ over an individual leaf's lifes-
750 pan and minimizes any effect of recent branch severance on our measurements. I
751 derived χ following the approach of Farquhar et al. (1989) described in Cernusak
752 et al. (2013):

$$\chi = \frac{\Delta^{13}C - a}{b - a} \quad (3.1)$$

753 where $\Delta^{13}\text{C}$ represents the relative difference between leaf $\delta^{13}\text{C}$ (‰) and air $\delta^{13}\text{C}$
754 (‰), and is calculated from the following equation:

$$\Delta^{13}C = \frac{\delta^{13}C_{\text{air}} - \delta^{13}C_{\text{leaf}}}{1 + \delta^{13}C_{\text{leaf}}} \quad (3.2)$$

755 where $\delta^{13}\text{C}_{\text{air}}$ is assumed to be -8‰ (Keeling et al. 1979; Farquhar et al. 1989), a
756 represents the fractionation between ¹²C and ¹³C due to diffusion in air, assumed
757 to be 4.4‰, and b represents the fractionation caused by Rubisco carboxylation,

758 assumed to be 27‰ (Farquhar et al. 1989).

759 3.2.4 A_{net}/C_i curve-fitting and parameter estimation

760 I fit A_{net}/C_i curves of each individual using the ‘fitaci’ function in the ‘plantecphys’ R package (Duursma 2015). This function estimates the maximum rate
761 of Rubisco carboxylation (V_{cmax} ; $\mu\text{mol m}^{-2} \text{s}^{-1}$) and maximum rate of electron
762 transport for RuBP regeneration (J_{max} ; $\mu\text{mol m}^{-2} \text{s}^{-1}$) based on the Farquhar,
763 von Caemmerer, and Berry biochemical model of C₃ photosynthesis (Farquhar
764 et al. 1980). For each curve fit, I included triose phosphate utilization (TPU)
765 limitation to avoid underestimating J_{max} (Gregory et al. 2021). Curves were
766 visually examined to confirm the likely presence of TPU limitation.

768 I determined Michaelis-Menten coefficients for Rubisco affinity to CO₂ (K_c ;
769 $\mu\text{mol mol}^{-1}$) and O₂ (K_o ; $\mu\text{mol mol}^{-1}$), and the CO₂ compensation point (Γ^* ;
770 $\mu\text{mol mol}^{-1}$) using leaf temperature and equations described in Medlyn et al.
771 (2002) and derived in Bernacchi et al. (2001). Specifically, K_c and K_o were
772 calculated as:

$$K_c = 404.9 * \exp^{\frac{79430(T_k - 298)}{298RT_k}} \quad (3.3)$$

773 and

$$K_o = 278.4 * \exp^{\frac{36380(T_k - 298)}{298RT_k}} \quad (3.4)$$

774 while Γ^* was calculated as:

$$\Gamma^* = 42.75 * \exp^{\frac{37830(T_k - 298)}{298RT_k}} \quad (3.5)$$

775 In all three equations, T_k is the leaf temperature (in Kelvin) during each A_{net}/C_i

776 curve and R is the universal gas constant ($8.314 \text{ J mol}^{-1} \text{ K}^{-1}$).

777 I standardized V_{cmax} and J_{max} estimates to 25°C using a modified Arrhe-

778 nius equation (Kattge and Knorr 2007):

$$k_{25} = \frac{k_{\text{obs}}}{e^{\frac{H_a(T_{\text{obs}} - T_{\text{ref}})}{T_{\text{ref}}RT_{\text{obs}}}} * \frac{1+e^{\frac{T_{\text{ref}}\Delta S - H_d}{T_{\text{ref}}}}}{1+e^{\frac{T_{\text{obs}}\Delta S - H_d}{T_{\text{obs}}}}}} \quad (3.6)$$

779 k_{25} represents the standardized V_{cmax} or J_{max} rate at 25°C , k_{obs} represents the

780 V_{cmax} or J_{max} estimate at the average leaf temperature measured inside the cuvette

781 during the A_{net}/C_i curve. H_a is the activation energy of V_{cmax} ($71,513 \text{ J mol}^{-1}$)

782 Kattge and Knorr (2007) or J_{max} ($49,884 \text{ J mol}^{-1}$) (Kattge and Knorr 2007).

783 H_d represents the deactivation energy of both V_{cmax} and J_{max} ($200,000 \text{ J mol}^{-1}$)

784 (Medlyn et al. 2002), and R represents the universal gas constant (8.314 J mol^{-1}

785 K^{-1}). T_{ref} represents the standardized temperature of 298.15 K (25°C) and T_{obs}

786 represents the mean leaf temperature (in K) during each A_{net}/C_i curve. ΔS is an

787 entropy term that (Kattge and Knorr 2007) derived as a linear relationship with

788 average growing season temperature (T_g ; $^\circ\text{C}$), where:

$$\Delta S_{vcmax} = -1.07 T_g + 668.39 \quad (3.7)$$

789 and

$$\Delta S_{j\max} = -0.75 T_g + 659.70 \quad (3.8)$$

790 I estimated T_g in Equations 3.7 and 3.8 based on mean daily (24-hour) air tem-
791 perature of the 30 days leading up to the day of each sample collection using the
792 same weather station reported in the site description. I used $V_{c\max 25}$ and $J_{\max 25}$
793 estimates to calculate the ratio of $J_{\max 25}$ to $V_{c\max 25}$ ($J_{\max 25}:V_{c\max 25}$; unitless).

794 3.2.5 *Proportion of leaf nitrogen allocated to photosynthesis and structure*

795 I used equations from Niinemets and Tenhunen (1997) to estimate the proportion
796 of leaf nitrogen content allocated to Rubisco and bioenergetics. The proportion of
797 leaf nitrogen allocated to Rubisco (ρ_{rubisco} ; gN gN⁻¹) was calculated as a function
798 of $V_{c\max 25}$ and N_{area} :

$$\rho_{\text{rubisco}} = \frac{V_{c\max 25} N_r}{V_{cr} N_{\text{area}}} \quad (3.9)$$

799 where N_r is the amount of nitrogen in Rubisco, set to 0.16 gN (gN in Rubisco)⁻¹
800 and V_{cr} is the maximum rate of RuBP carboxylation per unit Rubisco protein,
801 set to 20.5 μmol CO₂ (g Rubisco)⁻¹. The proportion of leaf nitrogen allocated to
802 bioenergetics (ρ_{bioe} ; gN gN⁻¹) was similarly calculated as a function of $J_{\max 25}$ and
803 N_{area} :

$$\rho_{\text{bioe}} = \frac{J_{\max 25} N_b}{J_{mc} N_{\text{area}}} \quad (3.10)$$

804 where N_b is the amount of nitrogen in cytochrome f, set to 0.12407 gN (μmol

805 cytochrome f)⁻¹ assuming a constant 1: 1: 1.2 cytochrome f: ferredoxin NADP
 806 reductase: coupling factor molar ratio (Evans and Seemann 1989; Niinemets and
 807 Tenhunen 1997), and J_{mc} is the capacity of electron transport per cytochrome f,
 808 set to 156 μmol electron (μmol cytochrome f)⁻¹s⁻¹.

809 I estimated the proportion of leaf nitrogen content allocated to photosynthetic
 810 tissue (ρ_{photo} ; gN gN⁻¹) as the sum of $\rho_{rubisco}$ and ρ_{bioe} . This calculation
 811 is an underestimate of the proportion of leaf nitrogen allocated to photosynthetic
 812 tissue because it does not include nitrogen allocated to light harvesting proteins.
 813 This leaf nitrogen pool was not included because I did not perform chlorophyll
 814 extractions on focal leaves. However, the proportion of leaf nitrogen content al-
 815 located to light harvesting proteins tends to be small relative to $\rho_{rubisco}$ and ρ_{bioe} ,
 816 and may scale with changes in $\rho_{rubisco}$ and ρ_{bioe} (Niinemets and Tenhunen 1997).

817 Finally, the proportion of leaf nitrogen content allocated to structural tissue
 818 ($\rho_{structure}$; gN gN⁻¹) was estimated as:

$$\rho_{structure} = \frac{N_{cw}}{N_{area}} \quad (3.11)$$

819 where N_{cw} is the leaf nitrogen content allocated to cell walls (gN m⁻²), calculated
 820 as a function of M_{area} using an empirical equation from Onoda et al. (2017):

$$N_{cw} = 0.000355 * M_{area}^{1.39} \quad (3.12)$$

821 3.2.6 *Tradeoffs between nitrogen and water use*

822 Photosynthetic nitrogen use efficiency (PNUE; $\mu\text{mol CO}_2 \text{ mol}^{-1} \text{ N s}^{-1}$) was cal-
823 culated by dividing A_{net} by N_{area} , first converting N_{area} to mol N m^{-2} using the
824 molar mass of nitrogen (14 g mol^{-1}). I used χ as an indicator of water use effi-
825 ciency, which exploratory analyses suggest had similar responses to soil nitrogen
826 availability and pH as intrinsic water use efficiency measured from gas exchange
827 ($A_{\text{net}}/g_{\text{sw}}$). Tradeoffs between nitrogen and water use were determined by cal-
828 culating the ratio of N_{area} to χ ($N_{\text{area}}:\chi$; gN m^{-2}) and V_{cmax25} to χ ($V_{\text{cmax25}}:\chi$;
829 $\mu\text{mol m}^{-2} \text{ s}^{-1}$). This approach is similar to tradeoff calculations in which nitrogen-
830 water use tradeoffs are measured as the ratio of N_{area} or V_{cmax25} to g_{sw} (Paillassa
831 et al. 2020; Bialic-Murphy et al. 2021). In this chapter, I quantify these rela-
832 tionships using χ in lieu of g_{sw} because g_{sw} rapidly changes with environmental
833 conditions and therefore may have been altered by recent tree branch severance
834 and/or placement in the cuvette.

835 3.2.7 *Soil nitrogen availability and pH*

836 To characterize soil nitrogen availability at the time of leaf gas exchange mea-
837 surements, I used mixed bed resin bags to quantify mobile ammonium-N and
838 nitrate-N concentrations in each plot. Lycra mesh bags were filled with 5 g of
839 Dowex® Marathon MR-3 hydrogen and hydroxide form resin (MilliporeSigma,
840 Burlington, MA USA) and sealed with a zip tie. Each bag was activated by soak-
841 ing in 0.5 M HCl for 20 minutes, then in 2 M NaCl until pH of the saline solution
842 stabilized, as described in Allison et al. (2008). Five resin bags were inserted
843 about 10 cm below the soil surface at each plot on June 25, 2019: one near each

844 of the four plot corners and one near the plot center. All resin bags were collected
845 24 days later on July 19, 2019 and were frozen until extracted.

846 Prior to anion and cation extraction, each resin bag was rinsed with ul-
847 trapure water (MilliQ IQ 7000; Millipore Sigma, Burlington, MA) to remove any
848 surface soil residues. Anions and cations were extracted from surface-cleaned
849 resin bags by individually soaking and shaking each bag in 100 mL of a 0.1 M
850 HCl/2.0 M NaCl matrix for one hour. Using a microplate reader (Biotek Synergy
851 H1; Biotek Instruments, Winooski, VT USA), I quantified nitrate-N concentra-
852 tions spectrophotometrically at 540 nm with the end product of a single reagent
853 vanadium (III) chloride reaction (Doane and Horwáth 2003), and ammonium-N
854 concentrations quantified at 650 nm with the end product of a modified phenol-
855 hypochlorite reaction (Weatherburn 1967; Rhine et al. 1998). Both the single
856 reagent vanadium (III) chloride and modified phenol-hypochlorite methodologies
857 are well established for determining nitrate-N and ammonium-N concentrations
858 in resin bag extracts (Arnone 1997; Allison et al. 2008). I used a series of nega-
859 tive and positive controls throughout each well plate to verify the accuracy and
860 precision of measurements, assaying each resin bag extract and control in trip-
861 licate. Soil nitrogen availability was estimated as the sum of the nitrate-N and
862 ammonium-N concentration in each resin bag, normalized per gram of resin and
863 duration in the field ($\mu\text{g N g}^{-1} \text{ resin d}^{-1}$), then subsequently averaged across all
864 resin bags in a plot for a plot-level mean.

865 Soil pH was measured on 0-10 cm mineral soil samples collected prior to
866 fertilization in 2019. Near each of the four plot corners, three 5.5 cm diameter soil
867 cores were collected after first removing the forest floor where present. Each set

868 of three cores was placed in a plastic bag, and later composited by hand mixing
869 and sieved to 4 mm. Soil pH was determined for a 1:2 soil:water slurry (10 g
870 field-moist soil to 20 mL DI water) of each sample using an Accumet AB15 pH
871 meter with flushable junction probe (Fisher Scientific; Hampton, NH, USA), and
872 was estimated at the plot level as the mean soil pH within each plot.

873 3.2.8 *Statistical analyses*

874 I built two separate series of linear mixed-effects models to explore effects of soil
875 nitrogen availability, soil pH, species, and leaf nitrogen content on leaf physiolog-
876 ical traits. In the first series of linear mixed-effects models, I explored the effect
877 of soil nitrogen availability, soil pH, and species on leaf nitrogen content, leaf
878 photosynthesis, stomatal conductance, and nitrogen-water use tradeoffs. Models
879 included plot-level soil nitrogen availability and plot-level soil pH as continuous
880 fixed effects, species as a categorical fixed effect, and site as a categorical ran-
881 dom intercept term. Interaction terms between fixed effects were not included
882 due to the small number of experimental plots. I built a series of separate mod-
883 els with this independent variable structure to quantify individual effects of soil
884 nitrogen availability, soil pH, and species on N_{area} , M_{area} , N_{mass} , A_{net} , V_{cmax25} ,
885 J_{max25} , $J_{\text{max25}}:V_{\text{cmax25}}$, ρ_{rubisco} , $\rho_{\text{bioenergetics}}$, ρ_{photo} , $\rho_{\text{structure}}$, χ , PNUE, $N_{\text{area}}:\chi$, and
886 $V_{\text{cmax25}}:\chi$.

887 A second series of linear mixed-effects models were built to investigate
888 relationships between leaf nitrogen content and photosynthetic parameters. Sta-
889 tistical models included N_{area} as a single continuous fixed effect with species and
890 site designated as individual random intercept terms. I used this independent

891 variable structure to quantify individual effects of leaf nitrogen content on A_{net} ,
892 $V_{\text{cmax}25}$, $J_{\text{max}25}$, $J_{\text{max}25}:V_{\text{cmax}25}$, and χ .

893 For all linear mixed-effects models, I used Shapiro-Wilk tests of normality
894 to determine whether linear mixed-effects models satisfied residual normality as-
895 sumptions. If residual normality assumptions were not met, then models were fit
896 using dependent variables that were natural log transformed. If residual normal-
897 ity assumptions were still not met (Shapiro-Wilk: $p < 0.05$), then models were fit
898 using dependent variables that were square root transformed. All residual nor-
899 mality assumptions for both sets of models that did not originally satisfy residual
900 normality assumptions were met with either a natural log or square root data
901 transformation (Shapiro-Wilk: $p > 0.05$ in all cases).

902 In the first series of models, models for N_{area} , M_{area} , N_{mass} , $V_{\text{cmax}25}$, $J_{\text{max}25}$,
903 χ , $N_{\text{area}}:\chi$, and $V_{\text{cmax}25}:\chi$, ρ_{rubisco} , $\rho_{\text{bioenergetics}}$, ρ_{photo} , $\rho_{\text{structure}}$ satisfied residual
904 normality assumptions without data transformations (Shapiro-Wilk: $p > 0.05$ in
905 all cases). The model for $J_{\text{max}25}:V_{\text{cmax}25}$ satisfied residual normality assumptions
906 with a natural log data transformation, while models for A_{net} and PNUE each
907 satisfied residual normality assumptions with square root data transformations.

908 In the second series of models, models for $V_{\text{cmax}25}$, $J_{\text{max}25}$, χ , and $V_{\text{cmax}25}:\chi$ satis-
909 fied residual normality assumptions without data transformations (Shapiro-Wilk:
910 $p > 0.05$ in all cases). The model for $J_{\text{max}25}:V_{\text{cmax}25}$ required a natural log data
911 transformation and the model for A_{net} required a square root data transformation
912 (Shapiro-Wilk: $p > 0.05$ in both cases).

913 In all models, I used the ‘lmer’ function in the ‘lme4’ R package (Bates
914 et al. 2015) to fit each model and the ‘Anova’ function in the ‘car’ R package

915 (Fox and Weisberg 2019) to calculate Type II Wald's χ^2 and determine the signif-
916 icance level ($\alpha=0.05$) of each fixed effect coefficient. Finally, I used the 'emmeans'
917 R package (Lenth 2019) to conduct post-hoc comparisons using Tukey's tests,
918 where degrees of freedom were approximated using the Kenward-Roger approach
919 (Kenward and Roger 1997). All analyses and plots were conducted in R version
920 4.1.1 (R Core Team 2021). All figure regression lines and associated 95% confi-
921 dence interval error bars were plotted using predictions generated across the soil
922 nitrogen availability gradient using the 'emmeans' R package (Lenth 2019).

923 3.3 Results

924 3.3.1 *Leaf nitrogen content*

925 Increasing soil nitrogen availability generally increased N_{area} (Table 3.1; Fig. 3.1a).
926 This pattern was driven by an increase in N_{mass} (Table 3.1; Fig. 3.1c) and a
927 marginal increase in M_{area} (Table 3.1; Fig. 3.1e) with increasing soil nitrogen
928 availability. There was no effect of soil pH on N_{area} , N_{mass} , or M_{area} (Table 3.1);
929 however, I also observed strong differences in N_{area} (Fig. 3.1b), N_{mass} (Fig. 3.1d),
930 and M_{area} (Fig. 3.1e) between species (Table 3.1).

Table 3.1. Effects of soil nitrogen availability, soil pH, and species on leaf nitrogen content per unit leaf area (N_{area} ; gN m⁻²), leaf nitrogen content per unit leaf mass (N_{mass} ; gN g⁻¹), and leaf mass per unit leaf area (M_{area} ; g m⁻²)*

	N_{area}			N_{mass}			M_{area}			
	df	Coefficient	χ^2	p	Coefficient	χ^2	p	Coefficient	χ^2	p
Intercept	-	$9.03 * 10^{-1}$	-	-	$1.68 * 10^0$	-	-	$4.60 * 10^1$	-	-
Soil N	1	$1.68 * 10^{-2}$	11.990	0.001	$1.25 * 10^{-2}$	6.902	0.009	$4.87 * 10^{-1}$	4.143	0.042
Soil pH	1	$9.28 * 10^{-2}$	0.836	0.361	$8.08 * 10^{-2}$	0.663	0.415	$4.05 * 10^0$	0.653	0.419
Species	4	-	72.128	<0.001	-	35.074	<0.001	-	29.869	<0.001

931 *Significance determined using Type II Wald χ^2 tests ($\alpha=0.05$). P-values<0.05 are in bold.

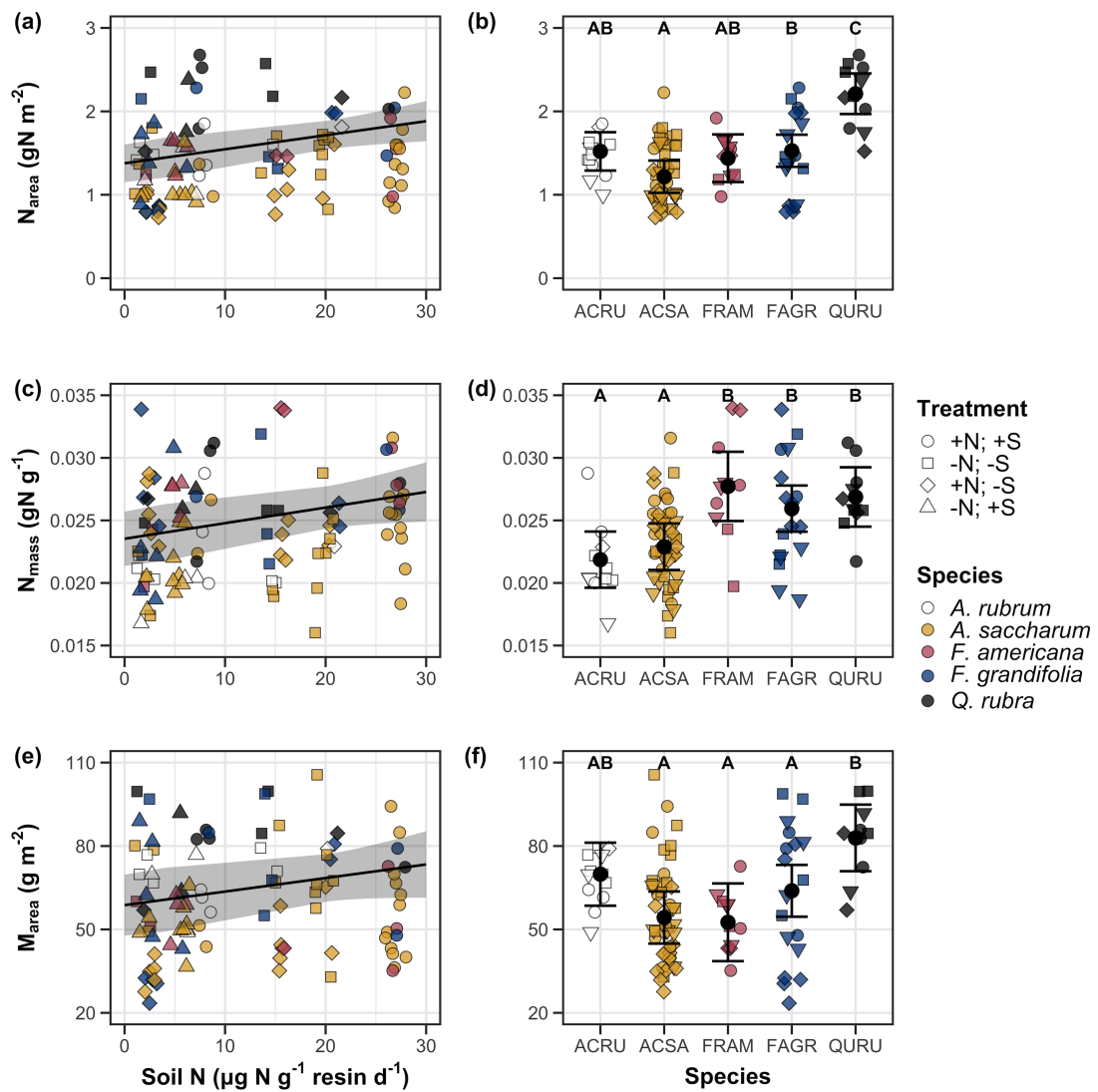


Figure 3.1. Effects of soil N availability and species on leaf nitrogen content per unit leaf area (a-b), leaf nitrogen content per unit leaf biomass (c-d), and leaf mass per unit leaf area (e-f). Soil nitrogen availability is represented on the x-axis in the left column of panels, while species is represented on the x-axis in the right column of panels. Tree species are represented as colored points and treatment plots are represented as shaped points, jittered for visibility. Species are abbreviated in the right column of panels through their assigned NRCS PLANTS Database symbol (USDA NRCS 2022), grouped along the x-axis per common mycorrhizal association, where the first three species commonly associate with arbuscular mycorrhizae (ACRU, ACSA, FAGR) and the second two species with ectomycorrhizae (FAGR, QURU). Trendlines are only included when the regression slope is statistically different from zero ($p < 0.05$).

932 3.3.2 *Net photosynthesis and leaf biochemistry*

933 Increasing soil nitrogen availability generally had no effect on A_{net} , V_{cmax25} , J_{max25} ,

934 or $J_{\text{max25}}:V_{\text{cmax25}}$ (Table 3.2, Figs. 3.2a, 3.2d, 3.2g). I also observed strong species

935 effects on all measured leaf photosynthetic traits (Table 3.2; Figs. 3.2b, 3.2e, 3.2h).

936 Increasing soil pH had a marginal negative effect on A_{net} , but had no effect on

937 V_{cmax25} , J_{max25} , or $J_{\text{max25}}:V_{\text{cmax25}}$ (Table 3.2). There was a weak positive effect of

938 increasing N_{area} on A_{net} (Fig. 3.2c), but quite strong positive effects of increasing

939 N_{area} on V_{cmax25} and J_{max25} (Table 3.2; Fig. 3.2f and 3.2i).

Table 3.2. Effects of soil nitrogen availability, soil pH, species, and N_{area} on net photosynthesis (A_{net} ; $\mu\text{mol m}^{-2} \text{s}^{-1}$), the maximum rate of Rubisco carboxylation (V_{cmax25} ; $\mu\text{mol m}^{-2} \text{s}^{-1}$), the maximum rate of RuBP regeneration (J_{max25} ; $\mu\text{mol m}^{-2} \text{s}^{-1}$), and the ratio of the maximum rate of RuBP regeneration to the maximum rate of Rubisco carboxylation ($J_{\text{max25}}:V_{\text{cmax25}}$; unitless)*

	A_{net}			V_{cmax25}			J_{max25}			
	df	Coefficient	χ^2	p	Coefficient	χ^2	p	Coefficient	χ^2	p
(Intercept)	-	$3.29 * 10^{0\text{b}}$	-	-	$6.38 * 10^1$	-	-	$1.12 * 10^2$	-	-
Soil N	1	$-1.23 * 10^{-3\text{b}}$	1.798	0.180	$-3.84 * 10^{-1}$	1.745	0.187	$-6.70 * 10^{-1}$	2.172	0.141
Soil pH	1	$-3.09 * 10^{-1\text{b}}$	3.312	0.069	$-4.91 * 10^0$	0.655	0.418	$-8.18 * 10^0$	0.742	0.389
Species	4	-	11.838	0.019	-	31.748	<0.001	-	27.291	<0.001
(N_{area} int.)	-	$6.59 * 10^{-1\text{b}}$	-	-	$1.45 * 10^{-1}$	-	-	$2.86 * 10^1$	-	-
N_{area}	4	$3.13 * 10^{-1\text{b}}$	4.790	0.029	$2.43 * 10^1$	22.616	<0.001	$4.04 * 10^1$	28.259	<0.001

	$J_{\text{max25}}:V_{\text{cmax25}}$			
	df	Coefficient	χ^2	p
(Intercept)	-	$6.59 * 10^{-1\text{a}}$	-	-
Soil N	1	$7.04 * 10^{-4\text{a}}$	0.088	0.767
Soil pH	1	$-7.84 * 10^{-3\text{a}}$	0.025	0.874
Species	4	-	12.745	0.013
(N_{area} int.)	-	$6.69 * 10^{-1\text{a}}$	-	-
N_{area}	4	$-4.69 * 10^{-2\text{a}}$	1.142	0.285

54

940 *Significance determined using Type II Wald χ^2 tests ($\alpha=0.05$). P-values less than 0.05 are in bold, while p-values
 941 between 0.05 and 0.1 are italicized. Superscript letters indicate model coefficients fit to natural-log ^(a) or square-root
 942 ^(b) transformed data. Relationships between N_{area} and each response variable were fit using the second series of
 943 bivariate mixed-effects models, so model coefficients and results are independent of model coefficients and results
 944 reported for relationships between soil nitrogen, soil pH, and species for each response variable.

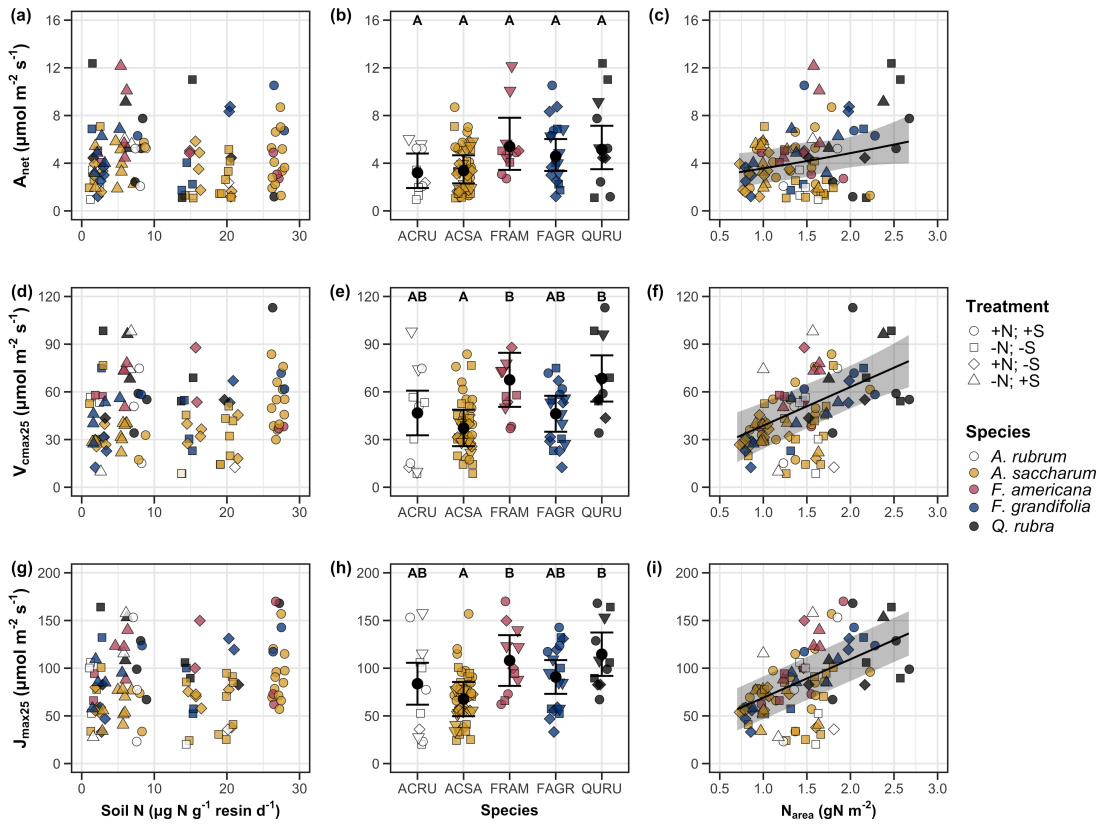


Figure 3.2. Effects of soil nitrogen availability (left column of panels), species (middle column of panels), and leaf nitrogen content per unit leaf area (right column of panels) on net photosynthesis (a-c), maximum Rubisco carboxylation rate (d-f), and maximum RuBP regeneration rate (g-i). Soil nitrogen availability is represented on the x-axis in the left column of panels, species is represented on the x-axis in the middle column of panels, and leaf nitrogen content per unit leaf area is represented continuously on the x-axis in the right column of panels. Species abbreviations and position along the x-axis in the middle column of panels, colored points, shapes, and trendlines are as explained in Figure 3.1.

945 3.3.3 *Leaf nitrogen allocation*

946 Neither soil nitrogen availability nor soil pH affected the proportion of leaf nitrogen
947 allocated to Rubisco or bioenergetics (Table 3.3; Fig. 3.3a, Fig. 3.3c). There was
948 also no effect of soil nitrogen availability or soil pH on the proportion of leaf
949 nitrogen allocated to photosynthesis (Table 3.3; Fig. 3.3f). I found no effect of
950 soil nitrogen availability or soil pH on the proportion of leaf nitrogen allocated to
951 structure (Table 3.3; Fig 3.3g). Species varied in the proportion of leaf nitrogen
952 allocated to Rubisco, photosynthesis, and structure (Fig 3.3b, Fig. 3.3f, Fig 3.3h),
953 with no detectable species effect on the proportion of leaf nitrogen allocated to
954 bioenergetics (Table 3.3, Fig. 3.3d).

Table 3.3. Effects of soil nitrogen availability, soil pH, and species on the proportion of leaf nitrogen content allocated to photosynthesis (ρ_{photo} ; gN gN $^{-1}$), Rubisco (ρ_{rubisco} ; gN gN $^{-1}$), bioenergetics (ρ_{bioe} ; gN gN $^{-1}$), and structure ($\rho_{\text{structure}}$; gN gN $^{-1}$)*

	ρ_{photo}			ρ_{rubisco}			ρ_{bioe}			
	df	Coefficient	χ^2	p	Coefficient	χ^2	p	Coefficient	χ^2	p
Intercept	-	$4.93 * 10^{-1}$	-	-	$4.17 * 10^{-1}$	-	-	$7.64 * 10^{-2}$	-	-
Soil N	1	$-1.23 * 10^{-3}$	0.521	0.470	$-1.04 * 10^{-3}$	0.501	0.479	$-1.77 * 10^{-4}$	0.557	0.455
Soil pH	1	$-4.37 * 10^{-2}$	1.581	0.209	$-3.70 * 10^{-2}$	1.511	0.219	$-6.84 * 10^{-3}$	1.941	0.164
Species	4	-	13.106	0.011	-	14.152	0.007	-	7.300	0.121

	$\rho_{\text{structure}}$			
	df	Coefficient	χ^2	p
Intercept	-	$9.77 * 10^{-2}$	-	-
Soil N	1	$-2.29 * 10^{-4}$	1.165	0.280
Soil pH	1	$-1.87 * 10^{-3}$	0.179	0.672
Species	4	-	16.428	0.002

955 *Significance determined using Type II Wald χ^2 tests ($\alpha=0.05$). P-values less than 0.05 are in bold.

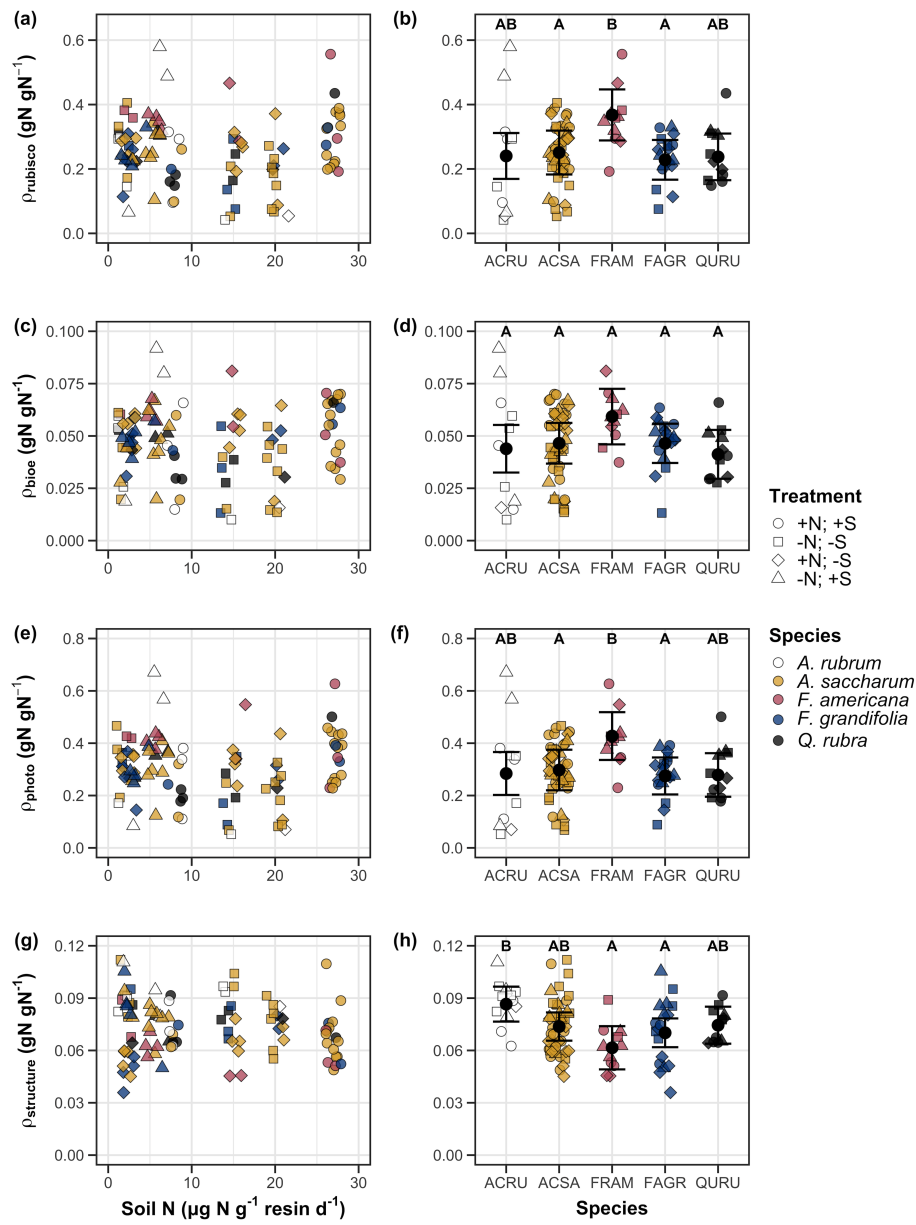


Figure 3.3. Effects of soil nitrogen availability and species on the proportion of leaf nitrogen content allocated to Rubisco (a-b), bioenergetics (c-d), photosynthesis (e-f), and structure (g-h). Soil nitrogen availability is represented on the x-axis in the left column of panels and species are represented on the x-axis in the right column of panels. Species abbreviations and position along the x-axis in the middle column of panels, colored points, shapes, trendlines, error bars, and compact lettering are as explained in Figure 3.1.

956 3.3.4 *Tradeoffs between nitrogen and water use*

957 Although soil nitrogen availability did not affect χ (Table 3.4; Fig. 3.4a), increasing
958 soil nitrogen availability decreased PNUE (Table 3.4; Fig. 3.4d) and increased
959 the ratio of $N_{\text{area}}:\chi$ (Table 3.4; Fig. 3.4f). Specifically, this response yielded a
960 26% reduction in PNUE and 37% stimulation in $N_{\text{area}}:\chi$ across the soil nitrogen
961 availability gradient. There was no apparent effect of soil nitrogen availability on
962 $V_{\text{cmax25}}:\chi$ (Table 3.4; Fig. 3.4h). Increasing soil pH had a weak marginal nega-
963 tive effect on PNUE, but did not influence χ , $N_{\text{area}}:\chi$, or $V_{\text{cmax25}}:\chi$ (Table 3.4). I
964 observed differences in χ (Fig. 3.4b), PNUE (Fig. 3.4e), $N_{\text{area}}:\chi$ (Fig. 3.4g), and
965 $V_{\text{cmax25}}:\chi$ (Fig. 3.4i) between species (Table 3.4). Finally, increasing N_{area} had a
966 strong negative effect on χ (Table 3.4; Fig. 3.4c) and a strong positive effect on
967 $V_{\text{cmax25}}:\chi$ (Table 3.4; Fig. 3.4j).

Table 3.4. Effects of soil nitrogen availability, soil pH, species, and N_{area} on χ (unitless), photosynthetic nitrogen use efficiency (PNUE; $\mu\text{mol CO}_2 \text{ mol}^{-1} \text{ N s}^{-1}$), leaf nitrogen content per unit χ ($N_{\text{area}}:\chi$; gN m^{-2}), and maximum Rubisco carboxylation rate per unit χ ($V_{\text{cmax25}}:\chi$; $\mu\text{mol m}^{-2} \text{ s}^{-1}$)^{*}

	χ			PNUE			$N_{\text{area}}:\chi$			
	df	Coefficient	χ^2	p	Coefficient	χ^2	p	Coefficient	χ^2	p
(Intercept)	-	$8.12 * 10^{-1}$	-	-	$9.57 * 10^{0\text{b}}$	-	-	$9.19 * 10^{-1}$	-	-
Soil N	1	$-1.14 * 10^{-3}$	1.698	0.193	$-6.63 * 10^{-2\text{b}}$	6.396	0.011	$2.60 * 10^{-2}$	9.533	0.002
Soil pH	1	$-1.91 * 10^{-2}$	1.087	0.297	$-9.25 * 10^{-1\text{b}}$	2.843	<i>0.092</i>	$2.03 * 10^{-1}$	1.321	0.250
Species	4	-	18.843	0.001	-	13.454	0.009	-	52.983	<0.001
(N_{area} int.)	-	$8.93 * 10^{-1}$	-	-	-	-	-	-	-	-
N_{area}	1	$-1.11 * 10^{-1}$	80.606	<0.001	-	-	-	-	-	-

	$V_{\text{cmax25}}:\chi$			
	df	Coefficient	χ^2	p
(Intercept)	-	$7.20 * 10^1$	-	-
Soil N	1	$3.99 * 10^{-1}$	0.963	0.326
Soil pH	1	$-3.12 * 10^0$	0.138	0.711
Species	4	-	31.450	<0.001
(N_{area} int.)	-	$1.18 * 10^1$	-	-
N_{area}	4	$3.87 * 10^1$	32.797	<0.001

968 *Significance determined using Type II Wald χ^2 tests ($\alpha = 0.05$). P-values less than 0.05 are in bold, while p-values
 969 between 0.05 and 0.1 are italicized. Superscript letters indicate model coefficients fit to natural-log ^(a) or square-root
 970 ^(b) transformed data. Relationships between N_{area} and each response variable were fit using the second series of
 971 bivariate mixed-effects models, so model coefficients and results are independent of model coefficients and results
 972 reported for relationships between soil nitrogen, soil pH, and species for each response variable.

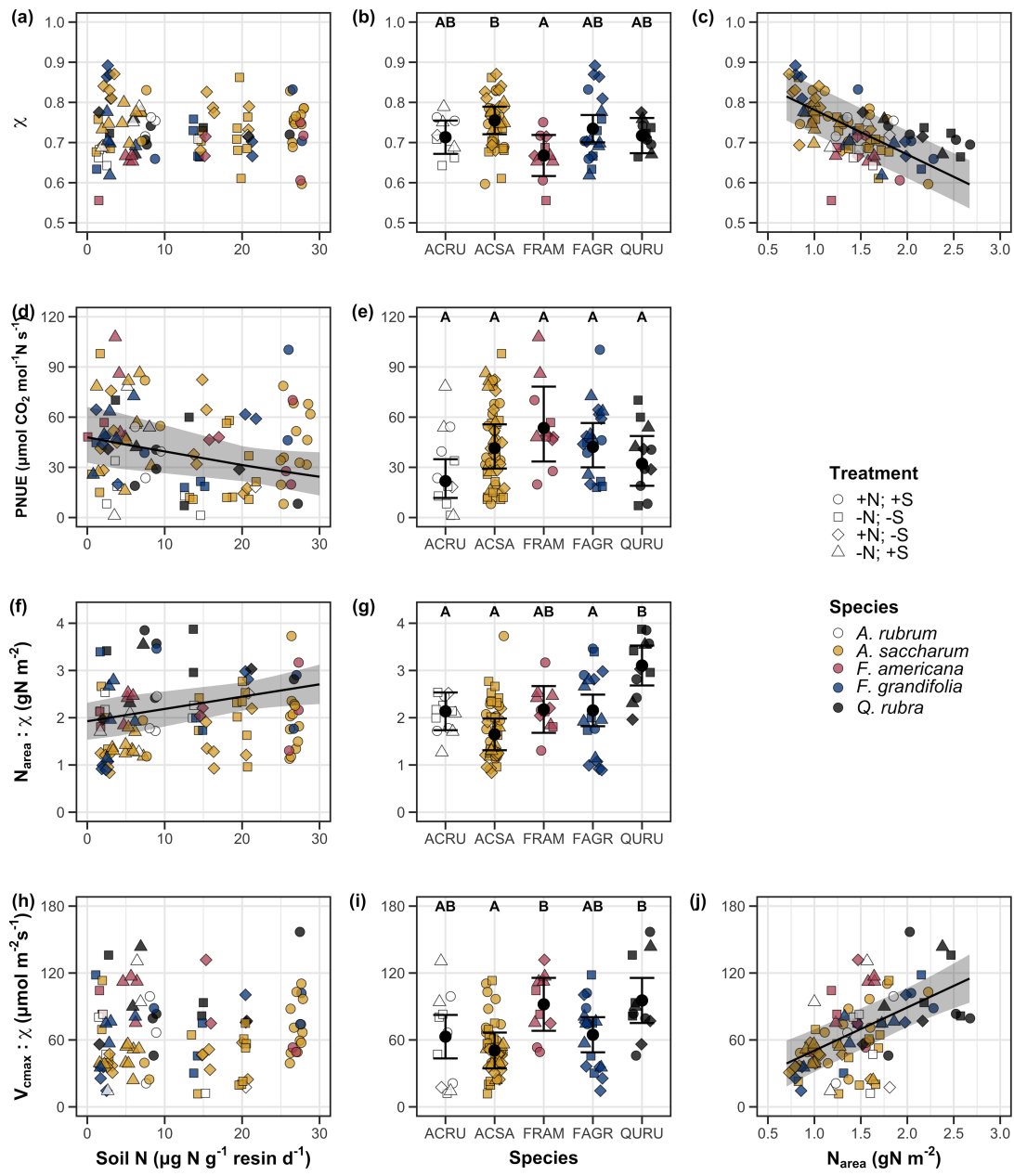


Figure 3.4. Effects of soil nitrogen availability and species on the proportion of leaf nitrogen content allocated to Rubisco (a-b), bioenergetics (c-d), photosynthesis (Rubisco + bioenergetics; e-f), and structure (g-h). Soil nitrogen availability is represented on the x-axis in the left column of panels and species are represented on the x-axis in the right column of panels. Species abbreviations and position along the x-axis in the middle column of panels, colored points, shapes, trendlines, error bars, and compact lettering are as explained in Figure 3.1.

973 3.4 Discussion

974 Photosynthetic least-cost theory provides an explanation for understanding rela-
975 tionships between soil nutrient availability, leaf nutrient allocation, and photosyn-
976 thetic capacity. The theory suggests that plants acclimate to a given environment
977 by optimizing leaf photosynthesis rates at the lowest summed cost of using nu-
978 trients and water (Prentice et al. 2014; Wang et al. 2017; Smith et al. 2019;
979 Paillassa et al. 2020). The theory predicts that an increase in soil nutrient avail-
980 ability should allow similar photosynthesis rates to be achieved with increased leaf
981 nutrient content and photosynthetic capacity (i.e., V_{cmax25} and J_{max25}) at reduced
982 leaf $C_i:C_a$ (χ), resulting in an increase in water use efficiency, decrease in nutrient
983 use efficiency, and increase in both leaf nutrient content and photosynthetic ca-
984 pacity per unit χ . The theory predicts similar leaf responses to increasing soil pH
985 under acidic conditions due to reduced costs of acquiring nutrients with increasing
986 soil pH (Wang et al. 2017; Paillassa et al. 2020; Dong et al. 2020).

987 Supporting the theory, increasing soil nitrogen availability was associated
988 with increased leaf nitrogen content, a pattern that reduced photosynthetic ni-
989 trogen use efficiency and increased leaf nitrogen content per unit χ . Increasing
990 soil nitrogen coincided with slight decreases in χ and increases in V_{cmax25} and
991 J_{max25} ($p < 0.2$, Table 3.2). The positive trend between soil nitrogen availability
992 and photosynthetic capacity was supported by the concurrent strong increase in
993 leaf nitrogen content with increasing soil nitrogen availability, which resulted in
994 no change in the proportion of leaf nitrogen content allocated to photosynthesis
995 across the soil nitrogen availability gradient. Additionally, leaf nitrogen content
996 exhibited a strong negative correlation with χ indicative of nitrogen-water use

997 tradeoffs at the leaf level. Responses tended to vary more due to soil nitrogen
998 availability than soil pH. Overall, these findings are consistent with the nutrient-
999 water use tradeoffs predicted from theory.

1000 3.4.1 *Soil nitrogen availability modifies tradeoffs between nitrogen and water use*

1001 Supporting expected least-cost outcomes and past environmental gradient stud-
1002 ies (Dong et al. 2017; Paillassa et al. 2020), increasing soil nitrogen availability
1003 was associated with increased leaf nitrogen content. Soil nitrogen availability had
1004 smaller impacts on net photosynthesis and χ , reducing PNUE and increasing leaf
1005 nitrogen content per unit χ , as expected from theory. Photosynthetic least-cost
1006 theory suggests that reductions in PNUE should be driven by increased propor-
1007 tions of leaf nitrogen allocated to photosynthetic tissue, a pattern that should
1008 allow plants to achieve optimal photosynthetic rates with greater photosynthetic
1009 capacity to make more efficient use of available light. Contrasting theory pre-
1010 dictions, I found no effect of soil nitrogen availability on photosynthetic capacity.
1011 However, photosynthetic capacity did tend to increase with increasing soil nitrogen
1012 availability ($p<0.20$; Table 3.2) resulting in no effect of soil nitrogen availability
1013 on the relative fraction of leaf nitrogen allocated to photosynthesis, Rubisco, or
1014 bioenergetics. These lines of evidence support the idea that trees use additional
1015 nitrogen to support increased leaf nitrogen allocation toward photosynthetic tissue
1016 and enhance photosynthetic capacity (Wright et al. 2003).

1017 Soil nitrogen availability had a stronger effect on leaf nitrogen than pho-
1018 tosynthetic capacity, suggesting that additional plant nitrogen uptake due to in-
1019 creased soil nitrogen availability was being used to support non-photosynthetic ni-

1020 trogen pools, possibly structural tissue or stress-induced amino acid and polyamine
1021 synthesis (Minocha et al. 2000; Onoda et al. 2004; Bubier et al. 2011). While
1022 I found no change in the proportion of leaf nitrogen allocated to leaf structural
1023 tissue, increased leaf nitrogen content with increasing soil nitrogen availability
1024 suggests that the net amount of nitrogen invested in leaf structural tissue in-
1025 creased with increasing soil nitrogen availability. Importantly, the proportion of
1026 leaf nitrogen allocated to leaf structural tissue was calculated using an empiri-
1027 cal relationship between M_{area} and the amount of leaf nitrogen allocated to cell
1028 walls (Onoda et al. 2017). As the generality of relationships between M_{area} and
1029 the amount of leaf nitrogen allocated to cell walls has been called into question
1030 (Harrison et al. 2009), future work should consider explicitly measuring nitrogen
1031 allocation to cell wall tissue and stress-induced amino acid synthesis to confirm
1032 these patterns.

1033 Opposing patterns expected from least-cost theory, increasing soil nitrogen
1034 availability had a null effect on χ . Despite this, I observed a strong negative effect
1035 of increasing N_{area} on χ , consistent with the nitrogen-water use tradeoffs expected
1036 from theory. The null response of χ to increasing soil nitrogen availability may
1037 have been due to a lack of water limitation in the system, given that the area
1038 received approximately 20% more precipitation (1167 mm) during the 12-month
1039 period leading up to our measurement period than normally expected (972 mm).
1040 However, droughts can and do occur in temperate forests of the northeastern
1041 United States (Sweet et al. 2017), so the observed increase in leaf nitrogen content
1042 with increasing soil nitrogen availability could be a strategy that allows trees
1043 to hedge bets against drier than normal growing seasons (Onoda et al. 2004;

1044 Onoda et al. 2017; Hallik et al. 2009). As suggested in Paillassa et al. (2020)
1045 and more recently by Querejeta et al. (2022), negative effects of soil nitrogen
1046 availability on χ may increase with increasing aridity. This strategy would be
1047 especially advantageous if it allows individuals growing in arid regions to maintain
1048 carbon assimilation rates with reduced water loss. Future work should attempt to
1049 quantify interactive roles of climate and soil nitrogen availability on nitrogen-water
1050 use tradeoffs, which could be done using coordinated and multifactor nutrient
1051 (Borer et al. 2014) and water (Knapp et al. 2017) manipulation experiments
1052 across broad climatic gradients.

1053 3.4.2 *Soil pH did not modify tradeoffs between nitrogen and water usage*

1054 While the primary purpose of this study was to examine the role of soil nitrogen
1055 availability on nitrogen-water use tradeoffs, this experiment manipulated both
1056 soil nitrogen and pH, thus providing an opportunity to isolate these variables.
1057 Previous correlational studies along environmental gradients have identified soil
1058 pH as an important factor that can modify tradeoffs between nutrient and water
1059 use (Smith et al. 2019; Paillassa et al. 2020; Westerband et al. 2023) and the
1060 proportion of leaf nitrogen allocated to photosynthesis (Luo et al. 2021). Such
1061 studies implied that these patterns may be driven by reduced costs of acquiring
1062 nutrients with increasing pH, which may be exacerbated in acidic soils.

1063 Consistent with theory (Wright et al. 2003; Prentice et al. 2014), results
1064 indicate that PNUE was negatively associated with increasing soil pH. However,
1065 there was no effect of soil pH on leaf nitrogen content, χ , or leaf nitrogen content
1066 per unit χ , most likely because the experimental nitrogen additions increased soil

1067 nitrogen supply while both increasing (sodium nitrate) and decreasing (ammo-
1068 nium sulfate) soil pH. These results suggest that soil pH did not play a major
1069 role in modifying expected photosynthetic least-cost theory patterns, contrasting
1070 findings from Paillassa et al. (2020) and other gradient studies that note positive
1071 effects of increasing soil pH on leaf nitrogen content, Rubisco carboxylation, and
1072 χ (Viet et al. 2013; Cornwell et al. 2018; Luo et al. 2021). Instead, null responses
1073 to soil pH show that leaf photosynthetic parameters depend more on soil nitrogen
1074 availability than pH per se, and that inferences from gradient studies might be
1075 confounding covariation between nitrogen availability and soil acidity.

1076 3.4.3 *Species identity explains a large amount of variation in leaf and whole*
1077 *plant traits*

1078 Species identity generally explained a larger amount of variation in measured leaf
1079 traits than soil nitrogen availability or soil pH. Interspecific variation is an im-
1080 portant factor to consider when deducing mechanisms that drive photosynthetic
1081 least-cost theory, particularly for species that form distinct mycorrhizal associ-
1082 ations or have different photosynthetic pathways, growth forms, or leaf habit
1083 (Espelta et al. 2005; Adams et al. 2016; Bialic-Murphy et al. 2021; Scott and
1084 Smith 2022). The need to consider species may also be important when com-
1085 paring nutrient-water use tradeoffs in early and late successional species, or in
1086 species with different resource economic strategies (Abrams and Mostoller 1995;
1087 Ellsworth and Reich 1996; Wright et al. 2004; Reich 2014; Onoda et al. 2017;
1088 Ziegler et al. 2020). The previous dissertation chapter notes species-specific car-
1089 bon cost to acquire nitrogen responses to soil nitrogen availability, a pattern that

1090 was either driven by differences in the dominant mode of nitrogen acquisition or
1091 growth form and duration.

1092 A strength of the study design and sampling effort is that it controls for
1093 many species differences that should modify nitrogen-water use tradeoffs expected
1094 from theory. All tree species measured in this study shared the leaf habit of de-
1095 ciduous broadleaves, were growing in forests of similar successional stage, but
1096 differed in mycorrhizal association and consequent resource economic strategies.
1097 As stands tended to be dominated by trees that associate with arbuscular myc-
1098 orrhizae (*Fraxinus* and both *Acer* species made up roughly 70% of total above-
1099 ground biomass across stands), ecosystem biogeochemical cycle dynamics may be
1100 more closely aligned to the inorganic nutrient economy proposed in Phillips et al.
1101 (2013), which may promote stronger nitrogen-water use tradeoffs in tree species
1102 that associate with arbuscular mycorrhizae. This result was not observed here,
1103 as photosynthetic properties varied as much within as across the two mycorrhizal
1104 associations represented.

1105 3.4.4 *Implications for photosynthetic least-cost theory model development*

1106 In the field, soil nutrient availability is heterogeneous across time and space (Ta-
1107 ble B4). Unaccounted within-plot heterogeneity may have contributed to the low
1108 amount of variation explained by soil nitrogen availability in statistical models, as
1109 resin bags are a coarse surrogate for soil nitrogen availability. Despite this, I still
1110 observed evidence for nutrient-water use tradeoffs, suggesting that observed re-
1111 sponses reported here may underestimate the net effect of soil nitrogen availability
1112 on such tradeoffs. While I urge caution in the interpretation of these results, they

1113 do provide a promising baseline for future studies investigating patterns expected
1114 from photosynthetic least-cost theory at finer spatiotemporal resolutions.

1115 The general stronger relationship between leaf nitrogen content and photo-
1116 synthetic parameters versus between leaf nitrogen content and soil nitrogen avail-
1117 ability suggests that leaf nitrogen content is more directly tied to photosynthesis
1118 than soil nitrogen availability. While this could be due to the high spatiotem-
1119 poral heterogeneity of soil nitrogen availability, principles from photosynthetic
1120 least-cost theory suggest that leaf nitrogen content is the downstream product
1121 of leaf nutrient demand to build and maintain photosynthetic machinery, which
1122 is set by aboveground environmental conditions such as light availability, CO₂,
1123 temperature, or vapor pressure deficit (Smith et al. 2019; Paillassa et al. 2020;
1124 Peng et al. 2021; Westerband et al. 2023). The stronger relationship between
1125 leaf nitrogen and photosynthetic parameters, paired with the strong negative re-
1126 lationship between leaf nitrogen and χ , could indicate a stronger effect of climate
1127 on leaf nitrogen-photosynthesis relationships than soil resource availability. How-
1128 ever, the short distance between plots and across sites limit my ability to test this
1129 hypothesis.

1130 Variation in soil pH affected least cost responses less than variations in soil
1131 nitrogen availability, in part because experimental treatments directly increased
1132 soil nitrogen and affected soil pH in opposite directions. While soil pH has been
1133 shown to drive nitrogen-water tradeoffs in global gradient analyses (Viet et al.
1134 2013; Paillassa et al. 2020), these responses may be due to covariations between
1135 soil pH and nutrient cycling rather than a role of pH per se. The direct manipula-
1136 tions of soil pH and soil nitrogen availability in this study partly disentangle these

1137 factors and show that variation in nitrogen availability matters more for least-cost
1138 tradeoffs than pH alone.

1139 3.4.5 *Conclusions*

1140 Increasing soil nitrogen availability generally increased leaf nitrogen content (both
1141 area- and mass-based) but did not significantly influence net photosynthesis or χ ,
1142 leading to a reduction in PNUE and an increase in leaf nitrogen per unit χ with
1143 increasing soil nitrogen availability. Despite null effects of soil nitrogen availabil-
1144 ity on χ , I observed a strong negative relationship between leaf nitrogen content
1145 and χ . These results provide empirical support for nutrient-water use tradeoffs
1146 expected from photosynthetic least-cost theory, but suggest that all tenets of the
1147 theory may not hold in every environment. Findings reported here experimen-
1148 tally test previous work suggesting that leaf nitrogen-water economies vary across
1149 gradients of soil nutrient availability and pH, and show that variations in nutrient
1150 availability matter more for predicting leaf photosynthetic traits than soil pH.

1151

Chapter 4

1152 The relative cost of resource use for photosynthesis drives variance in
1153 leaf nitrogen content across a climate and soil resource availability
1154 gradient

1155 4.1 Introduction

1156 Terrestrial biosphere models, which comprise the land surface component of Earth
1157 system models, are sensitive to the formulation of photosynthetic processes (Knorr
1158 and Heimann 2001; Ziehn et al. 2011; Booth et al. 2012; Walker et al. 2021).
1159 This is because photosynthesis is the largest carbon flux between the atmosphere
1160 and terrestrial biosphere (IPCC 2021), and is constrained by ecosystem carbon
1161 and nutrient cycles (Hungate et al. 2003; LeBauer and Treseder 2008; Fay et al.
1162 2015). Many terrestrial biosphere models formulate photosynthesis by parame-
1163 terizing photosynthetic capacity within plant functional groups through empiri-
1164 cal linear relationships between area-based leaf nitrogen content (N_{area}) and the
1165 maximum carboxylation rate of Ribulose-1,5-bisphosphate carboxylase/oxygenase
1166 (V_{cmax}) (Kattge et al. 2009; Rogers 2014; Rogers et al. 2017). Models are also
1167 beginning to include connected carbon-nitrogen cycles (Wieder et al. 2015; Shi
1168 et al. 2016; Davies-Barnard et al. 2020; Braghieri et al. 2022), which allows leaf
1169 photosynthesis to be predicted directly through changes in N_{area} and indirectly
1170 through changes in soil nitrogen availability (e.g., LPJ-GUESS, CLM5.0) (Smith
1171 et al. 2014; Lawrence et al. 2019). Despite recent model developments, open
1172 questions remain regarding the generality of ecological relationships between soil
1173 nitrogen availability, leaf nitrogen content, and leaf photosynthesis across edaphic
1174 and climatic gradients.

1175 Empirical support for positive relationships between soil nitrogen availabil-
1176 ity and N_{area} is abundant (Firn et al. 2019; Liang et al. 2020), and is a result
1177 often attributed to the high nitrogen cost of building and maintaining Rubisco
1178 (Evans 1989; Evans and Seemann 1989; Onoda et al. 2004; Walker et al. 2014;
1179 Onoda et al. 2017; Dong et al. 2020). Such patterns imply that positive relation-
1180 ships between soil nitrogen availability and N_{area} should increase leaf photosyn-
1181 thesis and photosynthetic capacity by increasing the maximum rate of Rubisco
1182 carboxylation through increased investments to Rubisco construction and mainte-
1183 nance. This integrated N_{area} -photosynthesis response to soil nitrogen availability
1184 has been observed both in manipulative experiments and across environmental
1185 gradients (Field and Mooney 1986; Evans 1989; Walker et al. 2014; Li et al.
1186 2020), and is thought to be driven by ecosystem nitrogen limitation, which lim-
1187 its primary productivity globally (LeBauer and Treseder 2008; Fay et al. 2015).
1188 However, this response is not consistently observed, as recent studies note variable
1189 N_{area} -photosynthesis relationships across edaphic and climatic gradients (Liang
1190 et al. 2020; Luo et al. 2021) and that aboveground growing conditions (e.g., light
1191 availability, temperature, vapor pressure deficit) or species identity traits (e.g.,
1192 photosynthetic pathway, nitrogen acquisition strategy) may be more important
1193 for explaining variance in N_{area} and photosynthetic capacity across environmental
1194 gradients (Adams et al. 2016; Dong et al. 2017; Smith et al. 2019; Dong et al.
1195 2020; Peng et al. 2021; Dong et al. 2022; Westerband et al. 2023).

1196 One hypothesized mechanism to explain variance in N_{area} across environ-
1197 mental gradients has been proposed via photosynthetic least-cost theory (Wright
1198 et al. 2003; Prentice et al. 2014; Paillassa et al. 2020; Harrison et al. 2021).

1199 The theory predicts that plants acclimate to environments by optimizing photo-
1200 synthetic assimilation rates at the lowest summed cost of nitrogen and water use
1201 (Wright et al. 2003; Prentice et al. 2014). In a given environment, the theory
1202 suggests that nitrogen and water use can be substituted for each other to maintain
1203 the lowest summed cost of resource use, such that optimal photosynthetic rates
1204 are achieved with less efficient use of the more abundant and less costly resource
1205 to acquire in exchange for more efficient use of the less abundant and more costly
1206 resource to acquire.

1207 Photosynthetic least-cost theory predicts that, all else equal, an increase in
1208 soil nitrogen availability should decrease the cost of acquiring and using nitrogen
1209 relative to water (a ratio referred to herein as β), resulting in optimal photosyn-
1210 thetic rates achieved with greater N_{area} at lower stomatal conductance and lower
1211 leaf $C_i:C_a$ (Wright et al. 2003; Prentice et al. 2014; Paillassa et al. 2020). Alter-
1212 natively, an increase in soil moisture should reduce costs of water acquisition and
1213 use, increasing β (Lavergne et al. 2020), stomatal conductance, and leaf $C_i:C_a$, re-
1214 sulting in optimal photosynthetic rates achieved with decreased N_{area} . The theory
1215 also predicts variability in stomatal conductance and N_{area} in response to climatic
1216 factors, suggesting that the optimal response to increased vapor pressure deficit
1217 should be a reduction in stomatal conductance and leaf $C_i:C_a$ that is counter-
1218 balanced by an increase in N_{area} to support the greater photosynthetic capacity
1219 needed to maintain high assimilation at lower conductance (Grossiord et al. 2020;
1220 Dong et al. 2020; López et al. 2021; Westerband et al. 2023).

1221 Leaf nitrogen allocation responses to changing climates or soil resource
1222 availability may also depend on their mode of nutrient acquisition or photo-

1223 synthetic pathway. For example, species that form associations with symbiotic
1224 nitrogen-fixing bacteria (referred as “N-fixing species” from this point forward)
1225 should, in theory, have access to less finite nitrogen supply than species not capa-
1226 ble of forming such associations (referred as “non-fixing species” from this point
1227 forward), which may result in lower β values in N-fixing species than non-fixing
1228 species. This result was previously shown in a greenhouse experiment, where a
1229 leguminous species generally had lower costs of nitrogen acquisition compared to a
1230 non-leguminous species, although these differences were generally stronger under
1231 increased nitrogen limitation (Perkowski et al. 2021). Lower β values could be an
1232 explanation for why N-fixing species commonly have greater leaf nitrogen content
1233 than non-fixing species (Adams et al. 2016; Dong et al. 2017).

1234 Similarly, leaf nitrogen allocation patterns across environmental gradients
1235 may be dependent on photosynthetic pathway. Lower leaf $C_i:C_a$ values in C₄
1236 species suggests that C₄ species should have lower β values than C₃ species (Scott
1237 and Smith 2022), a pattern that could be the result of increased costs associated
1238 with water acquisition and use or reduced costs of nitrogen acquisition and use
1239 relative to C₃ species. Theory predicts that this response in C₄ species will cause
1240 C₄ species to have higher leaf nitrogen content on average compared to C₃ species,
1241 though ample evidence exists documenting general lower leaf nitrogen content in
1242 C₄ species (Schmitt and Edwards 1981; Sage and Pearcy 1987; Ghannoum et al.
1243 2011). No study to date has directly quantified β in C₄ species aside from the
1244 initial parameterization of β in an optimality model for C₄ species (Scott and
1245 Smith 2022) using a global dataset of leaf $\delta^{13}\text{C}$ values (Cornwell et al. 2018).

1246 While photosynthetic least-cost theory provides a unified framework for

1247 understanding integrated effects of climate and soil resource availability on N_{area} ,
1248 empirical tests of the theory are sparse. Previous work shows that increasing
1249 soil nitrogen availability decreases costs of acquiring nutrients (Bae et al. 2015;
1250 Perkowski et al. 2021; Lu et al. 2022), which can induce predictable nutrient-
1251 water use tradeoffs expected from the theory across broad environmental gradients
1252 (Paillassa et al. 2020; Querejeta et al. 2022; Westerband et al. 2023) and in
1253 manipulation experiments (Bialic-Murphy et al. 2021). Additionally, increasing
1254 vapor pressure deficit has been shown to have a positive effect on N_{area} , which is
1255 commonly associated with reduced leaf $C_i:C_a$ (Dong et al. 2017; Dong et al. 2020;
1256 Firn et al. 2019; López et al. 2021).

1257 Despite evidence for patterns expected from photosynthetic least-cost the-
1258 ory, studies have been restricted to exploring these patterns in C₃ species and,
1259 while variance in N_{area} across environmental gradients has been shown to be driven
1260 by strong negative relationships with leaf $C_i:C_a$ (Dong et al. 2017; Paillassa et al.
1261 2020; Westerband et al. 2023), no study has explicitly investigated effects of soil
1262 resource availability or species identity on N_{area} using β as a direct predictor of
1263 leaf $C_i:C_a$. Furthermore, as N_{area} can be broken down into structural (leaf mass
1264 per area; M_{area} ; g m⁻²) and metabolic (mass-based leaf nitrogen content; N_{mass} ;
1265 gN g⁻¹) components (Dong et al. 2017), no study has investigated which compo-
1266 nent of N_{area} drives the hypothesized response of N_{area} to leaf $C_i:C_a$, which limits
1267 our ability to assess whether changes in N_{area} across environmental gradients are
1268 driven by changes in leaf morphology (i.e. M_{area}), leaf stoichiometry (i.e. N_{mass}),
1269 or both.

1270 In this study, I measured N_{area} , N_{mass} , M_{area} , leaf $\delta^{13}\text{C}$ -derived estimates

1271 of leaf $C_i:C_a$, and leaf $\delta^{13}\text{C}$ -derived estimates of β in 504 individuals spanning
1272 52 species scattered across 24 grassland sites in Texas, USA. The state of Texas
1273 contains a diverse climatic gradient, indicated by 2006-2020 mean annual precipi-
1274 tation totals ranging from 204 to 1803 mm and 2006-2020 mean annual tempera-
1275 ture ranging from 11.8° to 24.6°C within state boundaries (Fig. 4.1). Variability
1276 in soil nitrogen availability and soil moisture was expected across sites, owing to
1277 differences in soil texture and aboveground climate that would drive differential
1278 rates of water retention and nitrogen transformations to plant-available nitrogen
1279 substrate. I leveraged the expected climatic and soil resource variability across
1280 sites to test the following hypotheses:

- 1281 1. Soil nitrogen availability will decrease β through a reduction in costs of
1282 nitrogen acquisition and use, while soil moisture will increase β through a
1283 reduction in costs of water acquisition and use. Following previous results, I
1284 expected that N-fixing species would have lower β values and that C_4 species
1285 would have lower β values.
- 1286 2. Leaf $C_i:C_a$ will be positively related to β , a pattern that will result in a
1287 negative indirect effect of increasing soil nitrogen availability on leaf $C_i:C_a$,
1288 a positive indirect effect of increasing soil moisture on leaf $C_i:C_a$, and lower
1289 leaf $C_i:C_a$ in both N-fixing species and C_4 species. I expected that leaf
1290 $C_i:C_a$ would be negatively related to vapor pressure deficit, as increasing
1291 atmospheric dryness would cause plants to close stomata to minimize water
1292 loss.
- 1293 3. N_{area} will be negatively related to leaf $C_i:C_a$. This response will result in an
1294 indirect positive and negative effect of increasing soil nitrogen availability

1295 and soil moisture, respectively, on N_{area} , and larger N_{area} values in N-fixing
1296 species. While theory predicts that lower β values in C₄ species should
1297 yield larger N_{area} in C₄ species, I expected that C₄ species would have lower
1298 N_{area} than C₃ species due to greater nitrogen use efficiency in C₄ species.
1299 Additionally, I expected vapor pressure deficit to increase N_{area} , a pattern
1300 that would be directly mediated through the reduction in leaf $C_i:C_a$ with
1301 increasing vapor pressure deficit.

1302 4.2 Methods

1303 4.2.1 *Site descriptions and sampling methodology*

1304 Leaf and soil samples were collected from 24 open canopy grassland sites scattered
1305 across central and eastern Texas in summer 2020 and summer 2021 (Fig. 4.1).
1306 Twelve sites were visited between June and July 2020 and 14 sites (11 unique from
1307 2020) were visited between May and June 2021 (Table 4.1). Sites were chosen to
1308 maximize precipitation and edaphic variability across sites (Table 4.1). No site
1309 with personally communicated or anecdotal evidence of grazing or disturbance
1310 (e.g., mowing, feral hog activity, etc.) was used. Leaf material was collected
1311 from three individuals each of the five most abundant species at random locations
1312 at each site, only selecting species that were broadly classified as graminoid or
1313 forb/herb growth habits per the USDA PLANTS database (USDA NRCS 2022).
1314 All collected leaves were fully expanded with no visible herbivory or other external
1315 damage and also free from shading by nearby shrubs or trees. Five soil samples
1316 were collected from 0-15 cm below the soil surface at each site near the leaf
1317 collection sample locations. Soil samples were mixed together by hand to create

1318 one composite soil sample per site.

1319 4.2.2 *Leaf trait measurements*

1320 Images of each leaf were taken immediately following each site visit using a flat-
1321 bed scanner. Fresh leaf area was determined from each image using the ‘LeafArea’
1322 R package (Katabuchi 2015), which automates leaf area calculations using ImageJ
1323 software (Schneider et al. 2012). Each leaf was dried at 65°C for at least 48 hours
1324 to a constant mass, weighed, and manually ground in a mortar and pestle until
1325 homogenized. Leaf mass per area (M_{area} ; g m⁻²) was calculated as the ratio of
1326 dry leaf biomass to fresh leaf area. Subsamples of dried and homogenized leaf
1327 tissue were used to measure leaf nitrogen content (N_{mass} ; gN g⁻¹) through ele-
1328 mental combustion analysis (Costech-4010, Costech Instruments, Valencia, CA).
1329 Leaf nitrogen content per unit leaf area (N_{area} ; gN m⁻²) was calculated as the
1330 product of N_{mass} and M_{area} .

1331 Subsamples of dried and homogenized leaf tissue were sent to the University
1332 of California-Davis Stable Isotope Facility to determine leaf $\delta^{13}\text{C}$. Leaf $\delta^{13}\text{C}$ values
1333 were determined using an elemental analyzer (PDZ Europa ANCA-GSL; Sercon
1334 Ltd., Chestshire, UK) interfaced to an isotope ratio mass spectrometer (PDZ
1335 Europa 20-20 Isotope Ratio Mass Spectrometer, Sercon Ltd., Chestshire, UK).
1336 I used leaf $\delta^{13}\text{C}$ values (‰; relative to Vienna Pee Dee Belemnite international
1337 reference standard) to estimate the ratio of intercellular (C_i) to extracellular (C_a)
1338 CO₂ ratio (leaf $C_i:C_a$; unitless) following the approach of Farquhar et al. (1989)
1339 described in Cernusak et al. (2013). Specifically, I derived leaf $C_i:C_a$ as:

$$C_i : C_a = \frac{\Delta^{13}C - a}{b - a} \quad (4.1)$$

1340 where $\Delta^{13}C$ represents the relative difference between leaf $\delta^{13}\text{C}$ (‰) and air $\delta^{13}\text{C}$

1341 (‰), calculated as:

$$\Delta^{13}C = \frac{\delta^{13}C_{air} - \delta^{13}C_{leaf}}{1 + \delta^{13}C_{leaf}} \quad (4.2)$$

1342 $\delta^{13}\text{C}_{air}$, which is commonly assumed to be -8‰ (Keeling et al. 1979; Farquhar

1343 et al. 1989), was calculated as a function of calendar year t using an empirical

1344 equation derived in Feng (1999):

$$\delta^{13}C_{air} = -6.429 - 0.006e^{0.0217(t-1740)} \quad (4.3)$$

1345 Using this equation, $\delta^{13}\text{C}_{air}$ values were set to -9.04‰ and -9.09‰ for 2020 and

1346 2021, respectively. The parameter a represents the fractionation between ^{12}C

1347 and ^{13}C due to diffusion in air, assumed to be 4.4‰, while b represents the

1348 fractionation caused by Rubisco carboxylation, assumed to be 27‰ (Farquhar

1349 et al. 1989). For C_4 species, b in Eqn. 4.1 was set to 6.3‰, and was derived from:

$$b = c + (d \cdot \phi) \quad (4.4)$$

1350 Where c was set to -5.7‰ and d was set to 30‰ (Farquhar et al. 1989). ϕ , which

1351 is the bundle sheath leakiness term, was set to 0.4. All leaf $C_i:C_a$ values less than

1352 0.1 and greater than 0.95 were assumed to be incorrect and removed from the

1353 analysis.

1354 I derived the unit cost of resource use (β) using leaf $C_i:C_a$ and site climate

1355 data using equations first described in Prentice et al. (2014) and simplified in

1356 Lavergne et al. (2020):

$$\beta = 1.6\eta^*VPD \frac{\chi - (\frac{\Gamma^*}{C_a})^2}{(1 - \chi)^2(K_m + \Gamma^*)} \quad (4.5)$$

1357 where η^* is the viscosity of water relative to 25°C, calculated using elevation and

1358 mean air temperature of the seven days leading up to each site visit following equa-

1359 tions in Huber et al. (2009). VPD (Pa) was set to the mean vapor pressure deficit

1360 of the seven days leading up to each site visit, C_a represents atmospheric CO₂

1361 concentration, arbitrarily set to 420 μmol mol⁻¹ CO₂. K_m (Pa) is the Michaelis-

1362 Menten coefficient for Rubisco affinity to CO₂ and O₂, calculated as:

$$K_m = K_c \cdot \left(1 + \frac{O_i}{K_o}\right) \quad (4.6)$$

1363 where K_c (Pa) and K_o (Pa) are the Michaelis-Menten coefficients for Rubisco

1364 affinity to CO₂ and O₂, respectively, and O_i is the intercellular O₂ concentration.

1365 Γ^* (Pa) is the CO₂ compensation point in the absence of dark respiration. K_c , K_o ,

1366 and Γ^* were determined using equations described in Medlyn et al. (2002) and

1367 derived in Bernacchi et al. (2001), invoking an elevation correction for atmospheric

1368 pressure as explained in Stocker et al. (2020).

Table 4.1. Site locality information, sampling year, 2006-2020 mean annual precipitation (MAP; mm), mean annual temperature (MAT; °C), and water holding capacity (WHC; mm)*

Site	Latitude	Longitude	Sampling year	MAP	MAT	WHC
Edwards_2019_17	29.95	-100.36	2020	563.5	19.0	224.7
Uvalde_2020_02	29.59	-100.09	2020, 2021	648.5	19.5	224.7
Menard_2020_01	30.91	-99.59	2020	641.9	18.3	220.2
Kerr_2020_03	30.06	-99.34	2021	672.4	18.3	237.5
Bandera_2020_03	29.85	-99.30	2021	789.4	18.8	235.1
Sansaba_2020_01	31.29	-98.62	2020	733.0	18.8	234.3
Comal_2020_21	29.79	-98.43	2020	878.5	19.9	220.7
Blanco_2019_16	29.99	-98.43	2020	833.0	19.2	222.2
Bexar_2019_13	29.24	-98.43	2020	759.3	21.5	206.0
Burnet_2020_14	30.84	-98.34	2021	763.3	19.5	217.8
Comal_2020_19	30.01	-98.32	2021	845.0	19.3	220.4
Hays_2020_54	29.96	-98.17	2021	861.3	20.0	225.6
Burnet_2020_12	30.82	-98.06	2021	815.1	19.4	245.3
Williamson_2019_09	30.71	-97.86	2020	867.7	19.7	270.2
Williamson_2019_10	30.54	-97.77	2020	819.5	19.9	239.8
Bell_2021_08	31.06	-97.55	2021	937.3	19.6	232.3
Fayette_2021_12	29.86	-97.21	2021	985.7	20.4	165.6
Fayette_2019_04	30.09	-96.78	2020	1017.4	20.6	226.9
Fayette_2020_09	29.86	-96.71	2021	1002.7	20.8	187.6
Washington_2020_08	30.28	-96.41	2021	1077.4	20.4	203.9
Austin_2020_03	29.78	-96.24	2021	1108.7	20.6	253.0
Brazos_2020_16	30.93	-96.23	2021	1078.0	20.1	202.2
Brazos_2020_18	30.52	-96.21	2020, 2021	1099.4	20.4	233.5
Harris_2020_03	29.88	-95.31	2020, 2021	1492.0	21.6	265.6

1369 * Rows are arranged by longitude to visualize precipitation variability across sites

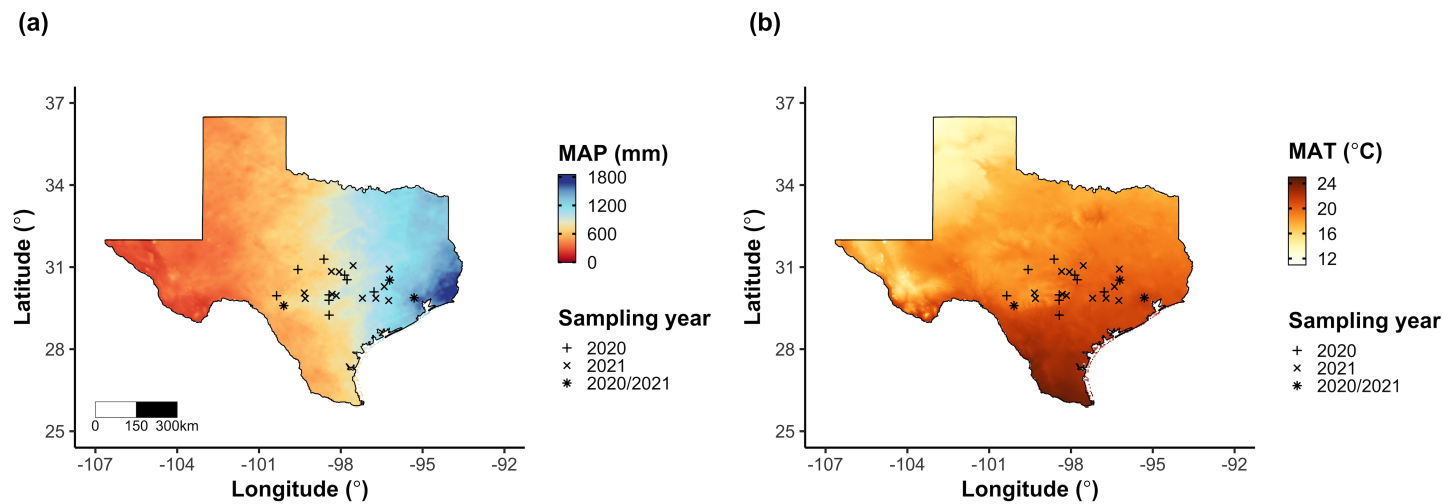


Figure 4.1. Site locations along 2006-2020 mean annual precipitation (a) and mean annual temperature (b) gradients in Texas, USA. Precipitation and temperature data were plotted using PRISM data at a 4-km grid resolution and are masked to include only grid cells that occur within the Texas state boundary of the United States. In both panels, addition signs refer to sites visited in 2020, multiplication signs to sites visited in 2021, and asterisks to sites visited in 2020 and 2021. The scale bar in (a) also applies to (b).

1370 4.2.3 *Site climate data*

1371 I used the Parameter elevation Regressions on Independent Slopes Model (PRISM)
1372 (Daly et al. 2008) climate product to access gridded daily temperature and precip-
1373 itation data for the coterminous United States at a 4-km grid resolution between
1374 January 1, 2006 and July 31, 2021 (PRISM Climate Group, Oregon State Uni-
1375 versity, <https://prism.oregonstate.edu>, data created 4 Feb 2014, accessed 24
1376 Mar 2022). Mean daily air temperature, mean daily vapor pressure deficit, and
1377 total daily precipitation data were extracted from the grid cell that contained the
1378 latitude and longitude of each property using the ‘extract’ function in the ‘terra’
1379 R package (Hijmans 2022). PRISM data were used in lieu of local weather sta-
1380 tion data because several rural sites did not have a local weather station present
1381 within a 20-km radius of the site. Daily site climate data were used to estimate
1382 mean annual precipitation and mean annual temperature for each site between
1383 2006 and 2020 (Table 4.1). I calculated total precipitation and mean daily vapor
1384 pressure deficit for the prior 1, 2, 3, 4, 5, 6, 7, 8, 9, 10, 15, 20, 25, 30, 60, and 90
1385 days leading up to each site visit. Temperature was not included in any analy-
1386 sis due to the close range in mean annual temperature between sites (mean±SD:
1387 $19.8 \pm 0.9^\circ\text{C}$; Table 4.1).

1388 4.2.4 *Site edaphic characteristics*

1389 Composted soil samples were sent to the Texas A&M Soil, Water and Forage
1390 Laboratory to quantify soil nitrate concentration ($\text{NO}_3\text{-N}$; ppm). Soil $\text{NO}_3\text{-N}$
1391 was determined by extracting composite soil samples in 1 M KCl, measuring
1392 absorbance values of extracts at 520 nm using the end product of a $\text{NO}_3\text{-N}$ to

1393 NO₂-N cadmium reduction reaction (Kachurina et al. 2000; Keeney and Nelson
1394 1983). Soil texture data from 0-15 cm below the soil surface were accessed using
1395 the SoilGrids2.0 data product (Poggio et al. 2021) through the ‘fetchSoilGrids’
1396 function in the ‘soilDB’ R package (Beaudette et al. 2022). I used SoilGrids2.0
1397 to access soil texture data in lieu of analyses using the composite soil sample due
1398 to a lack of soil material from some sites after sending samples for soil NO₃-N.

1399 Soil moisture was not measured in the field, but was estimated using the
1400 ‘Simple Process-Led Algorithms for Simulating Habitats’ model (SPLASH) (Davis
1401 et al. 2017). This model, derived from the STASH model (Cramer and Prentice
1402 1988), spins up a bucket model using Priestley-Taylor equations (Priestley and
1403 Taylor 1972) to calculate daily soil moisture (W_n ; mm) as a function of the previous
1404 day’s soil moisture (W_{n-1} ; mm), daily precipitation (P_n ; mm), condensation (C_n ;
1405 mm), actual evapotranspiration (E_n^a ; mm), and runoff (RO; mm):

$$W_n = W_{n-1} + P_n + C_n - E_n^a - RO \quad (4.7)$$

1406 Models were spun up by equilibrating the previous day’s soil moisture using succes-
1407 sive model iterations with daily mean air temperature, daily precipitation total,
1408 the number of daily sunlight hours, and latitude as model inputs (Davis et al.
1409 2017). Daily sunlight hours were estimated for each day at each site using the
1410 ‘getSunlightTimes’ function in the ‘suncalc’ R package, which estimated sunrise
1411 and sunset times of each property using date and site coordinates (Thieurmel and
1412 Elmarhraoui 2019). Water holding capacity (mm), or bucket size, was estimated
1413 as a function of soil texture using pedotransfer equations explained in Saxton and

1414 Rawls (2006), as done in Stocker et al. (2020) and Bloomfield et al. (2023). A
1415 summary of these equations is included in Appendix C.1.

1416 Daily soil moisture outputs from the SPLASH model for each site were
1417 used to calculate mean daily soil moisture for the prior 1, 2, 3, 4, 5, 6, 7, 8, 9,
1418 10, 15, 20, 25, 30, 60, and 90 days leading up to each site visit. Mean daily
1419 soil moisture values were then expressed as a fraction of water holding capacity
1420 to normalize across sites with different bucket depths, as done in Stocker et al.
1421 (2018). Site water holding capacity values are referenced in Table 4.1.

1422 4.2.5 *Plant functional group assignments*

1423 Plant functional group was assigned to each species and used as the primary de-
1424 scriptor of species identity. Specifically, plant functional groups were assigned
1425 based on photosynthetic pathway (C_3 , C_4) and ability to form associations with
1426 symbiotic nitrogen-fixing bacteria (N-fixer, non-fixer). The ability to form asso-
1427 ciations with symbiotic nitrogen-fixing bacteria was assigned based on whether
1428 species were in the *Fabaceae* family, and photosynthetic pathway of each species
1429 was determined from past literature and confirmed through leaf $\delta^{13}C$ values. I
1430 chose these plant functional groups based on *a priori* hypotheses regarding the
1431 functional role of nitrogen fixation and photosynthetic pathway on the sensitivity
1432 of plant nitrogen uptake and leaf nitrogen allocation to soil nitrogen availability
1433 and aboveground growing conditions. These plant functional group classifications
1434 resulted in three distinct plant functional groups within our dataset: C_3 N-fixers
1435 (n=53), C_3 non-fixers (n=334), and C_4 non-fixers (n=117).

1436 4.2.6 *Data analysis*

1437 All analyses and plotting were conducted in R version 4.1.1 (R Core Team 2021).

1438 I constructed a series of separate linear mixed-effects models to investigate en-

1439 vironmental drivers of β , leaf $C_i:C_a$, N_{area} , N_{mass} , and M_{area} , followed by a path

1440 analysis using a piecewise structural equation model to investigate direct and

1441 indirect effects of climate and soil resource availability on N_{area} .

1442 To explore environmental drivers of β , I built a linear mixed-effects model

1443 that included soil moisture, soil nitrogen availability, and plant functional group

1444 as fixed effect coefficients. Species were designated as a random intercept term.

1445 Interaction coefficients between all possible combinations of the three fixed effect

1446 coefficients were also included. β was natural log transformed to linearize data.

1447 I used an information-theoretic model selection approach to determine whether

1448 90-, 60-, 30-, 20-, 15-, 10-, 9-, 8-, 7-, 6-, 5-, 4-, 3-, 2-, or 1-day mean daily soil

1449 moisture conferred the best model fit for β . To do this, I constructed 16 separate

1450 linear mixed-effects models where log-transformed β was included as the response

1451 variable and each soil moisture time step was separately included as a single

1452 continuous fixed effect. Species were included as a random intercept term for all

1453 models. I used corrected Akaike Information Criterion (AICc) to select the soil

1454 moisture timescale that conferred the best model fit, indicated by the model with

1455 the lowest AICc score (Table C3; Fig. C1).

1456 To explore environmental drivers of leaf $C_i:C_a$, I constructed a second lin-

1457 ear mixed effects model that included vapor pressure deficit, soil moisture, soil

1458 nitrogen availability, and plant functional group as fixed effect coefficients. Two-

1459 way interactions between plant functional group and vapor pressure deficit, soil

1460 nitrogen availability, or soil moisture were included as additional fixed effect coef-
1461 ficients, in addition to a three-way interaction between soil moisture, soil nitrogen
1462 availability, and plant functional group. Species were included as a random inter-
1463 cept term. I used an information-theoretic model selection approach to determine
1464 whether 90-, 60-, 30-, 20-, 15-, 10-, 9-, 8-, 7-, 6-, 5-, 4-, 3-, 2-, or 1-day mean daily
1465 vapor pressure deficit conferred the best model fit for leaf $C_i:C_a$ using the same
1466 approach explained above for the soil moisture effect on β . The soil moisture
1467 timescale was set to the same timescale that conferred the best fit for β .

1468 To explore environmental drivers of N_{area} , N_{mass} , and M_{area} , I constructed
1469 a linear mixed effects model for each trait, including leaf $C_i:C_a$, soil nitrogen
1470 availability, soil moisture, and plant functional group as fixed effect coefficients
1471 for each model. Two-way interactions between plant functional group and β , leaf
1472 $C_i:C_a$, soil nitrogen availability, or soil moisture were included as additional fixed
1473 effect coefficients, in addition to a three-way interaction between soil nitrogen
1474 availability, soil moisture, and plant functional group. Species were included as a
1475 random intercept term, with the soil moisture timescale set to the same timescale
1476 that conferred the best fit for β .

1477 In all linear mixed-effects models explained above, including those to select
1478 relevant timescales, I used the ‘lmer’ function in the ‘lme4’ R package (Bates et al.
1479 2015) to fit each model and the ‘Anova’ function in the ‘car’ R package (Fox and
1480 Weisberg 2019) to calculate Type II Wald’s χ^2 and determine the significance
1481 level ($\alpha=0.05$) of each fixed effect coefficient. I used the ‘emmeans’ R package
1482 (Lenth 2019) to conduct post-hoc comparisons using Tukey’s tests, where degrees
1483 of freedom were approximated using the Kenward-Roger approach (Kenward and

1484 Roger 1997). Trendlines and error ribbons for all plots were drawn using a series
1485 of ‘emmeans’ outputs across the range in plotted x-axis values.

1486 Finally, I conducted a path analysis using a piecewise structural equation
1487 model to examine direct and indirect pathways that determined variance in N_{area} .
1488 Six separate linear mixed effects models were loaded into the piecewise structural
1489 equation model. Models were constructed per *a priori* hypotheses following pat-
1490 terns expected from photosynthetic least-cost theory. The first model regressed
1491 N_{area} against N_{mass} and M_{area} . The second model regressed M_{area} against leaf
1492 $C_i:C_a$ and soil nitrogen availability. The third model regressed N_{mass} against
1493 leaf $C_i:C_a$ and M_{area} (Dong et al. 2017; Dong et al. 2020). The fourth model re-
1494 gressed leaf $C_i:C_a$ against β and vapor pressure deficit. The fifth model regressed β
1495 against soil nitrogen availability, soil moisture, ability to associate with symbiotic
1496 nitrogen-fixing bacteria, and photosynthetic pathway. The sixth model regressed
1497 soil nitrogen availability against soil moisture. All models included the relevant
1498 timescale selected in the individual linear mixed effect models explained above.
1499 Models included species as a random intercept term, were built using the ‘lme’
1500 function in the ‘nlme’ R package (Pinheiro and Bates 2022), and subsequently
1501 loaded into the piecewise structural equation model using the ‘psem’ function in
1502 the ‘piecewiseSEM’ R package (Lefcheck 2016).

1503 4.3 Results

1504 4.3.1 *Cost to acquire nitrogen relative to water*

1505 Model selection indicated that 90-day mean soil moisture conferred the best model

1506 fit for β (AICc=1387.54; Table C3; Fig. C1).

1507 Increasing soil nitrogen availability generally decreased β ($p<0.001$; Table

1508 4.2; Fig. 4.2a), a pattern driven by a negative effect of increasing soil nitrogen on β

1509 in C₃ non-fixers (Tukey: $p=0.005$) and C₃ N-fixers (Tukey: $p=0.035$) despite a null

1510 effect of increasing soil nitrogen on β in C₄ non-fixers (Tukey: $p=0.856$). There

1511 was no effect of soil moisture on β ($p=0.872$; Table 4.2; Fig. 4.2b). A functional

1512 group effect ($p<0.001$; Table 4.2) indicated that C₄ non-fixers generally had lower

1513 β values than both C₃ N-fixers and C₃ non-fixers (Tukey: $p<0.001$ in both cases),

1514 while β values in C₃ N-fixers did not differ from C₃ non-fixers (Tukey: $p=0.854$).

Table 4.2. Effects of soil moisture, soil nitrogen availability, and plant functional group on β (unitless)*

	df	Coefficient	χ^2	p
Intercept	-	3.39E+00	-	-
Soil moisture (SM ₉₀)	1	-1.96E-01	0.026	0.872
Soil N (N)	1	-1.42E-02	12.031	<0.001
PFT	2	-	199.617	<0.001
SM ₉₀ *N	1	-3.02E-03	1.000	0.317
SM ₉₀ *PFT	2	-	0.623	0.732
N*PFT	2	-	5.271	0.072
SM ₉₀ *N*PFT	2	-	5.271	0.182

1515 *Significance determined using Type II Wald χ^2 tests ($\alpha=0.05$). P-values<0.05
1516 are in bold. Model coefficients are expressed on the natural-log scale and are only
1517 included for continuous fixed effects. Key: df=degrees of freedom; χ^2 =Wald Type
1518 II chi-square test statistic

1519 [DWS: exponential notation not used correctly in these tables. Looks

1520 copied from a graphing calculator output]

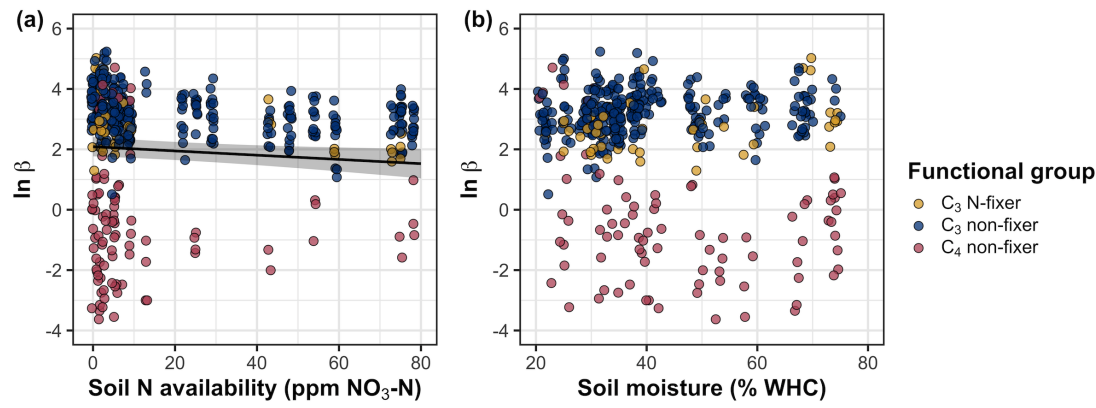


Figure 4.2. Effects of soil nitrogen availability (a) and soil moisture (b) on the cost of acquiring and using nitrogen (β ; unitless). Soil nitrogen availability is represented on the x-axis in (a), soil moisture is represented on the x-axis in (b) as a percent of site water holding capacity, and natural-log transformed β is represented on the y-axis for both panels. Yellow points represent C_3 N-fixers, blue points represent C_3 non-fixers, and red points represent C_4 non-fixers. Throughout, points are jittered for visibility. A black solid trendline is drawn to denote bivariate relationships where the slope is different from zero ($p < 0.05$), with error ribbons representing the upper and lower 95% confidence intervals.

1521 4.3.2 *Leaf C_i:C_a*

1522 Model selection indicated that 4-day mean vapor pressure deficit was the timescale

1523 that conferred the best model fit for leaf $C_i:C_a$ (AICc=-755.81; Table C3; Fig. C1).

1524 Model results revealed that increasing vapor pressure deficit generally de-

1525 creased leaf $C_i:C_a$ ($p<0.001$; Table 4.3; Fig. 4.3a). There was no effect of soil mois-

1526 ture ($p=0.549$; Table 4.3; Fig. 4.3b) or soil nitrogen availability ($p=0.549$; Table

1527 4.3; Fig. 4.3c) on leaf $C_i:C_a$. A strong plant functional group effect ($p<0.001$; Ta-

1528 ble 4.3) indicated that C₄ non-fixers had lower leaf $C_i:C_a$ than C₃ N-fixers and C₃

1529 non-fixers (Tukey: $p<0.001$ in both cases), with no difference between C₃ N-fixers

1530 and C₃ non-fixers (Tukey: $p=0.866$).

Table 4.3. Effects of soil moisture, soil nitrogen availability, and plant functional group on leaf $C_i:C_a$ (unitless)*

	df	Coefficient	χ^2	<i>p</i>
Intercept	-	1.32E+00	-	-
Vapor pressure deficit (VPD_4)	1	-4.53E-01	10.987	<0.001
Soil moisture (SM_{90})	1	-1.71E-01	0.039	0.843
Soil N (N)	1	-1.71E-03	0.043	0.549
PFT	2	-	205.274	<0.001
SM_{90}^*N	1	7.29E-03	2.266	0.132
VPD_4^*PFT	2	-	0.887	0.642
SM_{90}^*PFT	2	-	0.814	0.666
N^*PFT	2	-	4.158	0.125
$SM_{90}^*N^*PFT$	2	-	3.465	0.177

1531 *Significance determined using Type II Wald χ^2 tests ($\alpha=0.05$). *P*-values less
1532 than 0.05 are in bold and *p*-values where $0.05 < p < 0.1$ are italicized. Leaf $C_i:C_a$
1533 was not transformed prior to model fitting, so model coefficients are reported
1534 on the response scale. Model coefficients are only included for continuous fixed
1535 effects. Key: df=degrees of freedom; χ^2 =Wald Type II chi-square test statistic

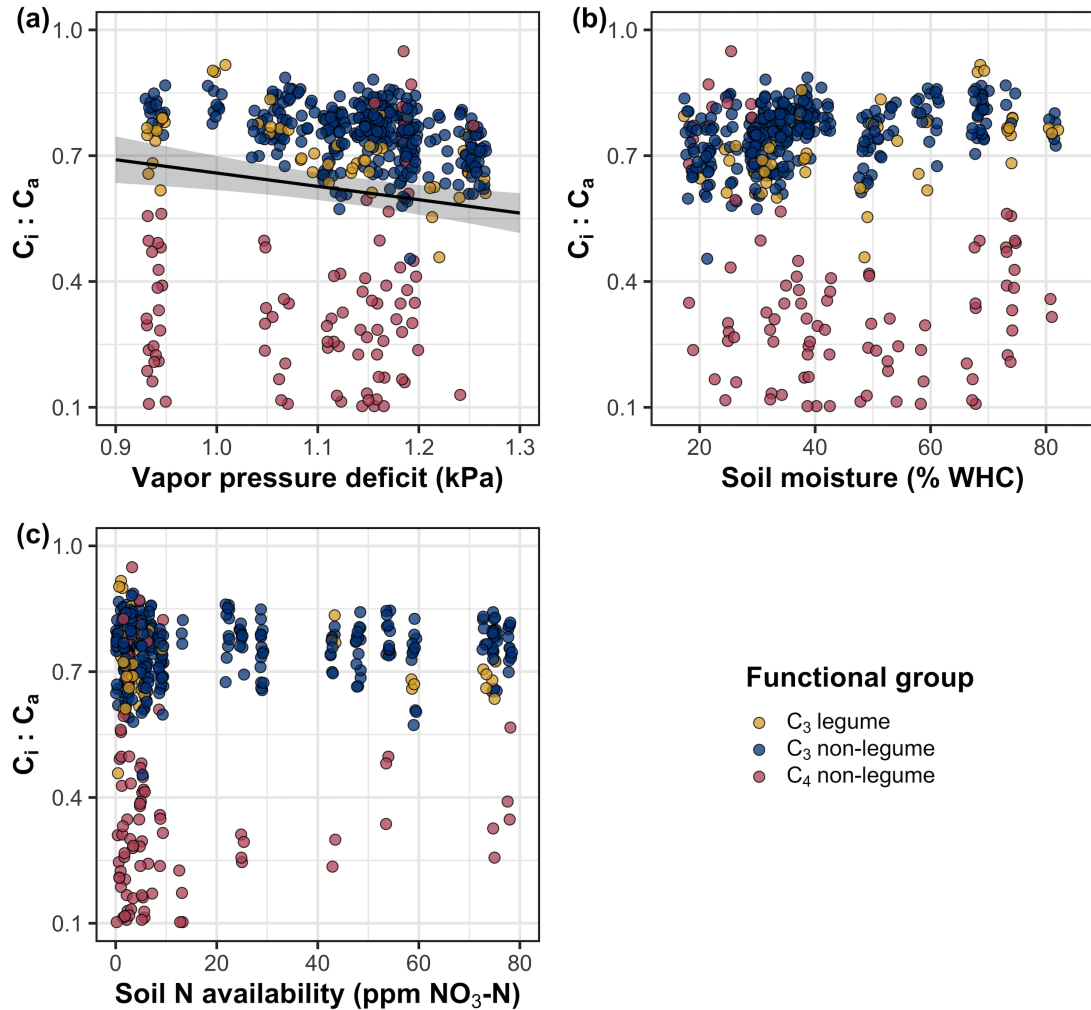


Figure 4.3. Effects of 4-day mean vapor pressure deficit (a), 90-day soil moisture (per water holding capacity; b), and soil nitrogen availability (c) on leaf $C_i:C_a$. Shading and trendlines are as explained in Figure 4.2. Points are jittered for visibility. Variably colored trendlines are only included if there is an interaction between the x-axis and plant functional group, where solid trendlines indicate slopes that are different from zero ($p < 0.05$) and dashed trendlines indicate slopes that are not different from zero ($p > 0.05$). Error ribbons represent the upper and lower 95% confidence intervals of each fitted trendline.

1536 4.3.3 *Leaf nitrogen content*

1537 An interaction between leaf $C_i:C_a$ and plant functional group ($p<0.001$; Table 4.4) revealed that the negative effect of increasing leaf $C_i:C_a$ on N_{area} ($p<0.001$; Table 4.4) was driven by a negative effect of increasing leaf $C_i:C_a$ on N_{area} in **1539** C_3 non-fixers and C_3 N-fixers (Tukey: $p<0.001$ in both cases), but not C_4 non-**1540** fixers (Tukey: $p=0.786$; Fig. 4.4a). A marginal interaction between soil nitrogen availability and plant functional group ($p=0.057$; Table 4.4) indicated that the positive effect of increasing soil nitrogen ($p=0.007$; Table 4.4) was only apparent **1542** in C_3 N-fixers (Tukey: $p<0.001$; Table 4.4; Fig. 4.4d), but not C_3 non-fixers **1543** (Tukey: $p=0.329$) or C_4 non-fixers (Tukey: $p=0.682$). Increasing soil moisture **1544** increased N_{area} ($p=0.011$, Table 4.4). A plant functional group effect ($p<0.001$; Table 4.4) indicated that C_4 non-fixers had lower N_{area} compared to C_3 N-fixers **1546** and C_3 non-fixers (Tukey: $p<0.001$ in both cases), while C_3 N-fixers had lower **1547** N_{area} compared to C_3 non-fixers (Tukey: $p=0.024$).

1550 Leaf $C_i:C_a$ had no effect on N_{mass} ($p=0.455$; Table 4.4; Fig. 4.4b). Increasing soil nitrogen availability and soil moisture each had a positive effect on N_{mass} ($p<0.001$ in both cases; Table 4.4; Fig. 4.4h). A plant functional group effect ($p<0.001$; Table 4.4) indicated that C_4 non-fixers had lower N_{mass} compared to C_3 N-fixers and C_3 non-fixers (Tukey: $p=0.001$ in both cases), while N_{mass} did not differ between C_3 N-fixers and C_3 non-fixers (Tukey: $p=0.323$).

1556 Variance in M_{area} was driven by a three-way interaction between soil nitrogen availability, soil moisture, and plant functional group ($p=0.018$; Table 4.4). **1557** This interaction indicated that increasing soil moisture increased the positive effect **1558** of increasing soil nitrogen availability on M_{area} in C_3 N-fixers (Tukey: $p=0.028$)

1560 but did not modify the negative effect of increasing soil nitrogen availability on
1561 M_{area} in C₄ non-fixers (Tukey: $p=0.806$) or C₃ non-fixers (Tukey: $p=0.998$). There
1562 was otherwise no effect of soil moisture on M_{area} ($p=0.436$; Table 4.4). An inter-
1563 action between leaf $C_i:C_a$ and plant functional group ($p<0.001$; Table 4.4; Fig.
1564 4.4c) indicated that the negative effect of increasing leaf $C_i:C_a$ on M_{area} ($p<0.001$;
1565 Table 4.4) was driven by a negative effect of increasing leaf $C_i:C_a$ on M_{area} in
1566 C₃ N-fixers (Tukey: $p<0.001$) and C₃ non-fixers(Tukey: $p=0.003$), but not C₄
1567 non-fixers (Tukey: $p=0.257$; Fig. 4.4c).

Table 4.4. Effects of soil moisture, soil nitrogen availability, plant functional group, and leaf $C_i:C_a$ on leaf nitrogen content per unit leaf area (N_{area} ; gN m⁻²), leaf nitrogen content per unit leaf biomass (N_{mass} ; gN g⁻¹), and leaf biomass per unit leaf area (M_{area} ; g m⁻²)

		N_{area}			N_{mass}			M_{area}		
	df	Coefficient	χ^2	p	Coefficient	χ^2	p	Coefficient	χ^2	p
(Intercept)	-	2.41E+00	-	-	7.72E-02	-	-	6.91E+00	-	-
$C_i:C_a$	1	-2.32E+00	6.841	0.009	7.91E-01	0.558	0.455	-3.13E+00	15.913	<0.001
Soil N (N)	1	1.26E-02	7.072	0.011	1.21E-02	87.457	<0.001	-2.66E-02	41.791	<0.001
Soil moisture (SM ₉₀)	1	5.60E-01	6.493	0.011	7.94E-01	10.889	<0.001	-2.54E-01	0.605	0.437
PFT	1	-	49.273	<0.001	-	21.786	<0.001	-	6.673	0.036
SM ₉₀ *N	1	5.45E-02	0.482	0.488	-2.18E-02	2.606	0.106	8.16E-02	0.791	0.374
$C_i:C_a$ *PFT	1	-	24.380	<0.001	-	5.367	0.068	-	30.073	<0.001
N*PFT	1	-	5.713	0.057	-	1.286	0.526	-	19.405	<0.001
SM ₉₀ *PFT	1	-	3.487	0.175	-	0.889	0.641	-	2.998	0.223
SM ₉₀ *N*PFT	1	-	3.523	0.172	-	0.161	0.923	-	7.996	0.018

97

1568 *Significance determined using Type II Wald χ^2 tests ($\alpha=0.05$). P-values less than 0.05 are in bold and p-values
 1569 where $0.05 < p < 0.1$ are italicized. Coefficients are reported on the natural-log scale for all traits and are only included
 1570 for continuous fixed effects. Key: df=degrees of freedom; χ^2 =Wald Type II chi-square test statistic

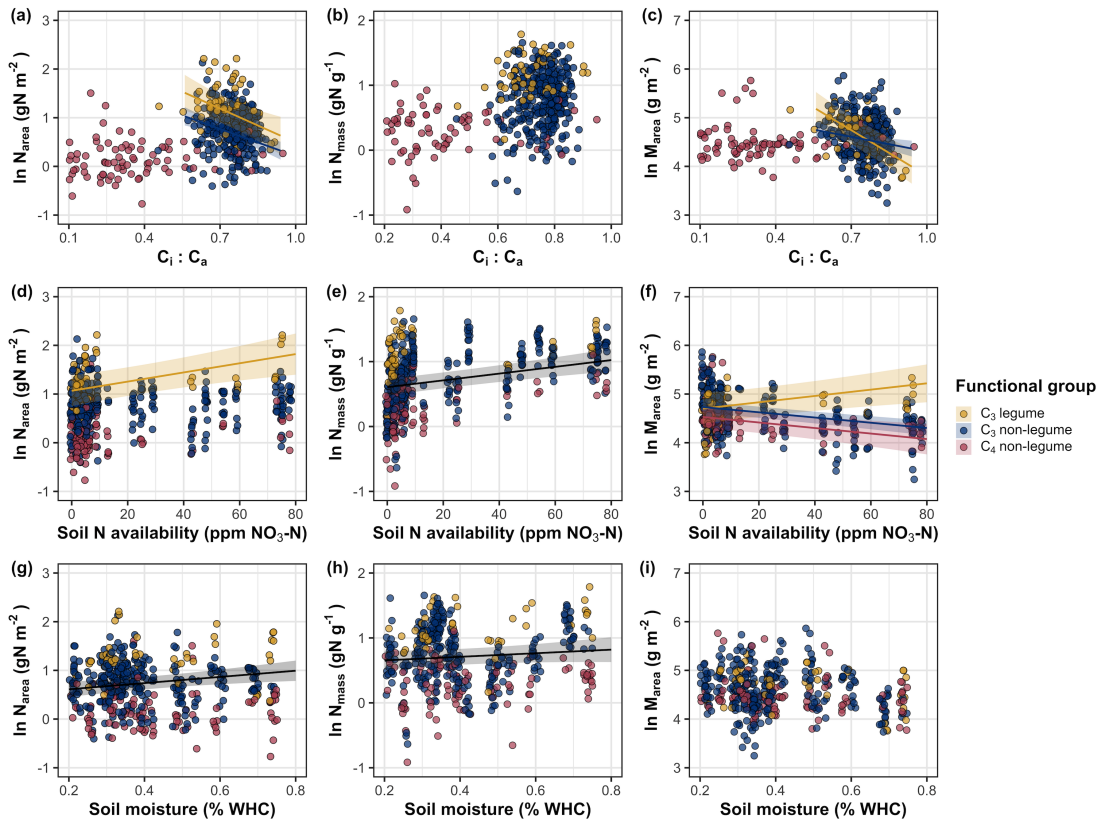


Figure 4.4. Effects of leaf $C_i:C_a$ (a-c), soil nitrogen availability (d-f), and soil moisture (g-i) on leaf nitrogen content per unit leaf area (a, d, g), leaf nitrogen content per unit leaf biomass (b, e, h), and leaf mass per area (c, f, i). Yellow points and trendlines indicate C_3 N-fixers, blue points and trendlines indicate C_3 non-fixers, and red points and trendlines indicate C_4 non-fixers. Points are jittered for visibility. Variably colored trendlines are only included if there is an interaction between plant functional group and the x-axis. Black solid trendlines denote bivariate slopes that are different from zero ($p < 0.05$) where there is no apparent interaction between plant functional group and the x-axis.

1571 4.3.4 *Structural equation model*

1572 The piecewise structural equation model explained 89%, 55%, 56%, 82%, and
1573 38% of variance in N_{area} , N_{mass} , M_{area} , leaf $C_i:C_a$, and β , respectively (Table
1574 4.5; Fig. 4.5). Increasing N_{mass} and M_{area} were each positively related to N_{area}
1575 ($p<0.001$ in both cases; Table 4.5; Fig. 4.5). N_{mass} increased with increasing
1576 soil nitrogen availability ($p<0.001$; Table 4.5) and leaf $C_i:C_a$ ($p=0.040$; Table
1577 4.5), and was generally larger in N-fixing species ($p<0.001$; Table 4.5), but was
1578 negatively related to increasing M_{area} ($p<0.001$; Table 4.5). M_{area} decreased with
1579 increasing leaf $C_i:C_a$ and soil nitrogen availability ($p<0.001$ in both cases; Table
1580 4.5). Leaf $C_i:C_a$ declined with increasing vapor pressure deficit, but was positively
1581 related to β ($p<0.001$ in both cases; Table 4.5). β decreased with increasing soil
1582 nitrogen availability and was higher in C₃ species ($p<0.001$ in both cases; Table
1583 4.5), but did not change with soil moisture ($p=0.895$; Table 4.5) or with ability
1584 to acquire nitrogen via symbiotic nitrogen fixation ($p=0.519$; Table 4.5). Finally,
1585 soil nitrogen availability was positively associated with increasing soil moisture
1586 ($p=0.003$; Table 4.5; Fig. 4.5).

Table 4.5. Structural equation model results investigating direct effects of climatic and soil resource availability on leaf nitrogen content (N_{area} ; g m⁻²)*

Predictor	Coefficient	<i>p</i>
N_{area} ($R^2_c=0.89$)		
M_{area}	0.714	<0.001
N_{mass}	0.778	<0.001
N_{mass} ($R^2_c=0.55$)		
Leaf $C_i:C_a$	0.113	0.040
M_{area}	-0.201	<0.001
Soil N	0.246	<0.001
N-fixing ability	0.326	<0.001
M_{area} ($R^2_c=0.56$)		
Leaf $C_i:C_a$	-0.224	<0.001
Soil N	-0.199	<0.001
Leaf $C_i:C_a$ ($R^2_c=0.82$)		
β	0.308	<0.001
VPD_4	-0.111	<0.001
β ($R^2_c=0.38$)		
Soil N	-0.207	<0.001
SM_{90}	-0.006	0.895
Photo. pathway	0.446	<0.001
N-fixing ability	-0.059	0.519
Soil N ($R^2_c=0.35$)		
SM_{90}	-0.148	0.003

1587 *Coefficients are standardized across the structural equation model. *P*-values less
 1588 than 0.05 are noted in bold. Positive coefficients for photosynthetic pathway
 1589 indicate generally larger values in C₃ species, while positive coefficients for N-
 1590 fixing ability indicate generally larger values in N-fixing species. Key: df=degrees
 1591 of freedom; χ^2 =Wald Type II chi-square test statistic; R^2_c =conditional R² value;
 1592 N_{mass} =leaf nitrogen content per unit leaf biomass (gN g⁻¹); M_{area} =leaf mass per
 1593 unit leaf biomass (g m⁻²); β =cost of acquiring nitrogen relative to water (unitless);
 1594 VPD_4 =4-day mean vapor pressure deficit (kPa); SM_{90} =90-day mean soil moisture
 1595 (mm)

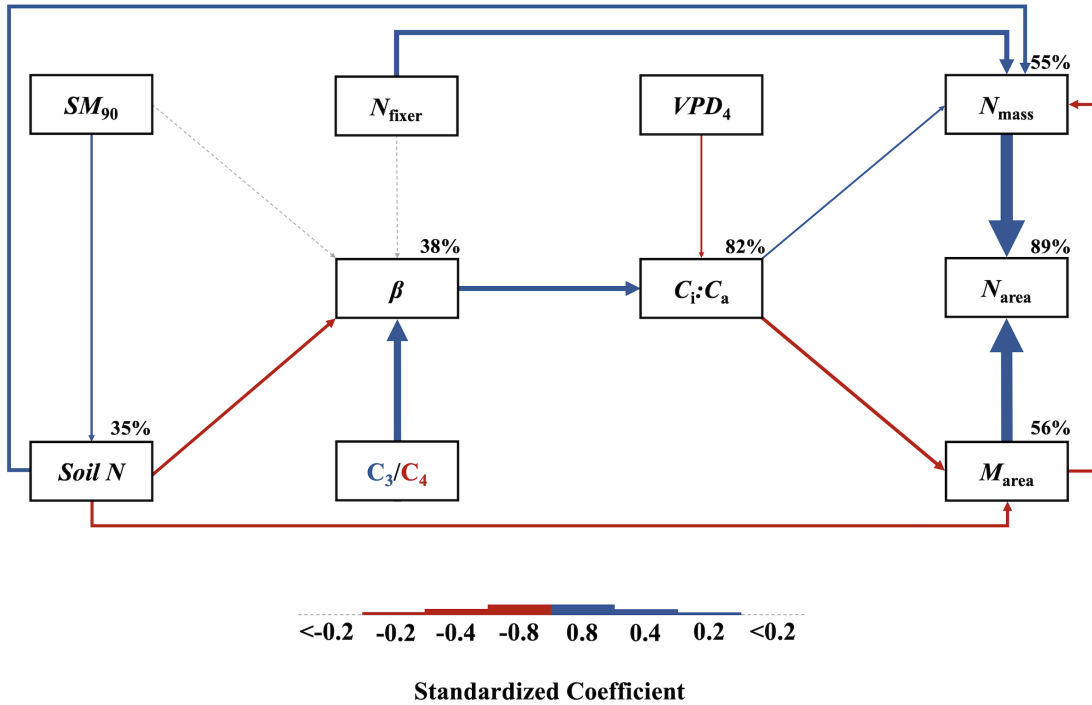


Figure 4.5. Structural equation model results exploring drivers of N_{area} . Boxes indicate measured edaphic factors, climatic factors, and leaf traits. Solid arrows indicate bivariate relationships where $p < 0.05$, while dashed arrows indicate relationships where $p > 0.05$. Positive model coefficients are indicated through blue arrows, negative model coefficients are indicated through red arrows, and insignificant coefficients are indicated through gray dashed arrows. Arrow thickness scales with the standardized model coefficient of each bivariate relationship. A positive coefficient for photosynthetic pathway indicates larger values in C_3 species, while a positive coefficient for N_{fixer} indicates larger values in N-fixing species. Standardized model coefficients and associated p -values are reported in Table 4.5, with conditional R^2 values for each response variable reported on the top right of each box.

1596 4.4 Discussion

1597 In this study, direct and indirect effects of edaphic and climatic characteristics on
1598 N_{area} and components of N_{area} (N_{mass} and M_{area}) were quantified in 504 individuals
1599 spanning across a soil resource availability and climate gradient in Texas, USA.
1600 Consistent patterns emerged in support of those expected from photosynthetic
1601 least-cost theory, a result driven by a strong direct negative relationship between
1602 leaf $C_i:C_a$ and N_{area} mediated through changes in M_{area} . In further support of
1603 patterns expected from theory, increasing soil nitrogen availability had a nega-
1604 tive effect on β , resulting in an indirect stimulation in N_{area} mediated through
1605 a positive relationship between β and $C_i:C_a$. Increasing vapor pressure deficit
1606 also indirectly increased N_{area} through a direct negative effect of increasing vapor
1607 pressure deficit on leaf $C_i:C_a$, following hypotheses and patterns expected from
1608 theory. Interestingly, a positive association between soil moisture and N_{area} was
1609 driven by covariance between soil moisture and soil nitrogen availability and was
1610 not associated with a direct effect of soil moisture on β . Overall, results provide
1611 strong and consistent support for patterns expected from photosynthetic least-cost
1612 theory, showing that both soil resource availability and climate drive variance in
1613 N_{area} through changes in leaf $C_i:C_a$.

1614 4.4.1 *Negative effects of leaf $C_i:C_a$ on N_{area} are driven by reductions in M_{area} ,*
1615 *not N_{mass}*

1616 The negative response of N_{area} to increasing leaf $C_i:C_a$ is consistent with pre-
1617 vious environmental gradient (Dong et al. 2017; Querejeta et al. 2022) and
1618 manipulation experiments (3.4c), showing strong support for the nitrogen-water

1619 use tradeoffs expected from photosynthetic least cost theory (Wright et al. 2003;
1620 Prentice et al. 2014). Negative effects of increasing leaf $C_i:C_a$ on N_{area} were driven
1621 by negative effect of increasing leaf $C_i:C_a$ on M_{area} coupled with a weak positive
1622 effect of increasing leaf $C_i:C_a$ on N_{mass} , suggesting that changes in N_{area} across
1623 the environmental gradient were driven more strongly by changes in leaf morphol-
1624 ogy than leaf chemistry. Interestingly, the negative relationship between M_{area}
1625 and N_{mass} suggested that stimulations in N_{mass} were often associated with larger,
1626 thinner leaves (i.e., lower M_{area}). These results are consistent with patterns re-
1627 ported from previous studies indicating that variance in N_{area} is driven by changes
1628 in M_{area} across environmental gradients, and that part of this response is due to
1629 negative covariance between M_{area} and N_{mass} (Dong et al. 2017; Dong et al. 2020).
1630 Negative covariance between M_{area} and N_{mass} could be a response associated with
1631 tradeoffs between leaf longevity and leaf productivity (Wright et al. 2004; Dong
1632 et al. 2017; Dong et al. 2022; Querejeta et al. 2022; Wang et al. 2023).

1633 The negative relationship between leaf $C_i:C_a$ and M_{area} could be indicative
1634 of tradeoffs between leaf longevity and leaf productivity. Tradeoffs between leaf
1635 longevity and leaf productivity are commonly observed and are included in a
1636 continuum of coordinated leaf traits that position individuals along a fast- or
1637 slow-growing leaf economics spectrum (Wright et al. 2003; Onoda et al. 2004;
1638 Reich 2014; Onoda et al. 2017; Wang et al. 2023). Negative relationships between
1639 leaf $C_i:C_a$ and M_{area} indicate that increased stomatal conductance and reduced
1640 water use efficiency were associated with thinner, larger leaves (i.e., lower M_{area}).
1641 Combined with the negative covariance between M_{area} and N_{mass} mentioned above,
1642 these responses may have allowed individuals to maximize light interception and

1643 productivity by exploiting high light environments at the expense of increased
1644 water loss and decreased water-use efficiency. This strategy may be especially
1645 advantageous for fast-growing species in open canopy systems. In this study, C₃
1646 N-fixers and C₃ non-fixers dominated the dataset (77% of total sampling effort),
1647 of which 23% (17% of total sampling effort) were classified as annual species with
1648 short growing seasons. We observed no effect of leaf $C_i:C_a$ on N_{area} or M_{area} in C₄
1649 non-fixers, which made up 23% of the sampling effort and were generally classified
1650 as warm season graminoid species with slower growth rates and longer growing
1651 seasons. These patterns indicate that stronger tradeoffs between nitrogen and
1652 water use may be more apparent in fast-growing species with high demand for
1653 building and maintaining productive leaf tissues.

1654 4.4.2 *Soil nitrogen availability increases N_{area} through changes in β*
1655 The structural equation model indicated multiple pathways where increasing soil
1656 nitrogen availability increased N_{area} . First, N_{area} increased with increasing soil
1657 nitrogen availability due to larger positive direct effects of increasing soil nitrogen
1658 availability on N_{mass} than the corresponding negative direct effect of increasing
1659 soil nitrogen availability on M_{area} . These patterns corroborate those observed in
1660 the individual linear mixed effect models and previous work. Second, soil nitrogen
1661 availability increased N_{area} indirectly through reductions in β , which increased leaf
1662 $C_i:C_a$ and stimulated N_{area} through a stronger negative effect of increasing leaf
1663 $C_i:C_a$ on M_{area} than corresponding positive effect of increasing leaf $C_i:C_a$ on N_{mass} .
1664 Reductions in β with increasing soil nitrogen availability were likely driven by re-
1665 ductions in the cost of acquiring and using nitrogen, following patterns observed

1666 in previous experiments (Bae et al. 2015; Eastman et al. 2021; Perkowski et al.
1667 2021; Lu et al. 2022). These pathways indicate that soil nitrogen availability can
1668 have direct positive effects on N_{area} by increasing leaf nitrogen concentration, fol-
1669 lowing previous work (Firn et al. 2019; Liang et al. 2020), or can alternatively have
1670 indirect positive effects on N_{area} through changes in leaf morphology associated
1671 with a reduction in the cost of acquiring nitrogen, following patterns expected
1672 from photosynthetic least-cost theory. Results reported here indicate that pho-
1673 tosynthetic least-cost frameworks are capable of detecting predictable variance in
1674 N_{area} and tradeoffs between nitrogen and water use across soil nitrogen availability
1675 gradients.

1676 4.4.3 *Soil moisture increases N_{area} by facilitating increases in soil nitrogen
1677 availability*

1678 Increasing soil moisture had a positive effect on N_{area} , though this response was
1679 associated with a null effect of soil moisture on β . These results contrast patterns
1680 expected from theory, where increasing soil moisture is expected to indirectly
1681 decrease N_{area} through an increase in β due to a reduction in costs associated
1682 with water acquisition and use (Wright et al. 2003; Prentice et al. 2014; Lavergne
1683 et al. 2020). Interestingly, structural equation model results revealed a strong
1684 positive association between soil moisture and soil nitrogen availability, indicating
1685 an indirect positive effect of increasing soil moisture on N_{area} mediated by the
1686 negative effect of increasing soil nitrogen availability on β . In Texan grasslands,
1687 productivity and nutrient uptake are often co-limited by precipitation and nutrient
1688 availability (Yahdjian et al. 2011; Wang et al. 2017). Thus, increases in soil
1689 moisture may have facilitated more favorable and productive environments for
1690 soil microbial communities (Reichman et al. 1966; Stark and Firestone 1995;

1691 Paul et al. 2003), or alternatively greater nitrogen mobility in soil solution. As
1692 discussed above, the positive indirect response of N_{area} to increasing soil nitrogen
1693 availability as mediated through reductions in β follow patterns expected from
1694 theory.

1695 4.4.4 *Indirect effects of climate on N_{area} are mediated through changes in leaf*
1696 $C_i:C_a$ *and β*

1697 In support of hypotheses and patterns expected from theory, increasing vapor
1698 pressure deficit indirectly increased N_{area} , mediated through the negative effect
1699 of increasing vapor pressure deficit on leaf $C_i:C_a$. These responses are consistent
1700 with previous work noting strong reductions in stomatal conductance with increas-
1701 ing vapor pressure deficit (Oren et al. 1999; Novick et al. 2016; Sulman et al.
1702 2016; Grossiord et al. 2020; López et al. 2021), a response that allows plants
1703 to minimize water loss as a result of high atmospheric water demand. Results
1704 also support findings from previous experiments across environmental gradients,
1705 where increasing vapor pressure deficit generally increases N_{area} at lower stomatal
1706 conductance across environmental gradients (Dong et al. 2017; Dong et al. 2022;
1707 Paillassa et al. 2020; Westerband et al. 2023). The increase in N_{area} with increas-
1708 ing vapor pressure deficit could allow plants to maximize photosynthetic capacity
1709 under reduced stomatal conductance (Dong et al. 2022), though this pattern con-
1710 trasts previous work suggesting that long-term increases in vapor pressure deficit
1711 are associated with increased plant mortality, reduced net primary productivity,
1712 and perhaps reductions in net photosynthesis rates over time due to prolonged
1713 stomatal closure (Eamus et al. 2013; Yuan et al. 2019; Grossiord et al. 2020).
1714 Importantly, such negative effects of increasing vapor pressure deficit often occur
1715 along much broader timescales compared to the timescale used here. Responses

1716 observed here suggest that variance in N_{area} across environmental gradients is
1717 a deterministic acclimation response to changing aboveground climate, allowing
1718 plants to satisfy demand to build and maintain photosynthetic enzymes and op-
1719 timize photosynthetic processes by maximizing resource use efficiency (Paillassa
1720 et al. 2020; Peng et al. 2021; Dong et al. 2022; Westerband et al. 2023).

1721 4.4.5 *Species identity traits modify effects of the environment on β , leaf $C_i:C_a$,*
1722 *and N_{area}*

1723 N-fixing species had greater N_{area} values on average compared to non-fixing species,
1724 a pattern driven by a stronger stimulation in N_{mass} in N-fixing species coupled with
1725 no change in M_{area} between species with different N-fixation ability. There was
1726 no evidence to suggest that N-fixing species had different β or leaf $C_i:C_a$ values
1727 compared to non-fixing species across the environmental gradient. These results
1728 follow patterns from previous environmental gradient experiments that investi-
1729 gate variance in leaf nitrogen allocation in N-fixing species (Adams et al. 2016;
1730 Dong et al. 2017; Dong et al. 2020), and that increases in N_{mass} and N_{area} in
1731 N-fixing species are not necessarily correlated to increases in water use efficiency
1732 or reductions in leaf $C_i:C_a$ (Adams et al. 2016). While results are consistent with
1733 results from previous environmental gradient experiments, they do not support
1734 hypotheses presented here or patterns expected from theory, which predicts that
1735 stimulations in N_{area} by N-fixing species should be driven by a reduction in β
1736 relative to non-fixing species, and that this response should decrease stomatal
1737 conductance and leaf $C_i:C_a$.

1738 C₄ species had reduced β , leaf $C_i:C_a$, and N_{area} than C₃ species. Reduced
1739 β and leaf $C_i:C_a$ values in C₄ species follow hypotheses listed above, a pattern

1740 that could be the result of either reduced costs of nitrogen acquisition and use,
1741 increased costs of water acquisition and use, or both (Wright et al. 2003; Prentice
1742 et al. 2014). Results also indicate that β in C₄ non-fixers was unresponsive to
1743 changes in soil nitrogen availability despite an apparent negative effect of increas-
1744 ing soil nitrogen availability on β in C₃ N-fixers and C₃ non-fixers. Combined
1745 with a general null response of β to soil moisture regardless of plant functional
1746 group, these patterns imply that reduced β values in C₄ species may be the re-
1747 sult of lower costs of nitrogen acquisition and use relative to C₃ species. While
1748 lower β values in C₄ species provides a possible explanation for why C₄ species
1749 often have lower leaf $C_i:C_a$ and greater water use efficiency, theory predicts that
1750 this response should cause C₄ species to have greater N_{area} values compared to
1751 C₃ species, though C₄ species commonly exhibit lower N_{area} and higher nitrogen
1752 use efficiency than C₃ species (Schmitt and Edwards 1981; Sage and Pearcy 1987;
1753 Ghannoum et al. 2011). We speculate that lowered costs of nitrogen acquisition
1754 and use in C₄ species could be driven by more efficient Rubisco carboxylation effi-
1755 ciency in C₄ species associated with CO₂ concentrating mechanisms that eliminate
1756 photorespiration (Ghannoum et al. 2011), which could reduce or eliminate the
1757 need to sacrifice inefficient nitrogen use for efficient water use to achieve optimal
1758 photosynthesis rates.

1759 4.4.6 *Next steps for optimality model development*

1760 Optimality models for both C₃ and C₄ species have been developed using principles
1761 from photosynthetic least-cost theory (Prentice et al. 2014; Wang et al. 2017;
1762 Smith et al. 2019; Stocker et al. 2020; Scott and Smith 2022). In both C₃ and C₄
1763 model variants, β values are held constant using global datasets of leaf $\delta^{13}\text{C}$ (Wang

1764 et al. 2017; Cornwell et al. 2018). Specifically, the C₃ optimality model initially
1765 assumed a constant β value of 240 (Wang et al. 2017), later corrected to 146
1766 (Stocker et al. 2020), while the C₄ optimality model assumes a constant β value of
1767 166 (Scott and Smith 2022). These results, which build on findings from Paillassa
1768 et al. (2020) and Lavergne et al. (2020), demonstrate high variability in calculated
1769 β values across the environmental gradient. Specifically, β values in C₃ species
1770 ranged from 1.7 to 188.0 (mean: 30.2; median: 23.1; standard deviation: 25.4),
1771 while ranged from 0.1 to 110.6 in C₄ species (mean: 7.2; median: 0.7; standard
1772 deviation: 18.6). Mean β values in both C₃ and C₄ species were consistently lower
1773 than values currently implemented in optimality models, though this was likely
1774 the result of increased water limitation across sites relative to global averages.
1775 Regardless, the high degree of β variability across this environmental gradient,
1776 together with findings from Lavergne et al. (2020) and Paillassa et al. (2020),
1777 suggests that the use of constant β values may contribute to erroneous errors when
1778 conducting optimality model simulations. Results from this experiment build
1779 on suggestions from Wang et al. (2017), suggesting that future photosynthetic
1780 least-cost optimality model developments should consider adopting frameworks
1781 for dynamically calculating β .

1782 4.4.7 *Conclusions*

1783 To summarize, variability in N_{area} across an environmental gradient in Texan
1784 grasslands was driven by indirect effects of climate and soil resource availability
1785 mediated by changes in β and leaf $C_i:C_a$. Results from this experiment provide
1786 strong and consistent support for patterns expected from photosynthetic least-

1787 cost theory, demonstrating that negative relationships between $C_i:C_a$ and N_{area}
1788 unify expected effects of climatic and edaphic characteristics on N_{area} across en-
1789 vironmental gradients. Results reported here also demonstrate a need to consider
1790 the dynamic nature of the relative cost of nitrogen versus water uptake (β) across
1791 environmental gradients in optimality models that leverage principles of photo-
1792 synthetic least-cost theory.

1793

Chapter 5

1794 Optimal resource investment to photosynthetic capacity maximizes
1795 nutrient allocation to whole plant growth under elevated CO₂

1796 5.1 Introduction

1797 Terrestrial ecosystems are regulated by complex carbon and nitrogen cycles. As
1798 a result, terrestrial biosphere models, which are beginning to include coupled
1799 carbon and nitrogen cycles (Shi et al. 2016; Davies-Barnard et al. 2020; Braghieri
1800 et al. 2022), must accurately represent these cycles under different environmental
1801 scenarios to reliably simulate carbon and nitrogen atmosphere-biosphere fluxes
1802 (Hungate et al. 2003; Prentice et al. 2015). While the inclusion of coupled carbon
1803 and nitrogen cycles tends to reduce model uncertainty (Arora et al. 2020), large
1804 uncertainty in role of soil nitrogen availability and nitrogen acquisition strategy
1805 on leaf and whole plant acclimation responses to CO₂ remains (Smith and Dukes
1806 2013; Terrer et al. 2018; Smith and Keenan 2020). This source of uncertainty
1807 likely contributes to the widespread divergence in future carbon and nitrogen flux
1808 simulations across terrestrial biosphere models (Friedlingstein et al. 2014; Zaehle
1809 et al. 2014; Meyerholt et al. 2020).

1810 Plants grown under elevated CO₂ generally have less leaf nitrogen content
1811 than those grown under ambient CO₂, a response that often corresponds with
1812 reductions in photosynthetic capacity and stomatal conductance at the leaf-level
1813 and biomass stimulation over time at the whole plant level (Curtis 1996; Drake
1814 et al. 1997; Ainsworth et al. 2002; Makino 2003; Morgan et al. 2004; Ainsworth
1815 and Long 2005; Ainsworth and Rogers 2007; Smith and Dukes 2013; Poorter et al.
1816 2022). As net primary productivity is generally limited by nitrogen availability

1817 (Vitousek and Howarth 1991; LeBauer and Treseder 2008; Fay et al. 2015), and
1818 soil nitrogen availability is often positively correlated with leaf nitrogen content
1819 and photosynthetic capacity (Field and Mooney 1986; Evans and Seemann 1989;
1820 Evans 1989; Walker et al. 2014; Firn et al. 2019; Liang et al. 2020), some
1821 have hypothesized that leaf and whole plant acclimation responses to CO₂ are
1822 constrained by soil nitrogen availability.

1823 The progressive nitrogen limitation hypothesis predicts that elevated CO₂
1824 will increase plant nitrogen demand, which will increase plant nitrogen uptake
1825 and progressively deplete soil nitrogen if soil nitrogen supply does not exceed
1826 plant nitrogen demand (Luo et al. 2004). The hypothesis predicts that this
1827 response should result in strong acute stimulations in whole plant growth and
1828 primary productivity that diminish over time as nitrogen becomes more limiting.
1829 Assuming a positive relationship between soil nitrogen availability, leaf nitrogen
1830 content, and photosynthetic capacity, this hypothesis also implies that progressive
1831 reductions in soil nitrogen availability should be the mechanism that drives the
1832 reduction in leaf nitrogen content and photosynthetic capacity under elevated
1833 CO₂. The progressive nitrogen limitation hypothesis has received some support
1834 from free air CO₂ enrichment experiments (Reich et al. 2006; Norby et al. 2010),
1835 although is not consistently observed across experiments (Finzi et al. 2006; Moore
1836 et al. 2006; Liang et al. 2016).

1837 While possible that progressive nitrogen limitation may determine leaf and
1838 whole plant acclimation responses to CO₂, growing evidence indicates that leaf ni-
1839 trogen content and photosynthetic capacity are more strongly determined through
1840 aboveground growing conditions than by soil resource availability (Dong et al.

1841 2017; Dong et al. 2020; Dong et al. 2022; Smith et al. 2019; Smith and Keenan
1842 2020; Paillassa et al. 2020; Peng et al. 2021; Querejeta et al. 2022; Wester-
1843 band et al. 2023), and satellite-derived chlorophyll fluorescence data indicate that
1844 increasing atmospheric CO₂ may decrease leaf and canopy demand for nitrogen
1845 (Dong et al. 2022). Together, results from these studies suggest that the re-
1846 duction in leaf nitrogen content and photosynthetic capacity due to increasing
1847 CO₂ may not be as tightly linked to progressive nitrogen limitation as previously
1848 hypothesized.

1849 A unification of optimal coordination and least-cost theories predicts that
1850 leaves acclimate to elevated CO₂ by reducing nitrogen allocation to Ribulose-
1851 1,5-bisphosphate (RuBP) carboxylase/oxygenase (Rubisco) to optimize resource
1852 use efficiencies at the leaf level, which allows for greater resource allocation to
1853 whole plant growth (Drake et al. 1997; Wright et al. 2003; Prentice et al. 2014;
1854 Smith et al. 2019). The theory predicts that the reduction in nitrogen allocation
1855 to Rubisco results in a stronger reduction in the maximum rate of Rubisco car-
1856 boxylation (V_{cmax}) than the maximum rate of RuBP regeneration (J_{max}), which
1857 maximizes photosynthetic efficiency by allowing net photosynthesis rates to be
1858 equally co-limited by Rubisco carboxylation and RuBP regeneration (Chen et al.
1859 1993; Maire et al. 2012). This acclimation response allows plants to make more
1860 efficient use of available light while avoiding overinvestment in Rubisco, which
1861 has high nitrogen and energetic costs of building and maintaining (Evans 1989;
1862 Evans and Clarke 2019). Instead, additional acquired resources not needed to
1863 optimize leaf photosynthesis are allocated to the maintenance of structures that
1864 support whole plant growth (e.g., total leaf area, whole plant biomass, etc.) or

1865 to allocation processes not related to leaf photosynthesis or growth, such as plant
1866 defense mechanisms. Regardless, optimized resource allocation at the leaf level
1867 should allow for greater resource allocation to whole plant growth. The theory
1868 indicates that leaf acclimation responses to CO₂ should be independent of changes
1869 in soil nitrogen availability. While this leaf acclimation response maximizes nitro-
1870 gen allocation to structures that support whole plant growth, the theory suggests
1871 that the positive effect of elevated CO₂ on whole plant growth may be further
1872 stimulated by soil nitrogen availability through reductions in the cost of acquiring
1873 nitrogen (Bae et al. 2015; Perkowski et al. 2021; Lu et al. 2022).

1874 Plants acquire nitrogen by allocating photosynthetically derived carbon be-
1875 lowground in exchange for nitrogen through different nitrogen acquisition strate-
1876 gies. These nitrogen acquisition strategies can include direct uptake pathways
1877 such as mass flow or diffusion (Barber 1962), symbioses with mycorrhizal fungi or
1878 symbiotic nitrogen-fixing bacteria (Vance and Heichel 1991; Marschner and Dell
1879 1994; Smith and Read 2008; Udvardi and Poole 2013), or through the release
1880 of root exudates that prime free-living soil microbial communities (Phillips et al.
1881 2011; Wen et al. 2022). Plants cannot acquire nitrogen without first allocating
1882 carbon belowground, which implies an inherent carbon cost to the plant for acquir-
1883 ing nitrogen regardless of nitrogen acquisition strategy. Carbon costs to acquire
1884 nitrogen often vary in species with different nitrogen acquisition strategies and
1885 are dependent on external environmental factors such as atmospheric CO₂, light
1886 availability, and soil nitrogen availability (Brzostek et al. 2014; Terrer et al. 2016;
1887 Terrer et al. 2018; Allen et al. 2020; Perkowski et al. 2021; Lu et al. 2022). These
1888 patterns suggest that acquisition strategy may at least partially determine the net

1889 effect of soil nitrogen availability on leaf and whole plant acclimation responses to
1890 elevated CO₂.

1891 A recent meta-analysis using data across 20 grassland and forest CO₂ en-
1892 richment experiments suggested that species which acquire nitrogen from sym-
1893 biotic nitrogen-fixing bacteria had reduced costs of nitrogen acquisition under
1894 elevated CO₂ (Terrer et al. 2018). Though these analyses included data from two
1895 experimental sites, findings from this meta-analysis indicated that reduced costs
1896 of nitrogen acquisition in species that form associations with symbiotic nitrogen-
1897 fixing bacteria under elevated CO₂ may drive stronger increases in whole plant
1898 growth and reductions in V_{cmax} than species that associate with arbuscular my-
1899 corrhizal fungi (Smith and Keenan 2020), which generally have greater costs of
1900 nitrogen acquisition under elevated CO₂ (Terrer et al. 2018). However, plant in-
1901 vestments in symbiotic nitrogen fixation generally decline with increasing nitrogen
1902 availability (Dovrat et al. 2018; Perkowski et al. 2021), a response that has been
1903 previously inferred to driven by a shift to direct uptake pathways as costs of direct
1904 uptake decrease (Rastetter et al. 2001; Perkowski et al. 2021). Thus, effects of
1905 symbiotic nitrogen fixation on plant acclimation responses to CO₂ should decline
1906 with increasing soil nitrogen availability, although manipulative experiments that
1907 directly test these patterns are rare.

1908 Here, I conducted a 7-week growth chamber experiment using *Glycine max*
1909 L. (Merr.) to examine the effects of soil nitrogen fertilization and inoculation with
1910 symbiotic nitrogen-fixing bacteria on leaf and whole plant acclimation responses to
1911 elevated CO₂. Following patterns expected from theory, I hypothesized that indi-
1912 vidual leaves should acclimate to elevated CO₂ by more strongly decreasing V_{cmax}

1913 relative to J_{\max} , allowing leaf photosynthesis to approach optimal coordination.
1914 I expected this response to correspond with a stronger reduction in leaf nitrogen
1915 content than $V_{c\max}$ and J_{\max} , which would increase the fraction of leaf nitrogen
1916 content allocated to photosynthesis. At the whole-plant level, I hypothesized that
1917 plants would acclimate to elevated CO₂ by increasing whole plant growth and
1918 productivity, a response that would be driven by an increase in total leaf area and
1919 aboveground biomass. I predicted that leaf acclimation responses to elevated CO₂
1920 would be independent of soil nitrogen fertilization and inoculation with symbiotic
1921 nitrogen-fixing bacteria. However, I expected that increasing fertilization would
1922 increase the positive effect of elevated CO₂ on total leaf area and aboveground
1923 biomass due to a stronger reduction in the cost of acquiring nitrogen under ele-
1924 vated CO₂ with increasing fertilization. Finally, I expected stronger increases in
1925 whole plant growth under elevated CO₂ in inoculated pots, but expected that this
1926 effect would only be apparent under low fertilization due to a reduction in root
1927 nodulation with increasing fertilization.

1928 5.2 Methods

1929 5.2.1 *Seed treatments and experimental design*

1930 *Glycine max* L. (Merr) seeds were planted in 144 6-liter surface sterilized pots (NS-
1931 600, Nursery Supplies, Orange, CA, USA) containing a steam-sterilized 70:30 v:v
1932 mix of *Sphagnum* peat moss (Premier Horticulture, Quakertown, PA, USA) to
1933 sand (Pavestone, subsidiary of Quikrete Companies, Atlanta, GA, USA). Before
1934 planting, all *G. max* seeds were surface sterilized in 2% sodium hypochlorite for 3
1935 minutes, followed by three separate 3-minute washes with ultrapure water (MilliQ

1936 7000; MilliporeSigma, Burlington, MA USA). A subset of surface sterilized seeds
1937 were inoculated with *Bradyrhizobium japonicum* (Verdesian N-DureTM Soybean,
1938 Cary, NC, USA) in a slurry following manufacturer recommendations (3.12 g
1939 inoculant and 241 g deionized water per 1 kg seed).

1940 Seventy-two pots were randomly planted with surface-sterilized seeds inoc-
1941 ulated with *B. japonicum*, while the remaining 72 pots were planted with surface-
1942 sterilized uninoculated seeds. Thirty-six pots within each inoculation treatment
1943 were randomly placed in one of two atmospheric CO₂ treatments (ambient and
1944 1000 $\mu\text{mol mol}^{-1}$ CO₂). Pots within each unique inoculation-by-CO₂ treatment
1945 combination randomly received one of nine soil nitrogen fertilization treatments
1946 equivalent to 0, 35, 70, 105, 140, 210, 280, 350, or 630 ppm N. Nitrogen fertil-
1947 ization treatments were created using a modified Hoagland solution (Hoagland
1948 and Arnon 1950) designed to keep concentrations of other macronutrients and
1949 micronutrients equivalent across treatments (Table D1). Pots received the same
1950 fertilization treatment throughout the entire duration experiment, which were ap-
1951 plied twice per week in 150 mL doses as topical agents to the soil surface. This
1952 experimental design yielded a fully factorial experiment with four replicates per
1953 unique fertilization-by-inoculation-by-CO₂ combination.

1954 5.2.2 *Growth chamber conditions*

1955 Upon experiment initiation, pots were randomly placed in one of six Percival
1956 LED-41L2 growth chambers (Percival Scientific Inc., Perry, IA, USA) over two
1957 experimental iterations due to chamber space limitation. Two iterations were
1958 conducted such that one iteration included all elevated CO₂ pots and the second

1959 iteration included all ambient CO₂ pots. Mean (\pm SD) CO₂ concentrations across
1960 chambers throughout the experiment were $439 \pm 5 \mu\text{mol mol}^{-1}$ CO₂ for the ambient
1961 CO₂ treatment and $989 \pm 4 \mu\text{mol mol}^{-1}$ CO₂ for the elevated CO₂ treatment.

1962 Daytime growing conditions were simulated using a 16-hour photoperiod,
1963 with incoming light radiation set to chamber maximum (mean \pm SD: 1240 ± 32
1964 $\mu\text{mol m}^{-2} \text{s}^{-1}$ across chambers), air temperature set to 25°C, and relative humid-
1965 ity set to 50%. The remaining 8 hours simulated nighttime growing conditions,
1966 with incoming light radiation set to 0 $\mu\text{mol m}^{-2} \text{s}^{-1}$, chamber temperature set
1967 to 17°C, and relative humidity set to 50%. Transitions between daytime and
1968 nighttime growing conditions were simulated by ramping incoming light radiation
1969 in 45-minute increments and temperature in 90-minute increments over a 3-hour
1970 period (Table D2).

1971 Including the two, 3-hour ramping periods, pots grew under average (\pm SD)
1972 daytime light intensity of $1049 \pm 27 \mu\text{mol m}^{-2} \text{s}^{-1}$. In the elevated CO₂ iteration,
1973 pots grew under $24.0 \pm 0.2^\circ\text{C}$ during the day, $16.4 \pm 0.8^\circ\text{C}$ during the night, and
1974 51.6 \pm 0.4% relative humidity. In the ambient CO₂ iteration, pots grew under
1975 $23.9 \pm 0.2^\circ\text{C}$ during the day, $16.0 \pm 1.4^\circ\text{C}$ during the night, and 50.3 \pm 0.2% relative
1976 humidity. I accounted for any climatic differences across the six chambers by
1977 shuffling the same group of pots daily throughout the growth chambers. This
1978 process was done by iteratively moving the group of pots on the top rack of a
1979 chamber to the bottom rack of the same chamber, while simultaneously moving
1980 the group of pots on the bottom rack of a chamber to the top rack of the adjacent
1981 chamber. I moved pots within and across chambers every day throughout the
1982 course of each experiment iteration.

1983 5.2.3 *Leaf gas exchange measurements*

1984 Gas exchange measurements were collected for all individuals on the seventh week
1985 of development. All gas exchange measurements were collected on the center leaf
1986 of the most recent fully expanded trifoliate leaf set. Specifically, I measured net
1987 photosynthesis (A_{net} ; $\mu\text{mol m}^{-2} \text{s}^{-1}$), stomatal conductance (g_{sw} ; $\text{mol m}^{-2} \text{s}^{-1}$),
1988 and intercellular CO_2 (C_i ; $\mu\text{mol mol}^{-1}$) concentrations across a range of atmo-
1989 spheric CO_2 concentrations (i.e., an A_{net}/C_i curve) using the Dynamic Assimila-
1990 tion Technique™. The Dynamic Assimilation Technique™ has been shown to
1991 correspond well with traditional steady-state CO_2 response curves in *G. max*
1992 (Saathoff and Welles 2021). A_{net}/C_i curves were generated along a reference CO_2
1993 ramp down from $420 \mu\text{mol mol}^{-1} \text{CO}_2$ to $20 \mu\text{mol mol}^{-1} \text{CO}_2$, followed by a ramp
1994 up from $420 \mu\text{mol mol}^{-1} \text{CO}_2$ to $1620 \mu\text{mol mol}^{-1} \text{CO}_2$ after a 90-second wait
1995 period at $420 \mu\text{mol mol}^{-1} \text{CO}_2$. The ramp rate for each curve was set to 200
1996 $\mu\text{mol mol}^{-1} \text{min}^{-1}$, logging every five seconds, which generated 96 data points per
1997 response curve. All A_{net}/C_i curves were generated after A_{net} and g_{sw} stabilized
1998 in a LI-6800 cuvette set to a 500 mol s^{-1} , 10,000 rpm mixing fan speed, 1.5 kPa
1999 vapor pressure deficit, 25°C leaf temperature, $2000 \mu\text{mol m}^{-2} \text{s}^{-1}$ incoming light
2000 radiation, and initial reference CO_2 set to $420 \mu\text{mol mol}^{-1}$.

2001 With the same focal leaf used to generate A_{net}/C_i curves, I measured dark
2002 respiration (R_{d25} ; $\mu\text{mol m}^{-2} \text{s}^{-1}$) following at least a 30-minute period of darkness.
2003 Measurements were collected on a 5-second log interval for 60 seconds after stabi-
2004 lizing in a LI-6800 cuvette set to a 500 mol s^{-1} , 10,000 rpm mixing fan speed, 1.5
2005 kPa vapor pressure deficit, 25°C leaf temperature, and $420 \mu\text{mol mol}^{-1}$ reference
2006 CO_2 concentration (for both CO_2 concentrations), with incoming light radiation

2007 set to 0 $\mu\text{mol m}^{-2} \text{s}^{-1}$. A single dark respiration value was determined for each
2008 focal leaf by calculating the mean dark respiration value (i.e. the absolute value
2009 of A_{net} during the logging period) across the logging interval.

2010 5.2.4 *Leaf trait measurements*

2011 The focal leaf used to generate A_{net}/C_i curves and dark respiration was harvested
2012 immediately following gas exchange measurements. Images of each focal leaf were
2013 curated using a flat-bed scanner to determine wet leaf area using the ‘LeafArea’ R
2014 package (Katabuchi 2015), which automates leaf area calculations using ImageJ
2015 software (Schneider et al. 2012). Each leaf was dried at 65°C for at least 48
2016 hours, and subsequently weighed and ground until homogenized. Leaf mass per
2017 area (M_{area} ; g m^{-2}) was calculated as the ratio of dry leaf biomass to fresh leaf
2018 area. Using subsamples of ground and homogenized leaf tissue, I measured leaf
2019 nitrogen content (N_{mass} ; gN g^{-1}) through elemental combustion analysis (Costech-
2020 4010, Costech, Inc., Valencia, CA, USA). Leaf nitrogen content per unit leaf area
2021 (N_{area} ; gN m^{-2}) was calculated by multiplying N_{mass} and M_{area} . Subsamples of
2022 ground and homogenized leaf tissue were also sent to the UC-Davis Stable Isotope
2023 Facility to quantify leaf $\delta^{15}\text{N}$, later used to estimate the fraction of leaf nitrogen
2024 derived from the atmosphere.

2025 I extracted chlorophyll content from a second leaf in the same trifoliolate
2026 leaf set as the focal leaf used to generate A_{net}/C_i curves. Prior to chlorophyll
2027 extraction, I used a cork borer to punch between 3 and 5 0.6 cm^2 disks from the
2028 leaf. Separate images of each punched leaf and set of leaf disks were curated using
2029 a flat-bed scanner to determine wet leaf area, again quantified using the ‘LeafArea’

2030 R package (Katabuchi 2015). The punched leaf was dried and weighed after at
2031 least 65°C in the drying oven to determine M_{area} of the chlorophyll leaf.

2032 Leaf disks were shuttled into a test tube containing 10mL dimethyl sulfoxide, vortexed, and incubated at 65°C for 120 minutes (Barnes et al. 1992). Incubated test tubes were vortexed again before loaded in 150 μL triplicate aliquots to a 96-well plate. Dimethyl sulfoxide was also loaded in a 150 μL triplicate aliquot as a blank. Absorbance measurements at 649.1 nm ($A_{649.1}$) and 665.1 nm ($A_{665.1}$) were read in each well using a plate reader (Biotek Synergy H1; Biotek Instruments, Winooski, VT USA) (Wellburn 1994), with triplicates subsequently averaged and corrected by the mean of the blank absorbance value. Blank-corrected absorbance values were used to estimate Chl_a ($\mu\text{g mL}^{-1}$) and Chl_b ($\mu\text{g mL}^{-1}$) following equations from Wellburn (1994):

$$Chl_a = 12.47A_{665.1} - 3.62A_{649.1} \quad (5.1)$$

2042 and

$$Chl_b = 25.06A_{665.1} - 6.50A_{649.1} \quad (5.2)$$

2043 Chl_a and Chl_b were converted to mmol mL^{-1} using the molar mass of chlorophyll a (893.51 g mol^{-1}) and the molar mass of chlorophyll b (907.47 g mol^{-1}), then added together to calculate total chlorophyll content in the dimethyl sulfoxide extractant (mmol mL^{-1}). Total chlorophyll content was multiplied by the volume of the dimethyl sulfoxide extractant (10 mL) and converted to area-based chlorophyll content by dividing by the total area of the leaf disks (Chl_{area} ; mmol m^{-2}). Mass-based chlorophyll content (Chl_{mass} ; mmol g^{-1}) was calculated by dividing Chl_{area}

2050 by the leaf mass per area of the punched leaf.

2051 5.2.5 *A/C_i curve fitting and parameter estimation*

2052 I fit A_{net}/C_i curves of each individual using the ‘fitaci’ function in the ‘plantecphys’ R package (Duursma 2015). This function estimates the maximum rate
2053 of Rubisco carboxylation (V_{cmax} ; $\mu\text{mol m}^{-2} \text{s}^{-1}$) and maximum rate of electron
2054 transport for RuBP regeneration (J_{max} ; $\mu\text{mol m}^{-2} \text{s}^{-1}$) based on the Farquhar
2055 biochemical model of C₃ photosynthesis (Farquhar et al. 1980). Triose phosphate
2056 utilization (TPU) limitation was included in all curve fits, and all curve fits in-
2057 cluded measured dark respiration values. As A_{net}/C_i curves were generated using
2058 a common leaf temperature, curves were fit using Michaelis-Menten coefficients
2059 for Rubisco affinity to CO₂ (K_c ; $\mu\text{mol mol}^{-1}$) and O₂ (K_o ; $\mu\text{mol mol}^{-1}$), and the
2060 CO₂ compensation point (Γ^* ; $\mu\text{mol mol}^{-1}$) reported in Bernacchi et al. (2001).
2061 Specifically, K_c was set to 404.9 $\mu\text{mol mol}^{-1}$, K_o was set to 278.4 $\mu\text{mol mol}^{-1}$,
2062 and Γ^* was set to 42.75 $\mu\text{mol mol}^{-1}$. All curve fits were visually examined for
2063 goodness-of-fit. The use of a common leaf temperature across curves and dark
2064 respiration measurements eliminated the need to temperature standardize rate
2065 estimates. For clarity, I reference V_{cmax} , J_{max} , and R_d estimates throughout the
2066 rest of the chapter as V_{cmax25} , J_{max25} , and R_{d25} .

2068 5.2.6 *Stomatal limitation*

2069 I quantified the extent by which stomatal conductance limited photosynthesis (l;
2070 unitless) following equations originally described in Farquhar and Sharkey (1982).
2071 Stomatal limitation was calculated as:

$$l = 1 - \frac{A_{net}}{A_{mod}} \quad (5.3)$$

2072 where A_{mod} represents the photosynthetic rate where $C_i=C_a$. A_{mod} was calculated

2073 as:

$$A_{mod} = V_{cmax25} - \frac{420 - \Gamma^*}{420 + K_m} - R_{d25} \quad (5.4)$$

2074 K_m is the Michaelis-Menten coefficient for Rubisco-limited photosynthesis, calcu-

2075 lated as:

$$K_m = K_c \cdot \left(1 + \frac{O_i}{K_o}\right) \quad (5.5)$$

2076 where O_i refers to leaf intercellular O_2 concentrations, set to $210 \mu\text{mol mol}^{-1}$.

2077 5.2.7 *Proportion of leaf nitrogen allocated to photosynthesis and structure*

2078 I used equations from Niinemets and Tenhunen (1997) to estimate the proportion

2079 of leaf nitrogen content allocated to Rubisco, bioenergetics, and light harvesting

2080 proteins. The proportion of leaf nitrogen allocated to Rubisco ($\rho_{rubisco}$; gN gN^{-1})

2081 was calculated as a function of V_{cmax25} and N_{area} :

$$\rho_{rubisco} = \frac{V_{cmax25} N_r}{V_{cr} N_{area}} \quad (5.6)$$

2082 where N_r is the amount of nitrogen in Rubisco, set to 0.16 gN (gN in Rubisco) $^{-1}$

2083 and V_{cr} is the maximum rate of RuBP carboxylation per unit Rubisco protein,

2084 set to $20.5 \mu\text{mol CO}_2 (\text{g Rubisco})^{-1}$. The proportion of leaf nitrogen allocated to

2085 bioenergetics (ρ_{bioe} ; gN gN^{-1}) was similarly calculated as a function of J_{max25} and

2086 N_{area} :

$$\rho_{\text{bioe}} = \frac{J_{\text{max}25} N_b}{J_{\text{mc}} N_{\text{area}}} \quad (5.7)$$

2087 where N_b is the amount of nitrogen in cytochrome f, set to 0.12407 gN (μmol cytochrome f) $^{-1}$ assuming a constant 1: 1: 1.2 cytochrome f: ferredoxin NADP reductase: coupling factor molar ratio (Evans and Seemann 1989; Niinemets and Tenhunen 1997), and J_{mc} is the capacity of electron transport per cytochrome f, set to 156 μmol electron (μmol cytochrome f) $^{-1}\text{s}^{-1}$.

2092 The proportion of leaf nitrogen allocated to light harvesting proteins (ρ_{light} ;
2093 gN gN $^{-1}$) was calculated as a function of Chl_{mass} and N_{mass} :

$$\rho_{\text{light}} = \frac{Chl_{\text{mass}}}{N_{\text{mass}} c_b} \quad (5.8)$$

2094 where c_b is the stoichiometry of the light-harvesting chlorophyll complexes of photosystem II, set to 2.75 mmol chlorophyll (gN in chlorophyll) $^{-1}$. I used the N_{mass} value of the focal leaf used to generate A_{net}/C_i curves instead of the leaf used to extract chlorophyll content, as the two leaves are from the same trifoliolate leaf set and are highly correlated (Figure D1).

2099 The proportion of leaf nitrogen content allocated to photosynthetic tissue
2100 (ρ_{photo} ; gN gN $^{-1}$) was estimated as the sum of ρ_{rubisco} , ρ_{bioe} , and ρ_{light} . Finally,
2101 the proportion of leaf nitrogen content allocated to structural tissue ($\rho_{\text{structure}}$; gN
2102 gN $^{-1}$) was estimated as:

$$\rho_{\text{structure}} = \frac{N_{\text{cw}}}{N_{\text{area}}} \quad (5.9)$$

2103 where N_{cw} is the leaf nitrogen content allocated to cell walls (gN m $^{-2}$), calculated

2104 as a function of M_{area} using an empirical equation from Onoda et al. (2017):

$$N_{cw} = 0.000355 * M_{area}^{1.39} \quad (5.10)$$

2105 5.2.8 *Whole plant traits*

2106 Seven weeks after experiment initiation and immediately following gas exchange
2107 measurements, I harvested all experimental individuals and separated biomass of
2108 each experimental individual into major organ types (leaves, stems, roots, and
2109 nodules when present). Fresh leaf area of all harvested leaves was measured using
2110 an LI-3100C (Li-COR Biosciences, Lincoln, Nebraska, USA). Total fresh leaf area
2111 (cm^2) was calculated as the sum of all leaf areas, including the focal leaf used to
2112 collect gas exchange data and the focal leaf used to extract chlorophyll content. All
2113 harvested material was dried in an oven set to 65°C for at least 48 hours, weighed,
2114 and ground to homogeneity. Leaves and nodules were manually ground with a
2115 mortar and pestle, while stems and roots were ground using a Wiley mill (E3300
2116 Mini Mill; Eberbach Corp., MI, USA). Total dry biomass (g) was calculated as
2117 the sum of dry leaf (including focal leaf for both the A_{net}/C_i curve and leaf used
2118 to extract chlorophyll content), stem, root, and root nodule biomass. I quantified
2119 carbon and nitrogen content of each respective organ type through elemental
2120 combustion (Costech-4010, Costech, Inc., Valencia, CA, USA) using subsamples
2121 of ground and homogenized organ tissue.

2122 Following the approach explained in the first experimental chapter, I calcu-
2123 lated structural carbon costs to acquire nitrogen as the ratio of total belowground
2124 carbon biomass to whole plant nitrogen biomass (N_{cost} ; gC gN^{-1}). Belowground

2125 carbon biomass (C_{bg} ; gC) was calculated as the sum of root carbon biomass
 2126 and root nodule carbon biomass. Root carbon biomass and root nodule carbon
 2127 biomass was calculated as the product of the organ biomass and the respective
 2128 organ carbon content. Whole plant nitrogen biomass (N_{wp} ; gN) was similarly
 2129 calculated as the sum of total leaf, stem, root, and root nodule nitrogen biomass,
 2130 including the focal leaf used for A_{net}/C_i curve and chlorophyll extractions. Leaf,
 2131 stem, root, and root nodule nitrogen biomass was calculated as the product of
 2132 the organ biomass and the respective organ nitrogen content. This calculation
 2133 only quantifies plant structural carbon costs to acquire nitrogen and does not
 2134 include any additional costs of nitrogen acquisition associated with respiration,
 2135 root exudation, or root turnover. An explicit explanation of the limitations for
 2136 interpreting this calculation can be found in Perkowski et al. (2021) and Terrer
 2137 et al. (2018).

2138 Finally, plant investments in nitrogen fixation were calculated as the ratio
 2139 of root nodule biomass to root biomass, where increasing values indicate an in-
 2140 crease in plant investments to nitrogen fixation (Dovrat et al. 2018; Dovrat et al.
 2141 2020; Perkowski et al. 2021). I also calculated the percent of leaf nitrogen ac-
 2142 quired from the atmosphere (% N_{dfa} ; %) using leaf $\delta^{15}\text{N}$ and the following equation
 2143 from Andrews et al. (2011):

$$\%N_{dfa} = \frac{\delta^{15}\text{N}_{reference} - \delta^{15}\text{N}_{sample}}{\delta^{15}\text{N}_{reference} - B} \quad (5.11)$$

2144 where $\delta^{15}\text{N}_{reference}$ refers to a reference plant that exclusively acquires nitrogen via
 2145 direct uptake, $\delta^{15}\text{N}_{sample}$ refers to an individual's leaf $\delta^{15}\text{N}$, and B refers to indi-

2146 individuals that are entirely reliant on nitrogen fixation. Within each unique nitrogen
2147 fertilization treatment-by-CO₂ treatment combination, I calculated the mean leaf
2148 δ¹⁵N for individuals growing in the non-inoculated treatment for δ¹⁵N_{reference}. Any
2149 individuals with visual confirmation of root nodule formation were omitted from
2150 the calculation of δ¹⁵N_{reference}. Following recommendations from Andrews et al.
2151 (2011) I calculated B within each CO₂ treatment using the mean leaf δ¹⁵N of
2152 inoculated individuals that received 0 ppm N. I did not calculate B within each
2153 unique soil nitrogen-by-CO₂ treatment combination, as previous studies suggest
2154 decreased reliance on nitrogen fixation with increasing soil nitrogen availability
2155 (Perkowski et al. 2021).

2156 5.2.9 *Statistical analyses*

2157 Uninoculated pots that had substantial root nodule formation (nodule biomass:
2158 root biomass values greater than 0.05 g g⁻¹) were removed from all analyses, as
2159 pots were assumed to have been colonized by symbiotic nitrogen-fixing bacteria
2160 from outside sources. This decision resulted in the removal of sixteen pots from
2161 analyses: two pots in the elevated CO₂ treatment that received 35 ppm N, three
2162 pots in the elevated CO₂ treatment that received 70 ppm N, one pot in the elevated
2163 CO₂ treatment that received 210 ppm N, two pots in the elevated CO₂ treatment
2164 that received 280 ppm N, two pots in the ambient CO₂ treatment that received
2165 0 ppm N, three pots in the ambient CO₂ treatment that received 70 ppm N, two
2166 pots in the ambient CO₂ treatment that received 105 ppm N, and one pot in the
2167 ambient CO₂ treatment that received 280 ppm N.

2168 I built a series of linear mixed effects models to investigate the impacts of

2169 CO₂ concentration, soil nitrogen fertilization, and inoculation with *B. japonicum*
2170 on *G. max* gas exchange, tradeoffs between nitrogen and water use, whole plant
2171 growth, and investment in nitrogen fixation. All models included CO₂ treatment
2172 as a categorical fixed effect, inoculation treatment as a categorical fixed effect,
2173 soil nitrogen fertilization as a continuous fixed effect, with interaction terms be-
2174 tween all three fixed effects. All models also accounted for climatic difference
2175 between chambers across experiment iterations by including a random intercept
2176 term that nested starting chamber rack by CO₂ treatment. Models with this
2177 independent variable structure were created for each of the following dependent
2178 variables: N_{area} , M_{area} , N_{mass} , Chl_{area} , V_{cmax25} , J_{max25} , $J_{\text{max25}}:V_{\text{cmax25}}$, R_{d25} , g_{sw} ,
2179 stomatal limitation, ρ_{rubisco} , ρ_{bioe} , ρ_{light} , ρ_{photo} , $\rho_{\text{structure}}$, total biomass, total leaf
2180 area, N_{cost} , C_{bg} , N_{wp} , nodule biomass, the ratio of nodule biomass to root biomass,
2181 and % N_{dfa} .

2182 I used Shapiro-Wilk tests of normality to determine whether linear mixed
2183 effects models satisfied residual normality assumptions. If residual normality as-
2184 sumptions were not met (Shapiro-Wilk: $p < 0.05$), then models were fit using de-
2185 pendent variables that were natural log transformed. If residual normality as-
2186 sumptions were still not met (Shapiro-Wilk: $p < 0.05$), then models were fit using
2187 dependent variables that were square root transformed. All residual normality
2188 assumptions that did not originally satisfy residual normality assumptions were
2189 met with either a natural log or square root data transformation (Shapiro-Wilk:
2190 $p > 0.05$ in all cases). Specifically, models for N_{area} , N_{mass} , Chl_{area} , V_{cmax25} , J_{max25} ,
2191 $J_{\text{max25}}:V_{\text{cmax25}}$, R_{d25} , g_{sw} , stomatal limitation, ρ_{rubisco} , ρ_{bioe} , ρ_{light} , ρ_{photo} , total leaf
2192 area, N_{cost} satisfied residual normality assumptions without data transformation.

2193 Models for M_{area} , $\rho_{\text{structure}}$, C_{bg} , and total biomass satisfied residual normality as
2194 assumptions with a natural log data transformation, while models for N_{wp} , nodule
2195 biomass, nodule biomass: root biomass, and $\%N_{\text{dfa}}$ satisfied residual normality
2196 assumptions with a square root data transformation.

2197 In all statistical models, I used the ‘lmer’ function in the ‘lme4’ R package
2198 (Bates et al. 2015) to fit each model and the ‘Anova’ function in the ‘car’ R
2199 package (Fox and Weisberg 2019) to calculate Type II Wald’s χ^2 and determine
2200 the significance ($\alpha=0.05$) of each fixed effect coefficient. I used the ‘emmeans’
2201 R package (Lenth 2019) to conduct post-hoc comparisons using Tukey’s tests,
2202 where degrees of freedom were approximated using the Kenward-Roger approach
2203 (Kenward and Roger 1997). All analyses and plots were conducted in R version
2204 4.2.0 (R Core Team 2021).

2205 5.3 Results

2206 5.3.1 Leaf nitrogen and chlorophyll content

2207 Elevated CO₂ reduced N_{area} , N_{mass} , and Chl_{area} by 29%, 50%, and 31%, respec-
2208 tively, and stimulated M_{area} by 44% ($p<0.001$ in all cases; Table 5.1). An inter-
2209 action between fertilization and CO₂ (CO₂-by-fertilization interaction: $p_{N_{\text{area}}}=$
2210 0.017, $p_{N_{\text{mass}}}<0.001$, $p_{Chl_{\text{area}}}=0.083$; Table 5.1) indicated that the positive effect
2211 of increasing fertilization on N_{area} , N_{mass} , and Chl_{area} ($p<0.001$ in all cases; Table
2212 5.1) was stronger under ambient CO₂ (Tukey _{N_{area}} : $p=0.026$; Tukey _{N_{mass}} : $p<0.001$;
2213 Tukey _{Chl_{area}} : $p=0.065$; Table 5.1; Figs. 5.1a, 5.1b, 5.1d). An interaction between
2214 fertilization and CO₂ on M_{area} (CO₂-by-fertilization interaction: $p=0.006$; Ta-
2215 ble 5.1) indicated that the positive effect of increasing fertilization on M_{area} was

2216 stronger under elevated CO₂ (Tukey: $p=0.009$; Fig. 5.1c). Overall, interactions
2217 between fertilization and CO₂ resulted in stronger reductions in N_{area} , N_{mass} , and
2218 Chl_{area} , and a stronger stimulation in M_{area} under elevated CO₂ with increasing
2219 fertilization.

2220 An interaction between inoculation and CO₂ on N_{area} (CO₂-by-inoculation
2221 interaction: $p=0.030$; Table 5.1) indicated that the positive effect of inoculation
2222 on N_{area} ($p<0.001$; Table 5.1) was stronger under elevated CO₂ (45% increase;
2223 Tukey: $p<0.001$) than under ambient CO₂ (18% increase; Tukey: $p<0.001$), a
2224 result that increased the reduction in N_{area} in inoculated pots under elevated
2225 CO₂. Inoculation treatment did not modify the reduction in N_{mass} (CO₂-by-
2226 inoculation interaction: $p=0.148$; Table 5.1) and Chl_{area} ($p = 0.147$; Table 5.1)
2227 or the stimulation in M_{area} ($p=0.866$; Table 5.1) under elevated CO₂. How-
2228 ever, interactions between fertilization and inoculation on N_{area} , N_{mass} , M_{area} ,
2229 and Chl_{area} (fertilization-by-inoculation interaction: $p_{N_{\text{area}}}<0.001$, $p_{N_{\text{mass}}}=0.001$,
2230 $p_{M_{\text{area}}}=0.025$, $p_{Chl_{\text{area}}}=0.083$; Table 5.1) indicated that the positive effect of in-
2231 creasing fertilization on each trait was stronger in uninoculated pots (Tukey N_{area} :
2232 $p<0.001$; Tukey N_{mass} : $p=0.001$; Tukey M_{area} : $p=0.031$; Tukey Chl_{area} : $p<0.001$;
2233 Figs. 5.1a-d).

Table 5.1. Effects of soil nitrogen fertilization, inoculation, and CO₂ treatments on leaf nitrogen content per unit leaf area (N_{area} ; gN m⁻²), leaf nitrogen content per unit leaf mass (N_{mass} , gN g⁻¹), leaf mass per unit leaf area (M_{area} ; g m⁻²), and chlorophyll content per unit leaf area (Chl_{area} ; mmol m⁻²)^{*}

	N_{area}			N_{mass}			M_{area}^a			
	df	Coefficient	χ^2	p	Coefficient	χ^2	p	Coefficient	χ^2	p
(Intercept)	-	1.10E+00	-	-	3.05E-02	-	-	3.64E+00	-	-
CO ₂	1	-5.67E-01	155.908	<0.001	-1.80E-02	272.362	<0.001	3.04E-01	151.319	<0.001
Inoculation (I)	1	6.21E-01	86.029	<0.001	7.54E-03	15.576	<0.001	1.81E-01	19.158	<0.001
Fertilization (N)	1	3.06E-03	316.408	<0.001	5.78E-05	106.659	<0.001	3.10E-04	21.440	<0.001
CO ₂ *I	1	2.63E-01	4.729	0.030	3.96E-03	2.025	0.155	-3.37E-02	0.029	0.866
CO ₂ *N	1	-3.68E-04	5.723	0.017	-2.85E-05	22.542	<0.001	2.80E-04	7.619	0.006
I*N	1	-1.36E-03	43.381	<0.001	-2.00E-05	11.137	0.001	-3.36E-04	5.022	0.025
CO ₂ *I*N	1	-3.23E-04	0.489	0.484	-2.59E-06	0.041	0.839	1.15E-04	0.208	0.649
Chl _{area}										
	df	Coefficient	χ^2	p						
(Intercept)	-	2.13E-02	-	-						
CO ₂	1	-1.33E-02	69.233	<0.001						
Inoculation (I)	1	1.24E-01	136.341	<0.001						
Fertilization (N)	1	3.35E-04	163.111	<0.001						
CO ₂ *I	1	-3.18E-02	2.102	0.147						
CO ₂ *N	1	-8.79E-05	2.999	0.083						
I*N	1	-2.65E-04	75.769	<0.001						
CO ₂ *I*N	1	7.68E-05	2.144	0.147						

2234 *Significance determined using Type II Wald χ^2 tests ($\alpha=0.05$). P-values less than 0.05 are in bold, while p-values
 2235 between 0.05 and 0.1 are italicized. A superscript “a” is included after trait labels to indicate if models were fit with
 2236 natural log transformed response variables. Key: df=degrees of freedom, χ^2 =Wald Type II chi-square test statistic.

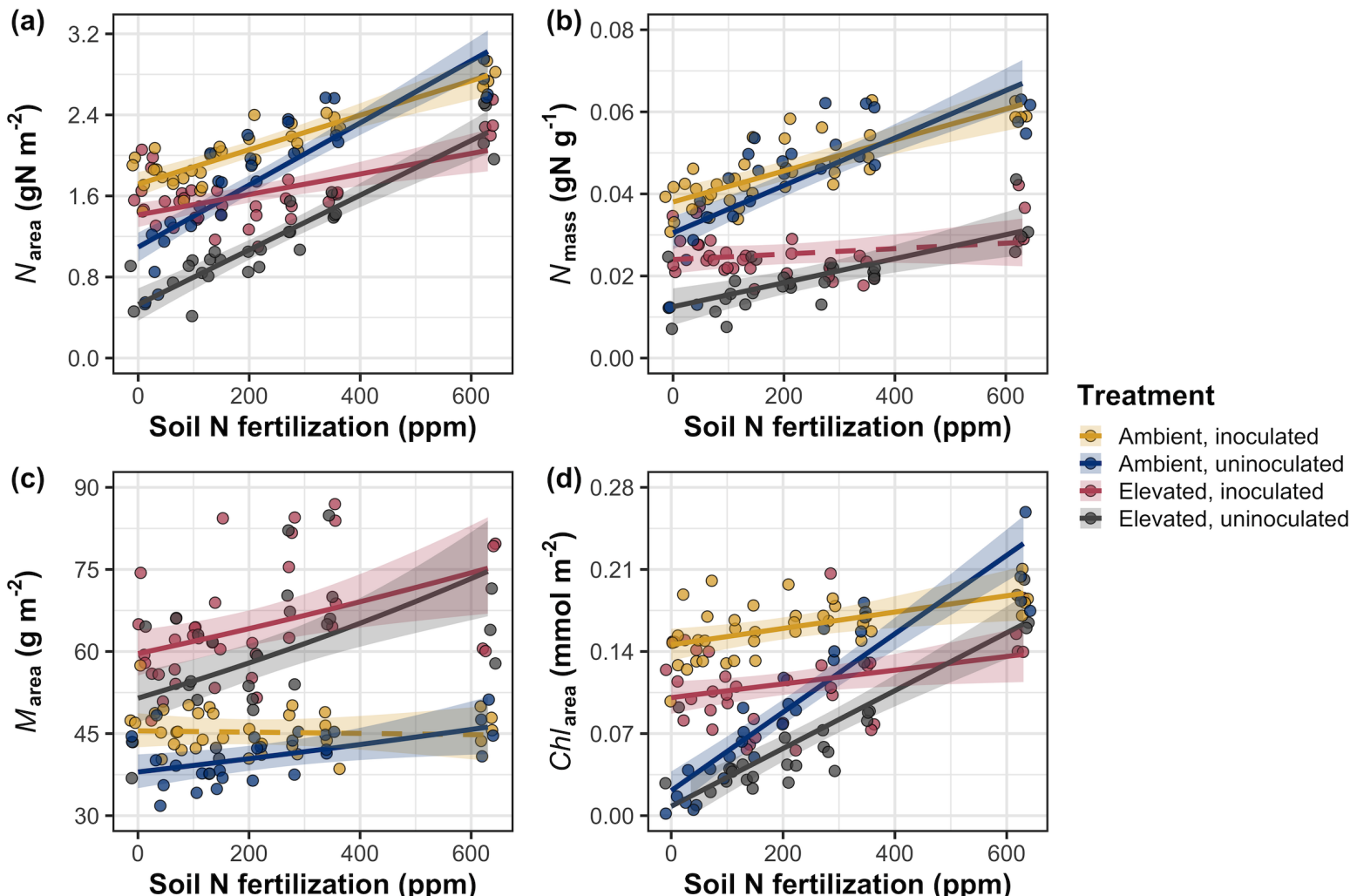


Figure 5.1. Effects of CO_2 , fertilization, and inoculation on leaf nitrogen per unit leaf area (a), leaf nitrogen content (b), leaf mass per unit leaf area (c), and chlorophyll content per unit leaf area (d). Soil nitrogen fertilization is represented on the x-axis in all panels. Yellow points and trendlines indicate inoculated individuals grown under ambient CO_2 , blue points and trendlines indicate uninoculated individuals grown under ambient CO_2 , red points and trendlines indicate inoculated individuals grown under elevated CO_2 , and gray points indicate uninoculated individuals grown under elevated CO_2 . Solid trendlines indicate regression slopes that are different from zero

2237 5.3.2 *Leaf biochemistry and stomatal conductance*

2238 Elevated CO₂ resulted in plants with 16% lower V_{cmax25} ($p<0.001$; Table 5.2) and
2239 10% lower J_{max25} ($p=0.014$; Table 5.2) compared to those grown under ambient
2240 CO₂. However, CO₂ concentration did not influence R_{d25} ($p=0.613$; Table 5.2;
2241 Fig. 5.2d). A relatively stronger reduction in V_{cmax25} than J_{max25} resulted in
2242 an 8% stimulation in $J_{max25}:V_{cmax25}$ under elevated CO₂ ($p<0.001$; Table 5.2).
2243 The negative effect of CO₂ on V_{cmax25} and J_{max25} was not modified across the
2244 fertilization gradient (CO₂-by-fertilization interaction: $p=0.185$ and $p=0.389$ for
2245 V_{cmax25} and J_{max25} , respectively; Table 5.2; Figs. 5.2a, 5.2b) or between inocula-
2246 tion treatments (CO₂-by-inoculation interaction: $p=0.799$ and $p=0.714$ for V_{cmax25}
2247 and J_{max25} , respectively; Table 5.2). However, a strong interaction between fer-
2248 tilization and inoculation (fertilization-by-inoculation interaction: $p\leq0.001$ in all
2249 cases; Table 5.2) indicated that the positive effect of increasing fertilization on
2250 V_{cmax25} ($p<0.001$; Table 5.2), J_{max25} ($p<0.001$; Table 5.2), and R_{d25} ($p=0.015$;
2251 Table 5.2) was only observed in uninoculated pots (Tukey: $p\leq0.001$ in all cases;
2252 Figs. 5.2a, 5.2b). A stronger positive effect of increasing fertilization on V_{cmax25}
2253 than J_{max25} resulted in a reduction in $J_{max25}:V_{cmax25}$ with increasing fertilization
2254 ($p<0.001$; Table 5.2), though this pattern was only observed in uninoculated pots
2255 (fertilization-by-inoculation interaction: $p=0.002$; Table 5.2; Fig. 5.2c).

2256 Elevated CO₂ reduced stomatal conductance by 20% ($p<0.001$; Table 5.2;
2257 Fig. 5.2e), but this pattern did not influence stomatal limitation of photosyn-
2258 thesis ($p=0.355$; Table 5.2; Fig. 5.2f). As with V_{cmax25} and J_{max25} , the reduction
2259 in stomatal conductance under elevated CO₂ was not modified across the fertil-
2260 ization gradient (CO₂-by-fertilization interaction: $p=0.141$; Table 5.2) or between

2261 inoculation treatments (CO_2 -by-inoculation interaction: $p=0.179$; Table 5.2). Fer-
2262 tilization did not modify the null effect of CO_2 on stomatal limitation (CO_2 -by-
2263 fertilization interaction: $p=0.554$; Table 5.2). An interaction between CO_2 and
2264 inoculation (CO_2 -by-inoculation interaction: $p=0.043$; Table 5.2) indicated that
2265 inoculation increased stomatal limitation under ambient CO_2 (Tukey: $p=0.021$),
2266 but not under elevated CO_2 (Tukey: $p>0.999$). An additional interaction between
2267 inoculation and fertilization on stomatal conductance (fertilization-by-inoculation
2268 interaction: $p<0.001$; Table 5.2) indicated that increasing fertilization increased
2269 stomatal conductance in uninoculated pots (Tukey: $p=0.003$) but decreased stom-
2270 atal conductance in inoculated pots (Tukey: $p=0.021$). The similar in magnitude,
2271 but opposite direction, trend in the effect of increasing fertilization on stomatal
2272 conductance between inoculation treatments likely drove a null response of stom-
2273 atal conductance to increasing fertilization ($p=0.642$; Table 5.2).

Table 5.2. Effects of soil nitrogen fertilization, inoculation, and CO₂ on the maximum rate of Rubisco carboxylation ($V_{\text{cmax}25}$; $\mu\text{mol m}^{-2} \text{s}^{-1}$), the maximum rate of RuBP regeneration ($J_{\text{max}25}$; $\mu\text{mol m}^{-2} \text{s}^{-1}$), dark respiration ($R_{\text{d}25}$; $\mu\text{mol m}^{-2} \text{s}^{-1}$), the ratio of the maximum rate of RuBP regeneration to the maximum rate of Rubisco carboxylation ($J_{\text{max}25}:V_{\text{cmax}25}$; unitless), stomatal conductance (g_{sw} ; $\text{mol m}^{-2} \text{s}^{-1}$), and stomatal limitation (unitless)*

	$V_{\text{cmax}25}$			$J_{\text{max}25}$			$R_{\text{d}25}$			
	df	Coefficient	χ^2	p	Coefficient	χ^2	p	Coefficient	χ^2	p
(Intercept)	-	4.36E+01	-	-	8.30E+01	-	-	1.69E+00	-	-
CO ₂	1	-7.05E+00	18.039	<0.001	-9.11E+00	6.042	0.014	4.53E-01	0.256	0.613
Inoculation (I)	1	5.87E+01	98.579	<0.001	9.62E+01	85.064	<0.001	1.04E+00	3.094	0.079
Fertilization (N)	1	1.32E-01	37.053	<0.001	2.09E-01	25.356	<0.001	2.86E-03	5.965	0.015
CO ₂ *I	1	-4.65E+00	0.065	0.799	7.84E-01	0.667	0.414	-5.71E-01	2.563	0.109
CO ₂ *N	1	-3.58E-02	1.758	0.185	-4.33E-02	0.742	0.389	-1.55E-03	2.675	0.102
I*N	1	-1.35E-01	60.394	<0.001	-2.30E-01	57.410	<0.001	-2.84E-03	12.083	0.001
CO ₂ *I*N	1	2.73E-02	0.748	0.387	3.46E-02	0.377	0.539	7.21E-04	0.244	0.622

	$J_{\text{max}25}:V_{\text{cmax}25}$			g_{sw}			Stomatal limitation			
	df	Coefficient	χ^2	p	Coefficient	χ^2	p	Coefficient	χ^2	p
(Intercept)	-	1.92E+00	-	-	1.95E-01	-	-	2.12E-01	-	-
CO ₂	1	5.71E-02	92.010	<0.001	-6.23E-02	9.718	0.002	3.91E-02	0.856	0.355
Inoculation (I)	1	-1.79E-01	27.768	<0.001	1.30E-01	22.351	<0.001	7.87E-02	4.582	0.032
Fertilization (N)	1	-4.61E-04	28.147	<0.001	2.50E-04	0.066	0.797	2.60E-04	32.218	<0.001
CO ₂ *I	1	8.94E-02	2.916	0.088	6.69E-02	1.810	0.179	-7.84E-02	4.093	0.043
CO ₂ *N	1	2.35E-04	3.210	0.073	-8.50E-05	2.165	0.141	-1.24E-04	0.350	0.554
I*N	1	3.27E-04	9.607	0.002	-3.09E-04	14.696	<0.001	-1.67E-04	2.547	0.110
CO ₂ *I*N	1	-1.66E-04	1.102	0.294	-8.89E-05	0.234	0.629	1.67E-04	2.231	0.135

2274 *Significance determined using Type II Wald χ^2 tests ($\alpha=0.05$). P-values less than 0.05 are in bold, while p-values
 2275 between 0.05 and 0.1 are italicized. Key: df=degrees of freedom; χ^2 =Wald Type II chi-square test statistic.

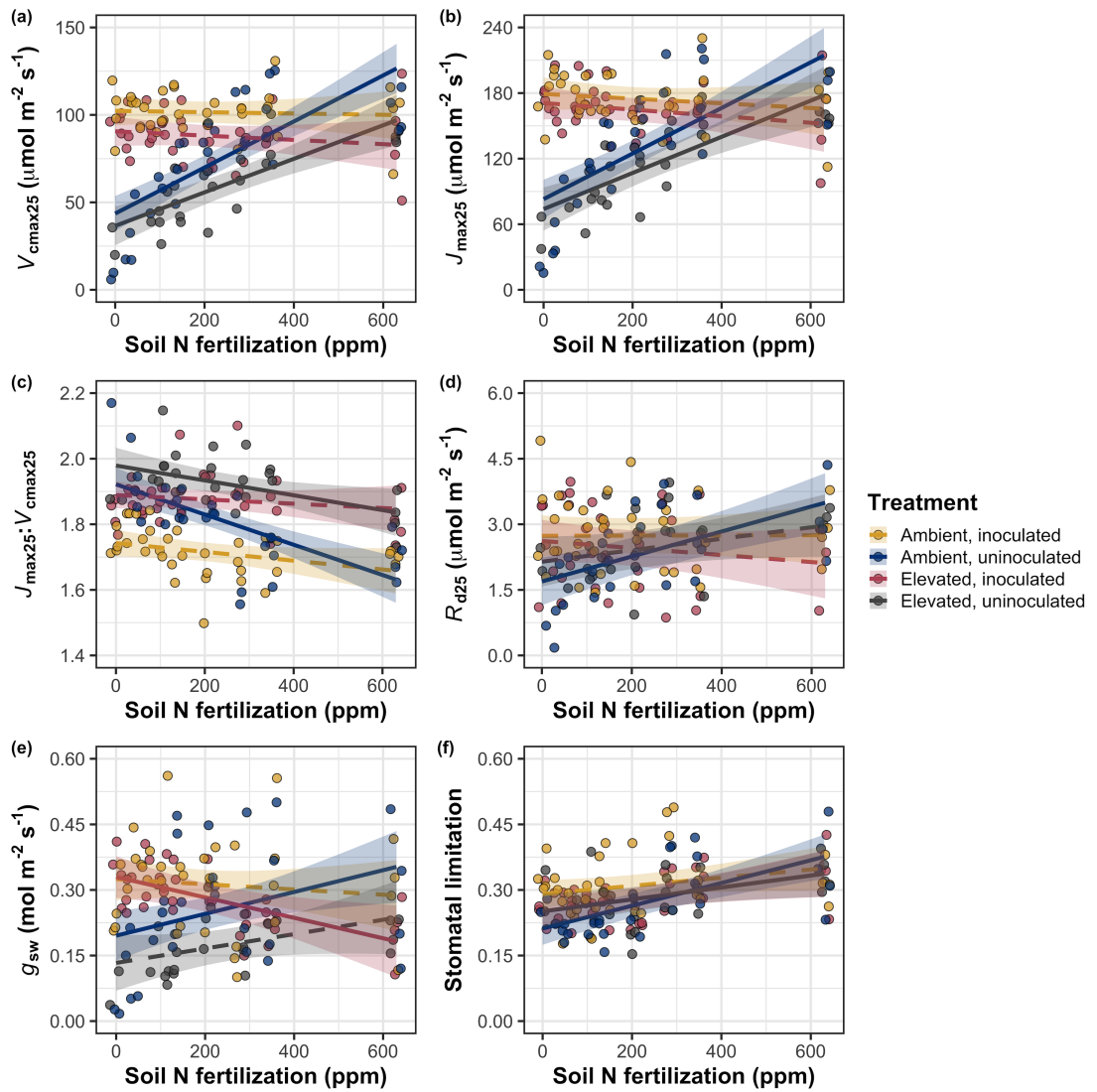


Figure 5.2. Effects of CO_2 , fertilization, and inoculation on maximum rate of Rubisco carboxylation (a), the maximum rate of RuBP regeneration (b), and the ratio of the maximum rate of RuBP regeneration to the maximum rate of Rubisco carboxylation leaf mass per unit leaf area (c), dark respiration (d), stomatal conductance (e), and stomatal limitation (f). Soil nitrogen fertilization is represented on the x-axis in all panels. Colored points and trendlines are as explained in Figure 5.1.

2276 5.3.3 *Leaf nitrogen allocation*

2277 A relatively stronger reduction in N_{area} than V_{cmax25} and J_{max25} under elevated
2278 CO_2 resulted in an 20% and 29% respective increase in ρ_{rubisco} and ρ_{bioe} ($p<0.001$
2279 in both cases; Table 5.3). There was no effect of CO_2 on ρ_{light} ($p=0.700$; Table
2280 5.3), but the increase in ρ_{rubisco} and ρ_{bioe} resulted in 21% greater ρ_{photo} under
2281 elevated CO_2 ($p<0.001$; Table 5.3; Fig. 5.3a). Effects of CO_2 on ρ_{rubisco} , ρ_{bioe} ,
2282 and ρ_{photo} were not modified across the fertilization gradient (CO_2 -by-fertilization
2283 interaction: $p_{\text{rubisco}}=0.269$, $p_{\text{bioe}}=0.298$, $p_{\text{photo}}=0.281$; Table 5.3). A marginal in-
2284 teraction between inoculation and CO_2 on ρ_{rubisco} and ρ_{photo} (CO_2 -by-inoculation
2285 interaction: $p_{\text{rubisco}}=0.057$, $p_{\text{photo}}=0.055$; Table 5.3) indicated that the positive ef-
2286 fect of inoculation on ρ_{rubisco} and ρ_{photo} ($p<0.001$ in both cases; Table 5.3) was only
2287 apparent under ambient CO_2 (Tukey: $p<0.001$ in both cases). Inoculation did
2288 not modify the positive effect of elevated CO_2 on ρ_{bioe} (CO_2 -by-inoculation inter-
2289 action: $p=0.122$; Table 5.3) or the null effect of CO_2 on ρ_{bioe} (CO_2 -by-inoculation
2290 interaction: $p=0.298$; Table 5.3). An interaction between fertilization and inocula-
2291 tion on ρ_{rubisco} , ρ_{bioe} , and ρ_{photo} (fertilization-by-inoculation interaction: $p<0.001$
2292 in all cases; Table 5.3) indicated that the negative effect of increasing fertilization
2293 on each trait ($p<0.001$ in all cases; Table 5.3) was only observed in inoculated pots
2294 (Tukey: $p<0.001$ in all cases). An additional interaction between fertilization and
2295 inoculation on ρ_{light} (fertilization-by-inoculation interaction: $p<0.001$; Table 5.3)
2296 indicated a negative effect of increasing fertilization on ρ_{light} in inoculated pots
2297 (Tukey: $p=0.041$), but a positive effect of increasing fertilization in uninoculated
2298 pots (Tukey: $p<0.001$).
2299 Increased M_{area} under elevated CO_2 resulted in an 133% stimulation of

2300 $\rho_{\text{structure}}$ ($p<0.001$; Table 5.3; Fig 5.3b). An interaction between fertilization and
2301 CO₂ (CO₂-by-fertilization interaction: $p=0.039$; Table 5.3) indicated that the
2302 negative effect of increasing fertilization ($p<0.001$; Table 5.3) on $\rho_{\text{structure}}$ was
2303 marginally stronger under ambient CO₂ (Tukey: $p=0.055$). A marginal inter-
2304 action between inoculation and CO₂ (CO₂-by-inoculation interaction: $p=0.057$;
2305 Table 5.3) indicated that the positive effect of inoculation on $\rho_{\text{structure}}$ ($p<0.001$;
2306 Table 5.3) was only observed under elevated CO₂ (Tukey: $p<0.001$), with no ap-
2307 parent inoculation effect observed under ambient CO₂ (Tukey: $p=0.513$). Finally,
2308 an interaction between fertilization and inoculation (fertilization-by-inoculation
2309 interaction: $p<0.001$; Table 5.3) indicated that, while increasing fertilization in-
2310 creased $\rho_{\text{structure}}$ ($p<0.001$; Table 5.3), this response was stronger in uninoculated
2311 pots (Tukey: $p=0.001$; Fig. 5.3b).

Table 5.3. Effects of soil nitrogen fertilization, inoculation, and CO₂ on the fraction of leaf nitrogen allocated to Rubisco (ρ_{rubisco} ; gN gN⁻¹), bioenergetics (ρ_{bioe} ; gN gN⁻¹), light harvesting proteins (ρ_{light} ; gN gN⁻¹), photosynthesis (ρ_{photo} ; gN gN⁻¹), and structure ($\rho_{\text{structure}}$; gN gN⁻¹)*

	ρ_{rubisco}			ρ_{bioe}			ρ_{light}			
	df	Coefficient	χ^2	p	Coefficient	χ^2	p	Coefficient	χ^2	p
(Intercept)	-	2.70E-01	-	-	5.26E-02	-	-	8.48E-03	-	-
CO ₂	1	1.42E-01	23.510	<0.001	3.00E-02	53.899	<0.001	2.03E-03	0.149	0.700
Inoculation (I)	1	1.83E-01	23.475	<0.001	2.80E-02	13.860	<0.001	2.04E-02	147.234	<0.001
Fertilization (N)	1	1.35E-04	16.609	<0.001	1.22E-05	26.827	<0.001	3.22E-05	19.378	<0.001
CO ₂ *I	1	-1.07E-01	3.629	0.057	-1.67E-02	2.390	0.122	-5.33E-03	0.684	0.408
CO ₂ *N	1	-2.16E-04	1.223	0.269	-3.59E-05	1.085	0.298	-7.01E-06	0.351	0.553
I*N	1	-4.26E-04	20.045	<0.001	-6.87E-05	15.458	<0.001	-4.37E-05	64.042	<0.001
CO ₂ *I*N	1	2.50E-04	3.327	0.068	4.08E-05	2.651	0.103	1.74E-05	3.735	0.053

	ρ_{photo}			$\rho_{\text{structure}}^a$			
	df	Coefficient	χ^2	p	Coefficient	χ^2	p
(Intercept)	-	3.32E-01	-	-	-2.93E+00	-	-
CO ₂	1	1.81E-01	27.651	<0.001	8.77E-01	229.571	<0.001
Inoculation (I)	1	2.31E-01	26.238	<0.001	-2.55E-01	13.872	<0.001
Fertilization (N)	1	1.76E-04	15.899	<0.001	-1.51E-03	38.128	<0.001
CO ₂ *I	1	-1.36E-01	3.671	0.055	-2.99E-01	3.622	0.057
CO ₂ *N	1	-2.72E-04	1.163	0.281	3.14E-04	4.266	0.039
I*N	1	-5.37E-04	21.355	<0.001	7.00E-04	11.025	0.001
CO ₂ *I*N	1	3.29E-04	4.009	0.045	4.52E-04	0.669	0.413

2312 *Significance determined using Type II Wald χ^2 tests ($\alpha=0.05$). P-values less than 0.05 are in bold, while p-values
 2313 between 0.05 and 0.1 are italicized. A superscript “a” is included after trait labels to indicate if models were fit with
 2314 natural log transformed response variable. Key: df=degrees of freedom; χ^2 =Wald Type II chi-square test statistic.

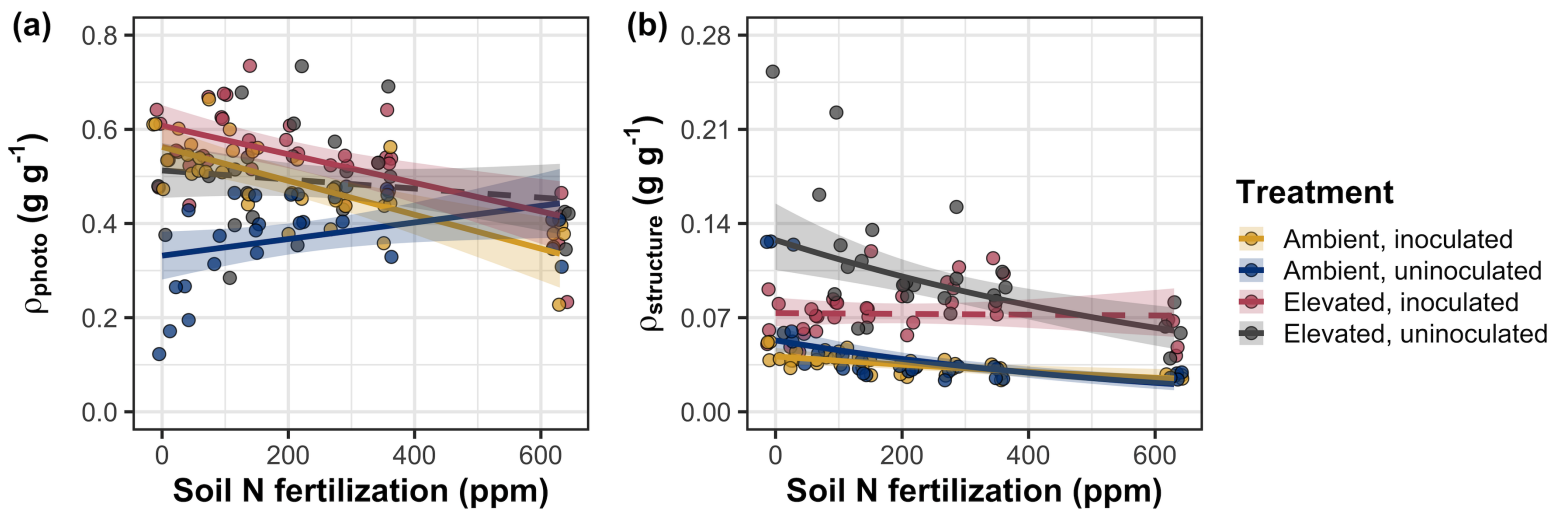


Figure 5.3. Effects of CO_2 , fertilization, and inoculation on the relative fraction of leaf nitrogen allocated to photosynthesis (a) and the fraction of leaf nitrogen allocated to structure (b). Soil nitrogen fertilization is represented on the x-axis in both panels. Colored points and trendlines are as explained in Figure 5.1.

2315 5.3.4 *Whole plant traits*

2316 Total leaf area and total biomass were 51% and 102% greater under elevated CO₂,
2317 respectively ($p<0.001$ in both cases; Table 5.4). The stimulation in total leaf area
2318 and total biomass under elevated CO₂ was enhanced by increasing fertilization
2319 (CO₂-by-fertilization interaction: $p<0.001$ in both cases; Table 5.4; Figs. 5.4a,
2320 5.4b) but was not modified across inoculation treatments (CO₂-by-inoculation
2321 interaction: $p_{total_leaf_area}=0.151$, $p_{total_biomass}=0.472$; Table 5.4). The positive
2322 effect of increasing fertilization on total leaf area and total biomass was modified by
2323 inoculation treatment (fertilization-by-inoculation interaction: $p<0.001$ in both
2324 cases; Table 5.4), indicating a stronger positive effect of increasing fertilization in
2325 uninoculated pots (Tukey: $p_{total_leaf_area}=0.002$, $p_{total_biomass}=0.001$, Figs. 5.4a,
2326 5.4b).

2327 A 62% stimulation in N_{cost} under elevated CO₂ was modified through a
2328 strong three-way interaction between CO₂, fertilization, and inoculation (CO₂-
2329 by-inoculation-by-fertilization interaction: $p<0.001$; Table 5.4; Fig. 5.4). This
2330 interaction revealed a general negative effect of increasing fertilization on N_{cost}
2331 ($p<0.001$; Table 5.4) that was observed in all treatment combinations (Tukey:
2332 $p<0.001$ in all cases) except for inoculated pots grown under elevated CO₂ (Tukey:
2333 $p=0.779$; Fig. 5.4c). This response also resulted in stronger negative effects of in-
2334 creasing fertilization on N_{cost} in uninoculated pots grown under elevated CO₂ than
2335 uninoculated pots grown under ambient CO₂ (Tukey: $p=0.001$) and inoculated
2336 pots grown under either ambient CO₂ (Tukey: $p<0.001$) or elevated CO₂ (Tukey:
2337 $p<0.001$), while uninoculated pots grown under ambient CO₂ had stronger nega-
2338 tive effects of increasing fertilization on N_{cost} than inoculated pots grown under

2339 elevated CO₂ (Tukey: $p=0.002$), but not inoculated pots grown under ambient
2340 CO₂ (Tukey: $p=0.216$; Fig. 5.4). The reduction in N_{cost} with increasing fertiliza-
2341 tion and in uninoculated pots were driven by a stronger positive effect of increasing
2342 fertilization on N_{wp} (denominator of N_{cost}) than C_{bg} (numerator of N_{cost}), while
2343 the stimulation in N_{cost} under elevated CO₂ was driven by a stronger positive
2344 effect of elevated CO₂ on C_{bg} than N_{wp} (Table 5.4).

Table 5.4. Effects of CO₂, fertilization, and inoculation on total leaf area (cm²), whole plant biomass (g), carbon costs to acquire nitrogen (N_{cost} ; gC gN⁻¹), belowground carbon biomass (C_{bg} ; gC), and whole plant nitrogen biomass (N_{wp} ; gN)*

Total leaf area				Total biomass ^b				<i>N</i> _{cost}		
	df	Coefficient	χ^2	p	Coefficient	χ^2	p	Coefficient	χ^2	p
(Intercept)	-	8.78E+01	-	-	9.96E-01	-	-	8.67E+00	-	-
CO ₂	1	3.36E+01	69.291	<0.001	5.07E-01	131.477	<0.001	8.75E+00	88.189	<0.001
Inoculation (I)	1	1.88E+02	35.715	<0.001	7.96E-01	34.264	<0.001	-1.68E+00	136.343	<0.001
Fertilization (N)	1	9.35E-01	274.199	<0.001	3.14E-03	269.046	<0.001	-8.50E-03	80.501	<0.001
CO ₂ *I	1	6.44E+01	2.064	0.151	-7.69E-02	0.518	0.472	-8.38E+00	85.237	<0.001
CO ₂ *N	1	5.05E-01	18.655	<0.001	1.61E-03	16.877	<0.001	-9.17E-03	1.050	0.306
I*N	1	-3.84E-01	10.804	0.001	-1.45E-03	15.779	<0.001	4.20E-03	46.489	<0.001
CO ₂ *I*N	1	-2.97E-03	<0.001	0.990	-1.14E-04	0.023	0.880	1.32E-02	18.125	<0.001

143

	C_{bg}^{a}	N_{wp}^{b}					
	df	Coefficient	χ^2	p	Coefficient	χ^2	p
(Intercept)	-	-1.70E+00	-	-	1.24E-01	-	-
CO ₂	1	9.21E-01	84.134	<0.001	-3.41E-03	23.890	<0.001
Inoculation (I)	1	1.18E+00	41.030	<0.001	1.68E-01	134.460	<0.001
N fertilization (N)	1	3.38E-03	152.248	<0.001	6.69E-04	529.021	<0.001
CO ₂ * I	1	-6.18E-01	8.965	0.003	3.68E-02	1.190	0.275
CO ₂ * N	1	-3.66E-05	1.188	0.276	1.58E-04	5.915	0.015
I * N	1	-2.22E-03	22.648	<0.001	-3.20E-04	55.562	<0.001
CO ₂ * I * N	1	8.09E-04	1.109	0.292	-7.54E-05	0.620	0.431

2345 *Significance determined using Type II Wald χ^2 tests ($\alpha=0.05$). *P*-values less than 0.05 are in bold. Superscripts
2346 included after trait labels indicate if models were fit with natural log (^a) or square root (^b) transformed response
2347 variables. Key: df=degrees of freedom; χ^2 =Wald Type II chi-square test statistic.

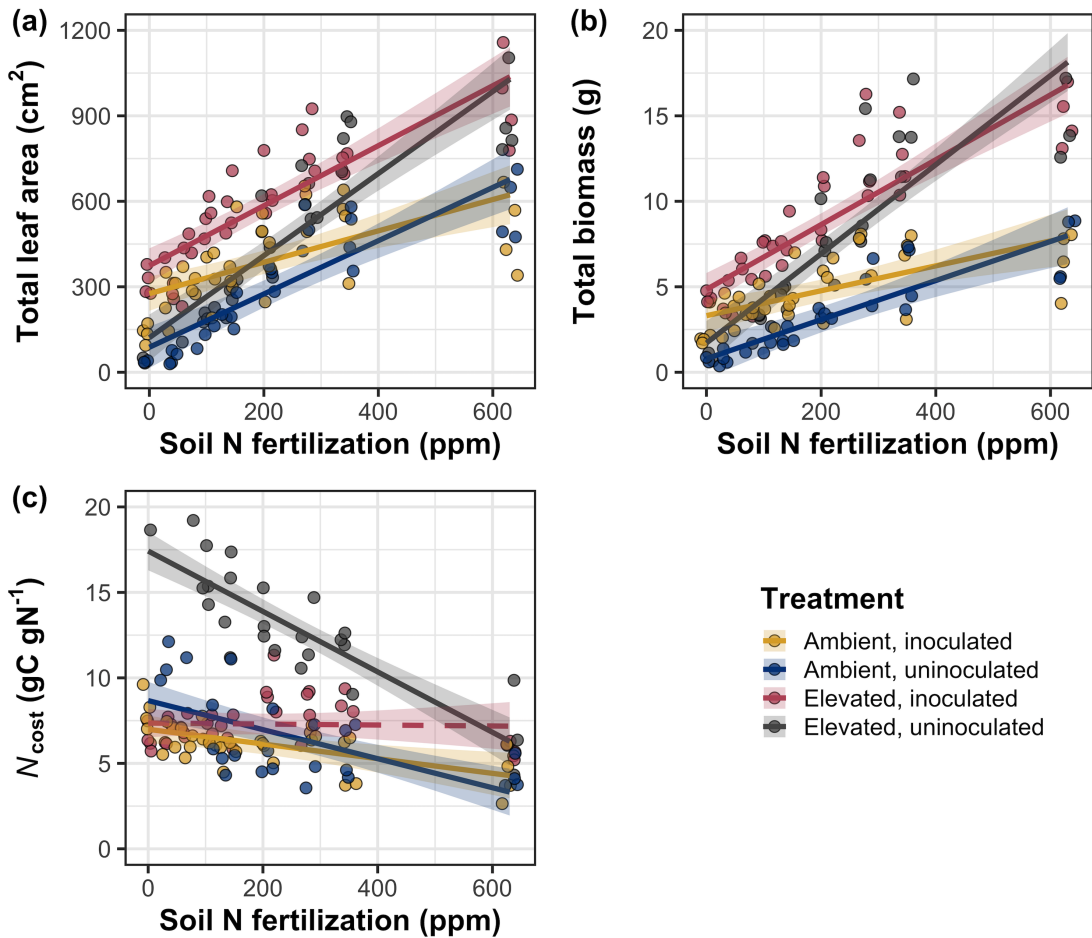


Figure 5.4. Effects of CO₂, fertilization, and inoculation on total leaf area (a), total biomass (b), and structural carbon costs to acquire nitrogen (c). Soil nitrogen fertilization is represented on the x-axis in all panels. Colored points and trendlines are as explained in Figure 5.1.

2348 5.3.5 *Nitrogen fixation*

2349 Nodule biomass was stimulated by 30% under elevated CO₂ ($p<0.001$; Table 5.5),
2350 a pattern that was modified across the fertilization gradient (CO₂-by-fertilization
2351 interaction: $p=0.479$; Table 5.5), but not between inoculation treatments (CO₂-
2352 by-inoculation interaction: $p=0.404$; Table 5.5). Specifically, the negative effect
2353 of increasing fertilization on nodule biomass ($p<0.001$; Table 5.5) was stronger
2354 under elevated CO₂ (Tukey: $p<0.001$; Fig. 5.5a). An interaction between fertil-
2355 ization and inoculation (fertilization-by-inoculation interaction: $p<0.001$; Table
2356 5.5) indicated a stronger negative effect of increasing fertilization in inoculated
2357 pots (Tukey: $p<0.001$; Fig. 5.5a).

2358 There was no effect of CO₂ on nodule: root biomass ($p=0.767$; Table 5.5),
2359 although an interaction between CO₂ and inoculation (CO₂-by-inoculation in-
2360 teraction: $p<0.001$; Table 5.5) indicated that the positive effect of inoculation
2361 on nodule: root biomass ($p<0.001$; Table 5.5) was stronger under ambient CO₂
2362 (3129% increase; Tukey: $p<0.001$) than elevated CO₂ (379% increase; Tukey:
2363 $p<0.001$; Fig. 5.5b). The null effect of CO₂ on nodule: root biomass was consis-
2364 tently observed across the fertilization gradient (CO₂-by-fertilization interaction:
2365 $p=0.183$; Table 5.5; Fig. 5.5b). An interaction between fertilization and inocula-
2366 tion (fertilization-by-inoculation interaction: $p<0.001$; Table 5.5) indicated that
2367 the negative effect of increasing fertilization on nodule: root biomass ($p<0.001$;
2368 Table 5.5) was stronger in inoculated pots (Tukey: $p<0.001$; Fig. 5.5b).

2369 There was no effect of CO₂ on %N_{dfa} ($p=0.472$; Table 5.5), a pattern
2370 that was not modified by inoculation (CO₂-by-inoculation interaction: $p=0.156$;
2371 Table 5.5) or fertilization (CO₂-by-fertilization interaction: $p=0.099$; Table 5.5).

- 2372** An interaction between fertilization and inoculation (fertilization-by-inoculation
2373 interaction: $p<0.001$; Table 5.5) indicated that the negative effect of increasing
2374 fertilization on $\%N_{dfa}$ ($p<0.001$; Table 5.5) was only observed in inoculated pots
2375 (Tukey: $p<0.001$; Fig. 5.5c).

Table 5.5. Effects of CO₂, fertilization, and inoculation on root nodule biomass (g), plant investments in symbiotic nitrogen fixation (unitless), and percent nitrogen fixed from the atmosphere (%N_{dfa}; unitless)*

	Root nodule biomass ^b			Root nodule: root biomass ^b			%N _{dfa} ^b			
	df	Coefficient	χ^2	p	Coefficient	χ^2	p	Coefficient	χ^2	p
(Intercept)	-	9.41E-03	-	-	1.33E-02	-	-	7.48E-01	-	-
CO ₂	1	1.20E-01	19.258	<0.001	9.94E-02	0.087	0.768	-1.00E-01	0.518	0.472
Inoculation (I)	1	5.74E-01	755.020	<0.001	5.40E-01	903.691	<0.001	9.01E+00	955.570	<0.001
Fertilization (N)	1	7.71E-06	84.376	<0.001	-5.99E-06	258.099	<0.001	3.64E-04	292.938	<0.001
CO ₂ *I	1	-4.68E-02	0.950	0.330	-1.38E-01	20.614	<0.001	-1.44E-01	2.010	0.156
CO ₂ *N	1	-1.59E-04	2.106	0.147	-1.73E-04	1.773	0.183	-6.21E-05	2.716	0.099
I*N	1	-5.82E-04	44.622	<0.001	-7.45E-04	133.918	<0.001	-1.58E-02	231.290	<0.001
CO ₂ *I*N	1	7.26E-05	0.196	0.658	1.76E-04	2.359	0.125	2.77E-03	2.119	0.145

2376 *Significance determined using Type II Wald χ^2 tests ($\alpha=0.05$). P-values less than 0.05 are in bold, while p-values
2377 between 0.05 and 0.1 are italicized. Superscript letters indicate model coefficients fit to square-root (^b) transformed
2378 data. Key: df=degrees of freedom; χ^2 =Wald Type II chi-square test statistic.

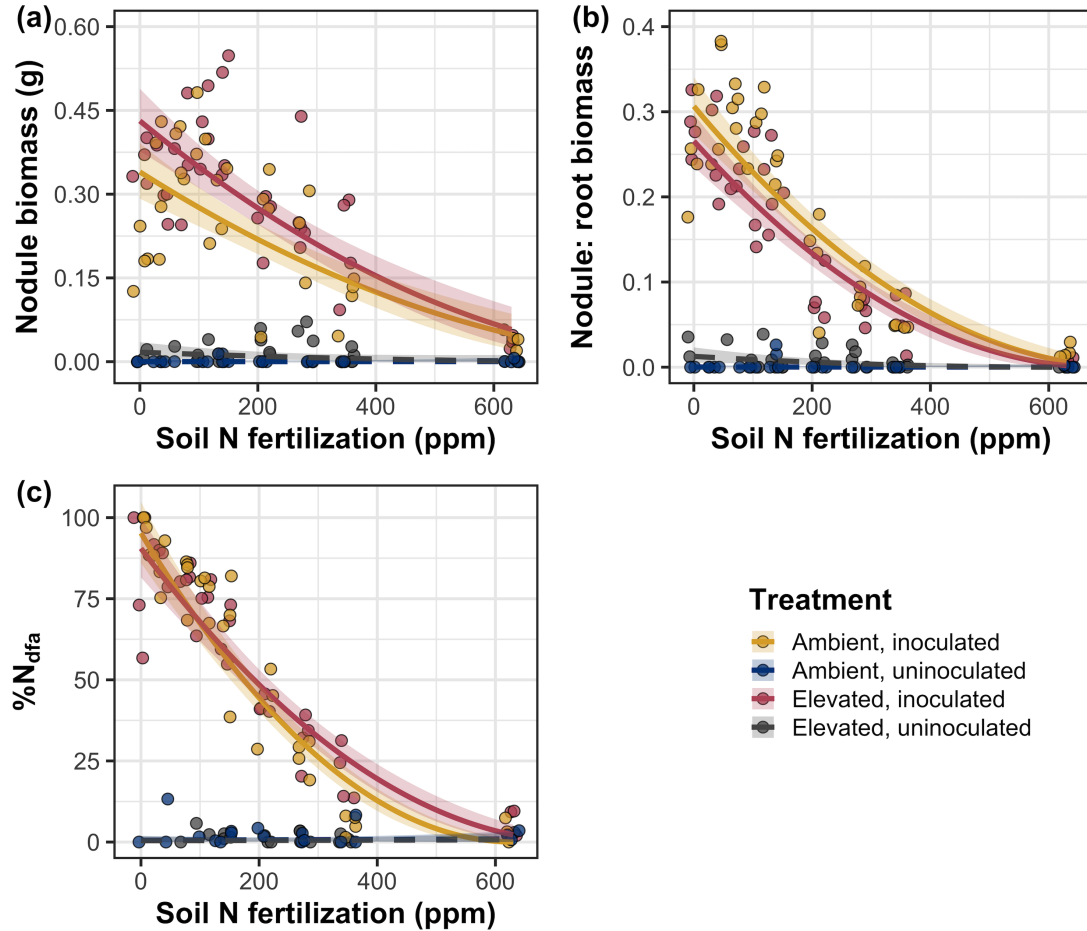


Figure 5.5. Effects of CO₂, fertilization, and inoculation on nodule biomass (a), nodule biomass: root biomass (b), and percent nitrogen fixed from the atmosphere (c). Soil nitrogen fertilization is represented on the x-axis. Colored points and trendlines are as explained in Figure 5.1. Curvilinear trendlines occur as a result of back-transforming models where response variables received either a natural log or square root transformation prior to fitting.

2379 5.4 Discussion

2380 In this study, I determined leaf and whole plant acclimation responses of 7-week *G.*
2381 *max* seedlings grown under two CO₂ concentrations, two inoculation treatments,
2382 and nine soil nitrogen fertilization treatments in a full-factorial growth chamber
2383 experiment. In support of hypotheses and patterns expected from theory, elevated
2384 CO₂ reduced N_{area} , V_{cmax25} , and J_{max25} . The relatively stronger reduction in
2385 V_{cmax25} than J_{max25} under elevated CO₂ resulted in a stimulation in $J_{\text{max25}}:V_{\text{cmax25}}$
2386 under elevated CO₂. Reduced V_{cmax25} and J_{max25} under elevated CO₂ was similar
2387 across fertilization and inoculation treatments, indicating that the CO₂ responses
2388 were not associated with nitrogen limitation. Interestingly, results indicate that
2389 elevated CO₂ increased the fraction of leaf nitrogen allocated to photosynthesis
2390 and structure, leading to a stimulation in nitrogen use efficiency under elevated
2391 CO₂ despite the apparent reduction in N_{area} , V_{cmax25} , and J_{max25} .

2392 Downregulated leaf biochemical process rates under elevated CO₂ corre-
2393 sponded with strong increases in total leaf area and total biomass. Increased
2394 whole plant growth under elevated CO₂ was generally enhanced with increasing
2395 fertilization and were negatively related to structural carbon costs to acquire ni-
2396 trogen. Inoculation generally did not modify whole plant responses to elevated
2397 CO₂ across the fertilization gradient, likely due to a strong reduction in root nodu-
2398 lation with increasing fertilization. However, strong positive effects of inoculation
2399 on whole plant growth were observed under low fertilization, consistent with hy-
2400 potheses. Overall, observed leaf and whole plant acclimation responses to CO₂
2401 support hypotheses and patterns expected from photosynthetic least-cost theory,
2402 showing that leaf acclimation responses to CO₂ were decoupled from soil nitrogen

2403 availability and ability to acquire nitrogen via symbiotic nitrogen fixation. In-
2404 stead, leaf and whole plant acclimation responses to CO₂ were driven by optimal
2405 resource investment to photosynthetic capacity, where optimal resource invest-
2406 ment at the leaf level maximized nitrogen allocation to structures that support
2407 whole plant growth.

2408 5.4.1 *Soil nitrogen fertilization has divergent effects on leaf and whole plant*
2409 *acclimation responses to CO₂*

2410 Elevated CO₂ reduced N_{area} , V_{cmax25} , J_{max25} , and stomatal conductance by 29%,
2411 16%, 10%, and 20%, respectively. The larger reduction in V_{cmax25} than J_{max25} led
2412 to an 8% stimulation in $J_{\text{max25}}:V_{\text{cmax25}}$, while the larger reduction in N_{area} than
2413 V_{cmax25} resulted in a 21% stimulation in the fraction of leaf nitrogen allocated to
2414 photosynthesis under elevated CO₂. These acclimation responses are directionally
2415 consistent with previous studies that have investigated or reviewed leaf acclima-
2416 tion responses to CO₂ (Drake et al. 1997; Makino et al. 1997; Ainsworth et al.
2417 2002; Ainsworth and Long 2005; Ainsworth and Rogers 2007; Smith and Dukes
2418 2013; Smith and Keenan 2020; Poorter et al. 2022), and follow patterns expected
2419 from photosynthetic least-cost theory (Wright et al. 2003; Prentice et al. 2014;
2420 Smith et al. 2019; Smith and Keenan 2020). Together, increased $J_{\text{max25}}:V_{\text{cmax25}}$
2421 and the fraction of leaf nitrogen allocated to photosynthesis under elevated CO₂
2422 provide strong support for the idea that leaves reduced V_{cmax25} such that net photo-
2423 synthesis rates approached becoming equally co-limited by Rubisco carboxylation
2424 and RuBP regeneration (Chen et al. 1993; Maire et al. 2012) while optimizing
2425 resource use efficiency.

2426 Increasing fertilization and inoculation induced strong positive effects on
2427 N_{area} , V_{cmax25} , J_{max25} . The positive effect of increasing fertilization on N_{area} was
2428 enhanced under ambient CO₂, which, paired with the reduction N_{area} under el-
2429 evated CO₂, resulted in a stronger reduction in N_{area} under elevated CO₂ with
2430 increasing fertilization and in inoculated pots. These patterns suggest that N_{area}
2431 responses to CO₂ were at least partially dependent on soil nitrogen fertilization
2432 and nitrogen acquisition strategy. However, increased fractions of leaf nitrogen
2433 allocated to Rubisco, bioenergetics, or photosynthesis under elevated CO₂ were
2434 not modified across the fertilization gradient and was only marginally enhanced in
2435 inoculated pots. These patterns suggest that increasing soil nitrogen fertilization
2436 and inoculation did not change relative nutrient investment in photosynthetic tis-
2437 sues, supporting the idea that leaf acclimation responses to CO₂ were decoupled
2438 from soil nitrogen availability.

2439 Leaf acclimation responses to elevated CO₂ corresponded with a 62% and
2440 100% increase in total leaf area and total biomass, respectively. Increases in to-
2441 tal leaf area and total biomass under elevated CO₂ corresponded with generally
2442 larger structural carbon costs to acquire nitrogen, a pattern driven by an increase
2443 in belowground carbon biomass and reduction in whole plant nitrogen biomass.
2444 This result suggests that elevated CO₂ reduces plant nitrogen uptake efficiency,
2445 which does not explain why plants grown under elevated CO₂ generally had higher
2446 biomass and total leaf area, unless growth stimulations under elevated CO₂ were
2447 driven by reductions in per-tissue nitrogen demand (Dong et al. 2022). Interest-
2448 ingly, strong negative effects of increasing fertilization on structural carbon costs
2449 to acquire nitrogen, which were generally similar between CO₂ concentrations,

2450 were driven by stronger increases in whole plant nitrogen biomass than below-
2451 ground carbon biomass. This response allowed plants to increase nitrogen uptake
2452 efficiency with increasing fertilization, providing a possible mechanism that ex-
2453 plains why increasing fertilization increased the positive effect of elevated CO₂ on
2454 whole plant growth.

2455 Interestingly, results indicate that increased total leaf area and whole plant
2456 growth under elevated CO₂ was not modified by inoculation despite an apparent
2457 general negative effect of inoculation on N_{cost} . This response could have been
2458 due to the strong negative effect of increasing fertilization on nodulation, which
2459 may have masked any effect of inoculation treatments in high fertilization treat-
2460 ments. Reductions in nodulation with increasing fertilization are commonly ob-
2461 served patterns that allow species optimize nitrogen uptake efficiency as costs to
2462 acquire nitrogen via direct uptake become more similar (Gibson and Harper 1985;
2463 Rastetter et al. 2001). In this study, pairwise comparisons indicated strong pos-
2464 itive effects of inoculation on total leaf area and total biomass (158% increase in
2465 total leaf area, 119% increase in total biomass) under elevated CO₂ at 0 ppm N
2466 ($p<0.05$ in both cases), but no observable inoculation effect on total leaf area or
2467 total biomass under elevated CO₂ at 350 ppm N or 630 ppm N ($p>0.05$ in both
2468 cases). While these responses did not generally differ from those observed under
2469 ambient CO₂, they do confirm the hypothesis that positive effects of inoculation
2470 on whole plant growth responses to elevated CO₂ would decrease with increasing
2471 fertilization. These results also support the paradigm that symbiotic nitrogen
2472 fixation is a nutrient acquisition strategy that may allow plants who sustain such
2473 symbioses to have competitive advantages for resources than species not capable

2474 of forming such symbioses.

2475 Combined, results reported here suggest that soil nitrogen availability plays
2476 divergent roles in shaping leaf and whole plant acclimation responses to CO₂. Leaf
2477 acclimation responses were generally decoupled from fertilization, while whole
2478 plant acclimation responses relied heavily on an increase in nitrogen uptake ef-
2479 ficiency and consequent reduction in costs of acquiring nitrogen associated with
2480 increasing fertilization. Whole plant responses to CO₂ indicated that fertilization
2481 may play a more important role in determining whole plant acclimation responses
2482 to CO₂ than nitrogen acquisition strategy, although any inoculation effect was
2483 likely masked by the strong reduction in root nodulation with increasing fertil-
2484 ization. These results suggest that plants acclimate to CO₂ in nitrogen-limited
2485 systems by minimizing the number of optimally coordinated leaves, and that re-
2486 ductions in leaf nitrogen content under elevated CO₂ are not driven by changes
2487 in soil nitrogen availability as has been previously implied.

2488 5.4.2 *Implications for future model development*

2489 Many terrestrial biosphere models predict photosynthetic capacity through plant
2490 functional group-specific linear regressions between N_{area} and V_{cmax} (Rogers 2014;
2491 Rogers et al. 2017), which assumes that leaf nitrogen-photosynthesis relation-
2492 ships are constant across growing environments. These results build on previ-
2493 ous work suggesting that leaf nitrogen-photosynthesis relationships dynamically
2494 change across growing environments (Luo et al. 2021; Dong et al. 2022), showing
2495 that CO₂ concentration increases the fraction of leaf nitrogen content allocated to
2496 photosynthesis independent of fertilization or acquisition strategy. Additionally,
2497 increasing fertilization strongly decreased the fraction of leaf nitrogen allocated

2498 to photosynthesis, a response that was largely determined by acquisition strategy.
2499 Specifically, reductions in the fraction of leaf nitrogen allocated to photosynthesis
2500 with increasing fertilization were only observed in inoculated pots that had less
2501 finite access to nitrogen, suggesting that constant leaf nitrogen-photosynthesis
2502 relationships may only be apparent in environments where nitrogen is limiting.
2503 Terrestrial biosphere models that parameterize photosynthetic capacity through
2504 linear relationships between N_{area} and V_{cmax} (Rogers 2014; Rogers et al. 2017) may
2505 therefore be overestimating photosynthetic capacity in systems where nitrogen is
2506 not as limiting. Such models are also not capable of detecting stimulations in the
2507 fraction of leaf nitrogen allocated to photosynthesis with increasing CO_2 concen-
2508 tration. The inability of models to predict these responses likely contributes to the
2509 widespread divergence of model simulations under future environmental scenarios
2510 (Friedlingstein et al. 2014; Davies-Barnard et al. 2020), and should therefore be
2511 a target for resolving in future generations of terrestrial biosphere models.

2512 These results demonstrate that optimal resource investment to photosyn-
2513 thetic capacity defines leaf acclimation responses to elevated CO_2 , and that these
2514 responses were independent of fertilization or inoculation treatment. Current
2515 model approaches for simulating photosynthetic responses to CO_2 generally in-
2516 voke patterns expected from progressive nitrogen limitation, where reductions
2517 in N_{area} , and therefore photosynthetic capacity, due to elevated CO_2 are formu-
2518 lated as a function of progressive reductions in soil nitrogen availability. Results
2519 reported here contradict this formulation, suggesting that the leaf acclimation re-
2520 sponse is driven by optimal resource investment to photosynthetic capacity and
2521 is independent of soil resource supply. Optimality models that leverage prin-

2522 ciples from optimal coordination and photosynthetic least-cost theories (Wang
2523 et al. 2017; Stocker et al. 2020; Scott and Smith 2022) are capable of capturing
2524 such acclimation responses to CO₂ (Smith and Keenan 2020), suggesting that the
2525 implementation of these models may improve the simulation of photosynthetic
2526 processes in terrestrial biosphere models under increasing CO₂ concentrations.

2527 5.4.3 *Study limitations and future directions*

2528 There are two study limitations that must be addressed to contextualize patterns
2529 observed in this study. First, restricting the volume of belowground substrate
2530 via a potted experiment does not adequately replicate belowground environments
2531 of natural systems, and therefore may modify effects of soil resource availability
2532 and inoculation on plant nitrogen uptake. This limitation may be particularly
2533 relevant if pot size limits whole plant growth (Poorter et al. 2012). I attempted
2534 to minimize the extent of pot size limitation experienced in the first experimen-
2535 tal chapter while accounting for the expected stimulation in whole plant growth
2536 under elevated CO₂ by using 6-liter pots. Despite attempts to minimize growth
2537 limitation imposed by pot volume, fertilization and CO₂ treatments increased the
2538 biomass: pot volume ratio such that all treatment combinations to exceed 1 g L⁻¹
2539 biomass: pot volume under high fertilization (Table D3; Fig. D2). The 1 g L⁻¹
2540 biomass: pot volume recommendation from Poorter et al. (2012) was designated
2541 to avoid growth limitation imposed by pot volume. However, if pot size limita-
2542 tion indeed limited whole plant growth, then structural carbon costs to acquire
2543 nitrogen, belowground carbon biomass, whole plant nitrogen biomass, and whole
2544 plant biomass should each exhibit strong saturation points with increasing fertil-

2545 ization, which was not observed here. Importantly, leaf acclimation responses to
2546 CO₂ observed in this study are consistent with findings reported in (Smith and
2547 Keenan 2020), who used data from field manipulation experiments that did not
2548 have any belowground space limitation.

2549 Second, this study evaluated leaf and whole plant responses to CO₂ in 7-
2550 week seedlings. Given the long-term scale of the progressive nitrogen limitation
2551 hypothesis, patterns observed here should be validated in longer-term nitrogen
2552 manipulation experiments. Previous work in free air CO₂ enrichment experiments
2553 show some support for patterns expected from the progressive nitrogen limitation
2554 hypothesis (Reich et al. 2006; Norby et al. 2010), although results are not consis-
2555 tent across experimental sites (Finzi et al. 2006; Moore et al. 2006; Liang et al.
2556 2016). I found some support for patterns expected by the progressive nitrogen
2557 limitation hypothesis, namely the increase in plant nitrogen uptake under elevated
2558 CO₂ (Luo et al. 2004), though leaf acclimation responses to CO₂ were strongly
2559 indicative of optimal resource investment to photosynthetic capacity as expected
2560 from photosynthetic least-cost theory (Prentice et al. 2014; Smith et al. 2019;
2561 Smith and Keenan 2020).

2562 5.4.4 *Conclusions*

2563 This study provides strong evidence suggesting that leaf acclimation responses
2564 to elevated CO₂ did not vary with soil nitrogen fertilization or ability to acquire
2565 nitrogen through symbiotic nitrogen fixation. However, whole plant acclimation
2566 responses to CO₂ were dependent on fertilization, where increasing fertilization
2567 increased the positive effect of whole plant growth under elevated CO₂. Results
2568 also indicate that fertilization played a relatively more important role in modify-

2569 ing whole plant responses to CO₂ than inoculation with symbiotic nitrogen-fixing
2570 bacteria, perhaps due to a reduction in nodulation across the fertilization gra-
2571 dient. These patterns strongly support the hypothesis that leaf and whole plant
2572 acclimation responses are driven by optimal resource investment to photosynthetic
2573 capacity, and that leaf acclimation responses to CO₂ were not modified by changes
2574 in soil nitrogen availability. These results build on previous work suggesting that
2575 constant leaf nitrogen-photosynthesis relationships are dynamic and change across
2576 growing environments, calling the current formulation of photosynthetic processes
2577 used in many terrestrial biosphere models into question.

2578

Chapter 6

2579

Conclusions

2580 The experiments included in this dissertation test mechanisms that drive patterns
2581 expected from photosynthetic least-cost theory across various edaphic and climatic
2582 gradients. Specifically, I investigate environmental drivers of carbon costs to ac-
2583 quire nitrogen, tradeoffs between nitrogen and water use, and plant acclimation
2584 responses to CO₂. These experiments provide important empirical data needed to
2585 test assumptions made in optimality models that leverage photosynthetic least-
2586 cost frameworks, and are among the first manipulative experiments to show sup-
2587 port for patterns expected from theory. Below, I summarize main findings of each
2588 chapter, synthesize common patterns observed across experiments, and conclude
2589 with a few study ideas that I think will help refine our understanding of plant
2590 nutrient acquisition and allocation responses to environmental change leveraging
2591 patterns predicted by photosynthetic least-cost theory.

2592 In the first experimental chapter, I quantified carbon costs to acquire ni-
2593 trogen in a species capable of forming associations with symbiotic nitrogen-fixing
2594 bacteria (*Glycine max*) and a species not capable of forming such associations
2595 (*Gossypium hirsutum*) grown under four soil nitrogen fertilization treatments and
2596 four light availability treatments in a full factorial greenhouse experiment. Sup-
2597 porting hypotheses, increasing light availability increased carbon costs to acquire
2598 nitrogen in both species due to a larger increase in belowground carbon biomass
2599 than whole plant nitrogen biomass. In further support of hypotheses, increasing
2600 fertilization decreased carbon costs to acquire nitrogen due to a larger increase in

2601 whole plant nitrogen biomass than belowground carbon biomass. Root nodulation
2602 data indicated that *G. max* shifted relative carbon allocation from nitrogen fixa-
2603 tion to direct uptake with increasing fertilization, which may explain the reduced
2604 responsiveness of *G. max* carbon costs to acquire nitrogen across the fertilization
2605 gradient.

2606 Despite evidence that reductions in the response of *G. max* carbon costs
2607 to acquire nitrogen to increasing fertilization may have been driven by shifts away
2608 from nitrogen fixation with increasing fertilization, I urge caution in assigning
2609 causality to the differential response of carbon costs to acquire nitrogen between
2610 species. This is because *G. max* and *G. hirsutum* are not phylogenetically related
2611 and have different life histories. Differences in life history between the two species
2612 limit my ability to assess whether reductions in the negative effect of increasing
2613 fertilization on carbon costs to acquire nitrogen in *G. max* were driven by shifts
2614 to direct uptake with increasing fertilization. However, these patterns were later
2615 confirmed in the fourth experimental chapter, where similar weaker negative ef-
2616 fects of increasing fertilization on carbon costs to acquire nitrogen were observed
2617 in *G. max* that were inoculated with symbiotic nitrogen-fixing bacteria compared
2618 to *G. max* that were left uninoculated across a similar soil nitrogen fertilization
2619 gradient.

2620 In the second experimental chapter, I assessed whether changes in soil
2621 nitrogen availability or soil pH drove changes in nitrogen-water use tradeoffs pre-
2622 dicted by photosynthetic least-cost theory. I measured leaf traits of mature upper
2623 canopy deciduous trees growing in a nine-year nitrogen-by-sulfur field manipula-
2624 tion experiment, where experimental sulfur additions were added with intent to

2625 acidify plots. Following patterns expected from the theory, increasing soil nitrogen
2626 availability was associated with increased leaf nitrogen content, but not net photo-
2627 tosynthesis, resulting in an increase in photosynthetic nitrogen use efficiency. In
2628 further support of theory, increasing soil nitrogen availability exhibited slight, but
2629 nonsignificant, decreases in leaf $C_i:C_a$ and increases in measures of photosynthetic
2630 capacity. Perhaps the strongest evidence for the theory was a strong negative
2631 relationship between leaf nitrogen content and leaf $C_i:C_a$, of which increased with
2632 increasing soil nitrogen availability through a stronger increase in leaf nitrogen
2633 content than leaf $C_i:C_a$.

2634 I found no effect of soil pH on nitrogen-water use tradeoffs aside from a
2635 marginal reduction in net photosynthesis rates that marginally reduced photosyn-
2636 thetic nitrogen use efficiency with increasing soil pH. Directionally, reductions in
2637 photosynthetic nitrogen use efficiency with increasing soil pH were expected per
2638 theory; however, this response was driven by no change in leaf nitrogen content
2639 and a reduction in net photosynthesis. Theory predicts that these tradeoffs should
2640 be driven by no change in net photosynthesis and an increase in leaf nitrogen con-
2641 tent. The general null leaf response to changing soil pH may have been due to
2642 experimental treatments directly increased soil nitrogen availability and affected
2643 soil pH in opposite patterns, suggesting that soil nitrogen availability may be more
2644 important in dictating nitrogen-water use tradeoffs than soil pH per se.

2645 In the third experimental chapter, I quantified variance in leaf nitrogen
2646 content across a precipitation and soil resource availability gradient in Texan
2647 grasslands. Specifically, I measured area-based leaf nitrogen content, components
2648 of area-based leaf nitrogen content (leaf mass per unit leaf area, leaf nitrogen per

2649 unit dry biomass), leaf $C_i:C_a$, and the unit cost of acquiring nitrogen relative to
2650 water in 520 individuals comprising 57 species. I found that variance in area-
2651 based leaf nitrogen content was positively associated with increasing soil nitrogen
2652 availability, soil moisture, vapor pressure deficit, and was negatively related to
2653 increasing leaf $C_i:C_a$. Following patterns expected from theory, a path analysis
2654 revealed that the positive soil nitrogen-leaf nitrogen relationship was driven by a
2655 positive relationship between soil nitrogen availability and the unit cost of acquir-
2656 ing and using nitrogen relative to water, a positive relationship between the unit
2657 cost of acquiring and using nitrogen relative to water, and negative relationship
2658 between leaf $C_i:C_a$ and leaf mass per unit leaf area. Interestingly, there was no
2659 effect of $C_i:C_a$ on leaf nitrogen content per unit dry biomass, indicating that vari-
2660 ance in area-based leaf nitrogen content across the environmental gradient was
2661 driven by a change in leaf morphology and not leaf chemistry.

2662 In the fourth experimental chapter, I quantified leaf and whole plant accli-
2663 mation responses in *G. max* grown under two atmospheric CO₂ levels, with and
2664 without inoculation with *Bradyrhizobium japonicum*, and across nine nitrogen fer-
2665 tilization treatments in a full factorial growth chamber experiment. I found strong
2666 evidence that leaf nitrogen content, V_{cmax} , and J_{max} were each downregulated un-
2667 der elevated CO₂. A stronger downregulation in V_{cmax} than J_{max} and stronger
2668 downregulation in leaf nitrogen content than V_{cmax} or J_{max} provided strong sup-
2669 port suggesting that leaves were acclimating to elevated CO₂ by optimizing leaf
2670 photosynthetic resource use efficiency to achieve optimal coordination. In striking
2671 support of my hypotheses, I find strong evidence suggesting that leaf acclimation
2672 responses to elevated CO₂ were decoupled from soil nitrogen fertilization and in-

2673 oculation treatment, despite apparent strong increases in leaf nitrogen content,
2674 V_{cmax} , and J_{max} with increasing fertilization and in inoculated pots. These find-
2675 ings contrast the current formulation of photosynthetic processes in terrestrial
2676 biosphere models, where many models simulate downregulations in leaf nitrogen
2677 content under elevated CO₂ as a function of progressive nitrogen limitation.

2678 There are currently two iterations of optimality models that employ the
2679 use of patterns expected from photosynthetic least-cost theory, one for C₃ species
2680 (Wang et al. 2017; Smith et al. 2019; Stocker et al. 2020) and one more recently
2681 developed for C₄ species (Scott and Smith 2022). In both model variants, costs
2682 to acquire and use nitrogen relative to water are held constant using a global
2683 dataset of δ¹³C (Cornwell et al. 2018). Throughout experiments, I show strong
2684 evidence suggesting that costs to acquire and use nitrogen are dynamic and vary
2685 predictably across environmental gradients, and that changes in these costs scale
2686 to alter leaf nitrogen-water use tradeoffs and acclimation responses to changing
2687 environments in ways predicted through photosynthetic least-cost theory. Thus,
2688 while optimality model simulations show good agreement with measured data
2689 (Smith et al. 2019; Stocker et al. 2020), such models may not be capturing an
2690 important source of variability in leaf nitrogen-water use tradeoffs by holding costs
2691 of resource use constant across environmental gradients.

2692 First principles of photosynthetic least-cost theory suggest that, in a given
2693 environment, plants optimize photosynthesis rates by sacrificing inefficient use of
2694 a relatively more abundant (and less costly to acquire) resource for more efficient
2695 use of a relatively less abundant (and more costly to acquire) resource. Through-
2696 out experimental chapters, I show strong support for these patterns across ex-

2697 periments, where increasing soil nitrogen fertilization generally decreased the cost
2698 of acquiring nitrogen relative to water, a pattern that scaled to influence leaf
2699 nitrogen-water use tradeoffs. I did not find evidence to suggest that soil moisture
2700 influenced nitrogen-water use tradeoffs, though this was due to strong covariation
2701 between soil moisture and soil nitrogen availability. Overall, findings across exper-
2702 iments provide empirical validation of photosynthetic least-cost theory needed to
2703 further develop optimality models and eventually implement such models in ter-
2704 restrial biosphere model products. Many terrestrial biosphere model products do
2705 not include robust frameworks for simulating acclimation responses to changing
2706 environmental conditions, and empirical findings shown here provide some support
2707 that optimality models that leverage photosynthetic least-cost theory predictions
2708 may improve the ability of terrestrial biosphere models to accurately simulate
2709 photosynthetic processes.

2710 Many terrestrial biosphere models predict photosynthetic capacity through
2711 plant functional group-specific linear regressions between area-based leaf nitrogen
2712 content and V_{cmax} (Rogers 2014; Rogers et al. 2017), which assumes that leaf
2713 nitrogen-photosynthesis relationships are constant across growing environments.
2714 I found constant leaf nitrogen-photosynthesis relationships with increasing soil ni-
2715 trogen availability in the nitrogen-by-sulfur field manipulation experiment. How-
2716 ever, results from the CO₂-by-nitrogen-by-inoculation manipulation experiment
2717 indicated that leaf nitrogen-photosynthesis responses to soil nitrogen availability
2718 were dependent on whether nitrogen was limiting. Further investigation regard-
2719 ing the effect of soil nitrogen availability in modifying leaf nitrogen-photosynthesis
2720 relationships is warranted to better understand the generality of leaf nitrogen pho-

2721 tosynthesis relationships across environmental gradients. However, findings from
2722 these experiments suggest that representing photosynthetic processes through pos-
2723 itive relationships between soil nitrogen availability, leaf nitrogen, and photosyn-
2724 thetic capacity are likely contributing to erroneous errors in model simulations and
2725 may explain the high degree of divergence in simulated processes across terrestrial
2726 biosphere models (Friedlingstein et al. 2014; Davies-Barnard et al. 2020).

2727 The experiments included in this dissertation have provided a strong foun-
2728 dation for me to continue growing as a plant physiological ecologist. I envision
2729 five primary avenues for future research that build on the work presented here,
2730 which are briefly summarized below:

2731 1. Manipulative and environmental gradient experiments included here were
2732 designed to provide empirical data needed to test photosynthetic least-cost
2733 theory assumptions. While these results show promising patterns for pat-
2734 terns expected from photosynthetic least-cost theory, they do not necessarily
2735 address whether these patterns follow those simulated by optimality models
2736 that leverage photosynthetic least-cost principles. Thus, a clear future di-
2737 rection of these experiments would be to conduct model-data comparisons
2738 using data collected here (or similar experiments) to compare against opti-
2739 mality model simulations.

2740 2. Experiments included here explicitly quantify effects of symbiotic nitrogen
2741 fixation on carbon costs to acquire nitrogen, nitrogen-water use tradeoffs,
2742 and leaf nitrogen-photosynthesis relationships. However, carbon costs to ac-
2743 quire nitrogen also vary in species that associate with different mycorrhizal
2744 types (Brzostek et al. 2014; Terrer et al. 2018), and dominant mycorrhizal

2745 type in an ecosystem has been shown to determine net biogeochemical cycle
2746 dynamics in deciduous forests of the northeastern United States (Phillips
2747 et al. 2013). Thus, future work should consider conducting similar experi-
2748 ments while manipulating mycorrhizal association to better understand how
2749 microbial symbioses modify leaf and whole plant acclimation responses to
2750 changing environments.

2751 3. Recent work indicates a high degree of variance in symbiotic nitrogen fixa-
2752 tion rates across terrestrial biosphere models (Meyerholt et al. 2016; Davies-
2753 Barnard et al. 2020), perhaps due to nitrogen fixation rates that are im-
2754 plemented across terrestrial biosphere models as a function of temperature
2755 (Houlton et al. 2008). While energetic costs of nitrogen fixation are de-
2756 pendent on temperature, I show that structural carbon costs to acquire
2757 nitrogen via symbiotic nitrogen fixation are driven by factors that influence
2758 demand to acquire nitrogen (i.e. CO₂, light) and are modified by soil ni-
2759 tragen supply. The light-by-nitrogen greenhouse experiment was published
2760 in *Journal of Experimental Botany*, and a reviewer encouraged future work
2761 to include a model-data comparison comparing structural carbon costs to
2762 acquire nitrogen measured in the experiment to carbon costs to acquire ni-
2763 tragen simulated by the FUN biogeochemical model (Fisher et al. 2010;
2764 Brzostek et al. 2014; Allen et al. 2020). Conveniently, FUN calculates car-
2765 bon costs to acquire nitrogen following the same calculation used in the first
2766 and fourth experimental chapter. Conducting such a model-data comparison
2767 would be a useful step toward identifying biases in the FUN biogeochemi-
2768 cal model, which is currently coupled to several terrestrial biosphere models

2769 (Clark et al. 2011; Shi et al. 2016; Lawrence et al. 2019; Davies-Barnard
2770 et al. 2020).

2771 4. Carbon costs to acquire nitrogen relative to water were quantified at the
2772 leaf level as a function of $\delta^{13}\text{C}$ and vapor pressure deficit, while structural
2773 carbon costs to acquire nitrogen were quantified at the whole plant level
2774 as the ratio of belowground carbon allocation per unit whole plant nitro-
2775 gen biomass. As increasing soil nitrogen availability decreases both leaf and
2776 whole plant estimates of costs to acquire and use nitrogen, one might expect
2777 leaf and whole plant carbon cost to acquire nitrogen estimates to covary. Fu-
2778 ture work should consider investigating if leaf and whole plant estimates of
2779 carbon costs to acquire nitrogen covary and evaluate whether environmental
2780 conditions (or species acquisition strategy) modifies any of this possible co-
2781 variance. Strong covariance between leaf and whole plant costs of nitrogen
2782 acquisition could be a possible avenue to implement frameworks for allowing
2783 costs of nitrogen acquisition to vary in optimality models, as the FUN model
2784 calculates carbon costs of nitrogen acquisition at the whole plant level.

2785 5. While experiments included here target effects of soil nitrogen availability
2786 on carbon costs to acquire nitrogen and associated leaf nitrogen-water use
2787 tradeoffs, photosynthetic least-cost theory predicts that plants acclimate
2788 their photosynthetic processes by minimizing the summed cost of nutrient
2789 (not just nitrogen) and water use. Therefore, the theory would predict
2790 similar leaf acclimation responses across soil phosphorus or other nutrient
2791 availability gradients. Recent iterations of the FUN biogeochemical cycle
2792 includes a framework for determining the carbon and nitrogen cost of ac-

2793 quiring and using phosphorus, which similarly varies in species with different
2794 nutrient acquisition strategies (Allen et al. 2020). The implementation of
2795 this model in a terrestrial biosphere model (E3SM) was also recently shown
2796 to improve model performance of ecosystem nutrient limitation (Braghieri
2797 et al. 2022). As nitrogen and phosphorus commonly co-limit leaf photo-
2798 synthesis and primary productivity, extending experiments reported here to
2799 investigate carbon and nitrogen costs of phosphorus use, and whether these
2800 patterns scale to leaf nutrient-water use tradeoffs would be a useful next
2801 step in understanding extensions and limitations of photosynthetic least-
2802 cost theory.

2803 The experiments included in this dissertation and the proposed experiments sum-
2804 marized above provide a snapshot view of the things that I have learned through-
2805 out my time as a graduate student. I am excited to continue learning and growing
2806 as a plant ecophysiologicalist, ecologist, and scientist, and look forward to continuing
2807 along my journey of investigating nutrient acquisition and allocation responses to
2808 global change.

2809

References

- 2810** Abrams, M. D. and S. A. Mostoller (1995). Gas exchange, leaf structure and
2811 nitrogen in contrasting successional tree species growing in open and under-
2812 story sites during a drought. *Tree Physiology* 15(6), 361–370.
- 2813** Adams, M. A., T. L. Turnbull, J. I. Sprent, and N. Buchmann (2016). Legumes
2814 are different: Leaf nitrogen, photosynthesis, and water use efficiency. *Pro-
2815 ceedings of the National Academy of Sciences of the United States of Amer-
2816 ica* 113(15), 4098–4103.
- 2817** Ainsworth, E. A., P. A. Davey, C. J. Bernacchi, O. C. Dermody, E. A. Heaton,
2818 D. J. Moore, P. B. Morgan, S. L. Naidu, H. S. Y. Ra, X. G. Zhu, P. S. Curtis,
2819 and S. P. Long (2002). A meta-analysis of elevated [CO₂] effects on soybean
2820 (*Glycine max*) physiology, growth and yield. *Global Change Biology* 8(8),
2821 695–709.
- 2822** Ainsworth, E. A. and S. P. Long (2005). What have we learned from 15 years of
2823 free-air CO₂ enrichment (FACE)? A meta-analytic review of the responses
2824 of photosynthesis, canopy properties and plant production to rising CO₂.
2825 *New Phytologist* 165(2), 351–372.
- 2826** Ainsworth, E. A. and A. Rogers (2007). The response of photosynthesis and
2827 stomatal conductance to rising [CO₂]: mechanisms and environmental in-
2828 teractions. *Plant, Cell and Environment* 30(3), 258–270.
- 2829** Allen, K., J. B. Fisher, R. P. Phillips, J. S. Powers, and E. R. Brzostek (2020).
2830 Modeling the carbon cost of plant nitrogen and phosphorus uptake across
2831 temperate and tropical forests. *Frontiers in Forests and Global Change* 3,

- 2832 1–12.
- 2833 Allison, S. D., C. I. Czimczik, and K. K. Treseder (2008). Microbial activity
- 2834 and soil respiration under nitrogen addition in Alaskan boreal forest. *Global*
- 2835 *Change Biology* 14(5), 1156–1168.
- 2836 Andersen, M. K., H. Hauggaard-Nielsen, P. Ambus, and E. S. Jensen (2005).
- 2837 Biomass production, symbiotic nitrogen fixation and inorganic N use in dual
- 2838 and tri-component annual intercrops. *Plant and Soil* 266(1-2), 273–287.
- 2839 Andrews, M., E. K. James, J. I. Sprent, R. M. Boddey, E. Gross, and F. B. dos
- 2840 Reis (2011). Nitrogen fixation in legumes and actinorhizal plants in natural
- 2841 ecosystems: Values obtained using ^{15}N natural abundance. *Plant Ecology*
- 2842 and *Diversity* 4(2-3), 117–130.
- 2843 Arndal, M. F., A. Tolver, K. S. Larsen, C. Beier, and I. K. Schmidt (2018). Fine
- 2844 root growth and vertical distribution in response to elevated CO₂, warming
- 2845 and drought in a mixed heathland–grassland. *Ecosystems* 21(1), 15–30.
- 2846 Arnone, J. A. (1997). Indices of plant N availability in an alpine grassland under
- 2847 elevated atmospheric CO₂. *Plant and Soil* 190(1), 61–66.
- 2848 Arora, V. K., A. Katavouta, R. G. Williams, C. D. Jones, V. Brovkin,
- 2849 P. Friedlingstein, J. Schwinger, L. Bopp, O. Boucher, P. Cadule, M. A.
- 2850 Chamberlain, J. R. Christian, C. Delire, R. A. Fisher, T. Hajima, T. Ilyina,
- 2851 E. Joetzjer, M. Kawamiya, C. D. Koven, J. P. Krasting, R. M. Law, D. M.
- 2852 Lawrence, A. Lenton, K. Lindsay, J. Pongratz, T. Raddatz, R. Séférian,
- 2853 K. Tachiiri, J. F. Tjiputra, A. Wiltshire, T. Wu, and T. Ziehn (2020).
- 2854 Carbon-concentration and carbon-climate feedbacks in CMIP6 models and
- 2855 their comparison to CMIP5 models. *Biogeosciences* 17(16), 4173–4222.

- 2856 Bae, K., T. J. Fahey, R. D. Yanai, and M. Fisk (2015). Soil nitrogen availabil-
2857 ity affects belowground carbon allocation and soil respiration in northern
2858 hardwood forests of New Hampshire. *Ecosystems* 18(7), 1179–1191.
- 2859 Barber, S. A. (1962). A diffusion and mass-flow concept of soil nutrient avail-
2860 ability. *Soil Science* 93(1), 39–49.
- 2861 Barnes, J. D., L. Balaguer, E. Manrique, S. Elvira, and A. W. Davison (1992).
2862 A reappraisal of the use of DMSO for the extraction and determination
2863 of chlorophylls a and b in lichens and higher plants. *Environmental and*
2864 *Experimental Botany* 32(2), 85–100.
- 2865 Bates, D., M. Mächler, B. Bolker, and S. Walker (2015). Fitting linear mixed-
2866 effects models using lme4. *Journal of Statistical Software* 67(1), 1–48.
- 2867 Beaudette, D., J. Skovlin, S. Roeker, and A. Brown (2022). soilDB: Soil
2868 Database Interface.
- 2869 Bengtson, P., J. Barker, and S. J. Grayston (2012). Evidence of a strong cou-
2870 pling between root exudation, C and N availability, and stimulated SOM
2871 decomposition caused by rhizosphere priming effects. *Ecology and Evolu-*
2872 *tion* 2(8), 1843–1852.
- 2873 Bernacchi, C. J., E. L. Singsaas, C. Pimentel, A. R. Portis, and S. P. Long
2874 (2001). Improved temperature response functions for models of Rubisco-
2875 limited photosynthesis. *Plant, Cell and Environment* 24(2), 253–259.
- 2876 Bialic-Murphy, L., N. G. Smith, P. Voothuluru, R. M. McElderry, M. D.
2877 Roche, S. T. Cassidy, S. N. Kivlin, and S. Kalisz (2021). Invasion-induced
2878 root–fungal disruptions alter plant water and nitrogen economies. *Ecology*

- 2879** *Letters* 24(6), 1145–1156.
- 2880** Bloom, A. J., F. S. Chapin, and H. A. Mooney (1985). Resource limitation
2881 in plants - an economic analogy. *Annual Review of Ecology and Systemat-*
2882 *ics* 16(1), 363–392.
- 2883** Bloomfield, K. J., B. D. Stocker, T. F. Keenan, and I. C. Prentice (2023).
2884 Environmental controls on the light use efficiency of terrestrial gross primary
2885 production. *Global Change Biology* 29(4), 0–2.
- 2886** Bonan, G. B., M. D. Hartman, W. J. Parton, and W. R. Wieder (2013). Eval-
2887 uating litter decomposition in earth system models with long-term litter
2888 bag experiments: an example using the Community Land Model version 4
2889 (CLM4). *Global Change Biology* 19(3), 957–974.
- 2890** Bonan, G. B., P. J. Lawrence, K. W. Oleson, S. Levis, M. Jung, M. Reich-
2891 stein, D. M. Lawrence, and S. C. Swenson (2011). Improving canopy pro-
2892 cesses in the Community Land Model version 4 (CLM4) using global flux
2893 fields empirically inferred from FLUXNET data. *Journal of Geophysical Re-*
2894 *search* 116(G2), G02014.
- 2895** Booth, B. B. B., C. D. Jones, M. Collins, I. J. Totterdell, P. M. Cox, S. Sitch,
2896 C. Huntingford, R. A. Betts, G. R. Harris, and J. Lloyd (2012). High sen-
2897 sitivity of future global warming to land carbon cycle processes. *Environ-*
2898 *mental Research Letters* 7(2), 024002.
- 2899** Borer, E. T., W. S. Harpole, P. B. Adler, E. M. Lind, J. L. Orrock, E. W.
2900 Seabloom, and M. D. Smith (2014). Finding generality in ecology: A model
2901 for globally distributed experiments. *Methods in Ecology and Evolution* 5(1),
2902 65–73.

- 2903** Braghieri, R. K., J. B. Fisher, K. Allen, E. Brzostek, M. Shi, X. Yang, D. M.
- 2904** Ricciuto, R. A. Fisher, Q. Zhu, and R. P. Phillips (2022). Modeling global
- 2905** carbon costs of plant nitrogen and phosphorus acquisition. *Journal of Ad-*
- 2906** *vances in Modeling Earth Systems* 14(8), 1–23.
- 2907** Brix, H. (1971). Effects of nitrogen fertilization on photosynthesis and respi-
- 2908** ration in Douglas-fir. *Forest Science* 17(4), 407–414.
- 2909** Brzostek, E. R., J. B. Fisher, and R. P. Phillips (2014). Modeling the carbon
- 2910** cost of plant nitrogen acquisition: Mycorrhizal trade-offs and multipath
- 2911** resistance uptake improve predictions of retranslocation. *Journal of Geo-*
- 2912** *physical Research: Biogeosciences* 119, 1684–1697.
- 2913** Bubier, J. L., R. Smith, S. Juutinen, T. R. Moore, R. Minocha, S. Long, and
- 2914** S. Minocha (2011). Effects of nutrient addition on leaf chemistry, morphol-
- 2915** ogy, and photosynthetic capacity of three bog shrubs. *Oecologia* 167(2),
- 2916** 355–368.
- 2917** Cernusak, L. A., N. Ubierna, K. Winter, J. A. M. Holtum, J. D. Marshall, and
- 2918** G. D. Farquhar (2013). Environmental and physiological determinants of
- 2919** carbon isotope discrimination in terrestrial plants. *New Phytologist* 200(4),
- 2920** 950–965.
- 2921** Chen, J.-L., J. F. Reynolds, P. C. Harley, and J. D. Tenhunen (1993). Coor-
- 2922** dination theory of leaf nitrogen distribution in a canopy. *Oecologia* 93(1),
- 2923** 63–69.
- 2924** Clark, D. B., L. M. Mercado, S. Sitch, C. D. Jones, N. Gedney, M. J. Best,
- 2925** M. Pryor, G. G. Rooney, R. L. H. Essery, E. Blyth, O. Boucher, R. J.
- 2926** Harding, C. Huntingford, and P. M. Cox (2011). The Joint UK Land Envi-

- 2927 ronment Simulator (JULES), model description. Part 2: Carbon fluxes and
2928 vegetation dynamics. *Geoscientific Model Development* 4(3), 701–722.
- 2929 Cornwell, W. K., J. H. C. Cornelissen, K. Amatangelo, E. Dorrepaal, V. T.
2930 Eviner, O. Godoy, S. E. Hobbie, B. Hoorens, H. Kurokawa, N. Pérez-
2931 Harguindeguy, H. M. Quested, L. S. Santiago, D. A. Wardle, I. J. Wright,
2932 R. Aerts, S. D. Allison, P. van Bodegom, V. Brovkin, A. Chatain, T. V.
2933 Callaghan, S. Díaz, E. Garnier, D. E. Gurvich, E. Kazakou, J. A. Klein,
2934 J. Read, P. B. Reich, N. A. Soudzilovskaia, M. V. Vaieretti, and M. Westoby
2935 (2008). Plant species traits are the predominant control on litter decompo-
2936 sition rates within biomes worldwide. *Ecology Letters* 11(10), 1065–1071.
- 2937 Cornwell, W. K., I. J. Wright, J. Turner, V. Maire, M. M. Barbour, L. A.
2938 Cernusak, T. E. Dawson, D. S. Ellsworth, G. D. Farquhar, H. Griffiths,
2939 C. Keitel, A. Knohl, P. B. Reich, D. G. Williams, R. Bhaskar, J. H. C. Cor-
2940 nelissen, A. Richards, S. Schmidt, F. Valladares, C. Körner, E.-D. Schulze,
2941 N. Buchmann, and L. S. Santiago (2018). Climate and soils together regulate
2942 photosynthetic carbon isotope discrimination within C₃ plants worldwide.
2943 *Global Ecology and Biogeography* 27(9), 1056–1067.
- 2944 Cramer, W. and I. C. Prentice (1988). Simulation of regional soil moisture
2945 deficits on a European scale. *Norsk Geografisk Tidsskrift - Norwegian Jour-*
2946 *nal of Geography* 42(2-3), 149–151.
- 2947 Curtis, P. S. (1996). A meta-analysis of leaf gas exchange and nitrogen in trees
2948 grown under elevated carbon dioxide. *Plant, Cell and Environment* 19(2),
2949 127–137.
- 2950 Daly, C., M. Halbleib, J. I. Smith, W. P. Gibson, M. K. Doggett, G. H. Taylor,

- 2951** J. Curtis, and P. P. Pasteris (2008). Physiographically sensitive mapping
2952 of climatological temperature and precipitation across the conterminous
2953 United States. *International Journal of Climatology* 28(15), 2031–2064.
- 2954** Davies-Barnard, T., J. Meyerholt, S. Zaehle, P. Friedlingstein, V. Brovkin,
2955 Y. Fan, R. A. Fisher, C. D. Jones, H. Lee, D. Peano, B. Smith, D. Wårlind,
2956 and A. J. Wiltshire (2020). Nitrogen cycling in CMIP6 land surface models:
2957 progress and limitations. *Biogeosciences* 17(20), 5129–5148.
- 2958** Davis, T. W., I. C. Prentice, B. D. Stocker, R. T. Thomas, R. J. Whitley,
2959 H. Wang, B. J. Evans, A. V. Gallego-Sala, M. T. Sykes, and W. Cramer
2960 (2017). Simple process-led algorithms for simulating habitats (SPLASH
2961 v.1.0): robust indices of radiation, evapotranspiration and plant-available
2962 moisture. *Geoscientific Model Development* 10, 689–708.
- 2963** Delaire, M., E. Frak, M. Sigogne, B. Adam, F. Beaujard, and X. Le Roux
2964 (2005). Sudden increase in atmospheric CO₂ concentration reveals strong
2965 coupling between shoot carbon uptake and root nutrient uptake in young
2966 walnut trees. *Tree Physiology* 25(2), 229–235.
- 2967** Doane, T. A. and W. R. Horwáth (2003). Spectrophotometric determination of
2968 nitrate with a single reagent. *Analytical Letters* 36(12), 2713–2722.
- 2969** Dong, N., I. C. Prentice, B. J. Evans, S. Caddy-Retalic, A. J. Lowe, and I. J.
2970 Wright (2017). Leaf nitrogen from first principles: field evidence for adaptive
2971 variation with climate. *Biogeosciences* 14(2), 481–495.
- 2972** Dong, N., I. C. Prentice, I. J. Wright, B. J. Evans, H. F. Togashi, S. Caddy-
2973 Retalic, F. A. McInerney, B. Sparrow, E. Leitch, and A. J. Lowe (2020).
2974 Components of leaf trait variation along environmental gradients. *New Phy-*

- 2975** *tologist* 228(1), 82–94.
- 2976** Dong, N., I. C. Prentice, I. J. Wright, H. Wang, O. K. Atkin, K. J. Bloomfield,
- 2977** T. F. Domingues, S. M. Gleason, V. Maire, Y. Onoda, H. Poorter, and N. G.
- 2978** Smith (2022). Leaf nitrogen from the perspective of optimal plant function.
- 2979** *Journal of Ecology* 110(11), 2585–2602.
- 2980** Dong, N., I. J. Wright, J. M. Chen, X. Luo, H. Wang, T. F. Keenan, N. G.
- 2981** Smith, and I. C. Prentice (2022). Rising CO₂ and warming reduce global
- 2982** canopy demand for nitrogen. *New Phytologist* 235(5), 1692–1700.
- 2983** Dovrat, G., H. Bakhshian, T. Masci, and E. Sheffer (2020). The nitrogen eco-
- 2984** nomic spectrum of legume stoichiometry and fixation strategy. *New Phytol-*
- 2985** *ogist* 227(2), 365–375.
- 2986** Dovrat, G., T. Masci, H. Bakhshian, E. Mayzlish Gati, S. Golan, and E. Shef-
- 2987** fer (2018). Drought-adapted plants dramatically downregulate dinitrogen
- 2988** fixation: Evidences from Mediterranean legume shrubs. *Journal of Ecol-*
- 2989** *ogy* 106(4), 1534–1544.
- 2990** Drake, B. G., M. A. Gonzàlez-Meler, and S. P. Long (1997). More efficient
- 2991** plants: a consequence of rising atmospheric CO₂? *Annual Review of Plant*
- 2992** *Biology* 48, 609–639.
- 2993** Duursma, R. A. (2015). Plantecophys - An R package for analyzing and mod-
- 2994** elling leaf gas exchange data. *PLOS ONE* 10(11), e0143346.
- 2995** Eamus, D., N. Boulain, J. Cleverly, and D. D. Breshears (2013). Global change-
- 2996** type drought-induced tree mortality: Vapor pressure deficit is more impor-
- 2997** tant than temperature per se in causing decline in tree health. *Ecology and*

- 2998** *Evolution* 3(8), 2711–2729.
- 2999** Eastman, B. A., M. B. Adams, E. R. Brzostek, M. B. Burnham, J. E. Carrara,
- 3000** C. Kelly, B. E. McNeil, C. A. Walter, and W. T. Peterjohn (2021). Altered
- 3001** plant carbon partitioning enhanced forest ecosystem carbon storage after 25
- 3002** years of nitrogen additions. *New Phytologist* 230(4), 1435–1448.
- 3003** Ellsworth, D. S. and P. B. Reich (1996). Photosynthesis and leaf nitrogen in five
- 3004** Amazonian tree species during early secondary succession. *Ecology* 77(2),
- 3005** 581–594.
- 3006** Espelta, J. M., P. Cortés, M. Mangirón, and J. Retana (2005). Differences
- 3007** in biomass partitioning, leaf nitrogen content, and water use efficiency δ^{13}
- 3008** result in similar performance of seedlings of two Mediterranean oaks with
- 3009** contrasting leaf habit. *Ecoscience* 12(4), 447–454.
- 3010** Evans, J. R. (1989). Photosynthesis and nitrogen relationships in leaves of C₃
- 3011** plants. *Oecologia* 78(1), 9–19.
- 3012** Evans, J. R. and V. C. Clarke (2019). The nitrogen cost of photosynthesis.
- 3013** *Journal of Experimental Botany* 70(1), 7–15.
- 3014** Evans, J. R. and H. Poorter (2001). Photosynthetic acclimation of plants to
- 3015** growth irradiance: the relative importance of specific leaf area and nitrogen
- 3016** partitioning in maximizing carbon gain. *Plant, Cell and Environment* 24(8),
- 3017** 755–767.
- 3018** Evans, J. R. and J. R. Seemann (1989). The allocation of protein nitrogen in
- 3019** the photosynthetic apparatus: costs, consequences, and control. *Photosyn-*
- 3020** *thesis* 8, 183–205.

- 3021** Exbrayat, J.-F., A. A. Bloom, P. Falloon, A. Ito, T. L. Smallman, and
3022 M. Williams (2018). Reliability ensemble averaging of 21st century projec-
3023 tions of terrestrial net primary productivity reduces global and regional
3024 uncertainties. *Earth System Dynamics* 9(1), 153–165.
- 3025** Farquhar, G. D., J. R. Ehleringer, and K. T. Hubick (1989). Carbon isotope
3026 discrimination and photosynthesis. *Annual Review of Plant Physiology and*
3027 *Plant Molecular Biology* 40(1), 503–537.
- 3028** Farquhar, G. D. and T. D. Sharkey (1982). Stomatal conductance and photo-
3029 synthesis. *Annual Review of Plant Physiology* 33(1), 317–345.
- 3030** Farquhar, G. D., S. von Caemmerer, and J. A. Berry (1980). A biochemical
3031 model of photosynthetic CO₂ assimilation in leaves of C₃ species.
3032 *Planta* 149(1), 78–90.
- 3033** Fay, P. A., S. M. Prober, W. S. Harpole, J. M. H. Knops, J. D. Bakker, E. T.
3034 Borer, E. M. Lind, A. S. MacDougall, E. W. Seabloom, P. D. Wragg, P. B.
3035 Adler, D. M. Blumenthal, Y. M. Buckley, C. Chu, E. E. Cleland, S. L.
3036 Collins, K. F. Davies, G. Du, X. Feng, J. Firn, D. S. Gruner, N. Hagenah,
3037 Y. Hautier, R. W. Heckman, V. L. Jin, K. P. Kirkman, J. A. Klein, L. M.
3038 Ladwig, Q. Li, R. L. McCulley, B. A. Melbourne, C. E. Mitchell, J. L. Moore,
3039 J. W. Morgan, A. C. Risch, M. Schütz, C. J. Stevens, D. A. Wedin, and
3040 L. H. Yang (2015). Grassland productivity limited by multiple nutrients.
3041 *Nature Plants* 1(7), 15080.
- 3042** Feng, X. (1999). Trends in intrinsic water-use efficiency of natural trees for the
3043 past 100-200 years: A response to atmospheric CO₂ concentration. *Geochim-
ica et Cosmochimica Acta* 63(13-14), 1891–1903.

- 3045 Field, C. B. and H. A. Mooney (1986). The photosynthesis-nitrogen relationship
3046 in wild plants. In T. J. Givnish (Ed.), *On the Economy of Plant Form and*
3047 *Function*, pp. 25–55. Cambridge: Cambridge University Press.
- 3048 Finzi, A. C., D. J. P. Moore, E. H. DeLucia, J. Lichter, K. S. Hofmockel, R. B.
3049 Jackson, H. S. Kim, R. Matamala, H. R. McCarthy, R. Oren, J. S. Pippen,
3050 and W. H. Schlesinger (2006). Progressive nitrogen limitation of ecosystem
3051 processes under elevated CO₂ in a warm-temperate forest. *Ecology* 87(1),
3052 15–25.
- 3053 Firn, J., J. M. McGree, E. Harvey, H. Flores Moreno, M. Schutz, Y. M. Buckley,
3054 E. T. Borer, E. W. Seabloom, K. J. La Pierre, A. M. MacDougall, S. M.
3055 Prober, C. J. Stevens, L. L. Sullivan, E. Porter, E. Ladouceur, C. Allen,
3056 K. H. Moromizato, J. W. Morgan, W. S. Harpole, Y. Hautier, N. Eisen-
3057 hauer, J. P. Wright, P. B. Adler, C. A. Arnillas, J. D. Bakker, L. Biederman,
3058 A. A. D. Broadbent, C. S. Brown, M. N. Bugalho, M. C. Caldeira, E. E. Cle-
3059 land, A. Ebeling, P. A. Fay, N. Hagenah, A. R. Kleinhesselink, R. Mitchell,
3060 J. L. Moore, C. Nogueira, P. L. Peri, C. Roscher, M. D. Smith, P. D. Wragg,
3061 and A. C. Risch (2019). Leaf nutrients, not specific leaf area, are consistent
3062 indicators of elevated nutrient inputs. *Nature Ecology and Evolution* 3(3),
3063 400–406.
- 3064 Fisher, J. B., S. Sitch, Y. Malhi, R. A. Fisher, C. Huntingford, and S.-Y. Tan
3065 (2010). Carbon cost of plant nitrogen acquisition: A mechanistic, globally
3066 applicable model of plant nitrogen uptake, retranslocation, and fixation.
3067 *Global Biogeochemical Cycles* 24(1), 1–17.
- 3068 Fox, J. and S. Weisberg (2019). *An R companion to applied regression* (Third

- 3069** edit ed.). Thousand Oaks, California: Sage.
- 3070** Franklin, O., R. E. McMurtrie, C. M. Iversen, K. Y. Crous, A. C. Finzi, D. Tis-
3071 sue, D. S. Ellsworth, R. Oren, and R. J. Norby (2009). Forest fine-root
3072 production and nitrogen use under elevated CO₂: contrasting responses
3073 in evergreen and deciduous trees explained by a common principle. *Global
3074 Change Biology* 15(1), 132–144.
- 3075** Friedlingstein, P., M. Meinshausen, V. K. Arora, C. D. Jones, A. Anav, S. K.
3076 Liddicoat, and R. Knutti (2014). Uncertainties in CMIP5 climate projections
3077 due to carbon cycle feedbacks. *Journal of Climate* 27(2), 511–526.
- 3078** Friel, C. A. and M. L. Friesen (2019). Legumes modulate allocation to rhizobial
3079 nitrogen fixation in response to factorial light and nitrogen manipulation.
3080 *Frontiers in Plant Science* 10, 1316.
- 3081** Fujikake, H., A. Yamazaki, N. Ohtake, K. Sueoshi, S. Matsuhashi, T. Ito,
3082 C. Mizuniwa, T. Kume, S. Hoshimoto, N.-S. Ishioka, S. Watanabe, A. Osa,
3083 T. Sekine, H. Uchida, A. Tsuji, and T. Ohyama (2003). Quick and reversible
3084 inhibition of soybean root nodule growth by nitrate involves a decrease in
3085 sucrose supply to nodules. *Journal of Experimental Botany* 54(386), 1379–
3086 1388.
- 3087** Ghannoum, O., J. R. Evans, and S. von Caemmerer (2011). Nitrogen and water
3088 use efficiency of C₄ plants. In A. S. Raghavendra and R. F. Sage (Eds.), *C₄
3089 Photosynthesis and Related CO₂ Concentrating Mechanisms*, Chapter 8, pp.
3090 129–146. Springer.
- 3091** Ghimire, B., W. J. Riley, C. D. Koven, J. Kattge, A. Rogers, P. B. Reich, and
3092 I. J. Wright (2017). A global trait-based approach to estimate leaf nitro-

- 3093** gen functional allocation from observations:. *Ecological Applications* 27(5),
3094 1421–1434.
- 3095** Giardina, C. P., M. D. Coleman, J. E. Hancock, J. S. King, E. A. Lilleskov,
3096 W. M. Loya, K. S. Pregitzer, M. G. Ryan, and C. C. Trettin (2005). The
3097 response of belowground carbon allocation in forests to global change. In
3098 D. Binkley and O. Manyailo (Eds.), *Tree Species Effects on Soils: Implica-*
3099 *tions for Global Change* (Volume 55 ed.), Chapter Chapter 7, pp. 119–154.
3100 Berlin/Heidelberg: Springer-Verlag.
- 3101** Gibson, A. H. and J. E. Harper (1985). Nitrate effect on nodulation of soybean
3102 by *Bradyrhizobium japonicum*. *Crop Science* 25(3), 497–501.
- 3103** Gill, A. L. and A. C. Finzi (2016). Belowground carbon flux links biogeochemical
3104 cycles and resource-use efficiency at the global scale. *Ecology Letters* 19(12),
3105 1419–1428.
- 3106** Goll, D. S., V. Brovkin, B. R. Parida, C. H. Reick, J. Kattge, P. B. Reich, P. M.
3107 van Bodegom, and Ü. Niinemets (2012). Nutrient limitation reduces land
3108 carbon uptake in simulations with a model of combined carbon, nitrogen
3109 and phosphorus cycling. *Biogeosciences Discussions* 9(3), 3173–3232.
- 3110** Gregory, L. M., A. M. McClain, D. M. Kramer, J. D. Pardo, K. E. Smith, O. L.
3111 Tessmer, B. J. Walker, L. G. Ziccardi, and T. D. Sharkey (2021, oct). The
3112 triose phosphate utilization limitation of photosynthetic rate: Out of global
3113 models but important for leaf models. *Plant, Cell and Environment* 44(10),
3114 3223–3226.
- 3115** Grossiord, C., T. N. Buckley, L. A. Cernusak, K. A. Novick, B. Poulter, R. T. W.
3116 Siegwolf, J. S. Sperry, and N. G. McDowell (2020). Plant responses to rising

- 3117** vapor pressure deficit. *New Phytologist* 226(6), 1550–1566.
- 3118** Gulmon, S. L. and C. C. Chu (1981). The effects of light and nitrogen on photo-
- 3119** synthesis, leaf characteristics, and dry matter allocation in the chaparral
- 3120** shrub, *Diplacus aurantiacus*. *Oecologia* 49(2), 207–212.
- 3121** Gutschick, V. P. (1981). Evolved strategies in nitrogen acquisition by plants.
- 3122** *The American Naturalist* 118(5), 607–637.
- 3123** Hallik, L., Ü. Niinemets, and I. J. Wright (2009). Are species shade and drought
- 3124** tolerance reflected in leaf-level structural and functional differentiation in
- 3125** Northern Hemisphere temperate woody flora? *New Phytologist* 184(1), 257–
- 3126** 274.
- 3127** Harrison, M. T., E. J. Edwards, G. D. Farquhar, A. B. Nicotra, and J. R.
- 3128** Evans (2009). Nitrogen in cell walls of sclerophyllous leaves accounts for
- 3129** little of the variation in photosynthetic nitrogen-use efficiency. *Plant, Cell*
- 3130** and *Environment* 32(3), 259–270.
- 3131** Harrison, S. P., W. Cramer, O. Franklin, I. C. Prentice, H. Wang,
- 3132** Å. Brännström, H. de Boer, U. Dieckmann, J. Joshi, T. F. Keenan,
- 3133** A. Lavergne, S. Manzoni, G. Mengoli, C. Morfopoulos, J. Peñuelas,
- 3134** S. Pietsch, K. T. Rebel, Y. Ryu, N. G. Smith, B. D. Stocker, and I. J.
- 3135** Wright (2021). Eco-evolutionary optimality as a means to improve vegetation
- 3136** and land-surface models. *New Phytologist* 231(6), 2125–2141.
- 3137** Henneron, L., P. Kardol, D. A. Wardle, C. Cros, and S. Fontaine (2020). Rhizo-
- 3138** sphere control of soil nitrogen cycling: a key component of plant economic
- 3139** strategies. *New Phytologist* 228(4), 1269–1282.

- 3140** Hijmans, R. J. (2022). *terra: Spatial Data Analysis*.
- 3141** Hikosaka, K. and A. Shigeno (2009). The role of Rubisco and cell walls in the
- 3142** interspecific variation in photosynthetic capacity. *Oecologia* 160(3), 443–
- 3143** 451.
- 3144** Hoagland, D. R. and D. I. Arnon (1950). The water culture method for growing
- 3145** plants without soil. *California Agricultural Experiment Station: 347* 347(2),
- 3146** 1–32.
- 3147** Hobbie, E. A. (2006). Carbon allocation to ectomycorrhizal fungi correlates
- 3148** with belowground allocation in culture studies. *Ecology* 87(3), 563–569.
- 3149** Hobbie, E. A. and J. E. Hobbie (2008). Natural abundance of ^{15}N in nitrogen-
- 3150** limited forests and tundra can estimate nitrogen cycling through mycorrhizal
- 3151** fungi: a review. *Ecosystems* 11(5), 815–830.
- 3152** Hoek, T. A., K. Axelrod, T. Biancalani, E. A. Yurtsev, J. Liu, and J. Gore
- 3153** (2016). Resource availability modulates the cooperative and competitive na-
- 3154** nature of a microbial cross-feeding mutualism. *PLOS Biology* 14(8), e1002540.
- 3155** Höglberg, M. N., M. J. I. Briones, S. G. Keel, D. B. Metcalfe, C. Campbell, A. J.
- 3156** Midwood, B. Thornton, V. Hurry, S. Linder, T. Näsholm, and P. Höglberg
- 3157** (2010). Quantification of effects of season and nitrogen supply on tree below-
- 3158** ground carbon transfer to ectomycorrhizal fungi and other soil organisms in
- 3159** a boreal pine forest. *New Phytologist* 187(2), 485–493.
- 3160** Höglberg, P., M. N. Höglberg, S. G. Göttlicher, N. R. Betson, S. G. Keel, D. B.
- 3161** Metcalfe, C. Campbell, A. Schindlbacher, V. Hurry, T. Lundmark, S. Linder,
- 3162** and T. Näsholm (2008). High temporal resolution tracing of photosynthate

- 3163** carbon from the tree canopy to forest soil microorganisms. *New Phytologist* 177(1), 220–228.
- 3165** Houlton, B. Z., Y.-P. Wang, P. M. Vitousek, and C. B. Field (2008). A unifying framework for dinitrogen fixation in the terrestrial biosphere. *Nature* 454(7202), 327–330.
- 3168** Huber, M. L., R. A. Perkins, A. Laesecke, D. G. Friend, J. V. Sengers, M. J.
- 3169** Assael, I. N. Metaxa, E. Vogel, R. Mareš, and K. Miyagawa (2009). New
- 3170** international formulation for the viscosity of H₂O. *Journal of Physical and*
- 3171** *Chemical Reference Data* 38(2), 101–125.
- 3172** Hungate, B. A., J. S. Dukes, M. R. Shaw, Y. Luo, and C. B. Field (2003).
- 3173** Nitrogen and climate change. *Science* 302(5650), 1512–1513.
- 3174** IPCC (2021). *Climate Change 2021: The Physical Science Basis. Contribution*
- 3175** *of Working Group I to the Sixth Assessment Report of the Intergovernmental*
- 3176** *Panel on Climate Change*, Volume In Press. Cambridge, United Kingdom
- 3177** and New York, NY, USA: Cambridge University Press.
- 3178** Johnson, N. C., J. H. Graham, and F. A. Smith (1997). Functioning of mycor-
- 3179** rhizal associations along the mutualism-parasitism continuum. *New Phytologist*
- 3180** 135(4), 575–585.
- 3181** Kachurina, O. M., H. Zhang, W. R. Raun, and E. G. Krenzer (2000). Simulta-
- 3182** neous determination of soil aluminum, ammonium- and nitrate- nitrogen
- 3183** using 1 M potassium chloride. *Communications in Soil Science and Plant*
- 3184** *Analysis* 31(7-8), 893–903.
- 3185** Kaiser, C., M. R. Kilburn, P. L. Clode, L. Fuchslueger, M. Koranda, J. B. Cliff,

- 3186** Z. M. Solaiman, and D. V. Murphy (2015). Exploring the transfer of recent
3187 plant photosynthates to soil microbes: mycorrhizal pathway vs direct root
3188 exudation. *New Phytologist* 205(4), 1537–1551.
- 3189** Katabuchi, M. (2015). LeafArea: An R package for rapid digital analysis of leaf
3190 area. *Ecological Research* 30(6), 1073–1077.
- 3191** Kattge, J. and W. Knorr (2007). Temperature acclimation in a biochemical
3192 model of photosynthesis: a reanalysis of data from 36 species. *Plant, Cell*
3193 and *Environment* 30(9), 1176–1190.
- 3194** Kattge, J., W. Knorr, T. Raddatz, and C. Wirth (2009). Quantifying photosyn-
3195 thetic capacity and its relationship to leaf nitrogen content for global-scale
3196 terrestrial biosphere models. *Global Change Biology* 15(4), 976–991.
- 3197** Kayler, Z., A. Gessler, and N. Buchmann (2010). What is the speed of link
3198 between aboveground and belowground processes? *New Phytologist* 187(4),
3199 885–888.
- 3200** Kayler, Z., C. Keitel, K. Jansen, and A. Gessler (2017). Experimental evidence
3201 of two mechanisms coupling leaf-level C assimilation to rhizosphere CO₂
3202 release. *Environmental and Experimental Botany* 135, 21–26.
- 3203** Keeling, C. D., W. G. Mook, and P. P. Tans (1979, jan). Recent trends in the
3204 ¹³C:¹²C ratio of atmospheric carbon dioxide. *Nature* 277(5692), 121–123.
- 3205** Keeney, D. R. and D. W. Nelson (1983). Nitrogen—Inorganic Forms. In A. L.
3206 Page (Ed.), *Methods of Soil Analysis* (2nd ed.), Chapter 33, pp. 643–698.
3207 Madison, WI, USA: ASA and SSSA.
- 3208** Kenward, M. G. and J. H. Roger (1997). Small sample inference for fixed effects

- 3209** from restricted maximum likelihood. *Biometrics* 53(3), 983.
- 3210** Knapp, A. K., M. L. Avolio, C. Beier, C. J. W. Carroll, S. L. Collins, J. S.
- 3211** Dukes, L. H. Fraser, R. J. Griffin-Nolan, D. L. Hoover, A. Jentsch, M. E.
- 3212** Loik, R. P. Phillips, A. K. Post, O. E. Sala, I. J. Slette, L. Yahdjian, and
- 3213** M. D. Smith (2017). Pushing precipitation to the extremes in distributed
- 3214** experiments: recommendations for simulating wet and dry years. *Global*
- 3215** *Change Biology* 23(5), 1774–1782.
- 3216** Knorr, W. (2000). Annual and interannual CO₂ exchanges of the
- 3217** terrestrial biosphere: process-based simulations and uncertainties. *Global*
- 3218** *Ecology and Biogeography* 9(3), 225–252.
- 3219** Knorr, W. and M. Heimann (2001). Uncertainties in global terrestrial biosphere
- 3220** modeling: 1. A comprehensive sensitivity analysis with a new photosynthesis
- 3221** and energy balance scheme. *Global Biogeochemical Cycles* 15(1), 207–225.
- 3222** Kulmatiski, A., P. B. Adler, J. M. Stark, and A. T. Tredennick (2017). Water
- 3223** and nitrogen uptake are better associated with resource availability than
- 3224** root biomass. *Ecosphere* 8(3), e01738.
- 3225** Lavergne, A., D. Sandoval, V. J. Hare, H. Graven, and I. C. Prentice (2020).
- 3226** Impacts of soil water stress on the acclimated stomatal limitation of pho-
- 3227** tosynthesis: Insights from stable carbon isotope data. *Global Change Biol-*
- 3228** *ogy* 26(12), 7158–7172.
- 3229** Lawrence, D. M., R. A. Fisher, C. D. Koven, K. W. Oleson, S. C. Swen-
- 3230** son, G. B. Bonan, N. Collier, B. Ghimire, L. Kampenhout, D. Kennedy,
- 3231** E. Kluzek, P. J. Lawrence, F. Li, H. Li, D. L. Lombardozzi, W. J. Riley,
- 3232** W. J. Sacks, M. Shi, M. Vertenstein, W. R. Wieder, C. Xu, A. A. Ali,

- 3233** A. M. Badger, G. Bisht, M. Broeke, M. A. Brunke, S. P. Burns, J. Buzan,
3234 M. Clark, A. Craig, K. M. Dahlin, B. Drewniak, J. B. Fisher, M. Flanner,
3235 A. M. Fox, P. Gentine, F. M. Hoffman, G. Keppel-Aleks, R. Knox, S. Ku-
3236 mar, J. Lenaerts, L. R. Leung, W. H. Lipscomb, Y. Lu, A. Pandey, J. D.
3237 Pelletier, J. Perket, J. T. Randerson, D. M. Ricciuto, B. M. Sanderson,
3238 A. Slater, Z. M. Subin, J. Tang, R. Q. Thomas, M. Val Martin, and X. Zeng
3239 (2019). The Community Land Model Version 5: description of new features,
3240 benchmarking, and impact of forcing uncertainty. *Journal of Advances in*
3241 *Modeling Earth Systems* 11(12), 4245–4287.
- 3242** LeBauer, D. S. and K. K. Treseder (2008). Nitrogen limitation of net primary
3243 productivity. *Ecology* 89(2), 371–379.
- 3244** Lefcheck, J. S. (2016). piecewiseSEM: Piecewise structural equation modelling
3245 in r for ecology, evolution, and systematics. *Methods in Ecology and Evolu-*
3246 *tion* 7(5), 573–579.
- 3247** Lenth, R. (2019). emmeans: estimated marginal means, aka least-squares
3248 means.
- 3249** Li, W., H. Zhang, G. Huang, R. Liu, H. Wu, C. Zhao, and N. G. McDowell
3250 (2020). Effects of nitrogen enrichment on tree carbon allocation: A global
3251 synthesis. *Global Ecology and Biogeography* 29(3), 573–589.
- 3252** Liang, J., X. Qi, L. Souza, and Y. Luo (2016). Processes regulating progressive
3253 nitrogen limitation under elevated carbon dioxide: a meta-analysis. *Bioge-
osciences* 13(9), 2689–2699.
- 3255** Liang, X., T. Zhang, X. Lu, D. S. Ellsworth, H. BassiriRad, C. You, D. Wang,
3256 P. He, Q. Deng, H. Liu, J. Mo, and Q. Ye (2020). Global response patterns of

- 3257** plant photosynthesis to nitrogen addition: A meta-analysis. *Global Change Biology* 26(6), 3585–3600.
- 3259** López, J., D. A. Way, and W. Sadok (2021). Systemic effects of rising atmospheric vapor pressure deficit on plant physiology and productivity. *Global Change Biology* 27(9), 1704–1720.
- 3262** Lu, J., J. Yang, C. Keitel, L. Yin, P. Wang, W. Cheng, and F. A. Dijkstra (2022). Belowground carbon efficiency for nitrogen and phosphorus acquisition varies between *Lolium perenne* and *Trifolium repens* and depends on phosphorus fertilization. *Frontiers in Plant Science* 13, 1–9.
- 3266** Luo, X., T. F. Keenan, J. M. Chen, H. Croft, I. C. Prentice, N. G. Smith, A. P. Walker, H. Wang, R. Wang, C. Xu, and Y. Zhang (2021). Global variation in the fraction of leaf nitrogen allocated to photosynthesis. *Nature Communications* 12(1), 4866.
- 3270** Luo, Y., W. S. Currie, J. S. Dukes, A. C. Finzi, U. A. Hartwig, B. A. Hungate, R. E. McMurtrie, R. Oren, W. J. Parton, D. E. Pataki, R. M. Shaw, D. R. Zak, and C. B. Field (2004). Progressive nitrogen limitation of ecosystem responses to rising atmospheric carbon dioxide. *BioScience* 54(8), 731–739.
- 3274** Maire, V., P. Martre, J. Kattge, F. Gastal, G. Esser, S. Fontaine, and J.-F. Soussana (2012). The coordination of leaf photosynthesis links C and N fluxes in C₃ plant species. *PLoS ONE* 7(6), e38345.
- 3277** Makino, A. (2003). Rubisco and nitrogen relationships in rice: leaf photosynthesis and plant growth. *Soil Science and Plant Nutrition* 49(3), 319–327.
- 3279** Makino, A., M. Harada, T. Sato, H. Nakano, and T. Mae (1997). Growth and N

- 3280** Allocation in Rice Plants under CO₂ Enrichment. *Plant Physiology* 115(1),
3281 199–203.
- 3282** Markham, J. H. and C. Zekveld (2007). Nitrogen fixation makes biomass al-
3283 location to roots independent of soil nitrogen supply. *Canadian Journal of*
3284 *Botany* (9), 787–793.
- 3285** Marschner, H. and B. Dell (1994). Nutrient uptake in mycorrhizal symbiosis.
3286 *Plant and Soil* 159(1), 89–102.
- 3287** Matamala, R. and W. H. Schlesinger (2000). Effects of elevated atmospheric
3288 CO₂ on fine root production and activity in an intact temperate forest
3289 ecosystem. *Global Change Biology* 6(8), 967–979.
- 3290** Medlyn, B. E., E. Dreyer, D. S. Ellsworth, M. Forstreuter, P. C. Harley,
3291 M. U. F. Kirschbaum, X. Le Roux, P. Montpied, J. Strassmeyer, A. Wal-
3292 croft, K. Wang, and D. Loustau (2002). Temperature response of parameters
3293 of a biochemically based model of photosynthesis. II. A review of experimen-
3294 tal data. *Plant, Cell and Environment* 25(9), 1167–1179.
- 3295** Menge, D. N. L., S. A. Levin, and L. O. Hedin (2008). Evolutionary tradeoffs can
3296 select against nitrogen fixation and thereby maintain nitrogen limitation.
3297 *Proceedings of the National Academy of Sciences* 105(5), 1573–1578.
- 3298** Menne, M. J., I. Durre, R. S. Vose, B. E. Gleason, and T. G. Houston (2012).
3299 An overview of the global historical climatology network-daily database.
3300 *Journal of Atmospheric and Oceanic Technology* 29(7), 897–910.
- 3301** Meyerholt, J., K. Sickel, and S. Zaehle (2020). Ensemble projections elucidate
3302 effects of uncertainty in terrestrial nitrogen limitation on future carbon up-

- 3303** take. *Global Change Biology* 26(7), 3978–3996.
- 3304** Meyerholt, J., S. Zaehle, and M. J. Smith (2016). Variability of projected ter-
3305 restrial biosphere responses to elevated levels of atmospheric CO₂ due to
3306 uncertainty in biological nitrogen fixation. *Biogeosciences* 13(5), 1491–1518.
- 3307** Minocha, R., S. Long, A. H. Magill, J. D. Aber, and W. H. McDowell (2000).
3308 Foliar free polyamine and inorganic ion content in relation to soil and soil
3309 solution chemistry in two fertilized forest stands at the Harvard Forest,
3310 Massachusetts. *Plant and Soil* 222(1-2), 119–137.
- 3311** Moore, D. J., S. Aref, R. M. Ho, J. S. Pippen, J. G. Hamilton, and E. H. De
3312 Lucia (2006). Annual basal area increment and growth duration of Pinus
3313 taeda in response to eight years of free-air carbon dioxide enrichment. *Global
Change Biology* 12(8), 1367–1377.
- 3315** Morgan, J. A., D. E. Pataki, C. Körner, H. Clark, S. J. Del Gross, J. M.
3316 Grünzweig, A. K. Knapp, A. R. Mosier, P. C. D. Newton, P. A. Niklaus,
3317 J. B. Nippert, R. S. Nowak, W. J. Parton, H. W. Polley, and M. R. Shaw
3318 (2004). Water relations in grassland and desert ecosystems exposed to ele-
3319 vated atmospheric CO₂. *Oecologia* 140(1), 11–25.
- 3320** Muñoz, N., X. Qi, M. W. Li, M. Xie, Y. Gao, M. Y. Cheung, F. L. Wong, and
3321 H.-M. Lam (2016). Improvement in nitrogen fixation capacity could be part
3322 of the domestication process in soybean. *Heredity* 117(2), 84–93.
- 3323** Nadelhoffer, K. J. and J. W. Raich (1992). Fine root production estimates and
3324 belowground carbon allocation in forest ecosystems. *Ecology* 73(4), 1139–
3325 1147.

- 3326 Niinemets, Ü. and J. D. Tenhunen (1997). A model separating leaf structural
3327 and physiological effects on carbon gain along light gradients for the shade-
3328 tolerant species *Acer saccharum*. *Plant, Cell and Environment* 20(7), 845–
3329 866.
- 3330 Norby, R. J., J. Ledford, C. D. Reilly, N. E. Miller, and E. G. O'Neill
3331 (2004). Fine-root production dominates response of a deciduous forest to
3332 atmospheric CO₂ enrichment. *Proceedings of the National Academy of Sci-
3333 ences* 101(26), 9689–9693.
- 3334 Norby, R. J., J. M. Warren, C. M. Iversen, B. E. Medlyn, and R. E. Mc-
3335 Murtrie (2010). CO₂ enhancement of forest productivity constrained by
3336 limited nitrogen availability. *Proceedings of the National Academy of Sci-
3337 ences* 107(45), 19368–19373.
- 3338 Novick, K. A., D. L. Ficklin, P. C. Stoy, C. A. Williams, G. Bohrer, A. C.
3339 Oishi, S. A. Papuga, P. D. Blanken, A. Noormets, B. N. Sulman, R. L.
3340 Scott, L. Wang, and R. P. Phillips (2016). The increasing importance of
3341 atmospheric demand for ecosystem water and carbon fluxes. *Nature Climate
3342 Change* 6(11), 1023–1027.
- 3343 Noyce, G. L., M. L. Kirwan, R. L. Rich, and J. P. Megonigal (2019). Asyn-
3344 chronous nitrogen supply and demand produce nonlinear plant allocation re-
3345 sponses to warming and elevated CO₂. *Proceedings of the National Academy
3346 of Sciences* 116(43), 21623–21628.
- 3347 Onoda, Y., K. Hikosaka, and T. Hirose (2004). Allocation of nitrogen to
3348 cell walls decreases photosynthetic nitrogen-use efficiency. *Functional Ecol-
3349 ogy* 18(3), 419–425.

- 3350** Onoda, Y., I. J. Wright, J. R. Evans, K. Hikosaka, K. Kitajima, Ü. Niinemets,
3351 H. Poorter, T. Tosens, and M. Westoby (2017). Physiological and structural
3352 trade-offs underlying the leaf economics spectrum. *New Phytologist* 214(4),
3353 1447–1463.
- 3354** Oren, R., J. S. Sperry, G. G. Katul, D. E. Pataki, B. E. Ewers, N. Phillips,
3355 and K. V. R. Schäfer (1999). Survey and synthesis of intra- and interspecific
3356 variation in stomatal sensitivity to vapor pressure deficit. *Plant, Cell and*
3357 *Environment* 22(12), 1515–1526.
- 3358** Oreskes, N., K. Shrader-Frechette, and K. Belitz (1994). Verification, vali-
3359 dation, and confirmation of numerical models in the Earth sciences. *Sci-
ence* 263(5147), 641–646.
- 3360** Paillassa, J., I. J. Wright, I. C. Prentice, S. Pepin, N. G. Smith, G. Ethier,
3361 A. C. Westerband, L. J. Lamarque, H. Wang, W. K. Cornwell, and V. Maire
3362 (2020). When and where soil is important to modify the carbon and water
3363 economy of leaves. *New Phytologist* 228(1), 121–135.
- 3364** Parvin, S., S. Uddin, S. Tausz Posch, R. Armstrong, and M. Tausz (2020). Car-
3365 bon sink strength of nodules but not other organs modulates photosynthesis
3366 of faba bean (*Vicia faba*) grown under elevated [CO₂] and different water
3367 supply. *New Phytologist* 227(1), 132–145.
- 3368** Paul, K. I., P. J. Polglase, A. M. O'Connell, J. C. Carlyle, P. J. Smethurst, and
3369 P. K. Khanna (2003). Defining the relation between soil water content and
3370 net nitrogen mineralization. *European Journal of Soil Science* 54(1), 39–48.
- 3371** Peng, Y., K. J. Bloomfield, L. A. Cernusak, T. F. Domingues, and I. C. Pre-
3372 nance (2021). Global climate and nutrient controls of photosynthetic capacity.
- 3373**

- 3374** *Communications Biology* 4(1), 462.
- 3375** Perkowski, E. A., E. F. Waring, and N. G. Smith (2021). Root mass carbon
3376 costs to acquire nitrogen are determined by nitrogen and light availability
3377 in two species with different nitrogen acquisition strategies. *Journal of*
3378 *Experimental Botany* 72(15), 5766–5776.
- 3379** Phillips, R. P., E. R. Brzostek, and M. G. Midgley (2013). The mycorrhizal-
3380 associated nutrient economy: a new framework for predicting carbon-
3381 nutrient couplings in temperate forests. *New Phytologist* 199(1), 41–51.
- 3382** Phillips, R. P., A. C. Finzi, and E. S. Bernhardt (2011). Enhanced root ex-
3383 udation induces microbial feedbacks to N cycling in a pine forest under
3384 long-term CO₂ fumigation. *Ecology Letters* 14(2), 187–194.
- 3385** Pinheiro, J. and D. Bates (2022). nlme: linear and nonlinear mixed effects
3386 models.
- 3387** Poggio, L., L. M. De Sousa, N. H. Batjes, G. B. M. Heuvelink, B. Kempen,
3388 E. Ribeiro, and D. Rossiter (2021). SoilGrids 2.0: Producing soil information
3389 for the globe with quantified spatial uncertainty. *Soil* 7(1), 217–240.
- 3390** Pons, T. L. and R. W. Pearcy (1994). Nitrogen reallocation and photosynthetic
3391 acclimation in response to partial shading in soybean plants. *Physiologia*
3392 *Plantarum* 92(4), 636–644.
- 3393** Poorter, H., J. Bühler, D. Van Dusschoten, J. Climent, and J. A. Postma (2012).
3394 Pot size matters: A meta-analysis of the effects of rooting volume on plant
3395 growth. *Functional Plant Biology* 39(11), 839–850.
- 3396** Poorter, H., O. Knopf, I. J. Wright, A. A. Temme, S. W. Hogewoning, A. Graf,

- 3397** L. A. Cernusak, and T. L. Pons (2022). A meta-analysis of responses of C₃
3398 plants to atmospheric CO₂: dose-response curves for 85 traits ranging from
3399 the molecular to the whole-plant level. *New Phytologist* 233(4), 1560–1596.
- 3400** Prentice, I. C., N. Dong, S. M. Gleason, V. Maire, and I. J. Wright (2014).
3401 Balancing the costs of carbon gain and water transport: testing a new theo-
3402 retical framework for plant functional ecology. *Ecology Letters* 17(1), 82–91.
- 3403** Prentice, I. C., X. Liang, B. E. Medlyn, and Y.-P. Wang (2015). Reliable, ro-
3404 bust and realistic: The three R's of next-generation land-surface modelling.
3405 *Atmospheric Chemistry and Physics* 15, 5987–6005.
- 3406** Priestley, C. H. B. and R. J. Taylor (1972). On the Assessment of Surface
3407 Heat Flux and Evaporation Using Large-Scale Parameters. *Monthly Weather
Review* 100(2), 81–92.
- 3409** Querejeta, J. I., I. Prieto, C. Armas, F. Casanoves, J. S. Diémé, M. Diouf,
3410 H. Yossi, B. Kaya, F. I. Pugnaire, and G. M. Rusch (2022). Higher leaf
3411 nitrogen content is linked to tighter stomatal regulation of transpiration
3412 and more efficient water use across dryland trees. *New Phytologist* 235(4),
3413 1351–1364.
- 3414** R Core Team (2021). R: A language and environment for statistical computing.
- 3415** Raich, J. W., D. A. Clark, L. Schwendenmann, and T. E. Wood (2014). Above-
3416 ground tree growth varies with belowground carbon allocation in a tropical
3417 rainforest environment. *PLoS ONE* 9(6), e100275.
- 3418** Rastetter, E. B., P. M. Vitousek, C. B. Field, G. R. Shaver, D. Herbert, and
3419 G. I. Ågren (2001). Resource optimization and symbiotic nitrogen fixation.

- 3420** *Ecosystems* 4(4), 369–388.
- 3421** Reich, P. B. (2014). The world-wide 'fast-slow' plant economics spectrum: a
3422 traits manifesto. *Journal of Ecology* 102(2), 275–301.
- 3423** Reich, P. B., S. E. Hobbie, T. Lee, D. S. Ellsworth, J. B. West, D. Tilman,
3424 J. M. H. Knops, S. Naeem, and J. Trost (2006). Nitrogen limitation con-
3425 strains sustainability of ecosystem response to CO₂. *Nature* 440(7086), 922–
3426 925.
- 3427** Reichman, G. A., D. L. Grunes, and F. G. Viets (1966). Effect of soil moisture
3428 on ammonification and nitrification in two Northern Plains soils. *Soil Science
Society of America Journal* 30(3), 363–366.
- 3430** Rhine, E. D., R. L. Mulvaney, E. J. Pratt, and G. K. Sims (1998). Improving
3431 the Berthelot reaction for determining ammonium in soil extracts and water.
3432 *Soil Science Society of America Journal* 62(2), 473.
- 3433** Rogers, A. (2014). The use and misuse of V_{cmax} in Earth System Models. *Pho-*
3434 *tosynthesis Research* 119(1-2), 15–29.
- 3435** Rogers, A., B. E. Medlyn, J. S. Dukes, G. B. Bonan, S. Caemmerer, M. C.
3436 Dietze, J. Kattge, A. D. B. Leakey, L. M. Mercado, Ü. Niinemets, I. C.
3437 Prentice, S. P. Serbin, S. Sitch, D. A. Way, and S. Zaehle (2017). A roadmap
3438 for improving the representation of photosynthesis in Earth system models.
3439 *New Phytologist* 213(1), 22–42.
- 3440** Saathoff, A. J. and J. Welles (2021). Gas exchange measurements in the un-
3441 steady state. *Plant Cell and Environment* 44(11), 3509–3523.
- 3442** Sage, R. F. and R. W. Pearcy (1987). The nitrogen use efficiency of C₃ and C₄

- 3443** plants: I. Leaf nitrogen, growth, and biomass partitioning in *Chenopodium*
3444 *album* (L.) and *Amaranthus retroflexus* (L.). *Plant Physiology* 84(3), 954–
3445 958.
- 3446** Saleh, A. M., M. Abdel-Mawgoud, A. R. Hassan, T. H. Habeeb, R. S. Yehia,
3447 and H. AbdElgawad (2020). Global metabolic changes induced by arbuscular
3448 mycorrhizal fungi in oregano plants grown under ambient and elevated levels
3449 of atmospheric CO₂. *Plant Physiology and Biochemistry* 151, 255–263.
- 3450** Saxton, K. E. and W. J. Rawls (2006). Soil water characteristic estimates by
3451 texture and organic matter for hydrologic solutions. *Soil Science Society of*
3452 *America Journal* 70(5), 1569–1578.
- 3453** Schaefer, K., C. R. Schwalm, C. Williams, M. A. Arain, A. Barr, J. M. Chen,
3454 K. J. Davis, D. Dimitrov, T. W. Hilton, D. Y. Hollinger, E. Humphreys,
3455 B. Poulter, B. M. Racza, A. D. Richardson, A. Sahoo, P. Thornton, R. Var-
3456 gas, H. Verbeeck, R. Anderson, I. Baker, T. A. Black, P. Bolstad, J. Chen,
3457 P. S. Curtis, A. R. Desai, M. C. Dietze, D. Dragoni, C. M. Gough, R. F.
3458 Grant, L. Gu, A. K. Jain, C. Kucharik, B. E. Law, S. Liu, E. Lokipitiya,
3459 H. A. Margolis, R. Matamala, J. H. McCaughey, R. Monson, J. W. Munger,
3460 W. Oechel, C. Peng, D. T. Price, D. Ricciuto, W. J. Riley, N. Roulet,
3461 H. Tian, C. Tonitto, M. Torn, E. Weng, and X. Zhou (2012). A model-
3462 data comparison of gross primary productivity: Results from the North
3463 American Carbon Program site synthesis. *Journal of Geophysical Research:*
3464 *Biogeosciences* 117(G3), G03010.
- 3465** Schmitt, M. R. and G. E. Edwards (1981). Photosynthetic capacity and nitrogen
3466 use efficiency of maize, wheat, and rice: A comparison between C₃ and C₄

- 3467** photosynthesis. *Journal of Experimental Botany* 32(3), 459–466.
- 3468** Schneider, C. A., W. S. Rasband, and K. W. Eliceiri (2012). NIH Image to
- 3469** ImageJ: 25 years of image analysis. *Nature Methods* 9(7), 671–675.
- 3470** Scott, H. G. and N. G. Smith (2022). A Model of C₄ photosynthetic acclima-
- 3471** tion based on least-cost optimality theory suitable for Earth system model
- 3472** incorporation. *Journal of Advances in Modeling Earth Systems* 14(3), 1–16.
- 3473** Shi, M., J. B. Fisher, E. R. Brzostek, and R. P. Phillips (2016). Carbon cost
- 3474** of plant nitrogen acquisition: Global carbon cycle impact from an improved
- 3475** plant nitrogen cycle in the Community Land Model. *Global Change Biol-*
- 3476** *ogy* 22(3), 1299–1314.
- 3477** Shi, M., J. B. Fisher, R. P. Phillips, and E. R. Brzostek (2019). Neglecting
- 3478** plant–microbe symbioses leads to underestimation of modeled climate im-
- 3479** pacts. *Biogeosciences* 16(2), 457–465.
- 3480** Smith, B., D. Wärldin, A. Arneth, T. Hickler, P. Leadley, J. Siltberg, and
- 3481** S. Zaehle (2014). Implications of incorporating N cycling and N limitations
- 3482** on primary production in an individual-based dynamic vegetation model.
- 3483** *Biogeosciences* 11(7), 2027–2054.
- 3484** Smith, N. G. and J. S. Dukes (2013). Plant respiration and photosynthesis in
- 3485** global-scale models: incorporating acclimation to temperature and CO₂.
- 3486** *Global Change Biology* 19(1), 45–63.
- 3487** Smith, N. G. and J. S. Dukes (2018). Drivers of leaf carbon exchange capacity
- 3488** across biomes at the continental scale. *Ecology* 99(7), 1610–1620.
- 3489** Smith, N. G. and T. F. Keenan (2020). Mechanisms underlying leaf photosyn-

- 3490 thetic acclimation to warming and elevated CO₂ as inferred from least-cost
3491 optimality theory. *Global Change Biology* 26(9), 5202–5216.
- 3492 Smith, N. G., T. F. Keenan, I. C. Prentice, H. Wang, I. J. Wright, Ü. Niinemets,
3493 K. Y. Crous, T. F. Domingues, R. Guerrieri, F. oko Ishida, J. Kattge, E. L.
3494 Kruger, V. Maire, A. Rogers, S. P. Serbin, L. Tarvainen, H. F. Togashi,
3495 P. A. Townsend, M. Wang, L. K. Weerasinghe, and S.-X. Zhou (2019).
3496 Global photosynthetic capacity is optimized to the environment. *Ecology*
3497 *Letters* 22(3), 506–517.
- 3498 Smith, N. G., D. L. Lombardozzi, A. Tawfik, G. B. Bonan, and J. S. Dukes
3499 (2017). Biophysical consequences of photosynthetic temperature acclimation
3500 for climate. *Journal of Advances in Modeling Earth Systems* 9(1), 536–547.
- 3501 Smith, N. G., S. L. Malyshev, E. Shevliakova, J. Kattge, and J. S. Dukes
3502 (2016). Foliar temperature acclimation reduces simulated carbon sensitivity
3503 to climate. *Nature Climate Change* 6(4), 407–411.
- 3504 Smith, S. E. and D. J. Read (2008). *Mycorrhizal Symbiosis*. Academic Press.
- 3505 Soil Survey Staff (2022). Web Soil Survey.
- 3506 Soudzilovskaia, N. A., J. C. Douma, A. A. Akhmetzhanova, P. M. van Bode-
3507 gom, W. K. Cornwell, E. J. Moens, K. K. Treseder, and J. H. C. Cornelissen
3508 (2015). Global patterns of plant root colonization intensity by mycorrhizal
3509 fungi explained by climate and soil chemistry. *Global Ecology and Biogeogra-*
3510 *phy* 24(3), 371–382.
- 3511 Stark, J. M. and M. K. Firestone (1995). Mechanisms for soil moisture ef-
3512 fects on activity of nitrifying bacteria. *Applied and Environmental Microbi-*

- 3513 *ology* 61(1), 218–221.
- 3514 Stocker, B. D., H. Wang, N. G. Smith, S. P. Harrison, T. F. Keenan, D. San-
- 3515 doval, T. Davis, and I. C. Prentice (2020). P-model v1.0: An optimality-
- 3516 based light use efficiency model for simulating ecosystem gross primary pro-
- 3517 duction. *Geoscientific Model Development* 13(3), 1545–1581.
- 3518 Stocker, B. D., J. Zscheischler, T. F. Keenan, I. C. Prentice, J. Peñuelas, and
- 3519 S. I. Seneviratne (2018). Quantifying soil moisture impacts on light use
- 3520 efficiency across biomes. *New Phytologist* 218(4), 1430–1449.
- 3521 Sulman, B. N., D. T. Roman, K. Yi, L. Wang, R. P. Phillips, and K. A.
- 3522 Novick (2016). High atmospheric demand for water can limit forest car-
- 3523 bon uptake and transpiration as severely as dry soil. *Geophysical Research*
- 3524 *Letters* 43(18), 9686–9695.
- 3525 Sulman, B. N., E. Shevliakova, E. R. Brzostek, S. N. Kivlin, S. L. Malyshev,
- 3526 D. N. L. Menge, and X. Zhang (2019). Diverse mycorrhizal associations
- 3527 enhance terrestrial C storage in a global model. *Global Biogeochemical Cy-*
- 3528 *cles* 33(4), 501–523.
- 3529 Sweet, S. K., D. W. Wolfe, A. DeGaetano, and R. Benner (2017). Anatomy
- 3530 of the 2016 drought in the Northeastern United States: Implications for
- 3531 agriculture and water resources in humid climates. *Agricultural and Forest*
- 3532 *Meteorology* 247, 571–581.
- 3533 Taylor, B. N. and D. N. L. Menge (2018). Light regulates tropical symbiotic
- 3534 nitrogen fixation more strongly than soil nitrogen. *Nature Plants* 4(9), 655–
- 3535 661.

- 3536** Terrer, C., S. Vicca, B. A. Hungate, R. P. Phillips, and I. C. Prentice (2016).
3537 Mycorrhizal association as a primary control of the CO₂ fertilization effect.
3538 *Science* 353(6294), 72–74.
- 3539** Terrer, C., S. Vicca, B. D. Stocker, B. A. Hungate, R. P. Phillips, P. B. Reich,
3540 A. C. Finzi, and I. C. Prentice (2018). Ecosystem responses to elevated CO₂
3541 governed by plant–soil interactions and the cost of nitrogen acquisition. *New*
3542 *Phytologist* 217(2), 507–522.
- 3543** Thieurmel, B. and A. Elmarhraoui (2019). suncalc: Compute sun position,
3544 sunlight phases, moon position, and lunar phase.
- 3545** Thomas, R. Q., E. N. J. Brookshire, and S. Gerber (2015). Nitrogen limita-
3546 tion on land: how can it occur in Earth system models? *Global Change*
3547 *Biology* 21(5), 1777–1793.
- 3548** Thomas, R. Q., S. Zaehle, P. H. Templer, and C. L. Goodale (2013). Global pat-
3549 terns of nitrogen limitation: confronting two global biogeochemical models
3550 with observations. *Global Change Biology* 19(10), 2986–2998.
- 3551** Thornton, P. E., J.-F. Lamarque, N. A. Rosenbloom, and N. M. Mahowald
3552 (2007). Influence of carbon-nitrogen cycle coupling on land model response
3553 to CO₂ fertilization and climate variability. *Global Biogeochemical Cy-*
3554 *cles* 21(4), GB4018.
- 3555** Tingey, D. T., D. L. Phillips, and M. G. Johnson (2000). Elevated CO₂ and
3556 conifer roots: effects on growth, life span and turnover. *New Phytolo-*
3557 *gist* 147(1), 87–103.
- 3558** Udvardi, M. and P. S. Poole (2013). Transport and metabolism in legume-

- 3559 rhizobia symbioses. *Annual Review of Plant Biology* 64, 781–805.
- 3560 USDA NRCS (2022). The PLANTS Database.
- 3561 Uselman, S. M., R. G. Qualls, and R. B. Thomas (2000). Effects of increased
3562 atmospheric CO₂, temperature, and soil N availability on root exudation
3563 of dissolved organic carbon by an N-fixing tree (*Robinia pseudoacacia* L.).
3564 *Plant and Soil* 222, 191–202.
- 3565 van Diepen, L. T. A., E. A. Lilleskov, K. S. Pregitzer, and R. M. Miller (2007).
3566 Decline of arbuscular mycorrhizal fungi in northern hardwood forests ex-
3567 posed to chronic nitrogen additions. *New Phytologist* 176(1), 175–183.
- 3568 Vance, C. P. and G. H. Heichel (1991). Carbon in N₂ fixation: Limitation or
3569 exquisite adaptation. *Annual Review of Plant Physiology and Plant Molec-*
3570 *ular Biology* 42(1), 373–392.
- 3571 Viet, H. D., J.-H. Kwak, K.-S. Lee, S.-S. Lim, M. Matsushima, S. X. Chang,
3572 K.-H. Lee, and W.-J. Choi (2013). Foliar chemistry and tree ring δ¹³C of
3573 *Pinus densiflora* in relation to tree growth along a soil pH gradient. *Plant*
3574 *and Soil* 363(1-2), 101–112.
- 3575 Vitousek, P. M., K. Cassman, C. C. Cleveland, T. Crews, C. B. Field, N. B.
3576 Grimm, R. W. Howarth, R. Marino, L. Martinelli, E. B. Rastetter, and
3577 J. I. Sprent (2002). Towards an ecological understanding of biological nitro-
3578 gen fixation. In *The Nitrogen Cycle at Regional to Global Scales*, pp. 1–45.
3579 Springer Netherlands.
- 3580 Vitousek, P. M. and R. W. Howarth (1991). Nitrogen limitation on land and in
3581 the sea: How can it occur? *Biogeochemistry* 13(2), 87–115.

- 3582 Vitousek, P. M., S. Porder, B. Z. Houlton, and O. A. Chadwick (2010).
- 3583 Terrestrial phosphorus limitation: mechanisms, implications, and nitro-
- 3584 gen–phosphorus interactions. *Ecological Applications* 20(1), 5–15.
- 3585 Walker, A. P., A. P. Beckerman, L. Gu, J. Kattge, L. A. Cernusak, T. F.
- 3586 Domingues, J. C. Scales, G. Wohlfahrt, S. D. Wullschleger, and F. I. Wood-
- 3587 ward (2014). The relationship of leaf photosynthetic traits - V_{cmax} and J_{max}
- 3588 - to leaf nitrogen, leaf phosphorus, and specific leaf area: a meta-analysis
- 3589 and modeling study. *Ecology and Evolution* 4(16), 3218–3235.
- 3590 Walker, A. P., A. L. Johnson, A. Rogers, J. Anderson, R. A. Bridges, R. A.
- 3591 Fisher, D. Lu, D. M. Ricciuto, S. P. Serbin, and M. Ye (2021). Multi-
- 3592 hypothesis comparison of Farquhar and Collatz photosynthesis models re-
- 3593 veals the unexpected influence of empirical assumptions at leaf and global
- 3594 scales. *Global Change Biology* 27(4), 804–822.
- 3595 Wang, H., I. C. Prentice, T. F. Keenan, T. W. Davis, I. J. Wright, W. K.
- 3596 Cornwell, B. J. Evans, and C. Peng (2017). Towards a universal model for
- 3597 carbon dioxide uptake by plants. *Nature Plants* 3(9), 734–741.
- 3598 Wang, H., I. C. Prentice, I. J. Wright, D. I. Warton, S. Qiao, X. Xu, J. Zhou,
- 3599 Kikuzawa, and N. C. Stenseth (2023). Leaf economics fundamentals ex-
- 3600 plained by optimality principles. *Science Advances* 9(3), eadd566.
- 3601 Wang, J., J. M. Knops, C. E. Brassil, and C. Mu (2017). Increased productivity
- 3602 in wet years drives a decline in ecosystem stability with nitrogen additions
- 3603 in arid grasslands. *Ecology* 98(7), 1779–1786.
- 3604 Wang, W., Y. Wang, G. Hoch, Z. Wang, and J. Gu (2018). Linkage of root mor-
- 3605 phology to anatomy with increasing nitrogen availability in six temperate

- 3606** tree species. *Plant and Soil* 425(1-2), 189–200.
- 3607** Weatherburn, M. W. (1967). Phenol-hypochlorite reaction for determination of
- 3608** ammonia. *Analytical Chemistry* 39(8), 971–974.
- 3609** Wellburn, A. R. (1994). The spectral determination of chlorophylls a and b, as
- 3610** well as total carotenoids, using various solvents with spectrophotometers of
- 3611** different resolution. *Journal of Plant Physiology* 144(3), 307–313.
- 3612** Wen, Z., P. J. White, J. Shen, and H. Lambers (2022). Linking root exuda-
- 3613** tion to belowground economic traits for resource acquisition. *New Phytolo-*
- 3614** *gist* 233(4), 1620–1635.
- 3615** Westerband, A. C., I. J. Wright, V. Maire, J. Paillassa, I. C. Prentice, O. K.
- 3616** Atkin, K. J. Bloomfield, L. A. Cernusak, N. Dong, S. M. Gleason, C. Guil-
- 3617** herme Pereira, H. Lambers, M. R. Leishman, Y. Malhi, and R. H. Nolan
- 3618** (2023). Coordination of photosynthetic traits across soil and climate gradi-
- 3619** ents. *Global Change Biology* 29(3), 1–29.
- 3620** Wieder, W. R., C. C. Cleveland, W. K. Smith, and K. Todd-Brown (2015).
- 3621** Future productivity and carbon storage limited by terrestrial nutrient avail-
- 3622** ability. *Nature Geoscience* 8(6), 441–444.
- 3623** Wieder, W. R., D. M. Lawrence, R. A. Fisher, G. B. Bonan, S. J. Cheng, C. L.
- 3624** Goodale, A. S. Grandy, C. D. Koven, D. L. Lombardozzi, K. W. Oleson,
- 3625** and R. Q. Thomas (2019). Beyond static benchmarking: using experimental
- 3626** manipulations to evaluate land model assumptions. *Global Biogeochemical*
- 3627** *Cycles* 33(10), 1289–1309.
- 3628** Wright, I. J., P. B. Reich, and M. Westoby (2003). Least-cost input mixtures

- 3629 of water and nitrogen for photosynthesis. *The American Naturalist* 161(1),
3630 98–111.
- 3631 Wright, I. J., P. B. Reich, M. Westoby, D. D. Ackerly, Z. Baruch, F. Bongers,
3632 J. Cavender-Bares, T. Chapin, J. H. C. Cornelissen, M. Diemer, J. Flexas,
3633 E. Garnier, P. K. Groom, J. Gulias, K. Hikosaka, B. B. Lamont, T. Lee,
3634 W. Lee, C. Lusk, J. J. Midgley, M.-L. Navas, Ü. Niinemets, J. Oleksyn,
3635 N. Osada, H. Poorter, P. Poot, L. Prior, V. I. Pyankov, C. Roumet, S. C.
3636 Thomas, M. G. Tjoelker, E. J. Veneklaas, and R. Villar (2004). The world-
3637 wide leaf economics spectrum. *Nature* 428(6985), 821–827.
- 3638 Xu-Ri and I. C. Prentice (2017). Modelling the demand for new nitrogen fixation
3639 by terrestrial ecosystems. *Biogeosciences* 14(7), 2003–2017.
- 3640 Yahdjian, L., L. A. Gherardi, and O. E. Sala (2011). Nitrogen limitation in
3641 arid-subhumid ecosystems: A meta-analysis of fertilization studies. *Journal
3642 of Arid Environments* 75(8), 675–680.
- 3643 Yuan, W., Y. Zheng, S. Piao, P. Ciais, D. Lombardozzi, Y. Wang, Y. Ryu,
3644 G. Chen, W. Dong, Z. Hu, A. K. Jain, C. Jiang, E. Kato, S. Li, S. Lienert,
3645 S. Liu, J. E. Nabel, Z. Qin, T. Quine, S. Sitch, W. K. Smith, F. Wang,
3646 C. Wu, Z. Xiao, and S. Yang (2019). Increased atmospheric vapor pressure
3647 deficit reduces global vegetation growth. *Science Advances* 5(8), 1–12.
- 3648 Zaehle, S., B. E. Medlyn, M. G. De Kauwe, A. P. Walker, M. C. Dietze, T. Hick-
3649 ler, Y. Luo, Y. P. Wang, B. El-Masri, P. Thornton, A. Jain, S. Wang,
3650 D. Warlind, E. Weng, W. Parton, C. M. Iversen, A. Gallet-Budynek, H. Mc-
3651 carthy, A. C. Finzi, P. J. Hanson, I. C. Prentice, R. Oren, and R. J. Norby
3652 (2014). Evaluation of 11 terrestrial carbon-nitrogen cycle models against

- 3653** observations from two temperate Free-Air CO₂ Enrichment studies. *New*
3654 *Phytologist* 202(3), 803–822.
- 3655** Zaehle, S., S. Sitch, B. Smith, and F. Hatterman (2005). Effects of parame-
3656 ter uncertainties on the modeling of terrestrial biosphere dynamics. *Global*
3657 *Biogeochemical Cycles* 19(3), GB3020.
- 3658** Zhu, Q., W. J. Riley, J. Tang, N. Collier, F. M. Hoffman, X. Yang, and G. Bisht
3659 (2019). Representing nitrogen, phosphorus, and carbon interactions in the
3660 E3SM land model: development and global benchmarking. *Journal of Ad-*
3661 *vances in Modeling Earth Systems* 11(7), 2238–2258.
- 3662** Ziegler, C., M. E. Dusenge, B. Nyirambangutse, E. Zibera, G. Wallin, and
3663 J. Uddling (2020). Contrasting dependencies of photosynthetic capacity on
3664 leaf nitrogen in early- and late-successional tropical montane tree species.
3665 *Frontiers in Plant Science* 11, 1–12.
- 3666** Ziehn, T., J. Kattge, W. Knorr, and M. Scholze (2011). Improving the pre-
3667 dictability of global CO₂ assimilation rates under climate change. *Geophys-*
3668 *ical Research Letters* 38(10), L10404.

3669 **Appendix A: Supplemental material for "Structural carbon costs to**
 3670 **acquire nitrogen are determined by nitrogen and light availability in**
 3671 **two species with different nitrogen acquisition strategies"**

Table A1. Summary table containing volumes of compounds used to create modified Hoagland's solutions for each soil nitrogen fertilization treatment. All volumes are expressed as milliliters per liter (mL L^{-1})

Compound	0 ppm N	70 ppm N	210 ppm N	630 ppm N
1 M $\text{NH}_4\text{H}_2\text{PO}_4$	0	0.33	1	1
2 M KNO_3	0	0.67	2	2
2 M $\text{Ca}(\text{NO}_3)_2$	0	0.67	2	2
1 M NH_4NO_3	0	0.33	1	0
8 M NH_4NO_3	0	0	0	2
1 M KH_2PO_4	1	0.67	0	0
1 M KCl	4	1.33	0	0
1 M CaCO_3	4	3	0	0
2 M MgSO_4	1	1	1	1
10% Fe-EDTA	1	1	1	1
Trace Elements	1	1	1	1

Table A2. Analysis of variance results exploring species-specific effects of light availability, nitrogen fertilization, and their interactions on the ratio of whole plant biomass to pot volume (g L^{-1})^{*}

	df	Coefficient	χ^2	p
<i>G. hirsutum</i>				
Intercept		0.740	-	-
Light (L)	1	-4.23E-03	189.581	<0.001
Nitrogen (N)	1	7.86E-04	17.927	<0.001
L*N	1	-6.61E-06	4.709	0.030
<i>G. max</i>				
Intercept		-0.233	-	-
Light (L)	1	-1.12E-02	69.500	<0.001
Nitrogen (N)	1	8.29E-04	40.297	<0.001
L*N	1	-8.51E-06	5.548	0.019

3672 *Significance determined using Wald's χ^2 tests ($p=0.05$). *P*-values less than 0.05
3673 are in bold and *p*-values between 0.05 and 0.1 are italicized. Negative coefficients
3674 for light treatments indicate a positive effect of increasing light availability on
3675 all response variables, as light availability is treated as percent shade cover in all
3676 linear mixed-effects models.

Table A3. Slopes of the regression line describing the relationship between each dependent variable and nitrogen fertilization at each light level*

Shade cover	Slope
<i>G. hirsutum</i>	
0%	8.29E-04^a
30%	5.74E-04^a
50%	4.03E-04^a
80%	1.48E-04 ^a
<i>G. max</i>	
0%	7.86E-04
30%	5.87E-04
50%	4.55E-04
80%	<i>2.57E-05</i>

3677 *Slopes represent estimated marginal mean slopes from linear mixed-effects models described in the Methods. Slopes
3678 were calculated using the ‘emmeans’ R package (Lenth 2019). Superscripts indicate slopes fit to natural-log (^a) or
3679 square root (^b) transformed data. Slopes statistically different from zero (Tukey: $p < 0.05$) are indicated in bold.
3680 Marginally significant slopes (Tukey: $0.05 < p < 0.1$) are italicized.

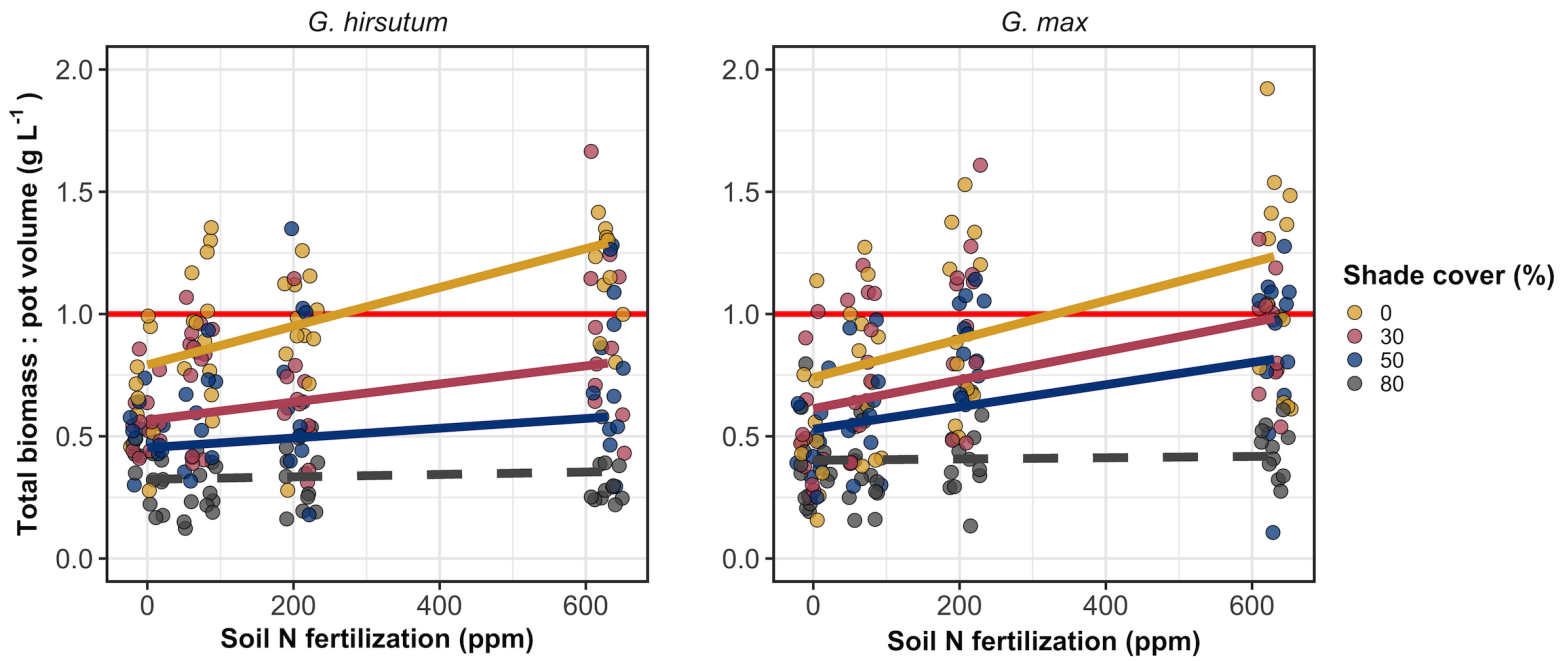


Figure A1. Effects of shade cover and nitrogen fertilization on the ratio of plant biomass to rooting volume in *G. hirsutum* (left panel) and *G. max* (right panel). The red horizontal line indicates the recommended 1 g L^{-1} threshold for biomass:pot volume recommended by Poorter et al. (2012) to avoid pot size-induced growth limitation. Nitrogen fertilization treatments are represented on the x-axis. Shade cover treatments are represented through colored points and trendlines. Points are jittered for visibility. Yellow points and trendlines represent the 0% shade cover treatment, blue points and trendlines represent the 30% shade cover treatment, green points and trendlines represent the 50% shade cover treatment, and purple points and trendlines represent the 80% shade cover treatment. Solid trendlines indicate slopes that are significantly different from zero (Tukey: $p < 0.05$), while dashed trendlines indicate slopes that are not statistically different from zero.

3681 Appendix B: Supplemental material for "Soil nitrogen availability
3682 modifies leaf nitrogen economies in mature temperate deciduous
3683 forests: a direct test of photosynthetic least-cost theory"

Table B1. Sample sizes of each species, abbreviated by their USDA NRCS PLANTS database code, within each plot at each site*

	ACRU	ACSA	FAGR	FRAM	QURU	N_{plot}
Bald Hill						
+N; +S	0	6	1	0	1	8
+N; -S	1	2	2	0	1	6
-N; +S	2	2	0	0	2	6
-N; -S	2	3	3	0	2	10
Carter Creek						
+N; +S	0	6	1	2	0	9
+N; -S	0	4	0	2	0	6
-N; +S	0	5	1	4	0	10
-N; -S	0	7	0	0	0	7
Mount Pleasant						
+N; +S	3	2	1	0	3	9
+N; -S	0	5	4	1	0	10
-N; +S	1	2	4	0	0	7
-N; -S	3	3	1	2	1	10
N_{spp}	12	47	18	11	10	98

3684 *Plots within each site are represented based on nitrogen and sulfur addition
3685 status. The final column on the right depicts total sample size per plot in each
3686 site (N_{plot}) and the final row on the bottom represents cumulative species sample
3687 size across all plots and all sites (N_{spp}). Key: ACRU=*A. rubrum*; ACSA=*A.*
3688 *saccharum*; FAGR=*F. grandifolia*; FRAM=*F. americana*; QURU=*Q. rubra*

Table B2. Analysis of variance results exploring the linear effect of leaf temperature on net photosynthesis rate (A_{net} ; $\mu\text{mol m}^{-2} \text{s}^{-1}$) and stomatal conductance (g_{sw} ; $\mu\text{mol m}^{-2} \text{s}^{-1}$) measured at $400 \mu\text{mol mol}^{-1} \text{CO}_2$

	df	A_{net}		g_{sw}	
		χ^2	p	χ^2	p
Leaf temperature	1	1.287	0.257	1.716	0.190

3689 *Results detail linear mixed effects model where temperature was regressed against
3690 net photosynthesis or stomatal conductance, with site and species designated as
3691 random intercept terms. Significance was determined using Type II Wald χ^2 tests
3692 ($\alpha=0.05$).

Table B3. Second order log-polynomial regression coefficients that described the effect of leaf temperature on net photosynthesis (A_{net} ; $\mu\text{mol m}^{-2} \text{s}^{-1}$) and stomatal conductance (g_s ; $\mu\text{mol m}^{-2} \text{s}^{-1}$) measured at 400 $\mu\text{mol mol}^{-1} \text{CO}_2$ *

	a	b	c
A_{net}	9.422	-0.573	0.010
g_s	-0.170	-0.186	0.003

3693 *Net photosynthesis and stomatal conductance values were fit to the log-polynomial
3694 equation $\log(y) = a + bx + cx^2$, where x is leaf temperature in °C.

Table B4. Mean, standard error, and 95% confidence interval ranges of soil nitrogen availability estimates across all measured plots. All units are expressed as $\mu\text{g N g}^{-1}$ resin d^{-1}

Site	Treatment	Mean	SE	Lower 95% CI	Upper 95% CI
Bald Hill	Ammonium sulfate	27.11	6.14	15.08	39.13
Bald Hill	Control	14.41	5.02	4.56	24.26
Bald Hill	Sodium nitrate	20.65	3.15	14.46	26.83
Bald Hill	Sulfur	6.33	2.19	2.04	10.62
Carter Creek	Ammonium sulfate	26.94	5.36	16.43	37.44
Carter Creek	Control	19.87	1.92	16.10	23.64
Carter Creek	Sodium nitrate	15.51	4.16	7.36	23.65
Carter Creek	Sulfur	5.50	1.40	2.75	8.25
Mount Pleasant	Ammonium sulfate	8.02	2.31	3.49	12.56
Mount Pleasant	Control	2.00	0.57	0.89	3.11
Mount Pleasant	Sodium nitrate	2.52	0.68	1.19	3.85
Mount Pleasant	Sulfur	2.42	0.39	1.66	3.17

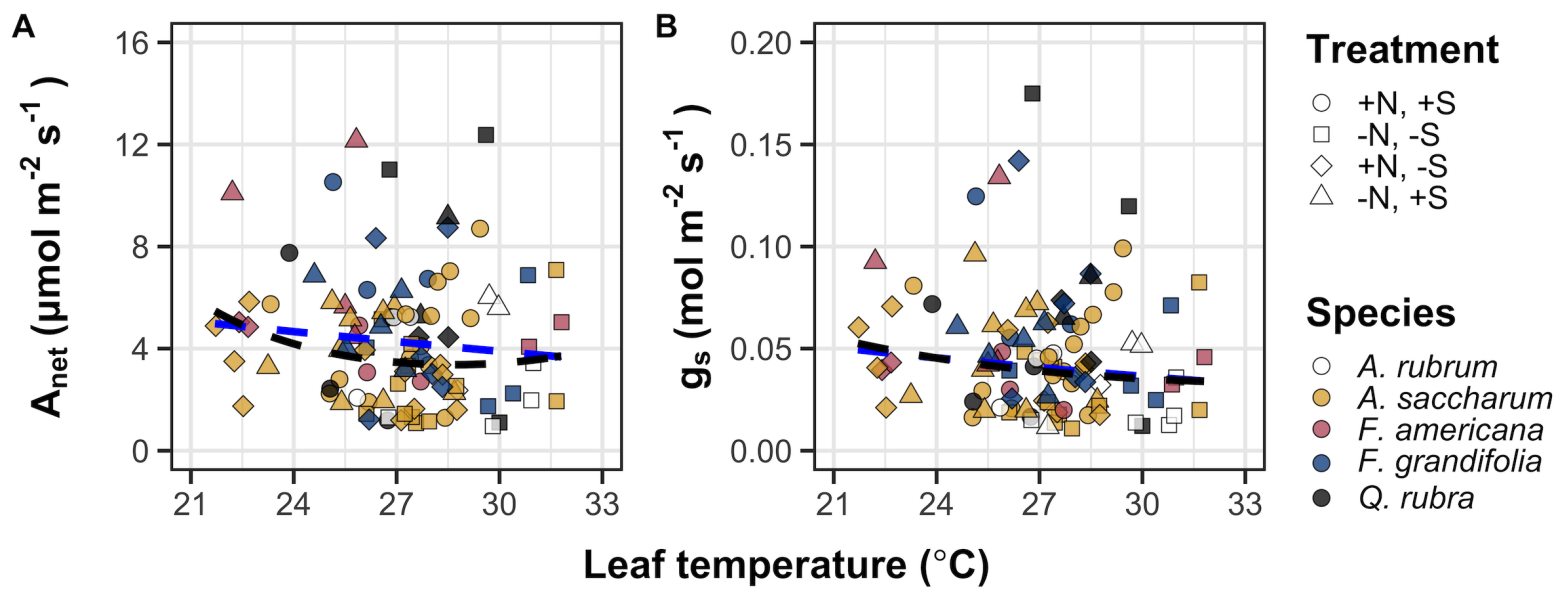


Figure B1. Effects of leaf temperature on net photosynthesis rate (A) and stomatal conductance (B) values when measured at $400 \mu\text{mol mol}^{-1} \text{CO}_2$. Leaf temperature is represented on the x-axis, while species are represented as colored points. Colored points and shapes are as explained in Figure 3.1. The dashed blue trendline describes the linear relationship between leaf temperature and each response variable, while the dashed black trendline describes the same relationship with a log-polynomial regression equation.

**3695 Appendix C: Supplemental material for "The relative cost of resource
3696 use for photosynthesis drives variance in leaf nitrogen content across a
3697 climate and soil resource availability gradient"**

3698 C.1 Calculations for soil water holding capacity

3699 Water holding capacity (θ_{WHC} ; mm) was calculated as a function of the volumetric
3700 soil water storage at field capacity (W_{FC} ; m³ m⁻³), and the volumetric soil water
3701 storage at wilting point (W_{PWP} ; m³ m⁻³):

$$\theta_{WHC} = (W_{FC} - W_{PWP})(1 - f_{gravel}) * \min(z_{bedrock}, z_{max}) \quad (\text{C4.1})$$

3702 where f_{gravel} (%) is the fraction of gravel content in soil, $z_{bedrock}$ (mm) is the
3703 distance to bedrock, and z_{max} (mm) is the maximum allowable distance to bedrock,
3704 set to 2000mm. W_{FC} is calculated as:

$$\theta_{FC} = k_{fc} + (1.283 * (k_{fc})^2 - 0.374 * k_{fc} - 0.015) \quad (\text{C4.2})$$

3705 where

$$\begin{aligned} k_{fc} = & -0.251 * f_{sand} + 0.195 * f_{clay} + 0.011 * f_{OM} \\ & + 0.006 * (f_{sand} * f_{OM}) - 0.027 * (f_{clay} \\ & * f_{OM}) + 0.452 * (f_{sand} * f_{clay}) + 0.299 \end{aligned} \quad (\text{C4.3})$$

3706 W_{PWP} is calculated as:

$$W_{PWP} = k_{pwp} + (0.14 * k_{pwp} - 0.02) \quad (\text{C4.4})$$

3707 where

$$\begin{aligned} k_{pwp} = & -0.024 * f_{sand} + 0.487 * f_{clay} + 0.006 * f_{OM} \\ & + 0.005 * (f_{sand} * f_{OM}) - 0.013 * (f_{clay} \\ & * f_{OM}) + 0.068 * (f_{sand} * f_{clay}) + 0.031 \end{aligned} \quad (\text{C4.5})$$

3708 In Equations C4.4 and C4.5, f_{sand} (%) is the fraction of sand content in soil

3709 (%), f_{clay} (%) is the fraction of clay content in soil (%), and f_{OM} is the fraction of

3710 organic matter in soil (%). Organic matter in the soil was calculated by converting

3711 soil organic carbon data extracted from SoilGrids 2.0 to soil organic matter using

3712 the van Bemmelen factor (1.724 conversion factor).

Table C1. List of sampled species and their plant functional group assignment

Symbol	Species	Photo. pathway	Growth duration	Growth habit	N-fixer?	Plant functional group	Number sampled
ACAN11	<i>Acaciella angustissima</i>	c3	perennial	forb	yes	c3_legume	3
AMAR2	<i>Ambrosia artemisiifolia</i>	c3	annual	forb	no	c3_nonlegume	25
AMPS	<i>Ambrosia psilostachya</i>	c3	perennial	forb	no	c3_nonlegume	32
ARAL3	<i>Argemone albiflora</i>	c3	annual	forb	no	c3_nonlegume	3
ARPU9	<i>Aristida purpurea</i>	c4	perennial	graminoid	no	c4_nonlegume	2
ASAS	<i>Asclepias asperula</i>	c3	perennial	forb	no	c3_nonlegume	3
ASLA4	<i>Asclepias latifolia</i>	c3	perennial	forb	no	c3_nonlegume	3
ASSY	<i>Asclepias syriaca</i>	c3	perennial	forb	no	c3_nonlegume	18
BOIS	<i>Bothriochloa ischaemum</i>	c4	perennial	graminoid	no	c4_nonlegume	6
BOSA	<i>Bothriochloa saccharoides</i>	c4	perennial	graminoid	no	c4_nonlegume	6
CAPL3	<i>Carex planostachys</i>	c4	perennial	graminoid	no	c4_nonlegume	3
CAREX	<i>Carex</i> spp.	c4	perennial	graminoid	no	c4_nonlegume	16
CHFE3	<i>Chamaesyce fendleri</i>	c3	perennial	forb	no	c3_nonlegume	2
CHPI8	<i>Chrysopsis pilosa</i>	c3	annual	forb	no	c3_nonlegume	3
COCO13	<i>Conoclinium coelestinum</i>	c3	perennial	forb	no	c3_nonlegume	3
COER	<i>Commelina erecta</i>	c3	perennial	forb	no	c3_nonlegume	3
CRGLL	<i>Croton glandulosus</i>	c3	annual	forb	no	c3_nonlegume	22
CYDA	<i>Cynodon dactylon</i>	c4	perennial	graminoid	no	c4_nonlegume	15
DIAN	<i>Dichanthium annulatum</i>	c4	perennial	graminoid	no	c4_nonlegume	8
ENPE4	<i>Engelmannia peristenia</i>	c3	perennial	forb	no	c3_nonlegume	6
EUMA8	<i>Euphorbia marginata</i>	c3	annual	forb	no	c3_nonlegume	6
GAPU	<i>Gaillardia pulchella</i>	c3	annual	forb	no	c3_nonlegume	16
GLGO	<i>Glandularia gooddngii</i>	c3	perennial	forb	no	c3_nonlegume	2
HEAN3	<i>Helianthus annuus</i>	c3	annual	forb	no	c3_nonlegume	6

Table C2. List of sampled species and their plant functional group assignment (cont.)

Symbol	Species	Photo. pathway	Growth duration	Growth habit	N-fixer?	Plant functional group	Number sampled
HECA8	<i>Heterotheca canescens</i>	c3	perennial	forb	no	c3_nonlegume	2
HETE3	<i>Heliotropium tenellum</i>	c3	annual	forb	no	c3_nonlegume	3
IVAX	<i>Iva axillaris</i>	c3	perennial	forb	no	c3_nonlegume	4
LIAT	<i>Lilaeopsis attenuata</i>	c3	perennial	forb	no	c3_nonlegume	3
LIPU	<i>Liatris punctata</i>	c3	perennial	forb	no	c3_nonlegume	3
LOPE	<i>Lolium perenne</i>	c3	perennial	graminoid	no	c3_nonlegume	9
MIQU2	<i>Mimosa quadrivalvis</i>	c3	perennial	forb	yes	c3_legume	15
NALE3	<i>Nassella leucotricha</i>	c3	perennial	graminoid	no	c3_nonlegume	19
OECU2	<i>Oenothera curtiflora</i>	c3	annual	forb	no	c3_nonlegume	3
OENOT	<i>Oenothera</i> spp.	c3	annual	forb	no	c3_nonlegume	1
PAVI2	<i>Panicum virgatum</i>	c4	perennial	graminoid	no	c4_nonlegume	12
RACO3	<i>Ratibida columnifera</i>	c3	perennial	forb	no	c3_nonlegume	40
RHSET	<i>Rhynchosia senna</i>	c3	perennial	forb	yes	c3_legume	1
RUHI2	<i>Rudbeckia hirta</i>	c3	perennial	forb	no	c3_nonlegume	3
RUNU	<i>Ruellia nudiflora</i>	c3	perennial	forb	no	c3_nonlegume	15
RUTR	<i>Rubus trivialis</i>	c3	perennial	vine	no	c3_nonlegume	3
SAFA2	<i>Salvia farinacea</i>	c3	perennial	forb	no	c3_nonlegume	7
SCHIZ4	<i>Schizachyrium</i> spp.	c4	perennial	graminoid	no	c4_nonlegume	8
SCSC	<i>Schizachyrium scoparium</i>	c4	perennial	graminoid	no	c4_nonlegume	3
SODI	<i>Solanum dimidiatum</i>	c3	perennial	forb	no	c3_nonlegume	1
SOEL	<i>Solanum elaeagnifolium</i>	c3	perennial	forb	no	c3_nonlegume	53
SOHA	<i>Sorghum halapense</i>	c4	perennial	graminoid	no	c4_nonlegume	38
STTE3	<i>Stillingia texana</i>	c3	perennial	forb	no	c3_nonlegume	3
VEOC	<i>Verbesina occidentalis</i>	c3	perennial	forb	no	c3_nonlegume	3
VEST	<i>Verbena stricta</i>	c3	perennial	forb	no	c3_nonlegume	3

Table C3. Model selection results for soil moisture and vapor pressure deficit. Soil moisture was used in a bivariate regression against log-transformed β , while vapor pressure deficit was used in bivariate regressions against leaf $C_l:C_a$

Day	Soil moisture		VPD	
	AICc	RMSE	AICc	RMSE
1	1431.77	0.8400	-772.71	0.0853
2	1431.76	0.8400	-775.47	0.0849
3	1431.78	0.8400	-770.86	0.0854
4	1431.79	0.8401	-793.49	0.0839
5	1431.79	0.8401	-771.66	0.0853
6	1431.78	0.8401	-771.66	0.0853
7	1431.78	0.8401	-771.05	0.0854
8	1431.76	0.8401	-770.94	0.0854
9	1431.75	0.8401	-770.11	0.0854
10	1431.74	0.8401	-770.08	0.0855
15	1431.54	0.8401	-768.64	0.0856
20	1431.40	0.8401	-769.77	0.0855
30	1431.23	0.8400	-772.18	0.0853
60	1429.84	0.8391	-779.06	0.0848
90	1429.14	0.8385	-773.99	0.0852

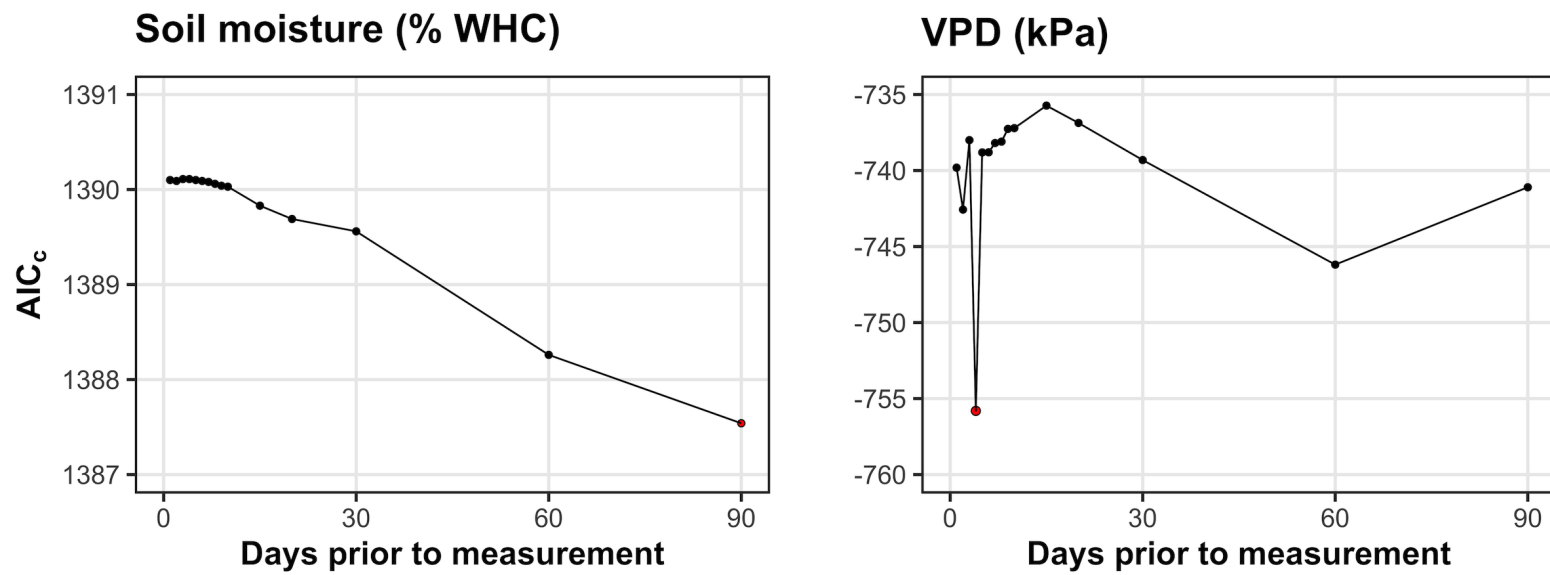


Figure C1. Model selection results exploring relevant timescales for soil moisture (left panel) and vapor pressure deficit (right panel). The x-axis indicates the number of days before each site visit and the y-axis notes the corrected Akaike Information Criterion value. The timescale with the lowest AICc value, and therefore most relevant timescale to include in statistical models, is noted as a red point.

**3713 Appendix D: Supplemental material for "Optimal resource investment
 3714 to photosynthetic capacity maximizes nutrient allocation to whole
 3715 plant growth under elevated CO₂"**

Table D1. Summary table containing volumes of compounds used to create modified Hoagland's solutions for each soil nitrogen fertilization treatment. All volumes are expressed as milliliters per liter (mL L⁻¹)

Compound	0 ppm N	35 ppm N	70 ppm N	105 ppm N	140 ppm N
1 M NH ₄ H ₂ PO ₄	0	0.165	0.33	0.5	0.67
2 M KNO ₃	0	0.335	0.67	1	1.33
2 M Ca(NO ₃) ₂	0	0.335	0.67	1	1.33
1 M NH ₄ NO ₃	0	0.165	0.33	0.5	0.67
8 M NH ₄ NO ₃	0	0	0	0	0
1 M KH ₂ PO ₄	1	0.85	0.67	0.5	0.33
1 M KCl	3	2.45	2	1.5	1
1 M CaCO ₃	4	3.33	2.67	2	1.33
2 M MgSO ₄	1	1	1	1	1
10% Fe-EDTA	1	1	1	1	1
Trace elements	1	1	1	1	1

Compound	210 ppm N	280 ppm N	350 ppm N	630 ppm N
1 M NH ₄ H ₂ PO ₄	1	1	1	1
2 M KNO ₃	2	2	2	2
2 M Ca(NO ₃) ₂	2	2	2	2
1 M NH ₄ NO ₃	1	3.5	0	0
8 M NH ₄ NO ₃	0	0	0.75	2
1 M KH ₂ PO ₄	0	0	0	0
1 M KCl	0	0	0	0
1 M CaCO ₃	0	0	0	0
2 M MgSO ₄	1	1	1	1
10% Fe-EDTA	1	1	1	1
Trace elements	1	1	1	1

Table D2. Summary of the daily growth chamber growing condition program

Time	Air temperature (°C)	Light (%)
09:00	21	25
09:45		50
10:30	25	75
11:15		100
22:45	21	75
23:30		50
00:15	17	25
01:00		0

Table D3. Effects of CO₂, fertilization, and inoculation on whole plant biomass: pot volume (BVR; g L⁻¹)*

	df	Coefficient	χ^2	p
(Intercept)	-	1.33E-01	-	-
CO ₂	1	1.53E-01	146.004	<0.001
Inoculation (I)	1	4.19E-01	19.320	<0.001
Fertilization (N)	1	1.90E-03	279.387	<0.001
CO ₂ *I	1	1.03E-01	0.007	0.934
CO ₂ *N	1	2.44E-03	49.725	<0.001
I*N	1	-6.90E-04	9.006	0.003
CO ₂ *I*N	1	-4.95E-04	0.640	0.424

3716 *Significance determined using Type II Wald χ^2 tests ($\alpha=0.05$). P-values less
3717 than 0.05 are in bold. Key: df=degrees of freedom; χ^2 =Wald Type II chi-square
3718 test statistic.

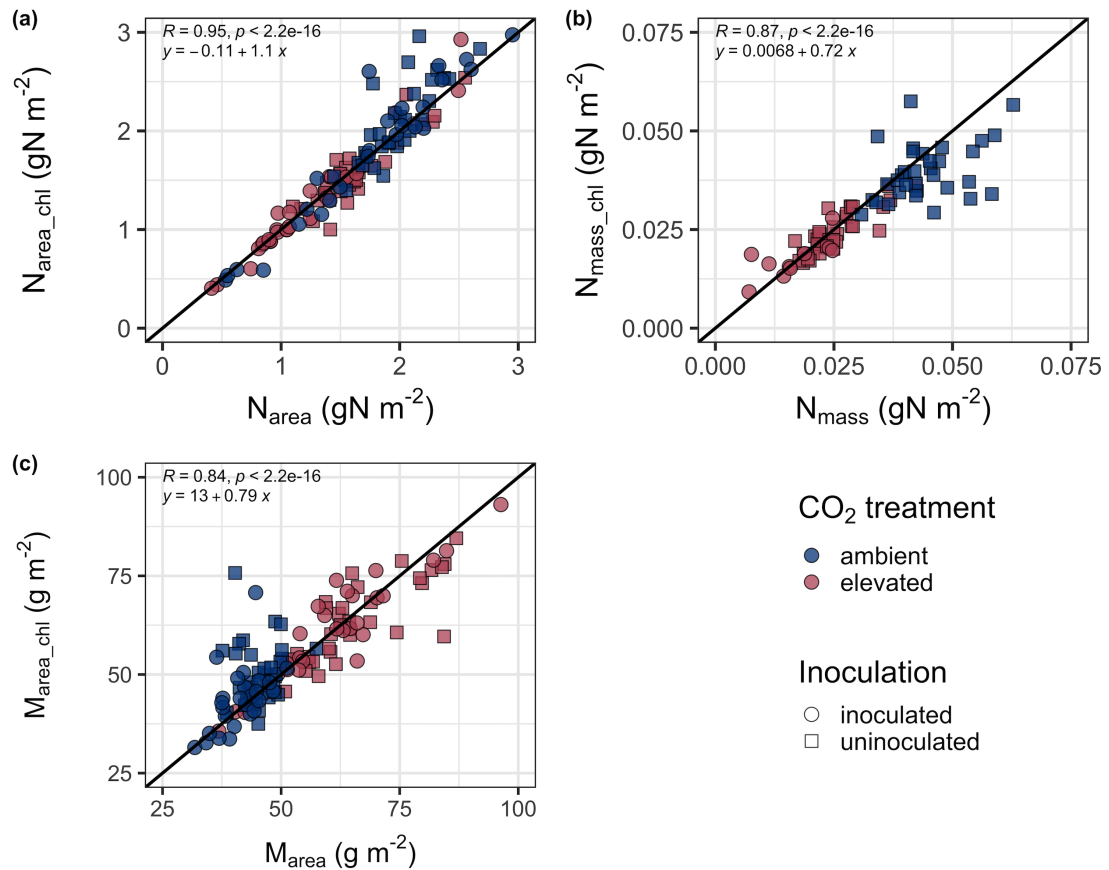


Figure D1. Relationships between area-based leaf nitrogen content (a), mass-based leaf nitrogen content (b), and leaf mass per unit leaf area (c) measured on the focal leaf used to generate A_{net}/C_i curves (x-axis) and leaf nitrogen content measured on the leaf used for chlorophyll extractions (y-axis). Blue points refer to leaves grown under ambient CO₂ and red points refer leaves grown under elevated CO₂. Square points indicate uninoculated pots and circular points indicate inoculated pots. Pearson's correlation coefficient, associated p -values, and the line of the regression line that described each bivariate are included in the top left corner of each plot. The solid black line visualizes the trend given a 1:1 bivariate relationship.

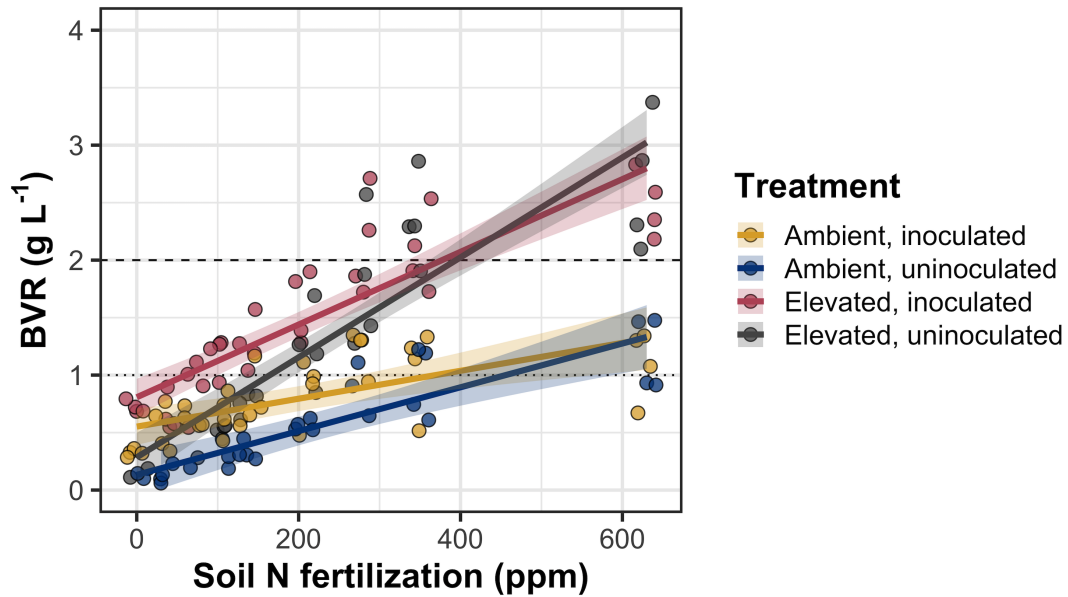


Figure D2. Effects of CO₂, fertilization, and inoculation on the ratio of whole plant biomass to pot volume. Soil nitrogen fertilization is represented on the x-axis in all panels. Yellow points and trendlines indicate inoculated individuals grown under ambient CO₂, blue points and trendlines indicate uninoculated individuals grown under ambient CO₂, red points and trendlines indicate inoculated individuals grown under elevated CO₂, and grey points indicate uninoculated individuals grown under elevated CO₂. Solid trendlines indicate regression slopes that are different from zero ($p<0.05$). The dotted horizontal line indicates the point where biomass:pot volume exceeds 1 g L⁻¹, and the dashed line indicates the point where biomass:pot volume exceeds 2 g L⁻¹.